Prosthetic Socket Design: From a Multi-Indenter Device for *in vivo* Biomechanical Tissue Measurement to a Quasi-passive Transtibial Socket Interface

by

Arthur Joseph Petron

B.S., Massachusetts Institute of Technology (2008)
S.M., Massachusetts Institute of Technology (2010)

Submitted to the Program in Media Arts and Sciences,
School of Architecture and Planning
in partial fulfillment of the requirements for the degree of

Doctor of Philosophy in Media Arts and Sciences

at the

MASSACHUSETTS INSTITUTE OF TECHNOLOGY

February 2016

Signature redacted

Author . . . . . .
Arthur Joseph Petron
Program in Media Arts and Sciences,
School of Architecture and Planning
December 18, 2015

Signature redacted

Certified by . . . . . .
Hugh M. Herr
Associate Professor, Program in Media Arts and Sciences
Associate Professor, Harvard-MIT Division of Health Sciences and Technology
Thesis Supervisor

Accepted by . . . . . Signature redacted . . . . . .
Pattie Maes
Academic Head, Program in Media Arts and Sciences

Prosthetic Socket Design: From a Multi-Indenter Device for *in vivo* Biomechanical Tissue Measurement to a Quasi-passive Transtibial Socket Interface

by

Arthur Joseph Petron

Submitted to the Program in Media Arts and Sciences,
School of Architecture and Planning
on December 18, 2015, in partial fulfillment of the
requirements for the degree of
Doctor of Philosophy in Media Arts and Sciences

Abstract

The prosthetic socket, the mechanical interface between an amputated residuum and an external prosthesis, is of critical importance to the performance of a prosthetic limb system. Conventional prosthetic socket technology is derived using a non-quantitative, artisan methodology. Consequently, a comfortable socket interface cannot be made reproducibly, and persons with limb amputation too often experience discomfort. As a resolution to this difficulty, the field of digital prosthetic socket design seeks to advance a quantitative CAD/CAM methodology for socket production to produce reproducible and comfortable interfaces. Prosthetic researchers have proposed a digital socket production work flow comprising the steps of 1) assessment of residuum tissue biomechanics; 2) modeling optimization of the residuum-socket interface, and 3) fabrication of a variable-impedance socket system based upon these optimizations. In this thesis, two novel technologies are designed, built and evaluated at either end of this work flow, namely a multi-indenter device for *in vivo* biomechanical tissue measurement and a quasi-passive variable-impedance transtibial socket interface.

An active indenter platform called the FitSocket is presented. To assess residual-limb tissue biomechanics, the FitSocket comprised 14 position and force controllable actuators that circumferentially surround a biological residuum to form an actuator ring. Each actuator is individually controllable in position (97.1?m accuracy) and force (330mN accuracy) at a PC controller feedback rate of 500Hz, allowing for a range of measurement across a residuum. At five distinct anatomical locations across the residual limb, force versus deflection data are presented, demonstrating the accuracy and versatility of the FitSocket for residual limb tissue characterization. A passive, single indenter version of the FitSocket, called the FitPen, is also presented. The FitPen is designed to be ultra-portable in order to take biomechanical measurements in the field outside the laboratory setting.

A quasi-passive socket (QPS) is presented having spatially and temporally varying socket wall impedances. The QPS is an autonomous computerized transtibial prosthetic interface that can stiffen or become compliant using computer-controlled electrolaminate actuators. The QPS measures forces applied by the limb on the socket, 3-axis acceleration of the socket, and the position of the electrolaminates. On a test participant with transtibial amputation, the socket was evaluated through sit-to-stand tests to de-

termine the viability of computer-controlled electrolaminate engagement, and through a walking study to evaluate the ability of the electrolaminates to maintain their clutched state during ambulation at a self-selected walking speed. The average deflections of forced tibia movement in the sit-to-stand tests were 7 $\pm$ 2mm while sitting with the electrolaminates in an unclutched state, and 2.1 $\pm$ 0.6 mm while standing with the electrolaminates in a clutched state. Further, the walking study showed a maximum unclutched deflection (3.7 $\pm$ 0.9 mm)16 times larger than that of the maximum deflection while clutched. This work was supported by the United States Department of Veteran Affairs through the VA Innovation Initiative (VAi2) program.

Thesis Supervisor: Hugh M. Herr
Title: Associate Professor, Program in Media Arts and Sciences
Associate Professor, Harvard-MIT Division of Health Sciences and Technology

Prosthetic Socket Design: From a Multi-Indenter Device for *in vivo* Biomechanical Tissue Measurement to a Quasi-passive Transtibial Socket Interface

by

Arthur Joseph Petron

Submitted to the Program in Media Arts and Sciences,
School of Architecture and Planning
on December 18, 2015, in partial fulfillment of the
requirements for the degree of
Doctor of Philosophy in Media Arts and Sciences

Signature redacted

Thesis Supervisor .....

Hugh M. Herr

Associate Professor, Program in Media Arts and Sciences

Associate Professor, Harvard-MIT Division of Health Sciences and Technology

Signature redacted

Thesis Reader .....

Neri Oxman

Associate Professor, Mediated Matter, Program in Media Arts and Sciences

Signature redacted

Thesis Reader .....

Joseph Paradiso

Alexander W. Dreyfoos (1954) Professor, Responsive Environments

Program in Media Arts and Sciences

Acknowledgments

Hugh Herr, Neri Oxman, Joe Paradiso, Bill Mitchell, Andy Lippman, David Sengeh, Ava Chen, Melody Liu, Reza Safai-Naini, Jean-Françios Duval, Akito van Troyer, David Cranor, Liz Tsai, Lindsey Reynolds and Chibly, Bevin Lin, Rebecca Kusko, Luke Mooney, Bryan Ranger, Katherine Song, Shuo Wang, Kevin Moerman, Michael Eilenberg, Bruce Deffenbaugh, Ken Pasch, Sarah Hunter, Jared Markowitz, Ernesto Martinez-Villalpando, Ken Endo, Grant Elliott, Jon Bruner, Rebecca Kleinberger, Jie Qi, Nan Zhao, Yoav Reches, Joichi Ito, Gershon Dublon, Nan-Wei Gong, Chia-Wei Lin, Spencer Russell and Ella, Brian Mayton, David Ramsey, Artem Dementyev, Juliana Cherston, Michael Lin, Juliana Nazaré, Peter Schmidt, Raul-David "retro" Poblano, Benjamin Weissman, Samantha Powers, Donald Guy, Philippa Mothersill, Todd Farrell, Christina Kang, Tim Dudley, Allison Jacobs, Micah Rae, Grace Woo, Phil Salesses, Viirj Kan, Xin Liu, Madeleine Abrombrowitz, Scott Greenwald, Jingni Wei, Roman Stolyarov, Benjamin Bloomberg, Lisa Katayama, Quentin Mitchell, David Hill, Andrew Petron, Tracey Petron, Gina Petron, Charles G. Petron, Susan Byrnes, Randy Byrnes, Thomas Petron, Corky Petron, Lydia Stern, Adam Linnert, Adam Setapen, Cameron Taylor, Nadya Peek, Christina Chase, David Wallace, Karthik Dinakar, Katie Byrnes, Krysten Byrnes, Chris Post, Evan Broder, Noah Jessop, Jifei Ou, Luke Vink, Mari Gallegos, Moni Gallegos, Christina Kang, Lauren Oldja, Justin Nelson, Tyler Clites, Chikara Inamura, Linda Peterson, Kiera Horowitz, Paula Aguilera, Jonathan Williams, Peter Pflanz, Will Glesnes, Xiao Xiao, Donald-Derek Haddad, Tim Dudley, Allie Jacobs, Devin Dersh, Nick Flytzanis, Dimitris Papanikolaou, Carson Teale, Brian Allen, Daniel Leitenger, Jacob Bernstien, Dan Oran, Joost Bonson, Anne Shen, Virginia Jo White, Ian Ferguson, Sandra Richter, Thaddeus Bromstrup, Nadia Chengovsky, Maxim Chengovsky, Denise Cheng, Svetlana Chekmasova, Alexis Hope, Edwina Portocarrero, Mitch Resnik, Pattie Maes, Cesar Hildago, Marko Ahtisaari, Aleksi Aaltonen, Elena Glassman, Chelsea Barabas, Alin Cristian Marin, Jutta Friedrichs, Palash Nandy, Dan Novy, Andrew Chen, Bianca Datta, Cheetiri Smith, Chris Pentacoff, Jonny Surick, Sara Ferry, Mike Grenier, Travis Rich, Valentin Heun, Mike Aponte, Vinayak Ranade, Chia Lynn Evers, John Silvio, Johnathan Marcus, Madeline Hickman, Michelle Chen, Margaret Wang, Frances Lenahan, Audrey Horst, Larissa Berger, Christie Lin, Daniel O'Niel, Greg Steinbrecher, Ian McFarland, Jasmina Aganovic, John Sylvan, Jeff Lieberman.

Contents

List of Figures

List of Tables

Listings

Chapter 1

Introduction

Imagine you are a spectator standing at the finish line on Boylston Steet watching some of the world's finest athletes finish running 26.2 miles and you think, "I want to do that someday." In a flash, your daydream of running the marathon on your own biological legs is no longer possible. Or, perhaps you are on a routine perimeter check off-base in Afghanistan and you walk over an IED. Or, maybe you are a child in Cambodia, whose dream is to play professional soccer for your country. So, you play soccer with your friends regularly on a nearby field. Until one day, your ball flies off into the shrubs by the field. As you go to retrieve the ball, you step on a mine.

The Biomechatronics group has developed bionic ankles, bionic knees, advanced exoskeletons for walking and running and other orthotic devices. Scientists in our program also develop musculo-skeletal models for walking and running. Others are attempting to interface these bionic prostheses with the peripheral nervous system to allow those with lower extremity amputation to receive tactile feedback from their prostheses and volitionally control them akin to biologically standard limbs.

For all these individuals with amputation, the current most important path is the one that allows them to maintain their livelihood – and that starts with walking. We can imagine a world where individuals voluntarily sacrifice their boring biological limbs for upgradable, bionic ones, but this is a topic for which the world is not quite ready. Thankfully, we finally have advanced prostheses that allow those with amputated lower limbs to not only walk again, but run and even compete professionally with individuals who have biologically standard limbs. The prosthetic socket – the interface that connects

the remaining or residual limb to the rest of the prostheses – is the most important part in the prosthetic system. Without a comfortable, direct, force-transferring socket, it doesn't matter how advanced the rest of a prosthesis is. We have seen extreme bionic hands, ankles, knees, and many other parts of the body, but the design and manufacture of sockets lags behind.

Whether you have the most advanced robotic ankle or a primitive wooden peg is secondary to the quality of attachment to the human body. Just like the slickest new smartphone of this era, if you do not have the right charger, it is not very useful. Today's sockets are primarily constructed using hard carbon-fiber or hard plastic. They are built to maximize strength while minimizing weight. When the Biomechatronics socket team started thinking about how to approach making better sockets, we started by examining why sockets are made the way they are. After many conversations with prosthetists and individuals with amputation, we learned that sockets do not need to be made in any particular way. In fact, they aren't. All over the world, sockets are made using different methods and the resulting "comfortable" socket shapes vary widely from a prosthetist in Nairobi to one in Boston to one in San Jose. The method of actual construction is strikingly similar everywhere, but the shapes are highly individual to the prosthetist who sculpts them.

Generally, sockets are not comfortable. David Sengeh, a graduate student with whom the author of this manuscript works closely on socket design in the Biomechatronics group, interacted with amputees who were sitting by the roadside in Sierra Leone four years ago. He was surprised to find out that they had in fact been given free prosthetic limbs by either the government or other organizations. Before he spoke to the patients, everyone else who he spoke to told him that those people just wanted to sit by the roadside to beg. He went to a camp to have a conversation with some of the patients. It was then that he was told that though they were given free legs, the reality of the matter was that their sockets did not fit well. As such, they were not able to use those legs to do anything else.

In fact, the use of poorly fit sockets is known to cause pressure ulcers, pressure sores, and bleeding as well as other secondary issues like back pain, weight gain, and more. These effects have been repeatedly observed to be related to poor socket fit. It is a vicious cycle for patients living with amputations.

An individual with amputation will not use a socket that is uncomfortable in the same way that you would not charge your phone no matter how fancy it is if it shocked you every time you charged it. This is not a developing world problem. It is a problem everywhere.

1.1 Introduction to the Field of Digital Socket Design

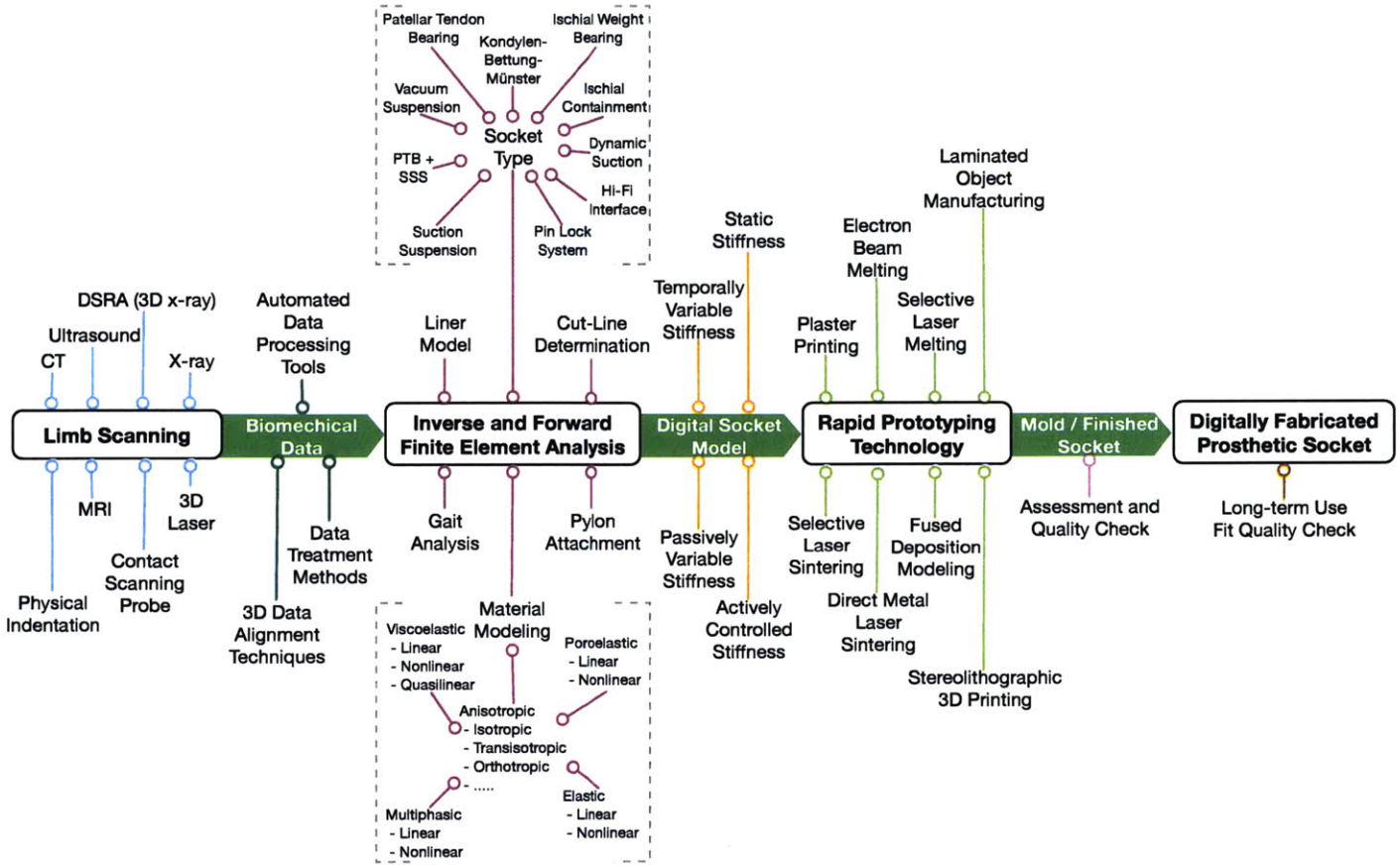

Figure 1-1: Pictured is the current state of the understanding of the digital socket design field. Note the many competing methodologies along the path from biomechanical data collection to long term, digitally fabricated socket use. This figure may be considered to be the visual representation of the topics that will be expanded upon throughout this chapter.

This manuscript seeks to demonstrate that an indenter device of varying forms is capable of providing reliable data for the creation of hyperviscoelastic mechanical deformation models of digital, 3D residual limbs[1], and that these models may be used to create spatially and temporally variable stiffness sockets. You will see that this work is not the effort of a single individual, but that of many – not only in the Biomechatronics group but all over the world. The work presented in this manuscript will be that of the author; however, a brief introduction to the work of others is necessary to understand the concept of the field as it stands today.

To begin, we will briefly overview the major topics of the field and this thesis, then break down each

[1]David Sengeh has taken countless MRI scans of our subjects and segmented the MRI data into useable 3D solids. Additionally, David Sengeh in collaboration with Kevin Moerman – a post-doc in Biomechatronics – have developed the mechanical deformation models necessary to go from these indentation data to a useable socket design

separately in order to elucidate the more subtle aspects. A description of the current state of the field of socket design aids in understanding the contributions of this thesis. The problems faced in digital socket design are many, spanning multiple academic disciplines (mainly math, mechanical engineering, physics, electrical engineering, computer science, biophysics, anatomy, dermatology, and neuroscience). This considered, it is possible to create quantitative knowledge across these fields when focused on the topic of digital socket design. The result of this endeavor is presented.

1.1.1 State of the Art of Lower Extremity Prosthetic Socket Design

The state-of-the art process for making prosthetic sockets is a tedious, cumbersome, and artisanal process that takes from a few days to a few months before a useable fit is designed and manufactured. Additionally, the residual limb does not stay exactly the same size or shape over time. Just like the rest of your body, losing or gaining weight or muscle will require a new socket for a comfortable fit.

Both patients and prosthetists have to continually modify their sockets in order to maintain a level of comfort required for them to do simple tasks, such as going to the grocery store. In order to move further, let's review how a prosthetist shapes a socket. Typically the prosthetist begins by wrapping the residual limb with plaster of Paris soaked gauze – the same material used to make casts if you were to break your arm. This is the female mold of the residual limb. Plaster of Paris is poured into the female mold to create a male replica of the residual limb. The plaster takes two days to cure. This heavy bit of plaster is not the final socket shape. If we were to make a carbon-fiber socket with this shape, it would be far too loose and would simply fall off on each step. This is because your tissue can compress. Go ahead, test it out on yourself. If you press on your shin bone it is very hard, while your calf located on the opposite side of your leg is softer.

A prosthetist uses this knowledge to alter the socket shape with one additional piece of information. It hurts a lot if you press on hard areas with too much force. A socket that applies too much force to areas of the body that are only skin and bone feels similar to crawling across a concrete floor on your knees and elbows. The prosthetist adds material in the red areas to create voids in the socket, while subtracting material in the green areas so that the socket can bear weight in those areas. Unfortunately, a side effect of this process is that the residual limb no longer makes full contact with the socket wall. It can't. The socket itself is hard. Direct contact with areas such as the shin would be very uncomfortable.

After the modifications have been made to the positive male mold, the prosthetist creates a test socket out of a semi flexible plastic. This test socket is checked on the patient for fit and can be modified with the application of heat if necessary. Once the test socket checks out, another plaster cast is poured into the plastic shell. Two days later the plaster can be cleaned and shaped for the application of carbon fiber composite to create the final socket.

In summary, sockets are difficult to make primarily because the process is completely analog. Sockets take a long time to make. The process is messy and non-repeatable. It is based solely on the experience of the prosthetist.

1.1.2 Improvements over the State of the Art

Sockets are the most important part of any prosthesis because they are the physical connection with the body. Most sockets are uncomfortable. No two sockets are alike. Each must be custom fit to every patient if any amount of comfort is expected.

To make new kinds of prosthetic sockets that improve the livelihood of patients, we would need to use scientific data to design prosthetic sockets in a repeatable process. Irrespective of where you are or who you are, you should be able to get customized prosthetic sockets based on scientifically validated principles. We now have the tools to accurately capture the shape and the biomechanical properties of the residual limb. Using these data, we can imagine a process by which we can save not only time, but the cost for the design and production of sockets.

For example, using Magnetic Resonance Imaging (MRI), we can scan the residual limbs of patients to see the density of soft tissue in the residual limb. We can use that MRI data to accurately represent the stiffness contours of the body. There are tools that can enable us to get accurate 3D models from MRI and we can better understand how the interface should be designed based on the underlying soft and hard tissue.

Other researchers have used computed tomography (CT), surface scanning, and ultrasound to accurately capture the shape of the residual limb and also get an understanding of the tissue. As you can see in Figure 1-1, many combinations of these limb scanning tools can be powerful for the design of mechanical interfaces for the body.

The FitSocket technology measures hyperviscoelastic biomechanical properties of soft tissue impedance of a patient's residual limb. These data can be correlated with other imaging tools, such as those developed by David Sengeh, and biomechanical modeling and computer aided manufacturing, such as those developed by David Sengeh and Kevin Moermon. The FitSocket is a rather large indentation device. In order to judge if indentation could be done with a more lightweight device, the FitPen was developed as a passive, single indenter version of the FitSocket. During initial experimentation with socket creation from measured data, the quasi-passive socket was developed as an extension of a spatially varied impedance prosthetic socket to explore the affordances offered by a spatially and temporally varied prosthetic socket.

1.1.2.1 The FitSocket

The FitSocket is a robotic, multi-indenter system that works by physically pressing on the patient's residual limb. Each of its 14 radial actuators is fitted with an extremely accurate position and force sensor. If we press on a certain area with 4 Newtons (about 1 lb) we can tell how much the tissue at that node moves. Essentially, we're measuring the body like it is made of springs; they are very non-linear springs. We don't know the properties of these springs, but the FitSocket allows measurement of them.

You may be wondering why this matters. Who cares how stiff one part of the residual limb is versus another? I thought this was about the right socket shape!

You're right. Shape is incredibly important. Today's sockets rely entirely on being the right shape for comfort. We think it should also be about stiffness, or how hard or soft the socket is.

When you pick up a paper cup, do you pick it up with a different force than a ceramic coffee mug? The shape of your hand matters but so does the force it is applying to the cup and the force the cup applies back on your hand. It turns out force and shape are intertwined. They are dependent on each other. To us it does not make sense to design a socket without knowing the impedance of the thing the socket is attaching to. By accurately measuring the shape of a residuum and its impedance, we enable designers to create sockets that minimize pressures within the prosthetic socket. These sockets fit better, and are much more comfortable, while increasing the surface area in contact with the patient.

Since we know the location and material property of the body at each node, we can match them

with material properties within our design for multi-material, 3D printed sockets. The resulting multi-material, 3D printed prostheses are fundamentally different from current solutions. By increasing the amount of comfortable contact with the socket wall, we are able to decrease the pressure required for a solid structural connection to the wearer.

1.1.2.2 The FitPen

The FitPen is a hand-held indenter with a passive (spring loaded) indentation mechanism. It has a capacitive sensor on the tip of the flat, circular indenter head that is 6.35mm in diameter. Internal to the device is a microcontroller, capacitive sensor circuitry, a deflection sensor, and communication circuitry via USB. When coupled with a digitizer arm, such as the Microscribe MX, or a motion capture system, such as a Vicon active IR system, the FitPen is capable of providing the same type of hyperviscoelastic impedance data as the FitSocket in a much smaller package.

The FitPen works by comparing the absolute position of the handheld indenter device with the deflection of its indenter head. Because the indenter head is spring loaded, this deflection also implies an indentation force. In order to know what the indentation distance is, we need to know the absolute location of the device – and this is what the digitizer arm or motion capture system accomplish. The complete system – a portable computer, digitizer arm, and the attached indenter device – is small enough to fit inside a medium sized suitcase. This means that the FitPen is capable of being relocated as easily as taking a flight from an airport.

1.1.2.3 The Quasi-Passive Socket

The Quasi-passive socket (QPS) is an exploration of a spatiotemporally varied impedance prosthetic socket. The tibial region on this socket has been made softer than our usual design for a spatially varied impedance socket and two electrostatic clutches have been placed across this area mounted to the supporting carbon fiber frame of the socket. Using the onboard microcontroller, it is possible to implement either motion specific clutch control or human operated, wireless clutch control.

The hypothesis for the temporal control component is that while the prosthetic socket must be able to transfer the forces commanded by the residuum to the rest of the prosthesis, it is not required to do

this at all times. In fact, when an individual with amputation is seated or (to a lesser degree) standing still, the forces necessary are quite low. If, during these reduced force requirement periods, the socket stiffness is reduced – lowering the overall pressure on the residuum – the wearer may enjoy a healthier, more comfortable prosthetic device.

1.1.3 Qualitative Benefits of Data Driven Socket Design

Recently, in one of our studies, we had a veteran try out a new type of 3D printed prosthetic socket generated by David Sengeh using the subject's prosthetist's socket shape but with spatially varying stiffness. He went on to tell us after the study that he'd had over 20 legs over the past 12 years of his amputation. As he walked out, he told us that this socket was most different from anything he'd ever experienced. Another patient whose profession requires that he is always on his legs and thus always in pain said it was like walking on pillows. The reason here is that we have a good understanding of where his muscles and bones are within his leg. As such, we are able to design custom sockets that minimize internal soft tissue strains and damage. Imagine if you could walk on high heels that felt like walking on a pillow. In general, those who have ever worn shoes have a leg up in understanding the benefits of this approach.

We validate the sockets we create and test on subjects by measuring the pressure inside the socket with a thin pressure sensor as the subject walks at their own pace. We wrap the residual limb with the sensor and ensure that it does not move within the socket. The patient walks at their own self-selected speeds on a treadmill that also has force plates. We put infrared reflective markers on the patients so that we can we better understand the joint angles and moments as they walk. When we compare the pressure values for the patient s normal socket with that of the socket we designed, we see high reductions of contact pressure.

1.1.4 Using this Data Driven Processes for Other Applications

How many of the mechanical interfaces that you use daily are customized for you? We've been talking about individuals with amputation, but these techniques can affect you as well. These techniques can be used to create incredibly comfortable orthotic braces to help with knee, elbow, and ankle injuries. We

can help design better backpacks that cause less back pain. Anything you can think of that attaches to your body to support some amount of force is fair game. Shoes, diving tank mounts, chairs, ski boots, climbing harnesses.

You may have seen some of the research into exoskeletons lately. A common problem plaguing designers in this field is mechanical attachment to the body. We can make an exoskeletal Iron Man suit that mechanically interfaces with the body in a very intimate way.

Don't want to be Iron Man? What about clothing that is designed with your exact physical properties in mind. Over places like the elbow, the cloth is stretchable to allow motion and less stretchable over areas like your triceps. It would be the most comfortable shirt you've ever worn. What about bras that are customized to a woman's specific physiology by not only providing the right support but also distributing the forces required for that support correctly on the body? The information we gather about the physical properties of your skin and the tissues and bones under it don't just make the lives of those with amputation better – it can be used in products we all wear every day. Those with amputation may have the most benefit, since they likely also wear shirts.

To summarize, socket design is a truly complicated process since the socket must be customized for each patient. This is truly an endeavor in mass customization. There are not enough prosthetists in the world. At the same time, the number of amputations will double by 2030 from increased cancer, cardiovascular diseases, and war.

The socket is the most important element of a prosthesis. If they are uncomfortable, a patient would not use them no matter how nice the prosthesis is. Their mobility will decrease. They will not have the life they would like to have. When this happens, these amazing people develop secondary challenges – some of which can lead to further amputation. This is an initial process into using quantitative data for the design of sockets.

1.2 Detail of the Problems with Current Socket Design

For an individual with lower-extremity amputation, one of the most cited problems is residual limb pain. This pain is generally associated with poor socket fit – either because the individual's limb has

changed shape since the original fitting [Sanders et al., 2009] or the original fitting was flawed. Flawed fittings may even be attributed to the patient's prior activity that day [Sanders et al., 2013]. Further, traditional sockets are made using a single material stiffness for the entire structure. While a single material socket is useful in order to guarantee that the socket supports the load associated with walking and running, it has a disadvantage in the way it loads the individual with amputation. Finally, the stiffness of the socket is constant over time. That means that when the individual wearing the socket is seated — and does not need secure control over their prosthetic device through the socket — the socket remains tightly adhered to the residual limb. Many individuals partially remove their residual limbs from the socket while seated to alleviate this problem.

1.2.1 More on Traditional Socket Manufacture

In the most common traditional socket manufacture, a male plaster mold [Bakody, 2009] is used to create a (usually clear) plastic test socket that a prosthetist uses to test the socket fit with a patient. The patient's residuum is wrapped with a fabric that has been coated in plaster. The prosthetist must take care to wrap the residuum with an even (or specifically varied) pressure over the entire surface of the limb to ensure proper socket shape. After the limb has been wrapped by hand, a male mold is created from the female plaster and fabric wrap. This male mold is modified by hand by the prosthetist in order to alter the spatial location of areas like the tibial crest, tibial and fibular heads, etc. in order to make the resulting socket more comfortable.

Current clinical practice is indeed an art. The creation of a comfortable socket takes months even when made by a trained, highly experienced prosthetist. There are approximately 1.7 million lower-limb amputees in the United States. Currently, there is no way to ensure that each patient has access to the same prosthetic skill when it comes to his or her socket. Uncomfortable sockets lead most directly to pain at the socket interface, which causes lower activity levels than normal from the patient, increasing their health risks in general.

Skin breakdown on the residual limb is a common occurrence, causing pain and discomfort in an amputee's daily life. Skin breakdown is usually due to high peak pressures at the interface between the socket wall and the residuum. Unfortunately, today's socket technology does not leverage current state-of-the-art robotic approaches that could facilitate socket designs that greatly improve both comfort and

joint flexibility. The problems that need to be addressed are pain, costly return-visits to a prosthetist, lower than desired activity, skin pathologies, changes in residual limb volume and shape over time, and limits in tolerable duration wearing the socket [Zheng et al., 2001, Mak et al., 2001].

1.2.2 Pain in Individuals with Lower Extremity Amputation

This thesis makes frequent mention of the terms "pain" and "comfort" for the purposes of describing how prosthetic sockets may be created that reduce pain or increase comfort. Lacking a scientific definition of comfort[2], we tend to suggest that these terms are also associated with injury. Pain over long periods of time likely causes physical and mental injury. Increased comfort is deemed to be a lack of pain *as compared to the individuals current pain levels.* When we describe a model as increasing comfort or reducing pain, we mean to say that the external pressures and internal stresses, put on the residuum by the prosthetic socket, that the model predicts — and we subsequently measure — are reduced in relation to current, state-of-the-art sockets. We know a good bit about the scientific, mechanical measures that lead to healthy tissue. We base our descriptions of comfort and pain on this basic understanding.

Pain for an individual with lower extremity amputation primarily occurs due to poor residual limb tissue integrity, the level of regiment of care to keep that tissue healthy, post-operative pain, phantom pain [Lacono et al., 1987, Molton et al., 2007, Davidson et al., 2010], and poor socket fit [Butler et al., 2014]. In those having one amputated limb, gait asymmetry associated with changes to walking speed – especially increased walking speed [Ferris et al., 1999] – can cause the intact limb to undergo increased rates of degeneration due to the higher loads it must bear during these activities [Nolan et al., 2003]. Total distance walked also plays a significant role in muscle fatigue, primarily in the sound-side plantar-flexor for those with trans-tibial amputations [Yeung et al., 2012]. Shock absorbing pylons help to mitigate these issues [Gard and Konz, 2003] but cannot eliminate them completely using current sockets. Tissue degeneration typical to trans-tibial or trans-femoral residua [Portnoy et al., 2007a] include debubitus ulcers, deep tissue breakdown, flap necrosis, and pressure sores. These edema can, in the dark, moist environment of the prosthetic socket, quickly lead to serious infections and, if left untreated, to further amputation.

Reduction of pain in the residual limb starts before (if possible) the amputation process and continues for

[2]Due to no shortcomings in due diligence; comfort is a very difficult word to scientifically define

the rest of the life of the individual [Arwert et al., 2007]. Pinzur et al. show that the angle between the femur and residual tibia, femur and prosthetic socket, and tibia and socket are useful measurements. The team concluded that significant differences between these measurements was a statistically significant indicator of pain [Pinzur et al., 1996]. During use, the socket and liner (which is essentially a silicone sock) heavily insulate the residual limb. The heat causes the skin inside the socket to sweat, resulting in unhealthy levels of moisture buildup inside the socket [Webber and Davis, 2015]. Not only can excess heat inside the prosthetic socket cause tissue edema, and infection, it can also be an indicator of the location of at risk tissue [Peery et al., 2005], since tissue that is irritated tends to increase in temperature before injury is unpreventable.

Poor socket fit can not only be the cause of tissue degeneration, it can also cause more widespread physiological pathologies [Behr et al., 2009] such as back and joint pain [Novacheck, 1998, McGeer, 1993, Pandy and Anderson, 1992, Kuo, 2001]. These effects further exacerbate the already reduced quality of life of an individual whose socket is already painful to use[3]. Acute phantom limb and residual limb pain, assessed 4 to 5 days after amputation have been found to be significant predictors of chronic pain at 6, 12, and 24 months respectively [Hanley et al., 2007].

1.2.3 Functional Requirements of a Lower-Limb Socket

Lower-limb sockets are responsible for bearing the forces associated with walking, running, jumping or any other type of full-body ambulation. These vertical forces range from the negative 100 Newton forces associated with an amputee dangling his or her prostheses from a stool to over positive 1000 newtons per leg associated with an amputee hopping on one leg [Dou et al., 2006, Polliack et al., 2000a]. In addition, the socket must be capable of transmitting rotational forces in the coronal, sagittal, and medial planes from the soft tissue of the residual limb to the prosthesis while mimicking the more rigid bone connection provided by biological limbs as closely as possible [Portnoy et al., 2007b, Bronzino, 2006].

The biological tissue of the residual limb has a separate set of functional requirements. These are that the residual limb is able to breathe through exposure to air, maintain good vascular condition, and be subject to minimal sustained forces [INMAN et al., 1961]. Excess moisture at the socket to residual

[3]It should be noted that a proper prosthesis is also very important for healthy body kinematic physiology [Hospital and Womwn´S, 2011, Lester et al., 2005].

limb interface will increase the likelihood of dangerous microbe buildup, soften tissue, and decrease the frictional coefficient of the skin with the socket wall. Excess pressure on the residual limb by the socket will force fluid (blood, lymphatic) out of the limb, reducing its volume and ability to repair damage caused by the socket [Mak et al., 2010]. High socket forces have the ability to cause acute tissue breakdown of both the dermal layers and the underlying muscle, nerve, facia, etc. tissues [Foisneau-Lottin et al., 2003]. It is common for amputees to experience all three of these problems during normal socket use, which in combination can present serious health risks to the amputee.

The tissue of the residual limb is capable of safely, comfortably supporting very high loads provided that these loads are properly applied and not sustained [Lee et al., 2005]. A properly applied load has a low impulse to the residual limb and is not capable of puncturing the skin [Portnoy et al., 2009]. In the same way that a weight lifter can support several hundred pounds during a squat with no permanent damage to his or her shoulders, an amputee can load their residual limb with large forces provided they are correctly applied.

The general strategy for the design of a prosthetic socket should take into account both the functional requirements associated with force transfer and residual skin health. Current clinical practice in sockets – such as rigid, carbon-fiber composite sockets – are able to transfer force well but tend to ignore the biological tissue requirements of the residual limb [Berke et al., 2010]. New socket paradigms that incorporate variable stiffness walls, new structural support morphologies, and/or active shape and pressure actuation show the ability to meet both the structural and biological functional requirements of a socket. To quantitatively verify these data, many develop pressure measurement systems for the explicit purpose of measuring the interface pressure between the residual limb and the prosthetic socket during normal use [Polliack et al., 2000b, Sanders and Daly, 1993b, Lang, 2004].

When an individual with amputation is stationary in the sitting or laying position, it is not necessary for him or her to transfer large forces through their socket to their prostheses. During stationary standing, the transfer forces are lower than those required of walking, and those transfer forces are lower than those required of running [Montgomery et al., 2010a]. Typically sockets are designed so that they are capable of transferring the forces associated with the most physically demanding action. This makes the socket tight and uncomfortable all of the time. This level of connection with the amputee is not necessary at all times.

1.2.4 Exploration of Requirements of Socket Design and Function

In order to explore the design and function of sockets with efficiency, it is necessary to group them logically. To begin, we will separate total surface bearing sockets from partial surface bearing sockets. Total surface bearing sockets seek to support the residual limb by maximizing the contact area between the socket wall and the residual limb. The current, rigid PTB sockets used by most amputees fit into this category [Yigiter et al., 2002]. Partial surface bearing sockets seek to support the residual limb through partial contact with the residual limb. The HiFi socket designed by biodesigns is a good example of a partial surface bearing socket.

Treating these two categories as a single dimension, we can create a two dimensional description of socket by suggesting that sockets can be rigid, passively dynamic, quasi-passively dynamic, or active. A socket that is partially rigid and partially active is considered an active socket [Montgomery et al., 2010a]. A socket that is partially rigid, partially passively dynamic and partially quasi-passively dynamic is considered a quasi-passively dynamic socket [Philen, 2009]. The rationale being that each successive quantification is merely an additional dimension of varying the stiffness or impedance of the socket wall. In the case of a passively dynamic socket, we vary stiffness spatially. Quasi-passive and active sockets are able to vary stiffness spatially and temporally with the latter capable of active deformation. A quasi-passive socket differs from an active socket in the method of control. Quasi-passive sockets are merely able to alter the passive stiffness of the same temporal area while active sockets are able to alter the position of a temporal area. In this way, an active socket can simulate a particular passive stiffness but also has the ability for more complicated functionality.

1.2.5 Useful Material Properties for Various Functions

Carbon-fiber composites and thermoformed plastic (HDPE, etc.) are the primary materials used to create the industry standard rigid, total surface bearing socket. These materials are chosen because they have very good strength to weight characteristics. Innovations in passively dynamic sockets have explored methods for creating spatially variable composite sockets by changing the structure of the socket. These sockets show promise but are somewhat labor intensive to fabricate.

Several researchers have experimented with 3D printed sockets in order to take advantage of the ability

to move directly from a 3D CAD model of a socket to a physical object [Frillici et al., 2008, Mak et al., 2001]. Some 3D printers are even capable of printing multiple different materials in the same print, allowing for passively variable stiffness sockets to be 3D printed. While this approach shows some promise, these sockets are generally far less structurally appealing than their carbon-fiber composite counterparts. The plastic from a 3D printer has much less strength and much more weight than a carbon-fiber composite. This approach is excellent for fast, in-house prototyping and testing of new socket designs, but it is not currently a viable manufacturing method for production sockets.

1.3 Introduction to the Primary Independent Variables Explored

By understanding the physical structure of residual limbs better we can develop a better idea about how to load the limb. For example, the boney protrusion just below the outside of your knee is called the fibular head. It's hard. It would seem like a great place to push against to transfer load, but if you do that, you'll end up crushing the skin between the bone and the socket. In reality, you can't push very much on the hard parts of the residual limb.

Three aspects of socket design that the devices described in this thesis hope to address are mentioned in this section's introduction: shape, stiffness, and time. Let's go into these in more detail to help elucidate the finer details.

The shape of the socket is of primary importance to the way it fits its wearer. In the case of a traditional socket, which is constructed entirely from a hard plastic or composite material, shape is the only variable that may change. Traditional socket manufacture determines this shape variable through the use of a prosthetist. A prosthetist is the orthopedist of amputated limbs, and is responsible for helping his or her patients maintain proper residual limb health and fitting them with prosthetic sockets so they may effectively operate a prosthetic arm or leg.

1.3.1 Shape of the Lower Extremity Prosthetic Socket

The shape of the lower extremity prosthetic socket is critically important to its function. A few tenths of a millimeter error in shape[4] can have a drastic effect on the comfort of the socket [Sanders et al., 2012a]. It may seem straightforward to simply 3D scan an individual with amputation's residual limb and use this as the shape of the prosthetic socket[5]. Just like any part of the human body, the residual limb does not stay the same shape when it is under load. Engsberg et al. have posited that an unrectified prosthetic socket[6] can perform as well as a prosthetist-crafted, rectified socket. However, given that the density of the alginate gel used in [Engsberg et al., 2008] ranges from $1.060\frac{g}{cm^3}$ to $1.123\frac{g}{cm^3}$ [Capone et al., 2013], it is quite possible that roughly $2.7kPa$ to $3.8kPa$ of pressure are uniformly acting on the distal end of the residual limb. Given the well known form of Navier-Stokes, namely $p - p_0 = \rho gh$, the pressure at the surface of the alginate gel is zero relative to atmospheric pressure. It is entirely possible that the pressure of the alginate gel in concert with the reduction of size of the cast produces a small amount of rectification that users of this type of socket find comfortable during chronic use. In general, a rectified socket has been shown to always result in a comfortable fit (discounting the number of test socket cycles required to get there) while unrectified sockets provide a comfortable fit about half of the time.

The shape that the prosthetist sculpts for the individual with amputation is very important [Lustig et al., 2013]. Unfortunately, the prosthetist's patient usually is not present during the sculpting process, so much of the shape change that occurs is done solely based upon the experience of the prosthetist with this particular patient and his or her other patients. Today's clinically available socket technology does not leverage current state-of-the-art material, fabrication and robotic measurement approaches [Fernie et al., 1985, Zheng et al., 2001, Milano et al., , Wu et al., 2003, Shuxian et al., 2005] that could facilitate socket designs that greatly improve both comfort and joint flexibility.

Given the large range of socket types and interventions to deal with limb shape change over time, some research has attempted to establish a methodology to perform long term measurements of deformation though the use of ultrasound indentation probes [Palousek et al., 2009]. A creative approach to this

[4]This is especially true in the case of a single material, hard socket

[5]Except that even 3D scanning can be a non-straightforward process [Sanders and Lee, 2008]

[6]An unrectified socket is one whose shape is identical to the shape of the residual limb, but may be uniformly shrunk in order to increase interface pressures

problem of monitoring limb volume change: a current at an specific frequency set between two electrodes that contact the skin of the residual limb. The voltage seen at the cathode changes throughout the day, allowing a fairly accurate, non-invasive way to continuously monitor limb shape change throughout the day [Shimazu et al., 1989]. Others [Geil, 2007] use a combination of non-contact optical and contact-based electromagnetic systems in order to measure 3D limb shape; however, this work was only able to achieve 0.96cm mean range across all measurements.

1.3.2 Spatial Impedance of the Lower Extremity Prosthetic Socket

In order to approach an understanding of a spatially varied mechanical impedance prosthetic socket for use by individuals having lower extremity amputation, we must first understand the biomechanical impedance of the residual limb. Measurement of pressure during normal socket use may provide some insight into this understanding, but what we really need is data relating many pressures to many shapes. Many techniques exist for this purpose [Vannah et al., 1999], and this particular topic will be a substantial focus of this manuscript. Dynamic Roentgen stereogrammetric analysis (3D x-ray) was performed on a trans-tibial amputee performing a fast stopping task for the purposes of determining the motion of the tibia and fibula during ambulation – showing that the internal movement of these bones can play an important role in the socket's impedance definitions [Papaioannou et al., 2010].

Spatially varied impedance sockets such as created by Sengeh et al. are generally created using a 3D printer [Sengeh and Herr, 2013a] but may also be created by altering the physical stiffness (changing the material or making cut-out shapes to decrease stiffness [Faustini et al., 2005, Awtar, 2004]) of the socket directly. Regarding quasi-static sockets, one version of the spiral slots produced the largest pressure relief with an average reduction in local interface pressure during single-leg stance (20-80% of the stance phase) from 172 to 66.4 kPa or 65.8% compared to a baseline socket with no compliant features. These results suggest that the integration of local compliant features is an effective method to reduce local contact pressure and improve the functional performance of prosthetic sockets [Faustini et al., 2006].

Ultimately, access to multi-material 3D printers that are capable of making a spatially varied stiffness socket is limited, considering that there are approximately three such printer brands that meet these criteria and they cost roughly $500k to purchase.

A more cost effective way to accomplish spatially varied impedance may be to 3D print a mold for a relatively soft liner material (Shore A of 30 to 40) whose Poisson ratio is greater than 0.40; in this case one may vary the thickness of the material in order to control the interface impedance.

Spatially varied impedance sockets have dramatic advantages over traditional non-spatially varied socket approaches. Because material is able to be relatively softer in some areas than others, it is possible to load portions of the anatomy previously too painful to load. This increased contact area can have the effect of feeling a greater level of control over the prosthesis, ultimately increasing the quality of life of the wearer.

1.3.3 Spatiotemporal Impedance of the Lower Extremity Prosthetic Socket

Let's say you're a sitting individual with amputation. There is very little force transfer from your feet to your torso, so the socket would not need to squeeze very hard on your residual limb. When you stand up however, much more force is transferred and thus the socket must tighten or stiffen in order for you to continue to be able to reliably control your prosthesis.

Generally, lower extremity, active prosthetic sockets make use of bladders that are actuated with either air or liquid [Montgomery et al., 2010b]. Some instantiations of this variation are human adjustable [Jr, 2006]. When given the option of control over fluid-bladder inserts, however, subjects tended to prefer settings that "induced higher measured socket stresses" because they found them "more comfortable than those that induced lower measured stresses.." Possible explanations for this could be that the subjects prefer the high level of control over their prosthesis and will deal with increased pain [Sanders et al., 2006]. During walking, the knee flexion inertia plays a large role in the dynamic loading at the interface between the prosthetic socket and the residual limb [Jia et al., 2005]. Highest pressures were observed at the popliteal depression, mid-patellar tendon, and the lateral and medial tibial regions. Some research has shown reasonable ability to predict with artificial neural networks across 16 pressure sensors located throughout the prosthetic socket to predict socket interface pressures during walking to within 8.7% [Sewell et al., 2012]. Pressure sensors, especially those that are multi-axis, can provide extremely useful data to inform proper socket spatial position for socket impedance interventions at well chosen temporal location [Mcelligott et al., 2002].

A temporally and spatially varied socket and its corresponding gait data is presented in Chapter 3 of this manuscript. This quasi-passive socket (QPS) utilizes electrolaminate devices to quasi-passively clutch the deflection of the tibial region of a prosthetic socket. The socket contains a custom PCB with two force sensitive resistors placed between the socket wall and the carbon fiber support layer, two analog deflection sensors for the electrolaminate devices, a three-axis accelerometer, X-BEE radio for wireless communication, a STM32 series microprocessor, and an up to 1200V driver circuit to turn on and off the electrolaminate devices. The socket may be wirelessly controlled or may use its sensor data to control the electrolaminate in a biomechanically informed feedback loop [Herr and Maes, 2013].

1.4 Review of the Ideological Components of Digital Socket Design

1.4.1 Limb Scanning and Measurement

As quantitative biomechanical measurement becomes an increasingly important factor in progressing toward digitally fabricated prosthetic sockets, there is a need to increase communication of data and techniques [Zheng et al., 2001, Mak et al., 2001]. Measurement of limb shape has been a topic of focus for the last 30 years [Fernie et al., 1985]. Volume change over the course of the day, week, and month is an important factor to consider when attempting to measure a residual limb [Sanders et al., 2009]. Surface contour measurement with contacting probes can be difficult due to the low forces needed to deflect human tissue [Shirley and Mermelstien,]. An interesting technique using thermoplastic elastomer strain sensor in cloth can be used to accurately measure posture and maybe shape as well [Mattmann et al., 2007].

1.4.1.1 Pressure and Shear

Basic pressure measurements at the interface between the socket and the residual limb during walking have been becoming both higher fidelity and well known [Sanders et al., 1992]. More advanced, three-dimensional stress measurements have also been completed [Sanders and Daly, 1993a]. Some who see the

benefit in deep tissue injury prevention measure the effects of intentionally painful pressures [Finocchietti et al., 2013].

It has been shown that a nonlinear increase in force occurs from standing to walking [Zachariah and Sanders, 2001]. In addition to showing regional variation (0.24:1), the highest correlation between walking and standing was 0.88 for pressure over the lateral region of the residual limb. Pressure at the residual limb depends on the knee moments involved in each walking condition [Wolf et al., 2009]. Adapting the prosthetic ankle angle is a valuable means of modifying joint kinetics and thereby the pressure distribution at the stump. However, large inter-individual differences in local pressures underline the importance of individual socket fitting. These interface pressures have a substantial effect on long-term transtibial prosthesis deformation [Kisiel et al., 2007].

1.4.1.2 Optical Scanning

Surface scanning technologies such as 3D optical or laser and physical contact probe scanning are able to provide accurate models of the external physical shape of the residuum. Recent advances in optical scanning have lead to short-cuts for topology and shape optimization [Lin and Chao, 2000]. This is necessary because the residual limb is difficult to mount securely during an optical scan [Sanders and Lee, 2008]. Some techniques also have the ability to measure surface skin strain through Delaunay meshing [Mahmud et al., 2012]. Others use topologically adaptive surface and contour information to provide good digital data from medical imaging [Terzopoulos, 2011]. Topology based approaches can seek to aid in the design of the socket by solving the topology problem whereby stiffness is maximized [Yang and Chuang, 1994].

1.4.1.3 MRI and CT

Internal scanning technologies such as MRI, ultrasound, CT, x-ray [Lilja et al., 1993], and dynamic roentgen stereophotogrammetric analysis (DSRA) are capable of providing information about tissue location and density below the surface of the skin. Some approaches describe the creation of software packages specifically for converting between CT scan data and a 3D reconstructed model of the residual limb [Shuxian et al., 2005], while others are focusing on simpler use of the data [Avril et al., 2010]. There is a chemical shift when scanning materials such as plaster of Paris or silicone that can possibly distort

the images taken by the MRI machine [Buis et al., 2006, Safari et al., 2013]. Buis et al. find that this distortion is within acceptable levels for accurate segmentation, and Safari et al. find an error of 0.30% to 14.03% (0.13mm to 5.47mm, st. dev. 0.89mm). Through image processing of CT data and reverse engineering approaches, one group was able to reconstruct solid models of the residual limb for the use of prosthetic socket design [Shuxian et al., 2005].

1.4.1.4 Ultrasound

Ultrasound has the ability to not only provide biomechanical indentation-like data [Han et al., 2003], it can also be used to provide information about general skin elastography [Wu et al., 2012, Monetti and Minafra, 2007, Hoskins and Svensson, 2012], tomography [Natterer and Wubbeling, 1995], blood flow [Radegran, 1997] (including microcirculatory flow [Christopher et al., 1996]), perfusion [Cosgrove and Lassau, 2010], bone density [Zagzebski et al., 1991, Laugier et al., 1997, Antich et al., 1991], and much more.

The role that muscle contraction plays inside the prosthetic socket has been shown to be measurable through sonomyographic techniques that, unlike the normally used muscle assessment technique of electromyography, are able to see more fine, dynamic muscle movements [Zhou and Zheng, 2012, Kane et al., 2004]. In fact, tomographic and sonomyographic techniques can reliably resolve 3D, dynamic, volumetric information about the residual limb [He et al., 1997, He et al., 1999, Wachinger et al., 2007], and those data may be used for the purposes of prosthetic socket design [He et al., 1996, Morimoto et al., 1995]. Validated elsewhere, error with this type of measurement can be less than 0.40 mm in all three orthagonal directions [Huang et al., 2005].

In addition to 3D reconstruction of the unloaded tissue of the residual limb, indentation elastography may be done (properly [Gilbertson and Anthony, 2012]) to assess the internal tissue strains during the compression of the tissue [Ophir, 1991]. High frequency ultrasound may be used to directly extract physical properties of tissue as well [Wang et al., 2007, Krouskop et al., 1987a], including viscoelastic properties [Catheline et al., 1999]. Another technique uses suction to deform the tissue but obtains similarly useful results [Diridollou et al., 1998].

Secondary information about the residual limb, such as arterial wall stiffness and blood pressure can be gathered using quantitative elastography in a way that provides a method of continuous blood pressure

measurement [Zakrzewski and Anthony, 2013, Zakrzewski et al., 2013]. High resolution modeling of human gait is also possible using this technique [Geisheimer et al., 2002, Convery and Murray, 2000].

Assessment of musculoskeletal recovery can be found in a rehabilitation by heavily contributing to the diagnostic tools that are available [Ozcakar et al., 2013, Deimel et al., 2013].

1.4.1.5 Indentation

Biomechanical tests, such as those performed with an indentation probe, allow researchers to gain insight into the mechanical properties of the residuum under loading.

While the topic of biomechanical measurement through indentation has seen increasing research focus throughout the last two decades [Zheng et al., 2001, Mak et al., 2001], indenter design deficiencies still remain. Firstly, biological indenters must be able to collect data that are accurate and repeatable in both position and force. Secondly, the indentation process must be position and force controllable in order to generate the necessary data required for the identification and evaluation of biomechanical models of tissue. The state of the art of research in the area of biomechanical indentation of human tissue in vivo can be split into two categories: passive and active.

Passive biological indenters are generally hand-held devices that collect data to inform hyperelastic and/or viscoelastic models through imaging techniques [Tran et al., 2007] or through the use of sensors mounted on the indenter device [Zheng et al., 1999, Oflaz and Baran, 2014, Ziegert and Lewis, 1978, Ahn and Kim, 2010]. Imaging techniques have an increased ability to aid in inverse finite element analysis (IFEA) through a more comprehensive 3D reconstruction of how tissue deforms near the indentation site. Sensor based, handheld, passive indenters are able to take measurements with shorter processing times when compared to passive indenters used in imaging based techniques [Mak et al., 2001, Zheng et al., 1999, Khatyr et al., 2004].

Active biological indenters are robotic or actuated mechanisms that are either mounted to an actuated arm [Mojra et al., 2011] or to a static base [Ahn and Kim, 2010, Khatyr et al., 2004, Xiong et al., 2010, Moerman et al., 2013]. These computer controlled devices are either MRI machine compliant [Tran et al., 2007, Moerman et al., 2012] or not. Significant design challenges exist with MRI-compliant active indenters since ferrous materials cannot be employed in their construction [Moerman et al., 2013].

Limitations of passive indenters primarily manifest in an inability to control force and position referenced to the residual limb. Such a deficiency in control limits the breadth of data that may be collected. Active indenters are able to control their position precisely, but many lack the ability to control the indentation force.

This lack of control complicates measurement of deflection of the tissue at a given force or pressure; however, Khatyr et al. (2004) present an indenter device that is capable of controlling for force, but the clamping procedure uses jaws thats contact area changes during indentation, complicating biomechanical modeling efforts. Further, Mojra et al. (2003) present a device that is limited in the directionality of the applied force, which complicates the measurement process and does not allow for tangential application of load to all areas of measurement. Various indenter geometries are considered [Ziegert and Lewis, 1978]. Most use cylindrical indenters with flat contact surfaces [Vannah and Childress, 1996]. A hemispherical indenter contact shape is better for providing data that may be easily processed by iFEA algorithms. Better diagnosis of breast cancer through indentation measurement has provided basic estimation of these tissues' properties which agree with the studies by others on limb tissues [Han et al., 2002, Wiskin et al., 2007, Zhi et al., 2007, Lalitha et al., 2011, Hansen et al., 2008].

1.4.2 Digital Biomechanical Data

In addition to scanning data, biomechanical gait dynamics studies – some of which include muscle dynamics – provide useful data to drive FEA techniques [Coleman, 1998, Zajac et al., 2002, Vukobratović and Borovac, 2004, Neptune et al., 2008]. Age [Silver et al., 2002, Agache et al., 1980], gender, and anatomical location may play a role in explaining some variability in biomechanical data [Cua et al., 1990]. These factors serve to normalize the measured data such that they may be used in the following steps of the digital socket design process in a way that guarantees independence of measurement. A thorough sensitivity analysis of all factors that may affect the creation of a quantitative, universal digital biomechanical model is still required in the field. Surveys have narrowed in on the major problem areas (for example, type of non-linear hyperviscoelastic model), but currently no strong consensus exists. Indeed, most of these scanning methods have a goal of resolving some kind of quasi-linear model of the tissue biomechanics [Zheng and Mak, 1999]. A linear model is not suggested by the author of this manuscript.

Imaging approaches such as MRI, CAT, or Ultrasound generally require tomography processing algorithms to render an objective 3D representation of the data output by the scanning device. These algorithms range from non-linear traveltime tomography [Berryman, 1989] to synchrotron microtomography [Bossy et al., 2005] to transmission tomography [OK-Denis et al., 1995] to non-local Shepard interpolation for structural topology [Kang and Wang, 2011]. General shape fitting algorithms help to make otherwise noisy data more readable to software that requires cleaned models [Lempitsky and Boykov, 2007, Candes et al., 2011]. Segmentation of tissue types can also be determined through the use of recently developed algorithmic techniques that operate on any number of raw data types [Lempitsky et al., 2009, Zach and Pollefeys, 2010, Nowozin and Lampert, 2009, Fuchs et al., 1999].

1.4.3 Forward and Inverse Finite Element Analysis

There is no doubt that the use of simulation software is able to enhance our ability to design prosthetic sockets [Frillici et al., 2008, Krouskop et al., 1987b]. The question is, do we need to use inverse FEA to do it [Delalleau et al., 2008, Sewell et al., 2012]? Inverse finite element analysis is the process of specifying the loads on an object as well as a bounding box and allowing the algorithm to specify the form of the object that must bear these loads [Oxman et al., 2010]. In the case of iFEA for tissue properties identification, we use the results of a real indentation experiment to inform the constants of a model of a simulation of the experiment. Iteratively adjusting the constants provides the values in which results most closely match the data.

1.4.3.1 Modeling of Tissue Biomechanics

Biomechanical engineering remains one of the most difficult fields in medicine and science [Bronzino, 2006]. Many non-linear biomechanical models have been suggested to model human tissue biomechanics. Non-linear system identification can be applied quite successfully to human tissues provided the data are of good quality and broad frequency content [Chen, 2010, Korenberg, 1990, Keesman, 2011]. System identification is a technique that makes use of statistical methods in order to model dynamical systems. Most generally, the system is perturbed mechanically and the response of the system is measured. The input-output relationship defines a model or model-class. System identification techniques have been shown to produce fairly robust models of human tissue.

Many do not take the common – some would say required – gel liner into account during their modeling [Zhang et al., 1998]. It may be possible to use a thinner liner with a better fitting socket [Boutwell et al., 2012]. In addition to considering the thickness of the gel liner, Lin et al, describes the effects of varying the liner's bulk stiffness [Lin et al., 2004]. In vivo characterization of the human dermal mechanical properties are well published [Hendriks, 2005]. Because tissue behaves in a nonlinear, time-variant way it must either be identified using a model that reflects these characteristics or approximated to a nonlinear, time-invariant system or linear, time-invariant system (LTI). Some success has been shown using a LTI model that includes a static Wiener nonlinearity. Other approaches, such as models that use Volterra series, are able to capture tissue dynamics more accurately through memory effects of the system. In a Volterra system, the response at time t is a function of all previous inputs. These approaches may utilize Kelvin-Voigt [Boyer et al., 2007], Mooney-Rivlin, or Maxwell models in order to capture viscoelastic effects of the system. Other models show high correlation with experimental data using a James-Green-Simpson material formulation that has been expanded with a Prony series to capture viscoelastic effects. The James-Green-Simpson material formulation is commonly used to model the dynamics of the residual limb because it produces reasonable results and is a part of many standard FEA nonlinear packages.

Finite element analysis is a computational method used to solve partial differential equations through numerical approaches. In material analysis such as that used in socket biomechanics, FEA is used to determine material deflection under load by breaking the material into infinitesimal elements. FEA has proven to be an invaluable tool in the study of the forces between the residual limb and the socket because the computer models are accurate enough to iterate quickly over socket designs or even determine ideal socket shape.

Many experiments have been performed to assess the ability of FEA techniques to predict pressure distributions between the residual limb and socket wall under load in both standing and walking simulations. Other experiments use FEA to model the ideal liner thickness. Still others seek to identify situations where the amputee is at risk of deep-tissue injury.

The increased use of FEA techniques helps researchers share real data about socket designs. Unfortunately FEA relies on boundary conditions that are not well defined. Generally, researchers fail to see that it is much easier to model the skin and underlying tissue as two mechanically distinct materials (but not all of them do [Pailler-Mattei et al., 2008]). Two- or even three-layer models create a situation

where simulation data are much easier to fit with experimental data.

Additionally, successful designs have come from FEA simulation, but they generally require very technical knowledge of CAD software to create. Data from MRI or CT scans must be converted to appropriate CAD models. This technique is far from straight forward, and in many cases involves tracing tissue and bone contours from transverse scan slice data by hand. Proposals have been made that embrace a process that may be more easily reduced to clinical practice.

1.4.3.2 Static FEA Techniques

There were no evident relations between socket type and changes in interface pressure, though there is some evidence that gait symmetry is improved with CAD/CAM sockets. Comfort scores were not directly related to interface pressures, indicating that prosthetists should take care when relying on patient feedback to determine quality of socket fit. Quantifying the regional load-bearing ability of trans-tibial residua show that the patellar tendon and the distal end of the fibula were the best and worst load-tolerant region, respectively.

The most promising result common to FEA papers involving prosthesis design is that both the mechanical properties of the residual limb and the socket are important [Silver-Thorn and Childress, 1996]. MIMICS is a popular FEA software package used to generate FEA driven socket designs – such as one a patellar tendon bearing socket [Moo et al., 2009]. Contact mechanics methods have been employed to predict the contact interface between socket and residual limb, but these approaches tend to fail against more robust FEA approaches [Lee et al., 2004, Omasta et al., 2011]. Well fitting tissue FEA models have existed for quite some time [Larrabee, 1986].

1.4.3.3 Dynamic FEA Techniques

Dynamic residual limb tissue stress during walking is useful information for determining a prosthetic socket whose purpose would be to reduce these stresses [Portnoy et al., 2006]. Non-linear analysis in other fields – such as spacecraft tethers [Lee et al., 2011] – may provide some insight into helpful methodologies. The propagation of shear waves across skin has been measured and one study suggests that frequencies above 500Hz propagate only as bulk shear waves [Potts et al., 1983]. The use of force

sensors to gather real-time data for use in a FEA model have seen slight reductions in residual limb pain in a study with five trans-tibial patients [Portnoy et al., 2007a].

1.4.4 Digital Socket Model

Groups are already working to provide software tools specifically for socket modeling [Milano et al.,]. One such tool, called the Socket Modeling Assistant (SMA) is designed specifically to help prosthetists create digital models of the prosthetic socket [Colombo et al., 2011]. The ideal process is one that is quantitative from measurement to socket creation, using a well-proven methodology [Krouskop et al., 1987c].

The digital socket model needs to be a well-standardized, agreed upon package of files that can effectively describe a prosthetic socket. One approach currently used by Sengeh and Moerman et al. is the use of STL files that are grouped in a single directory per socket and named with the material properties they are required to have. In this case these are the possible materials printable by a Stratasys Connex500 3D Printer, which have been mechanically tested using the standard ASME testing techniques to provide data for FEA modeling. This approach is effective at describing a spatially varied stiffness socket in a simple, understandable way, but is merely a single piece of the required information in order to describe a temporally and spatially varied prosthetic socket.

1.4.5 Rapid Prototyping Technologies

FDM technologies tend to be a popular choice for prosthetic socket 3D printing because of the strength of material that the FDM process is able to produce [Hsu et al., 2008]. Polyjet multi-material 3D printers have been shown to produce functional spatially varied impedance prosthetic sockets that reduce peak interface pressures during walking [Sengeh and Herr, 2013b]. Some combat the strength issue in 3D printed parts by coating the socket with resin after the print [Lu et al., 2009]. SLS is another widely used 3D printing technology, as shown by Montgomery et al. in their adaptive socket research. Research in the Mediated Matter group at the MIT Media Lab has demonstrated the ability to define the voxel properties required to command a multi-material 3D printer to print with specific material properties [Doubrovski et al., 2014].

One benefit of using a 3D printer to make a prosthetic socket is the ability to add interesting affordances such as cooling channels [Webber and Davis, 2015]. Another is the much more widely varied material selection having even more varied material properties [Lenka, 2011]. Some consider the cost to benefit ratio of digital fabrication tools such as 3D printing because the capital investments required are generally quite high [Freeman and Wontorcik, 1998].

3D printing is not the only option for rapid production of prosthetic sockets. A review of high speed computer numerical control (CNC) milling methods of molds for composite layup and gel liners describes many alternatives [Aherwar et al., 2014].

1.4.6 The Physical Socket or Socket Mold

Some approaches involve modularizing the components of the prosthetic socket for single prosthetist visit fittings albeit at higher monetary cost [Normann et al., 2011]. Post rapid production, the socket will require cleaning, and in many cases, attachment to the standard pyramid joint that will allow it to mate with off the shelf prosthetic components (shanks, knees, feet). This process of post-processing may involve wrapping a 3D printed socket in carbon fiber to add additional structural security. Even so, the craft work required to post process a digitally fabricated socket into a functional prosthesis does not rely on the skill of the craftsmanship for proper prosthetic fit[7]

In the case of a mold – which is the preferred way to construct custom gel liners – the post-processing would involve casting the gel liner or socket in the mold and finishing the process from that point. Silicone, such as Fast Dragon Skin by SmoothOn, cures remarkably fast. Two custom gel liners could me made per hour using these methods. This speed is much faster than current 3D printing technology can print the molds.

1.4.7 Evaluation of Digital Sockets

Evaluation of the socket fit is exceedingly important since we still do not have a scientific definition of "comfort." Checklists [Rheinstein, 2001] are available that can help to standardize the evaluation procedures. A more specific "Socket Fit Comfort Score" has been developed by Hanspal et al. and

[7]Unless the craftsman somehow puts the shank on crooked, or something more unimaginable

showed consistency over multiple trials with 44 subjects [Hanspal et al., 2003]. The author recommends an online database, such as Digibody or others for the collection of data and the associated experimental requirements of those data (basic standards for tests). Communication of these data across research groups and locations can help us provide a more complete picture of what interventions are yielding the most positive results through quantitative data reporting. Given the small population of those having lower extremity amputation, a large database of subjects is incredibly helpful when attempting to define FEA models or to understand the life expectancy of a certain type of 3D printed prosthetic socket.

On the accuracy of CAD/CAM transtibial prosthetic sockets from central fabrication facilities, around 65% of the surveyed companies managed to make sockets within +/ 1.1% volume of the file sent describing the socket shape. Six of the manufacturers consistently undersized their sockets [Sanders et al., 2007]. One estimate suggests that only 24% of prosthetists use CAD tools in their processes. Most do not rely on central manufacturing for socket production, and thus the low volumes may account for poor quality control (QC).

Joint replacement therapies routinely make use of CAD/CAM technologies in to aid in mating with the biologically portion of the body [Werner et al., 2000]. Dental prosthesis procedures are especially well known in this are [Davidowitz and Kotick, 2011]. These practices are generally oriented towards bone-to-bone mates, and therefore are able to utilize linear elastic, high Young's modulus, material models for their designs. In many cases, no material model at all is necessary and the 3D objects being designed are simply treated as static bodies. Soft tissue, on the other hand, presents a much more challenging problem.

Sanders et al. have developed assessment technique for trans-tibial sockets with specific guidelines for how to take the measurements [Sanders and Severance, 2011]. They define mean radial error (MRE) as the average difference between two shapes radii can be a key indicator to quality of sizing. Further, they have found that a MRE of more than 0.25mm were "clinically unacceptable," and unusable without some kind of adjustment [Sanders et al., 2012b].

Chapter 2

The FitSocket

2.1 A Robotic, Multi-Indenter Device for *in vivo* Measurement of Biomechanical Tissue Properties

The objective of this study is to present the design and evaluation of an active biological indenter that addresses the limitations of these previous works. The proposed indenter is designed specifically for residual-limb tissue characterizations for the quantification of prosthetic socket production for individuals with limb amputation. The indenter platform employs a 16 degree-of-freedom (DoF) system (15 actuated, linear, 1 passive, rotational) comprising 14 position and force-controllable actuators that circumferentially surround a biological residuum to form an actuator ring, and one additional active degree of freedom for longitudinal positioning of the actuator ring relative to the residuum. The indenter platform is capable of measuring circumferential rings of the residual limb in a single reading, as well as single point readings while the limb is clamped by the remaining 13 actuators.

This work describes the design, function, and measurement capability of a computer-controlled biological indenter consisting of 14 actuators that surround a biological limb. The indenter design is presented and its performance evaluated. The indenter is characterized by position and force accuracy across multiple, separate experimental sessions of the device, current and position controller responses of the actuators, as well as basic geometric properties. As a further evaluation of the indenter platform, biological hyperviscoelastic tissue data are collected on a human test participant with bi-lateral transtibial

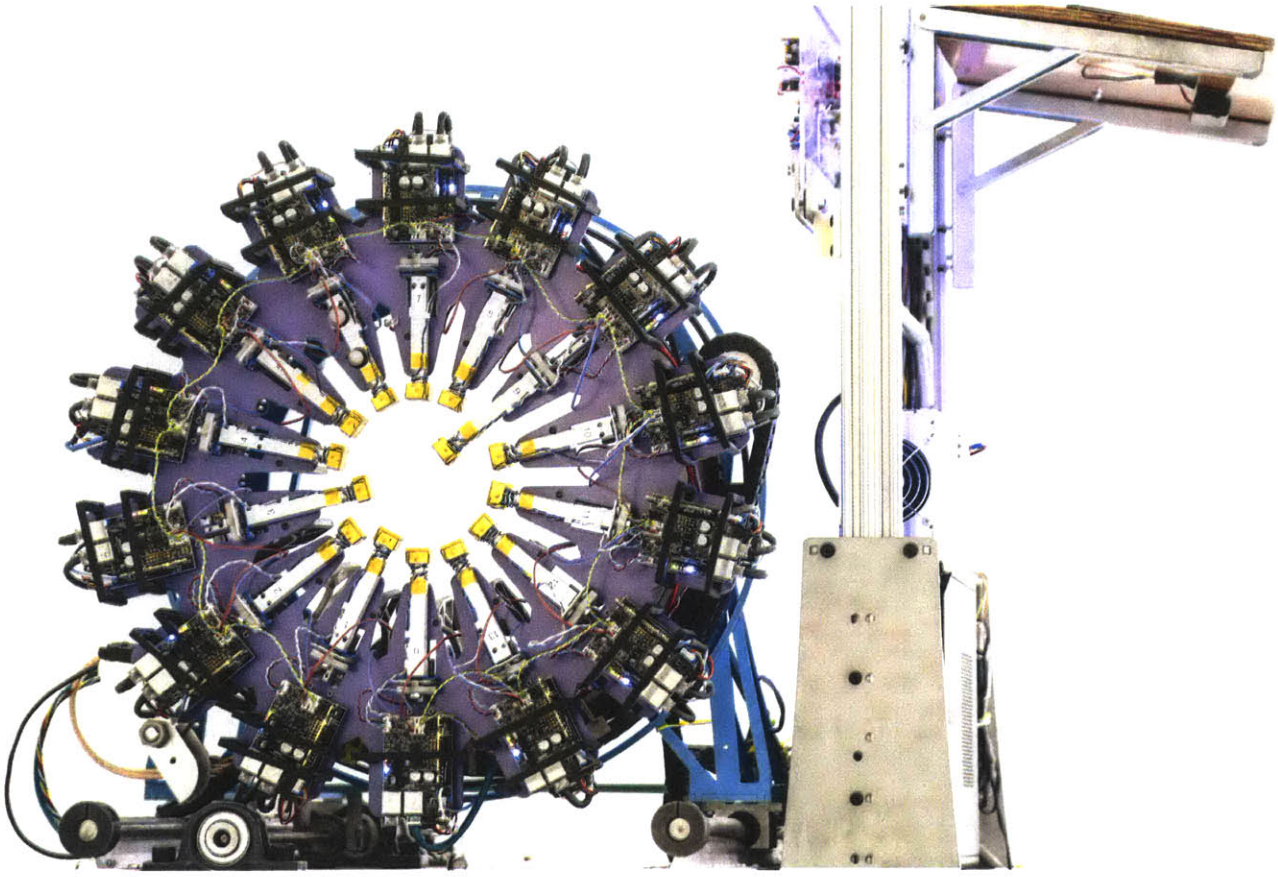

Figure 2-1: A detail image of the FitSocket's main actuator ring comprising fourteen linear actuators that are force and position controllable.

amputations. These data may be used to validate mechanical hyperviscoelastic constants of the same model. We show sufficient accuracy and repeatability for the purposes of biomechanical modeling.

The FitSocket is a device that can be used to measure the stiffness of body tissue through physical contact with the human. The data are used to identify a linear or non-linear transfer function, which describes the physical response of the tissue to a given load (force) or deflection. The device's actuators are capable of operating in force-control or position-control modes. In other words, taking force-control as an example, the actuators of the FitSocket are able to exert a desired force. This desired force is provided either by an operator or a computer program running a test cycle. Position control works in very much the same way. It is not possible to control for both position and force at the same time. In the case that force-control is used, position will be the output (dependent) variable, and the converse is true for a position-controlled scenario.

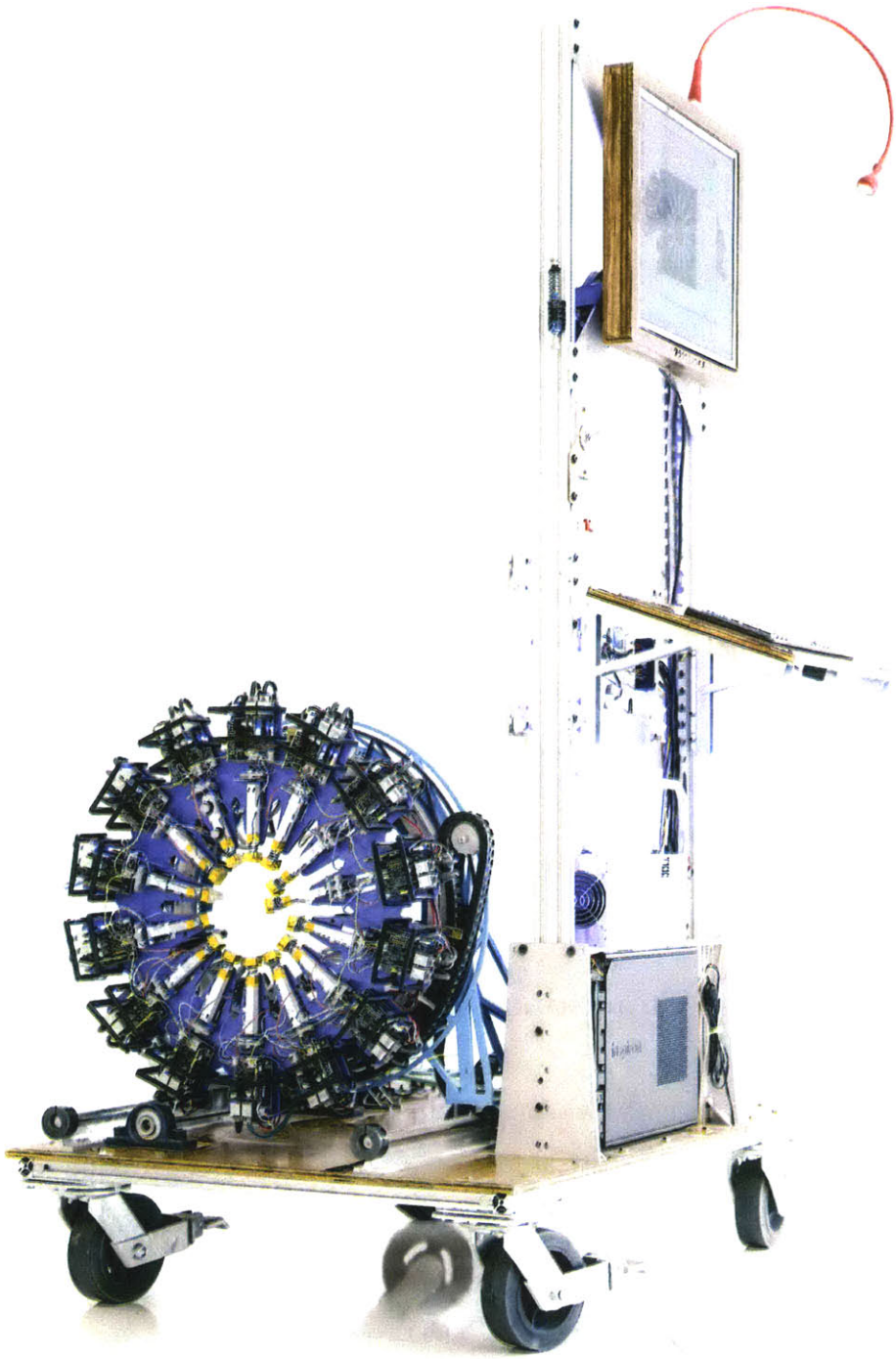

Figure 2-2: The FitSocket is a fully self-contained, mobile measurement platform. It includes a built in LCD display in order to interact with the device's main computer.

2.2 Method

2.2.1 Design Description and Specification

An active multi-indenter device was designed, fabricated, and evaluated that enables the measurement of tissue biomechanics across the residual limb of a person with limb amputation. The device, shown in Figure 2-3, comprised 14 individual indenters directed radially inwards towards the longitudinal axis of a biological limb inserted into the device. Using the device, tissue hyperviscoelastic properties can be measured for tissue state disturbances (position and speed) applied perpendicular[1] to the body's surface.

Forming a multi-indenter ring, the radial array of indenters was designed to rotate passively 360 degrees about the longitudinal axis of an inserted biological limb. Further, the ring and rotation mechanism were mounted to an actuated linear stage with position feedback. This linear stage DoF enabled the multi-indenter ring to translate along the longitudinal axis of the inserted biological limb. The ring could therefore be repositioned longitudinally down the leg without requiring the study participant to move from a fixed seated position. In summary, the multi-indenter had 16-DoF comprising 14 linear-actuated indenters, 1 rotational multi-indenter ring DoF, and 1 actuated translational multi-indenter ring DoF.

2.2.2 Specification of Functional Requirements

Design specifications for the mechanical components are presented in Table 2.1. The Main Ring (L in Figure 2-3) is the steel support ring of all 14 actuators. This ring was required to support the weight of the resting biological leg, as well as the weight of all 14 indenter components. With an added safety factor of 2X, the functional requirement was set at 500N. This requirement is based on the 15kg mass of the multi-indenter ring plus the 10kg mass of the resting biological residuum, resulting in a 250N downward force in the plane of the multi-indenter ring. Additionally, the ring was designed not to move due to a loading of up to 100N perpendicular to the plane of the ring. Each actuator's motor was required to withstand up to 10Nm of torque, 200N of linear force in the direction of the ball screw, and 500N of off-axis force against the steel ring (in order to preserve position sensing).

[1]One may also imagine this loading as radial loading

Table 2.1: Electromechanical Requirements

Structural Requirements		
Main Ring Load	500N vertical	Body weight with safety factor for rigidity
	100N axial	Body weight with safety factor for rigidity
Motor Support	10Nm torque	Rigidity for rotational position sensor
	200N linear	Rigidity for ballscrew element
	500N off-axis	Rigidity for ballscrew element
Linear Kinematic Support	200N off-axis	Body weight with safety factor
	500N radial	Able to hold the load of the main ring
Sensor Decoupling	Rotation only for position	Off axis loading will cause miscounts or break the sensor
	Linear only for force	Strain gauges are designed for uniaxial loading
Electrical Requirements		
Power	36A at 24V (nominal, 1.5A per motor)	Allow motors to reach their nominal power
	44.8A at 24V (peak, 3.2A per motor)	Allow motors to reach their peak power
Feedback	At least 15kHz	Inaudible motor drive
Sensor Amplification	Less than 5% noise	Reliable data is a primary requirement
Temperature Sensing	Onboard overtemp	Safety
Sensor Feedback	>100Hz	High quality data collection and control at speed. Ability to capture viscoelastic effects
Actuator State Information	Robust comm. protocol	Prevent communication faults where possible
Safety Requirements		
Fault Condition Sensing	Onboard fault condition sense	Subject safety
User Stop	Easily accessible power kill switch	Subject safety
Intrinsic Force Limit	Unable to push with more than 20N	Subject safety
Kinematic Requirements		
Motor Velocity	> 6000 RPM	Linear stage moves at least 0.2 m/s
Motor Torque	> 5mNm	Force at indenter is at least 15N
Motor Size	Eq. or less than 25mm diameter	Volume requirement for motor to fit into space
Force Sensor	Range from 500mN to 20N	Must be able to measure the full range of possible forces
	At least 100mN sensitivity	Soft tissue deflects readily at small changes in force
	Less than 25mm x 25mm	Volume requirement for sensor to fit into space
Position Sensor	At least 100μm sensitivity	Bony prominences deflect less than 2mm total
	At least 50,000 counts/s sensor	Assures maximum positional resolution at maximum motor velocity
	Less than 25mm x 25mm	Spatial requirement for sensor to fit into space

The bearing block that houses two thrust bearings and one radial bearing (G in Figure 2-3) satisfied these requirements. The linear stage was designed to transfer loads applied to the actuators through the main ring (L in Figure 2-3) to the base of the multi-indenter device, requiring the 200N off-axis relative to linear stage's axis of movement and 500N radial functional requirements. Sensors were mechanically decoupled in order to preserve data validity. A 5-DoF flexure (leaving only one degree locked) was included to actuate the strain gauge force sensor (E in Figure 2-3). The rotational position sensor was mounted directly to the motor body, taking advantage of its bearing arrangement for decoupling.

When all 14 indenter motors were operational at once, the multi-indenter device required up to 44.8A at 24V. Motor controller PWM frequency was set to be in the inaudible frequency range. In order to capture hyperviscoelastic properties, the rate of sensory feedback to the top-level controller was at least 100Hz. A robust communication protocol (Ethernet for Control Automation Technology or EtherCAT) was necessary to prevent data loss. Primary fault condition sensing was handled by the EtherCAT

fieldbus protocol and the corresponding CANopen device state machine. Secondary fault condition sensing specific to the indentation procedure (e.g. maximum force, position commands outside physical possibility) were written into the controller software. The multi-indenter device was designed with an easily accessible, emergency-stop switch to turn off power to the device.

The pitch of the ball screw was 2mm per rotation. In order to achieve a desired actuator velocity of 20mm/s, the motor therefore had to spin at a rotational velocity of 630rad/s. A 15N force at the indenter head required that the motor supply at least 5mNm of torque, assuming 90% efficiency of the ball screw components. In order to provide useful biomechanical tissue data, the force sensor was designed to have both high sensitivity (100mN) and large range (500mN to 20N). Similarly, the position sensor was designed to have high sensitivity (100µm) and high encoder count speed in order to accurately track the position of the indenter. Both force and position sensors were designed to fit into a 25mm x 25mm space defined by indenter size constraints.

Table 2.2: Functional Requirements of Indenter System

Requirement Name	Required Value	Actual Value
Position Accuracy	< 0.15mm	0.109mm
Position Sensitivity	< 0.10mm	0.00139mm
Force Accuracy	< 0.50N	0.330N
Force Sensitivity	< 0.10N	0.0150N
Step Response Time	< 150ms	120ms
Maximum Force	> 15N	22.755N
Minimum Radius	< 50mm	42.90mm
Maximum Radius	> 130mm	132.48mm

Functional requirements of the multi-indenter system are presented in Table 2.2. Position and force accuracies were achieved through specific design that allowed for $3-\sigma$ ranges of 100µm and 500mN, respectively. The step response time of the assembled actuator system was less than 150ms. This value allows the indenter to create, via feedback control, a zero-hysteresis force versus displacement plot based on the Bode response of soft tissue. The actuators were able to supply at least 15N of force to the residual limb (38.2kPa). Based on the average size range for a transtibial residual limb, the minimum and maximum radii the actuators were able to achieve was set at 50mm and 130mm, respectively. See Table 2.1 for a full electromechanical requirement listing for the indenter device.

2.2.3 Specification of Physical Components

In this section, the electromechanical and functional requirements are presented and used to specify the components used in the construction of the multi-indenter system. The hardware description is followed by a description of the software controller. The main mechanical components of the multi-indenter are shown in Figure 2-3.

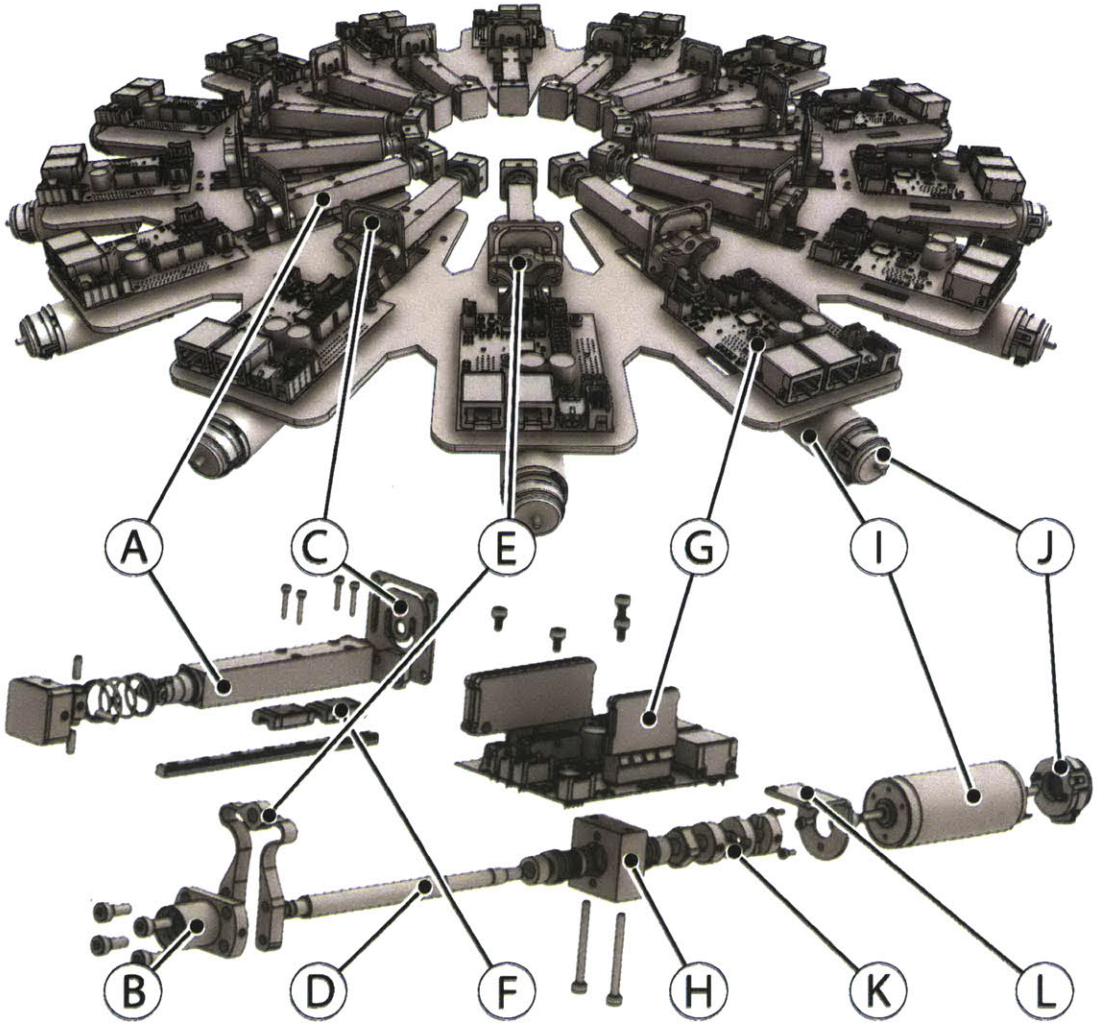

Figure 2-3: A mechanical diagram of the multi-indenter system. The exploded view is one of the fourteen linear actuators that make up the main multi-indenter assembly. Each individual indenter is radially directed towards the longitudinal axis of the limb, such that actuator forces are aligned in an orthogonal direction to the body's surface in order to provide easily reproducible boundary conditions for modeling.

These components include the following: (A) a custom load-transfer pin with a 2-DoF, spring-centered head (head shape: flat, 20mm square with 3mm rounds); (B) a Whemulti-indenter systemtone bridge strain-gauge force sensor [MLC700-10KG, Manyyear Technology Inc., Shenzen, China]; (C) a linear ball-

bearing [SSE2B-N6-100-MC, Misumi Corp., Schaumburg, IL, USA]; (D) ball-screw nut [BSSC0802-115, Misumi Corp., Schaumburg, IL, USA]; (E) a 5-DoF flexural force transfer beam that mounts to the strain-gauge; (F) a 2mm pitch, 8mm diameter ball-screw [BSSC0802-115, Misumi Corp., Schaumburg, IL, USA]; (G) a custom bearing enclosure housing two thrust bearings [6x12x4.5, Dynaroll, Sylmar, CA, USA] on either side of one roller bearing [6x10x3, Dynaroll, Sylmar, CA, USA]; (H) shaft-coupling [MCO15-6-6, , Misumi, Schaumburg, IL, USA]; (I) a custom L' bracket motor mount; (J) 20W, 24V brushed Maxon motor [339152, Maxon Precision Motors Inc., Fall River, MA, USA]; (K) U.S. Digital relative reflective optical shaft encoder with 360 pulses per revolution (1440 quadrature counts) [E4P-360-118-N-D-D-T-B, US Digital Corp., Vancouver, WA, USA]; and (L) a custom steel plate to mount the 14 indenter actuators.

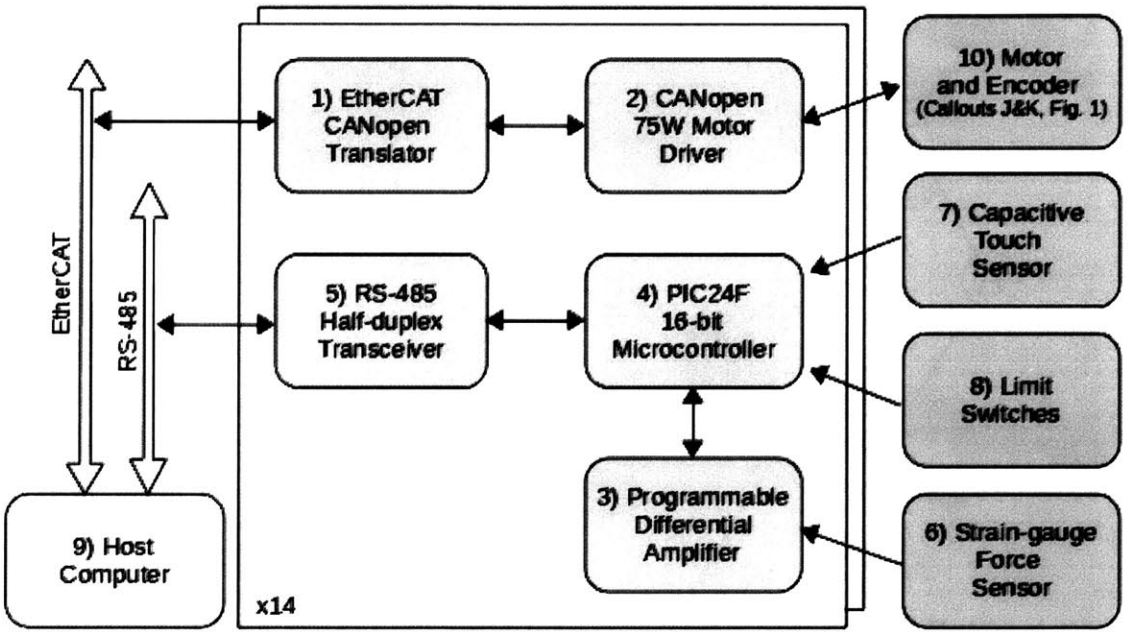

Figure 2-4: A basic diagram of the electrical system that drives the multi-indenter device. Note that there are two separate communication busses: EtherCAT^{TM} and RS-485.

Figure 2-3, callout M (detailed in Figure 2-4), shows the location of the electrical system for each indenter. The system is comprised of: 1) EtherCAT to CANopen communication electronics [P038.011.E001, Technosoft SA, 2000 Neuch tel, Switzerland]; 2) a 75W CANopen motor driver [P028.001.E001, Technosoft Motion^{TM}, 2000 Neuch tel, Switzerland]; 3) a custom dual-stage differential instrumentation operational amplifier for strain gauge amplification with real-time adjustable gain; 4) a PIC24FV16KM204-I/ML microcontroller [Microchip Technology Inc., Chandler, AZ, USA]; 5) RS-485 half-duplex transceiver

for communication with the PIC; 6) amplifier management; 7) digital I/O; 8) capacitive sensing for detecting contact with the residuum; and 9) limit switches [Omron Corp., D5A-1100, Kyoto 600-8530 Japan] for position calibration. EtherCAT is an Ethernet-based fieldbus protocol based on the CANopen and EtherCAT Technology Group 6010 specifications. Capable of running at full-duplex Ethernet speeds (>100Mbps), EtherCAT enabled a sophisticated communication topology as well as a wide-range of supported devices.

2.2.4 Device Calibration and Characterization

In this section, the position and force calibration methodology is described. Further, device characterization experiments are explained, including experimental design and data analysis methodology. The multi-indenter device was characterized by its position/force accuracy and resolution.

Data were collected from 162 sensors over an EtherCAT fieldbus at 500Hz. Two Windows^{TM}-based programs were required for operation of the multi-indenter system: TwinCAT^{TM} [19] and a custom controller program written in Java^{TM}. Position calibration of the multi-indenter device was required for each actuator on start-up. Position calibration was completed by retracting each actuator until contact was made with a hard stop of known position. Actuator contact with the hard stop was determined using a limit switch. This position plus a small safety increment (decrease in indenter radius) was set as the zero position where the actual encoder count was zeroed. Position accuracy was determined by starting with the multi-indenter device powered off, turning it on, running the position calibration and measuring the distance between linearly-opposing indenter pairs using digital calipers. This process was repeated 15 times. Each measurement was recorded separately, and the average and standard deviation of the mean were calculated. The average value was used as the position calibration setting for the indenter device.

Position sensitivity was measured by determining the minimum repeatable difference between any two successive position readings from the raw data saved by the testing software. Specifically, data were processed as shown in the equation where n is the number of samples in the data and x_i is a single position reading. Position sensitivity was measured in this way to ensure the entire system configuration was taken into account.

Force sensor calibration was accomplished through the use of a calibrated compression spring (stiffness measured as 2.44kN/m). During force calibration, two opposing indenters were controlled to move inwardly at the same time to compress the calibration spring to its maximum-allowable deflection, then controlled to translate the spring while maintaining constant spring deflection three times to ensure that the force measurements were uncorrelated with position before calibration was accepted. The resulting force sensor signal was plotted versus spring displacement. The linear regression of these data (the slope) was multiplied by the spring constant. The resulting value was taken as the calibration constant, a value that converts the analog signal measured by the Whemulti-indenter systemtone-bridge strain gauge into a force in Newtons. Force error was estimated by subtracting the linear regression predicted force from the force reported in the experimental calibration data and then analyzing the >1000 data points gathered during force calibration for error. The root mean square error, standard deviation, and r-squared results are presented.

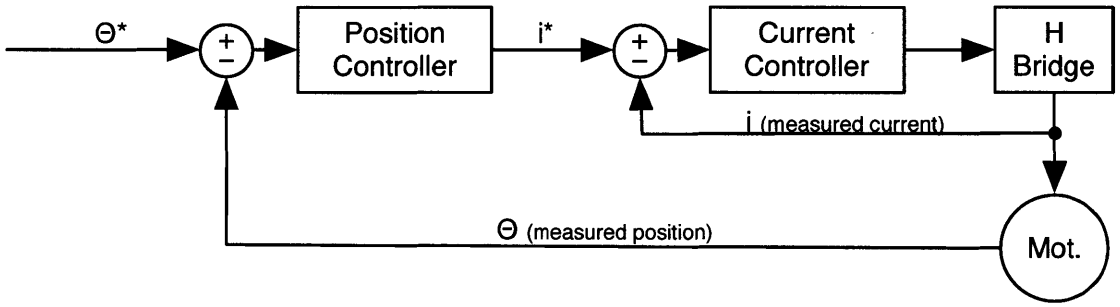

Figure 2-5: Each indenter is controlled by a separate controller. The current controller is a lower-level controller than the position controller, however both run at 20kHz.

The internal control system used by each indenter can be seen in Figure 2-5. The position and current controllers have separate PID and PI controllers, respectively. These low level controllers each run at 20kHz. Tuning was done using a methodology similar to the Ziegler-Nichols technique.

The PI current controller was tuned for acceptable stability and high fastness. In other words, rise time was prioritized over settling time. The position controller was tuned to achieve acceptable stability and medium fastness. With the derivative and integral terms set to zero, the proportional gain was increased until the system reached instability. The derivative gain was increased until the system was over-damped, then set to 75% of the over-damped value. The integral gain was then increased until the system was well damped. These initial values were then adjusted slightly to hone the performance of the system. The current controller was tested by clamping the motor shaft and examining the current response to a command from the main controller. The position controller was tested through position

commands of repeated 2mm ramped step movements.

2.2.5 Electrical System Description

Figure 2-6 shows the basic electrical connections of the FitSocket. The 120V power from the wall is split to two power switches. One switch connects the computer and its peripherals and the other can be seen in Figure 2-2 as the large toggle switch just below the left corner of the control PC's LC display. The latter toggle switch provides power to three power supplies. The smallest is a 1A at 5V power supply that provides TTL level voltage for circuits and small devices (sensors, etc.) that need more power than a linear regulator can supply.

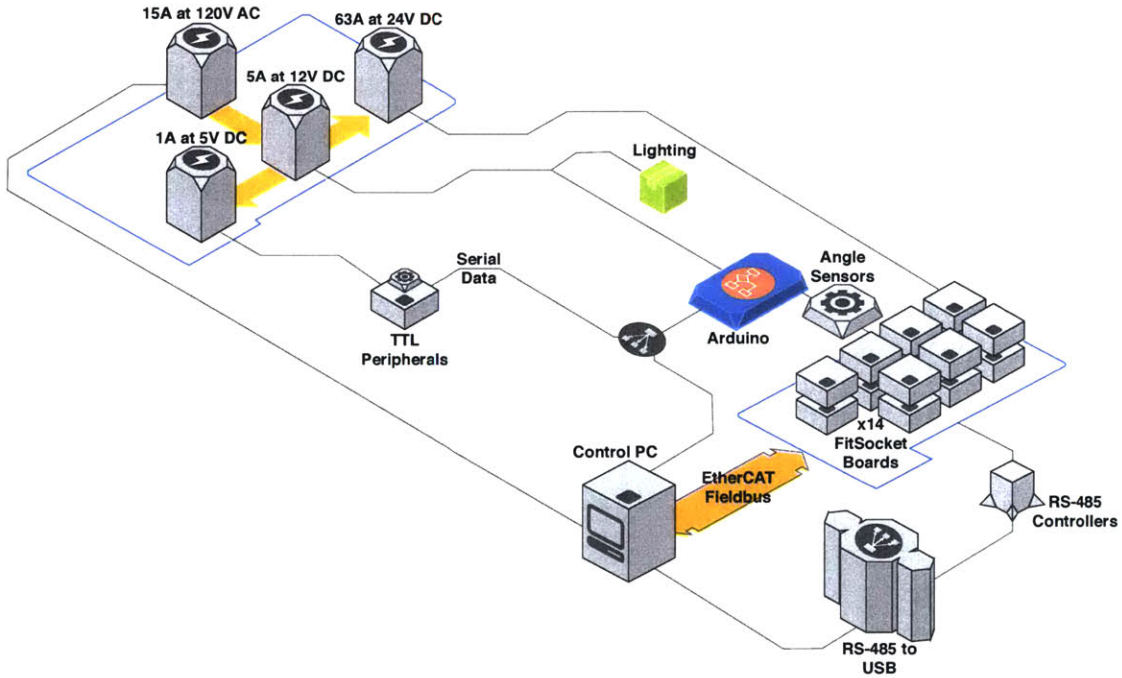

Figure 2-6: The primary electrical subsystems include: three power supplies – 63A at 24V, 5A at 12V, and 1A at 5V; a two USB busses to the controller PC – one for RS-485 and one for the Arduino microprocessor; an EtherCAT fieldbus that connects the controller PC to the 14 EtherCAT controller PCBs; three accelerometer based angle sensors for sensing the rotation of the main actuator ring; and a motor controller and continuous rotary position encoder (not shown) for controlling the base linear stage controlled by the Arduino.

In the middle, the 5A at 12V power supply provides potential to the regulator contained on the Arduino board and 12V LED power indicator lights. The largest power supply is a 63A at 24V power supply for the FitSocket's main actuator ring. This power supply is used to power the 14 controller boards, including the EtherCAT to CANopen translator PCBs and the Motor Controller PCBs, both by Technosoft

Motion (the 5V TTL power is derived from the motor controllers, which helpfully provide a very clean 5V output), the 14 20W continuous Maxon motors, and the base linear actuator that is controlled by the Arduino using position feedback from a continuous rotational potentiometer.

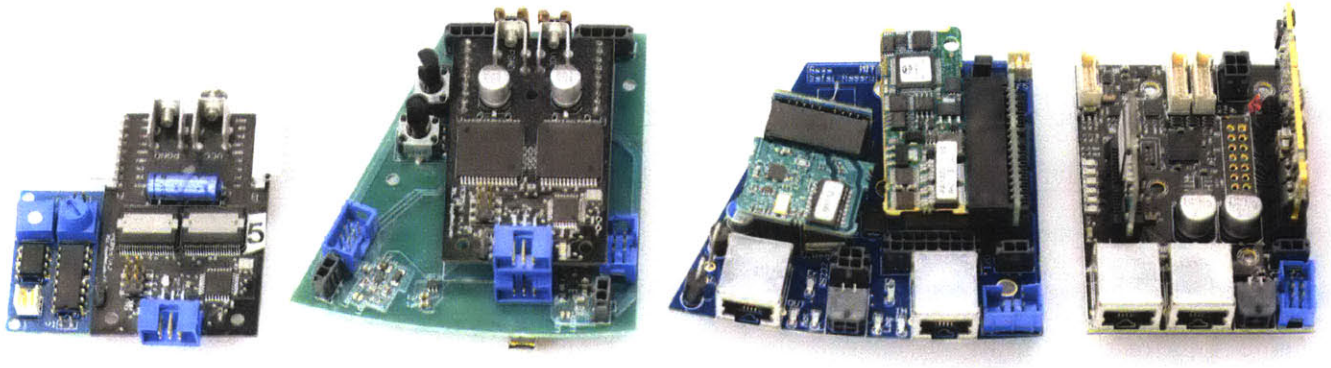

Figure 2-7: The historical progression of the FitSocket controller boards from left to right: the MCBMini controller with external strain-gauge amplifier; a carrier board for the MCBMiniV2 that includes additional peripherals including a strain-gauge amplifier as well as power and communication management; the HALOBOT EtherCAT host board that has built in strain-gauge amplifiers, power distribution, and communication; and the final FitSocket host board featuring a two-stage strain-gauge amplifier, PIC16 microcontroller, RS-485 communication hardware and capacitive sensing (among many other GPIOs).

The first and second versions (the left-most two boards in Figure 2-7) of the FitSocket controller board were based on boards that were designed and built by Sigurður Örn Aðalgeirsson (Siggi), then a graduate student in Cynthia Breazeal's Personal Robots group. The board, called the MCBMini, is a feedback capable dual motor driver that communicates via serial (and eventually USB) to a control PC that uses a custom Java API for control. Siggi developed the basic control framework prior to the boards use in the FitSocket, so getting started with his hardware was quite straightforward. Unfortunately these boards did not have the power, GPIOs, or high resolution encoders that were eventually required, so they could not be the final solution. The MCBMini was a wonderful way to get started with the FitSocket because of the ease at which they could be used.

The third and fourth (see Figure 2-7) FitSocket controller boards were based on the Technosoft Motion iPOS-3602VX-CAT 75W motion controllers. These are EtherCAT capable controllers and must be controlled through the EtherCAT protocol. The third board, designed primarily by Reza Safai-Naeeni, featured a built in strain-gauge amplifier and custom connectors for the motors, encoders, and data wiring. The fourth board, designed primarily by Jean-François Duval, added a PIC24F microcontroller to aid with capacitive sensing, digital gain, and offset tuning of the strain-gauge amplifier, in addition

to a few extra GPIO pins for limit switches, etc. The PIC communicates with the computer through an RS485 bus, which terminates in an RS-485 to USB transceiver.

2.2.6 Software System Description

The software for the multi-indenter system can be thought of as having four distinct functions: Calibration, Experimentation, Results, and Communication. The calibration object is responsible for creating a way by which we can take the electrical signals from the force and position sensors and make them into human readable units such as millimeters and Newtons. The experiment object is responsible for performing a robust test on a residual limb. The results object is responsible for saving the data gathered from testing and calibration in a useful way for retrieval and data manipulation. The communication object maintains the state of the actuators so they are always ready. Additionally, the communication object maintains the data in the system on a separate process that runs continuously no matter what other operations the control program is doing. The communication thread is also responsible for translating the command signals – which are in the form of a byte stream – into readable values and vise versa for reading the state of the multi-indenter system.

2.2.6.1 High Level Software Organization

The software that controls the multi-indenter robots is organized into the following main and sub packages:

- Communication
  - Arduino
  - RS-485
  - EtherCAT
- Data
  - Experimental Data
  - Calibration Data
- Experiment
- Robot

  - Actuator
  - Calibration
  - Pin
  - Sensor
- Test
  - Concrete Tests
  - Test Manager
  - Test Worker
- UI
  - Actions
  - Event Handlers
  - Interfaces
  - Views

2.2.6.2 Communication

Let's begin with the main communication thread, which is the first thread that begins on the "Initialize Robot" GUI command. The loop is fairly simple but handles all of the communication between the physical robot and the software through the use of the AdsReaderWriter dynamic link library provided by Beckhoff Automation. The functionality of the commands in this library are fairly low level, so the communication consists entirely of a 154 byte long byte array. Each pin's (what we call the linear actuators in the software but you may see both terms) data is contained in 11 bytes. Listing 2.1 below shows how these functions are used. Not shown is the debug portion of this loop, which outputs a time-averaged loop frequency. This frequency is always 500Hz.

To begin, 154 bytes are read from the device. A response byte array is instantiated next so that while the pins are being populated with the newly acquired sensor data from the actuators, they can also send their commands to the device. Note that the readData object is the instance of ReadDataStructure, which *reads in data from* the physical robot while the writeData object, the instance of the WriteDataStructure *writes data to* the physical robot. Both of these data structures are actually classes containing structures that are thread-safe storage vaults for data as well as thread-safe functions for modifying those data. After each pin has added its command data to the write buffer, it is sent to the robot via

the AdsReaderWriter.

The next for-loop checks the status of each pin, as they are running state machines on the hardware level. If any thing changes with the state of a pin, the software needs to shut down the pin and restart it immediately in order to preserve smooth operation of the device. This is checked by asserting that the voltage state of the pin is "on." If this is not true and the pin is not already running its state executor, then a new thread is created through the instantiation of a pinWorker whose job is to shut down the pin and bring it back online through the state transitions necessitated by the EtherCAT state machine rules.

You may notice that the pinStateExecutor object appears to be a ThreadPoolExecutor type object. At its heart, this is true. In reality it is a NamedThreadPoolExecutor, created by wrapping a ThreadPoolExecutor with an external runnable such that it is possible to query the object (1) which IDs are currently running or (2) if an ID is currently running. This was necessary because multiple threads must not be trying to shut down a particular pin and reinitialize it at the same time, as this would be counter-productive.

Listing 2.1: Main Communication Thread

```
while (isCommunicationOpen) {
      // Read bytes from the ADS stream
      byte[] readBytes = AdsReaderWriter.readAll(address);
      // Instantiate an output stream for adding each pin's data
      ByteArrayOutputStream outputStream = new ByteArrayOutputStream();
      for (int pinNum = 0; pinNum < pinCount; pinNum++) {
        // Put data from ADS into the ReadDataStructure for each pin
        int start = pinNum * 11, end = start + 11;
        readData[pinNum].writeAll(Arrays.copyOfRange(readBytes, start, end));
        try {
          // Add each pin's data to the output stream
          outputStream.write(writeData[pinNum].getByteArray());
        } catch (IOException e) {
          Logger.log(CALLER, e.getMessage());
        }
      }
      // Write the data to the ADS stream
      AdsReaderWriter.writeAll(address, outputStream.toByteArray());
      // Check the status of the pins
      for (int pinNum = 0; pinNum < pinCount; pinNum++) {
        if (!readData[pinNum].getVoltageOnState() && !pinStateExecutor.isRunningId(pinNum)) {
          // Execute a pin worker thread that walks through the state machine
          pinStateExecutor.execute(pinWorker.get(pinNum), pinNum);
        } else {
          Robot.getInstance().getPins().get(pinNum).update();
        }
      }
    }
```

2.2.6.3 Pin Movement

Now that we have stable communication and state management of our 14 pins, we want to be able to send commands and receive sensor data from them. Listing 2.2 shows how this is accomplished. The PinData object interacts directly with the WriteDataStructure object to set its values to the position requested through this function[2]. At this point, it is as easy as telling a particular Pin object to set its position to a particular radial value. Because these position values are radial, an *increase* in position denotes a movement of the pin *outward*. One note of particular interest is the forced inclusion of units in this setting. Not only does this make the code more readable, it prevents accidental unit errors and other unpredictable situations. All units are stored in one of the Constants objects (see Appendix H.1) and are reasonably inclusive (to the point of containing beard-seconds as a unit).

On top of this requirement, after a position calibration check, the actual position command sent to the robot is passed through a protected position function that determines if it is within the physical bounds of the linear actuators that make up the pins. These bounds are accessible in the Constants object[3].

Each pin has a calibration zero that is stored in a volatile way when the robot is calibrated. This is the theoretical zero radius position of the pin, since the pins are not actually capable of moving to this position physically. It is important to note (again) that the pin position commands are commands of the pin's radius, so a larger value means that the pin will move more outward.

Listing 2.2: Setting the Position of an Actuator

```
// This function is generally used of the (full, expanded) form:
// Robot.getInstance().getPins().get(foo).setPosition(bar, Constants.MM);

public void setPosition(double position, int unit) {

    if (!this.pinCalibrationData.isPositionCalibrated()) {
      pinData.setPosition(position * (double) unit);
      System.err.println("Warning: Pin " + pinData.getId() + " not calibrated. Moving
          anyway.");
    } else {
      double actualPositionTicks = (position * (double) unit) +
          pinCalibrationData.getPositionZero();
      actualPositionTicks = getProtectedPosition(actualPositionTicks);
      pinData.setPosition(actualPositionTicks);
    }
  }
```

[2]The PinData object is a boring list of helper functions and simple safety checks, so it is not shown

[3]The definition of these bounds is reliant upon the individual position calibration settings (in the PinGeometricConstants object) Be mindful if you intend to modify these values as errors will result in sad actuators

2.2.6.4 Anatomy of a Test

Listing 2.3 is an example of a *concrete test.* Concrete tests are objects that should implement a test interface (and that exists, it is just not implemented), as all concrete tests have the same runFooTest() function that is called by the TestSwingWorker object that manages the test through the TestManager object. This can be seen in Figure 2-8.

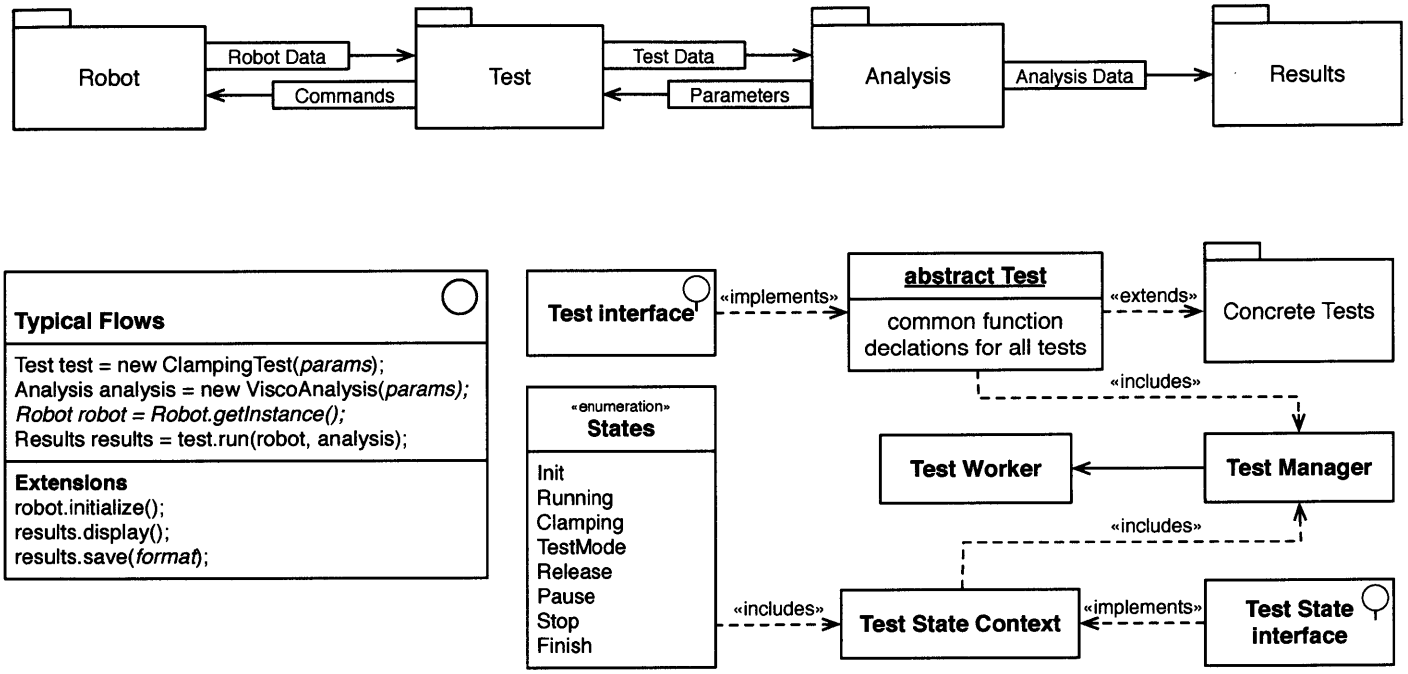

Figure 2-8: The basic layout of the command structure (top), typical interaction flows (bottom left) and the basic layout of the testing structure (bottom right).

This method of organization allows the concrete test to be separated from much of the context dependent requirements of a test and focus on the movement and processing of data. The concrete test contains the functions that are required for it to function, and the type of concrete test defines which functions those are. In the case of a biomechanical measurement test, there are several functions corresponding to the different states of the test (e.g., initialization, clamping, testing, and possible special modes). It is the job of the TestManager object to communicate between the user interacting with the current GUI view and the concrete test to determine what should happen next.

Most seasoned computer scientists will understand Figure 2-8 as a basic state machine design pattern. One complicating factor in this design pattern is that each test does not implement exactly the same functionality nor does it necessarily require the use of the state machine at all. In the example seen in Listing 2.3, this is the case. This concrete test simply displays the current time – with the 12 hours

mapped to 14 pins. In order for the time to make sense, Pin 0 must be rotated to the bottom of the actuator ring.

Most of the concrete tests are of similar complexity to this test that is referenced. The idea being that one does not need to understand the entire codebase in order to create an experimental test.

Listing 2.3: An Example of a Test

```
public static void runClock() {
    Robot.getInstance().setVelocityAllPins(7);
    ArrayList<Pin> pins = (ArrayList<Pin>) Robot.getInstance().getPins();
    Calendar calendar = Calendar.getInstance();

    System.out.println("Clock Test Running...");
    try {
      while(System.in.available() == 0) {

        calendar.setTime(new Date());

        double hours = calendar.get(Calendar.HOUR_OF_DAY);
        double minutes = calendar.get(Calendar.MINUTE);
        double seconds = calendar.get(Calendar.SECOND);

        //System.out.println("Time: " + hours + ":" + minutes + ":" + seconds);

        int robotHours = (int) Math.floor((hours * 28.0) / 24.0);
        int robotMinutes = (int) Math.floor((minutes * 14.0) / 60.0);
        int robotSeconds = (int) Math.floor((seconds * 14.0) / 60.0);

        robotHours = NumberUtilities.getCircularIndex(pins.size(), robotHours, 7);
        robotMinutes = NumberUtilities.getCircularIndex(pins.size(), robotMinutes, 7);
        robotSeconds = NumberUtilities.getCircularIndex(pins.size(), robotSeconds, 7);

        //System.out.println("Robot Time: " + robotHours + ":" + robotMinutes + ":" +
            robotSeconds);

        for (int pinNum = 0; pinNum < pins.size(); pinNum++) {

          if (pinNum == robotHours) {
            pins.get(pinNum).setPosition(Constants.MAX_LINEAR_TRAVEL_MM - 38, Constants.MM);
          } else if (pinNum == robotMinutes) {
            pins.get(pinNum).setPosition(Constants.MAX_LINEAR_TRAVEL_MM - 22, Constants.MM);
          } else if (pinNum == robotSeconds) {
            pins.get(pinNum).setPosition(Constants.MAX_LINEAR_TRAVEL_MM - 16, Constants.MM);
          } else {
            pins.get(pinNum).setPosition(Constants.MAX_LINEAR_TRAVEL_MM, Constants.MM);
          }
        }
      }
    } catch (IOException e) {
      // TODO Auto-generated catch block
      e.printStackTrace();
    }
    System.out.println("Clock Test Stopped.");
    Robot.getInstance().releaseAllPins();
  }
```

2.2.7 Clinical Experimental Design

To evaluate the capabilities of the multi-indenter system for in vivo biomechanical tissue measurement, four anatomical locations across the transtibial residual limbs of a person with bi-lateral amputations were selected for measurement: 1) fibula head, 2) patellar tendon, 3) mid-tibia, and 4) mid-posterior. The participant in this study was consented through a research protocol approved by the Committee on the Use of Humans as Experimental Subjects (COUHES) through the Massachusetts Institute of Technology (MIT).

2.2.7.1 Subject Setup

The experimental participant was seated comfortably facing the multi-indenter system ring, and asked to insert his residual limb into the device. The multi-indenter was passively rotated and actively translated down the longitudinal axis of the limb until the tissue indenter was positioned adjacent the anatomical location of interest. During the tissue measurement phase, a single indenter, or a test indenter, was used. To minimize whole-limb translation, the remaining indenters were used to clamp the residual limb, with the exception of the two indenters immediately adjacent to the test indenter, totaling 11 clamped indenters. The indenters adjacent to the test indenter were not engaged in clamping in order to abate mechanical interference due to the relative incompressibility of human soft tissue. By allowing the tissue around the indenter to remain uncompressed, the measured stiffness data more closely resemble single indenter data.

2.2.7.2 Test Indenter Pre-Test Alignment

Force control was applied to enable indenter clamping at a specific force to ensure study participant comfort and safety, as well as to provide data that were readily processed by IFEA algorithms. At each anatomical location, the multi-indenter system clamped the limb using 11 indenters. Using the GUI shown in Figure 2-9, the limb was clamped with an operator-selectable clamping force of 14N. The specific clamping force was selected to prevent whole-limb translation of the residuum. After clamping, the subject was allowed to relax their residual limb. The starting position of the remaining test indenter relative to the body's surface was determined by simple linear force regression. The indenter measured

the radial positions associated with 500mN and 1N force on the residuum, then backed away from the limb to the linearly interpolated 0N radial position plus one additional millimeter away from the residual limb.

2.2.7.3 Clinical Data Collection

Following this positioning (the residual limb remained clamped), the test indenter was moved to push against the residual limb until it reached the operator specified maximum testing force in under two seconds in order to determine the displacement of the soft tissue related to the safe and comfortable testing force. This testing force was chosen to be distinct from the clamping force. In this experiment, the force was selected to be 12N.

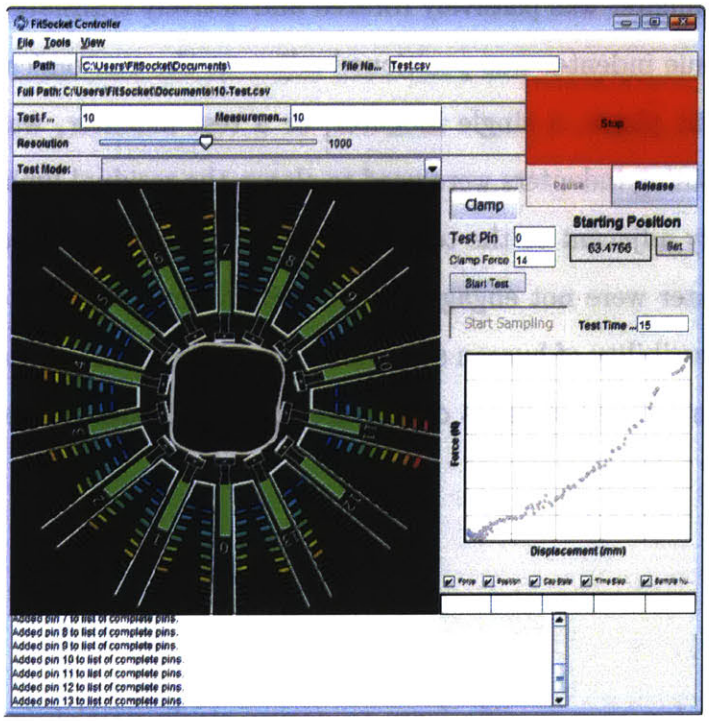

Figure 2-9: The graphical user interface that controls the multi-indenter system. The interface allowed for complete control of the device, including data processing and storage for use with other software such as Matlab^{TM}. Note the colored ticks on test indenter 11, indicating the real-time force applied by the indenter on underlying residual limb tissues. The remaining indenters (0-9, 13) were used for residual limb clamping.

After determining the tissue deflection corresponding to the maximum testing force, the test indenter moved back to its starting position while the 11 opposing indenters remained clamped. The test indenter then completed a constant velocity movement lasting 7.5 seconds to the determined position corresponding to the maximum testing force, measuring the force-displacement relationship of the tissues directly beneath its head. Following this data collection, the test indenter then moved back out again to the starting position in a velocity controlled way, also lasting 7.5 seconds.

Velocity varied according to total indentation per experimental trial; however, the velocity during any one indentation is constant throughout the indentation. These data were also recorded in the same file as the inward movement of the indenter. After the test indenter reached its starting location, all clamped indenters were released, and the

data (force [N], radial position [mm], time elapsed at each sample [ms], indenter number, sample number) were saved. This process was repeated across all four selected anatomical locations on the limb three times.

Successive trials were analyzed for similarity (see Figure 2-14). Similarity was defined as the standard deviations in force and deflection calculated as the mean difference for each sample of three trials each, then the calulated standard deviation of these differences for both deflection (x axis) and force (y axis) – a total of 1500 samples, each comprised of standard deviation of force and deflection defined by three data points.

2.2.7.4 Viscoelastic Clinical Data Collection

In a second experiment, an identical method was followed with a single change. Instead of immediately moving away from the residuum after the maximum deflection had been reached, the indenter was held at a constant position for 10 seconds while continuing to record the same data as in the first experiment (force [N], radial position [mm], time elapsed at each sample [ms], indenter number, sample number). The indenter was then moved away from the residuum just as in the previous experiment. Each trial of this experiment is completed three times in order to prove consistency across trials. Data are averaged between trials, and the standard deviation across trials is presented.

2.2.7.5 Force and Position Calibration Methods

The multi-indenter system was calibrated in position and force no more than one hour prior to data collection to avoid strain-gauge drift. Prior to data collection, motion capture markers were placed on the residual limb, the multi-indenter system (reference points), and the tissue indenter itself. To determine if any movement of the residual limb occurred during tissue measurement, each trial was recorded using a Vicon^{TM} 12-camera motion capture system that captured data at 100Hz. Motion capture data were analyzed using Vicon Nexus^{TM} 1.815 and Matlab^{TM}.

Three reference point xyz locations were averaged and subtracted from two averaged reference points. The magnitude of each distance between the reference point and the residual limb point was calculated and the mean subtracted. Whole-limb translational data are presented in the subsequent Results section.

2.3 Results

We present the results of the device characterization experiments as well as the clinical experiments. The device characterization experiments include position calibration, force calibration, current PI, and position PID control loop tuning.

The clinical experiments show the force displacement plots for the four anatomical locations previously mentioned: 1) fibula head, 2) patellar tendon, 3) mid-tibia, and 4) mid-posterior, as well as the repeatability of these measurements.

2.3.1 Robotic Multi-Indenter System Characterization Experimental Results

Functional requirement results are detailed in Table 2.2. Position accuracy is 100µm, with a position sensitivity of 1.4µm. Force accuracy is 330µN and sensitivity is 15µN. The step response time is 120ms. The maximum force is 22.8N. The minimum and maximum radii achievable by the indenter system is 43mm and 132mm respectively.

Position calibration results are shown in Figure 2-10. The maximum difference from the mean is 287µm, and mean standard deviation across all indenter pairs of 109µm.

Force calibration results from indenter 2 consisting of 1110 data points are shown in Figure 2-11. Indenter 2 has an r-squared value of 0.99786. Analysis of all indenters was completed, resulting in a mean r-squared value of 0.9952 and a mean RMSE of 341mN. The standard deviation of the mean for all fourteen indenters' data subtracted from their linear trend lines is 90.2mN.

The indenter's internal current controller plot is shown in Figure 2-12. The indenter's shaft was locked in place for this measurement. A current of 750mA was requested, and the internal PI controller of the actuator attempted to match the command. Settling time is roughly 6ms (or 120 discreet PI cycles).

Figure 2-13 results of the position controller PID turning during a 2mm ramped step movement – each section (ramp down, hold, ramp up, hold) lasting 100ms. The position response shows overshoot typical of a well-damped system. The overshoot is roughly 3.1% of the total movement in this test, lasting

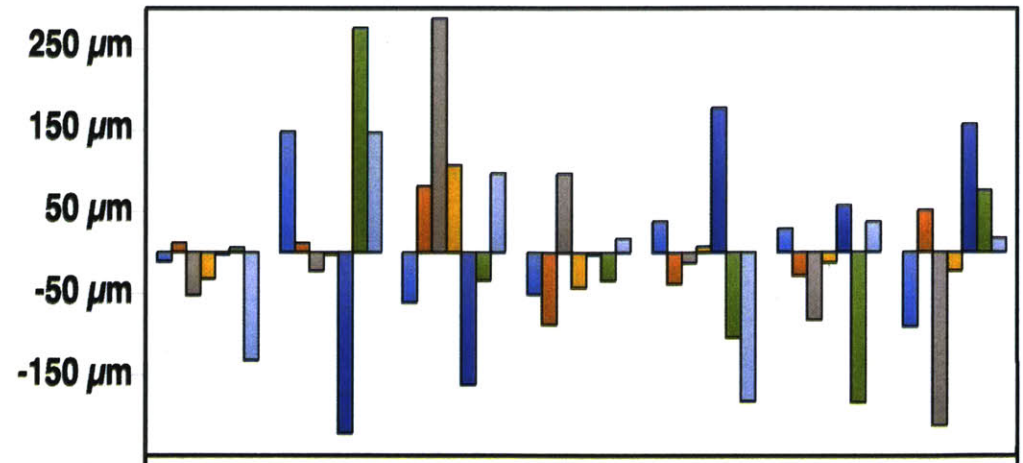

Ind. Pair	Trial 1	Trial 2	Trial 3	Trial 4	Trial 5	Trial 6	Trial 7
0&7	-11.43	148.57	-61.43	-51.43	38.57	28.57	-91.43
1&8	11.43	11.43	81.43	-88.57	-38.57	-28.57	51.43
2&9	-52.86	-22.86	287.14	97.14	-12.86	-82.86	-212.86
3&10	-32.86	-2.86	107.14	-42.86	7.14	-12.86	-22.86
4&11	-2.86	-222.86	-162.86	-2.86	177.14	57.14	157.14
5&12	5.71	275.71	-34.29	-34.29	-104.29	-184.29	75.71
6&13	-132.86	147.14	97.14	17.14	-182.86	37.14	17.14

Figure 2-10: Position calibration residuals are measured between opposing pairs of indenters. Each of seven position calibration verification trials is shown here. Note the grey highlighted table cells. These cells' residuals are above 1.5 standard deviations from the mean. The standard deviation of these data is 109μm.

approximately 20% of the 100ms section time. Additionally, the current response shows acceptable stability both during movement and standstill.

2.3.2 Robotic Multi-Indenter System Clinical Experimental Results

Figure 2-14 shows indentation data collected at the same anatomical location for three trials. Recalling from the methods, the subject remained clamped by eleven actuators during these three indentation trials. Over the entire 1.8mm deflection of the fibula head region consisting of 1500 force and deflection readings for each trial, the standard deviation of force is 194.3mN and the standard deviation of deflection is 47.7μm across trials for all data in each trial. For reference, these standard deviations are calculated by calculating the mean difference for each sample of three trials each, then calculating the standard deviation of these differences for both deflection (x axis) and force (y axis).

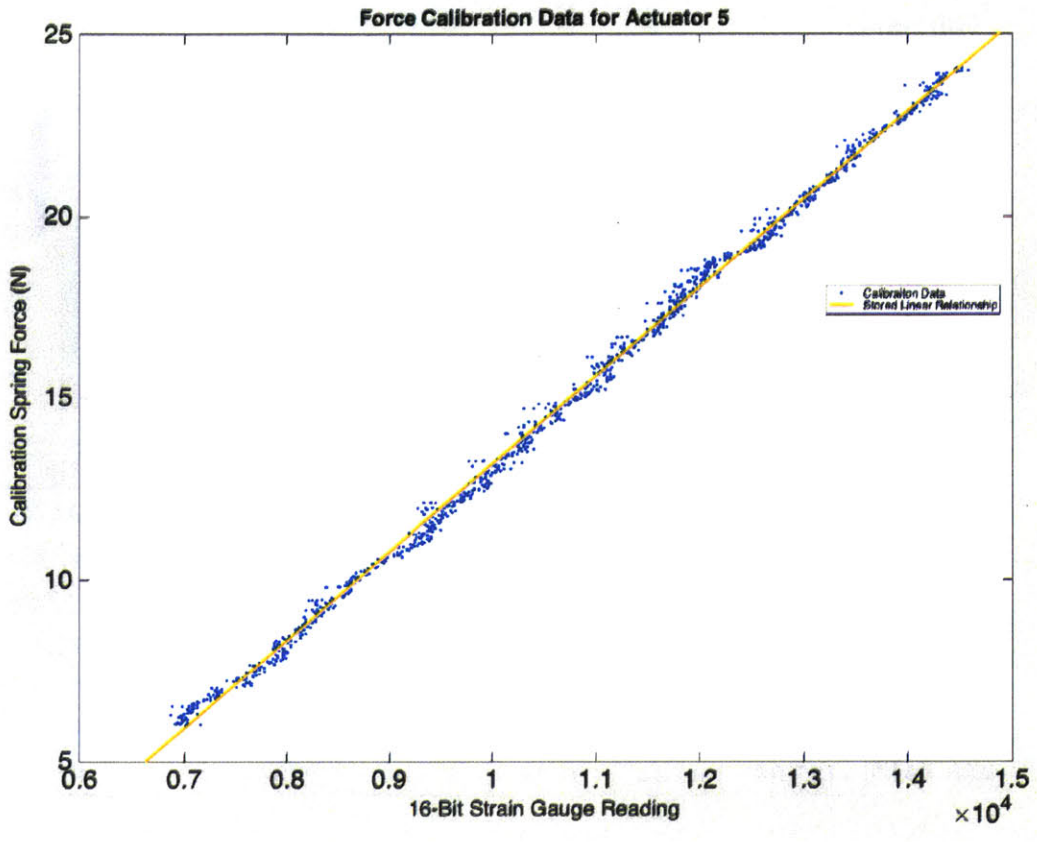

Figure 2-11: The robotic indenter device saves its force calibration data so that it may be checked for calibration quality. This plot shows a force calibration curve for indenter 5. The mean RMSE of all actuators' calibration plots combined is 0.341N and the mean R-squared of all actuators is 0.9952.

Note the hysteresis effect in Figure 2-14 and Figure 2-15 caused by the hyperviscoelastic properties of the tissue. Figure 2-16 details this during the plotted force versus time during a 10-second relaxation time wherein the indenter is held at a constant position during the relation time, allowing the hyperviscoelastic effects to be observed. Aside from the relaxation time, the test is identical to that in Figure 2-15. Computer controlled measurements allow repeated measurements of the same location to be reproducible with mean standard deviation across position controlled indentations below 200mN in force and 50µm in position.

Analysis of the motion capture data taken during trials with subjects show a standard deviation in distance between the five averaged reference points and two averaged residual limb points of 155.34µm. The standard deviation of a non-moving single reference marker that is physically attached to the structure of the room that was not averaged with multiple points is 627.27µm (Note the larger standard deviation because this is the data from a single marker). No statistically significant correlation with the indenter movement was observed in the motion capture data.

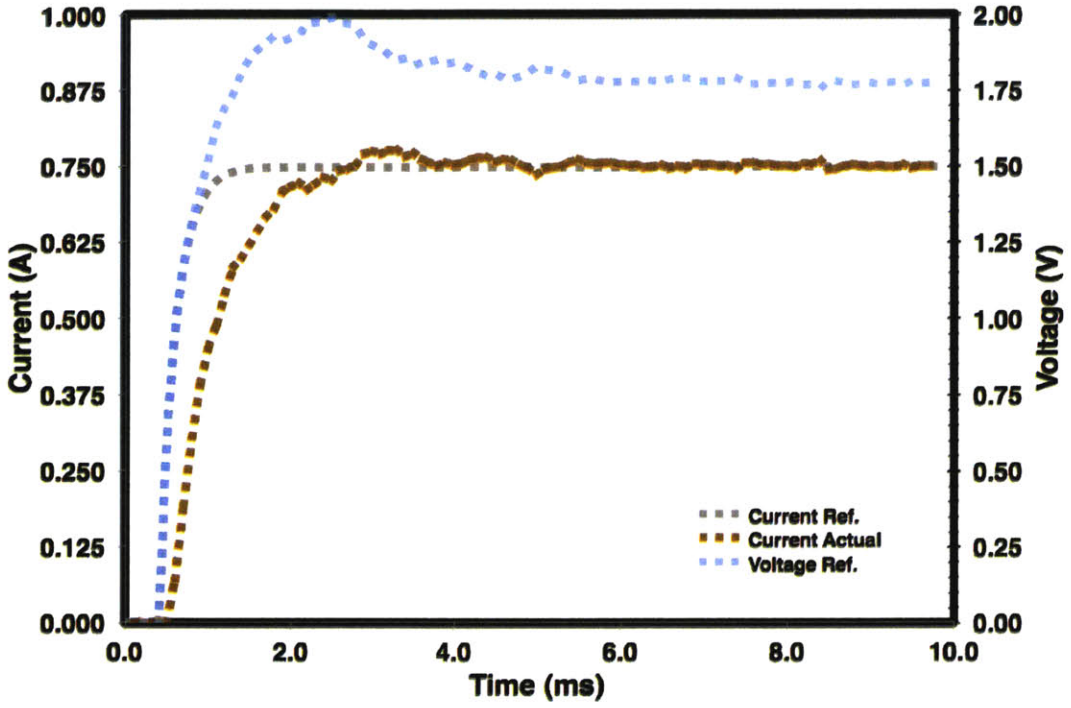

Figure 2-12: PI current control of the intender while the motor shaft is blocked. The current controller has a steady–state rise time of roughly 6ms.

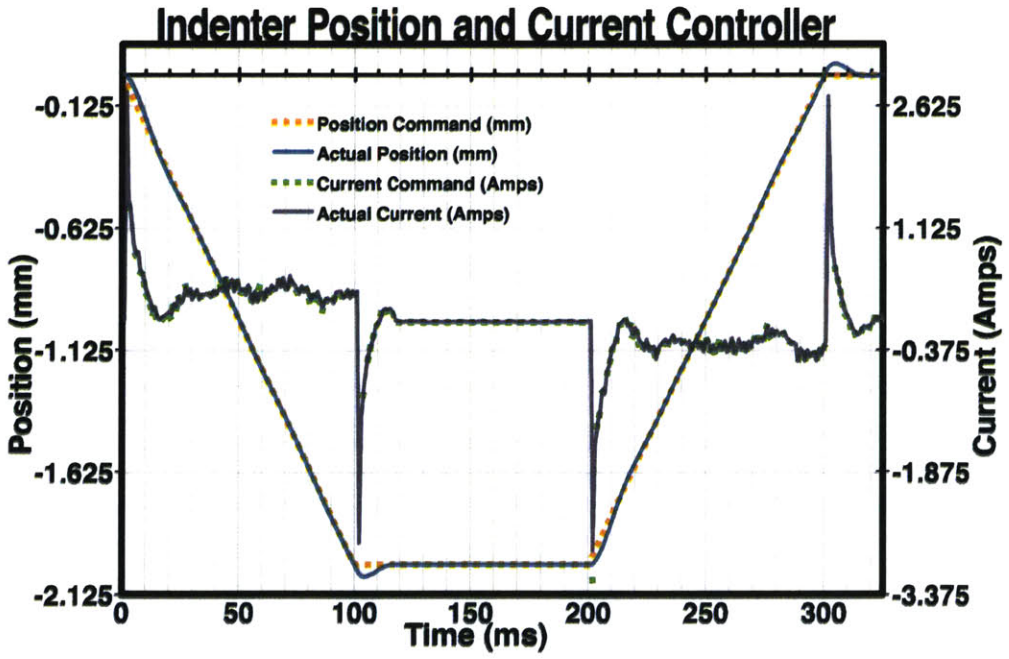

Figure 2-13: Dashed lines are commands while solid lines are measurements. Settling time is about 20ms for the PID controller in position at this velocity (20mm/s). Current commands are limited to $\pm$3.2A as seen on the supplementary right vertical axis of this plot.

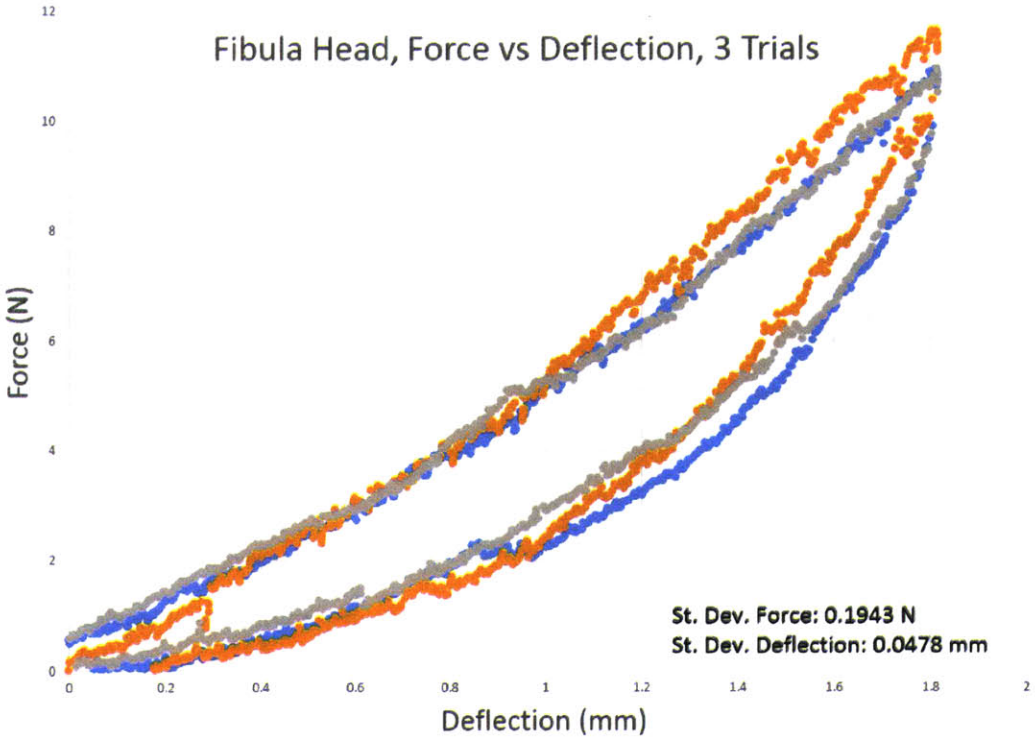

Figure 2-14: Controlled movements allow repeated measurements of a location to be reproducible with mean standard deviation for controlled indentations below 200mN in force and 50µm in position. Note that the total deflection in this test is only 1.8mm.

2.4 Discussion

Individuals having lower-limb amputation cite prosthetic socket fit as the primary source of discomfort [20]. In order to improve upon the current state-of-the-art, a better understanding of the mechanical interaction between the prosthetic socket and the tissues of the residual limb is required. To this end, we present a multi-indenter device whose purpose is to accurately measure the biomechanical properties of trans-tibial residua. We show that this device can capture repeatable data of high dimensionality: orthogonal force, deflection, and time. These data may help to inform the design of more comfortable prosthetic sockets.

Originally, it was thought that the force-displacement data of all 14 indenters could be collected at once, but the hyperviscoelastic nature of human tissue prevents accurate decoupling of the tissue's mechanical deformation. It was determined that limb translation during a trial could not be easily quantified or guaranteed to be zero. A 3D video or motion capture system could be used to quantify limb motion, but due to the deformation of the limb during the measurement process, accurate determination of

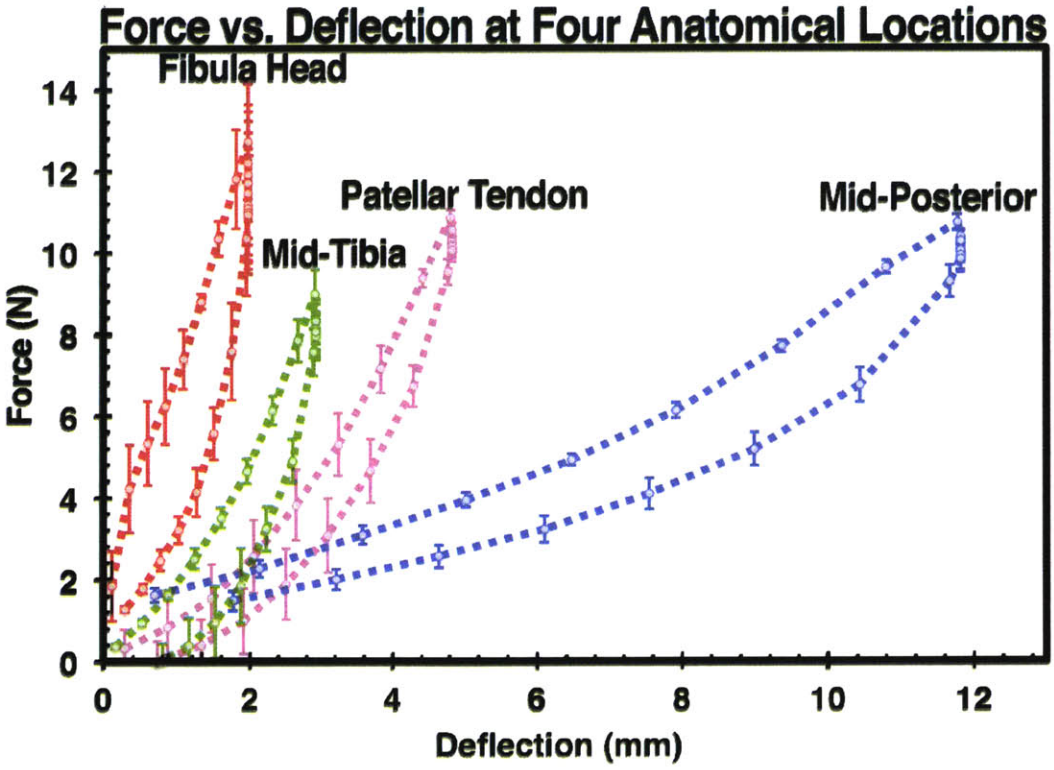

Figure 2-15: Force versus deflection with a 4 square centimeter indenter for three trials at each of four anatomical locations on the transtibial residual limb: (1) fibula head, (2) mid-tibia, (3) patellar tendon, and (4) mid-posterior. Error bars denote one standard deviation from the mean of the three trials.

exact translation would be an involved process. Considering limb deformation, 11 of the indenters were used to clamp the limb while a single opposing indenter was used for measurement in order to remove deformation effects from nearby indenters. This process was much slower in terms of data collection, but – as determined in the motion capture studies – shows good physical restriction of the residuum during measurement in a comfortable, controllable way. Additionally, the force readings in the clamping indenters increased evenly during testing, further supporting the motion capture study results.

2.4.1 Viscoelastic and boundary condition considerations

Boundary conditions of the experimental process are extremely sensitive. In the experiments that were buffered by at least 600 seconds between trials on the same anatomical location – in order to allow hyperviscoelastic conditions of that anatomical location to return to initial conditions – it was found that even with this buffer, the limb continued to experience hyperviscoelastic effects even after 20 minutes. In addition, the hyperviscoelastic components of data taken after 20 minutes more closely resembled the initial indenter data, just after clamping of the limb. Some of these effects are due to

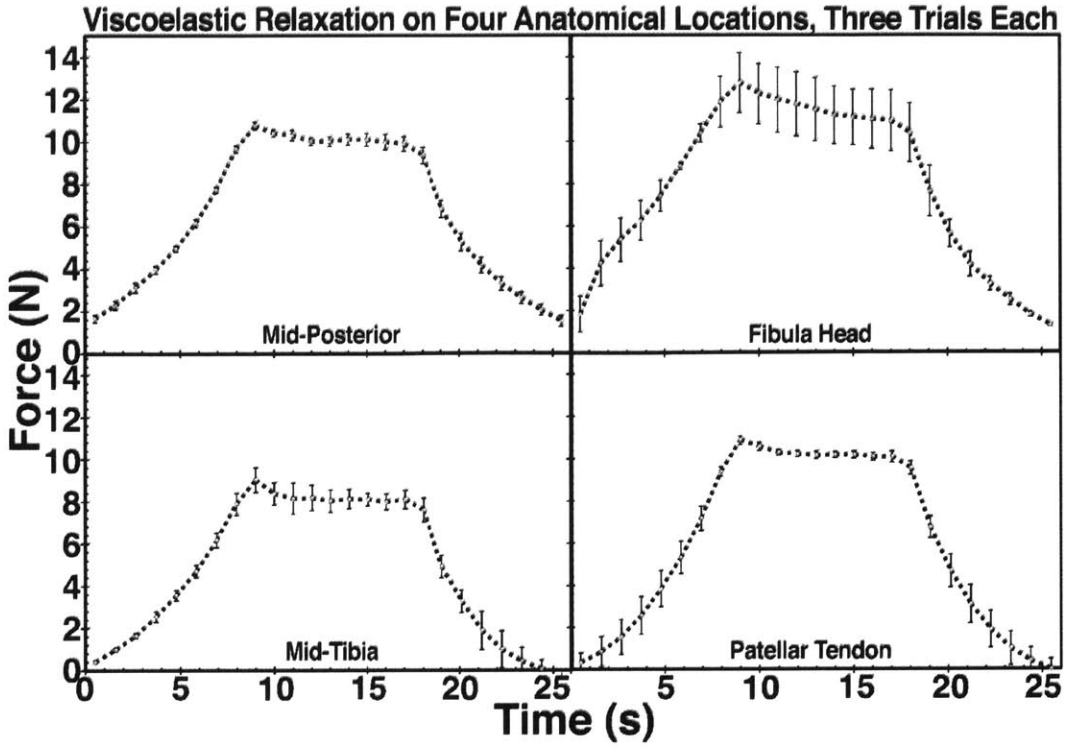

Figure 2-16: A subject is measured as in Figure 2-15, but the indenter is held at its maximum indentation position for a period of 10 seconds and the resulting hyperviscoelastic relaxation is recorded via the indenter's force sensor. Error bars denote one standard deviation from the mean of the three trials at each location.

the method of clamping the limb (11 of the indenters remained in contact with the limb during the entire duration of the experiment). The clamping force was readjusted – automatically, by sending a force request to the robotic controller – after each trial to account for the hyperviscoelastic relaxation of the residuum. If this force was adjusted just before each trial as well, some of these effects may be mitigated.

2.4.2 Difficulty in measurement of small bony prominences

The fibula head hyperviscoelastic response data show a much higher standard deviation across the three trials than the mid-posterior, mid-tibia, and patellar tendon plots in Figure 2-16. This higher discrepancy across trials is due to the difficulty of aligning the indenter (which has a 2 DoF head) exactly on the small bony prominence that defines the fibula head. As the indenter moves inward to take measurements, it may rotate around the fibula head differently at each measurement, making it difficult to take consistent readings at this location. Solutions to this problem include hemispherical indenter heads with no DoF and/or smaller indenter heads.

2.4.3 Future considerations for indenter head design

In general, after collecting hundreds of indenter samples using a 2 DoF indenter head, it is clear that a semi-spherical indenter head that is rigidly mounted to the load-transfer pin (A in Figure 2-3) would produce more predictable biomechanical data, especially if those data were to be used to inform finite element modeling of residua.

2.4.4 Data acquisition time and method

Data collection with a single subject takes roughly 60 minutes from subject arrival at the testing location to their departure. The actual measurement of 4 or 5 test locations takes 20-30 minutes. As stated in the methods, each location is measured three times, which each measurement taking 15 seconds, plus up to 60 seconds for measurement prep (measurement and subject information, verification of test and clamping forces, selecting the testing indenter, etc.) and any additional time between measurements for viscoelastic effects. While the multi-indenter system is capable of measuring with each of its actuators in sequence with only 15 to 20 seconds between each indenter, the purpose of the experimental data presented in this manuscript is to show the level of sensitivity of the device as well as the broad measurement affordances offered, so extra care was taken in the design of the experimental protocol and time was not a factor for minimization.

2.4.5 Comparison of clinical results to existing literature values for mechanical properties of human tissue

Data collected during the above experiments are consistent with those seen in existing literature. Considering that the exact data are dependent on the physical location of measurement on the body, the characteristic hyperviscoelastic shape, including viscoelastic properties are well represented in both data sets. Additionally, the data are well within the same order of magnitude in terms of force (or pressure) and versus displacement cross all cited and measured values.

2.4.6 Future considerations for full limb data capture

As previously referenced, a relatively high frame rate (15Hz), 3D imaging system would be capable of imaging the residuum during indentation. This would not only provide information about limb translation – allowing all indenters to measure the limb at once – but also provide surface deflection information and unloaded limb shape. These data could allow for nearly direct to socket measurements to be made – provided that a well-tuned, generalizable biomechanical FEA model of the residuum backs them.

2.5 Conclusion

In this manuscript, we demonstrate the ability of a multi-indenter device having 14 robotic indenters to measure data regarding the biomechanical properties (force, deflection, and time) of human, trans-tibial residua in vivo. We show that these data may be measured in a precise, repeatable way. Additionally we show that this method of indentation minimizes limb movement during measurement. We present data that depicts the hyperviscoelastic behavior of tissue undergoing orthogonal displacement and show the differences – both for force (N) versus displacement (mm) and for force (N) versus time (ms) – for four anatomical locations on a trans-tibial residuum: fibula head, mid-posterior, mid-tibia, and patellar tendon.

Chapter 3

The FitPen

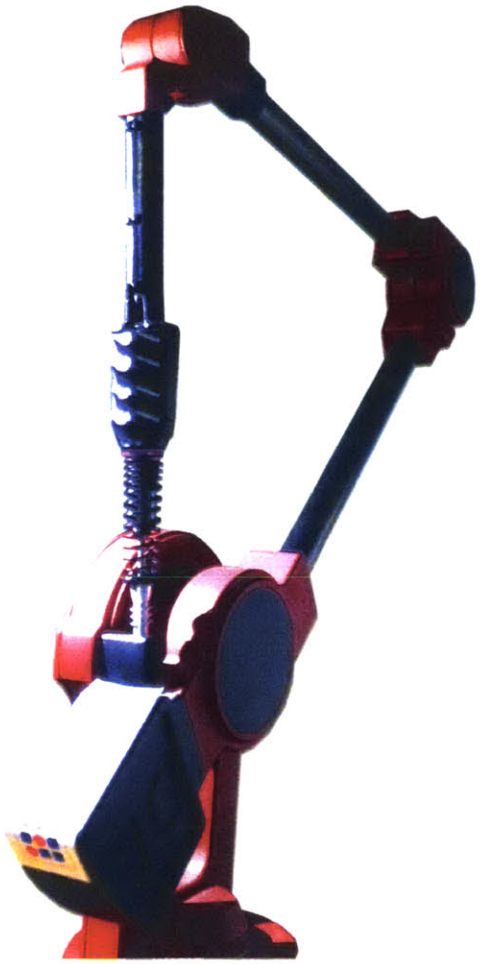

Figure 3-1: The FitPen is a portable version of the same measurement ideology as the FitSocket.

Another way of measuring stiffness is with a location aware object that has a force sensitive tip. Additionally, the body part under measurement must be tracked in the same three-dimensional reference frame as the measurement object (let's call it a pen). This pen can be placed on the surface of the human with varying forces, and since it is aware of its position, we are left with the same data as discussed in Chapter 2. Essentially, the FitPen is a single, passive indenter from the FitSocket with a smaller tip. In the current instantiation, the FitPen is mounted to a Microscribe x y z digitizer in order to know its position in spacetime while it is performing an indentation on tissue. Because the tip size is much smaller than that on the FitSocket, the indentation forces are low enough to negate whole limb movement events during testing. Additionally, the testing may be done in much more remote locations.

3.1 Preliminary Remote Testing

The FitPen was primarily designed to be a lightweight, transportable version of the basic capabilities of the FitSocket. To this end, it was taken to Nairobi, Kenya, and used to measure a person with unilateral, trans-tibial amputation at eight biomechanically distinct locations. The hosting prosthetist was very interested to see the different parts of the limb presented simply in terms of varying impedance on a simple graph. This basic proof of concept experiment showed that we can reliably discern between different impedances in different areas of a single subject, and quite likely, allow a prosthetist to quantitatively compare across his or her patients.

The positioning system can be physically connected to the pen, such as a structure of linkages similar to that of an industrial robot arm where each linkage has angle sensors that are capable of determining the exact position of the pen's tip from a grounded reference frame. In addition, the pen could have markers on its surface that can be seen by cameras. These cameras can be used to triangulate the position of the pen. The pen could also broadcast electromagnetic signals that are picked up by nearby electromagnetic sensors for the purposes of determining the position of the pen. The pen can use a combination of gyroscopes, accelerometers, and magnetometers to aid in determining its position.

The force data from the pen can be communicated wirelessly or wired. The wireless method can be IR-based, Bluetooth, or any other wireless communication method, such as an open electromagnetic frequency.

The location of the human body part under measurement can be determined in much the same way as the location of the pen. Using electromagnetic signals, accelerometers, gyroscopes, magnetometers, location markers for cameras, or any other location technology or combination of location technologies.

The pen could also have a force sensor that is either capacitive, strain-gauge based, resistive, or ultrasonic. Ultrasonic transducers on the pen's tip could be used to gather very detailed tissue density data during deflection in order to have a high fidelity measurement.

3.2 Hardware and Mechanical Description

The pen measures force with a simple spring and linear position measurement device (Bournes 3048 linear potentiometer) to know the deflection of the spring ($F = -kx$). The pen also contains a STM32 series microcontroller (Teensy3.1), capacitive sensor on the pen tip, LEDs for status indication, and serial communication with a host computer. The Microscribe 3DLX device also connects to the host computer, both through USB interfaces, to a Java program which combines the x y z location (and pitch, roll, yaw) of the FitPen's main body with the deflection information read by the FitPen itself. The result is a realtime plot of force versus deflection on the GUI of the Java program. These data may be saved as a CSV file and used in other applications such as Matlab or Excel.

At 17.7mm x 35.6mm, the Teensy 3.1 by PJRC is an Arduino, Maple, C, and C++ compatible development platform known for its very small size. It features a 72MHz, MK20DX256VLH7, Cortex M4 processor that is overclockable to 96MHz. This version of the Cortex M4 has 256kB of flash memory, 34 5V tolerant digital inputs/outputs, 21 analog inputs at 13bits resolution (12 of which support capacitive touch sensing), and SPI, I2C, I2S, CAN, and USB communication. These specifications make the Teensy 3.1 ideal for development and eventual deployment in a possible product, as the PCB only contains 26 components.

The Microscribe 3DLX is an off-the-shelf digitizer that can be controlled through c libraries included with the device. This code allows complete interaction with all the the serial level functions associated with the device.

The 3D printed body of the FitPen is designed such that it slides on to another 3D printed part that mates with the Microscribe 3DLX. This sliding interface also locks the two halves of the FitPen's main body together, simplifying the development and maintenance of the internals of the device. The spring mechanism is created from a modified type II alloy shock for the Axial AX10 Scorpion. In general, it was found that RC car shocks have a very good spring constant for use with human tissue displacement and are much easier to acquire than custom springs or off-the-shelf springs from a spring supplier[1]. One warning on using RC car shocks as linear springs: it is important to remove the damping fluid from the shocks before attempting to get a linear force-displacement response from them.

[1]This is because custom springs take over a month and cost a fortune, and off-the-shelf springs have ridiculously confusing specifications almost as if the manufacturers do not know what the units of stiffness are

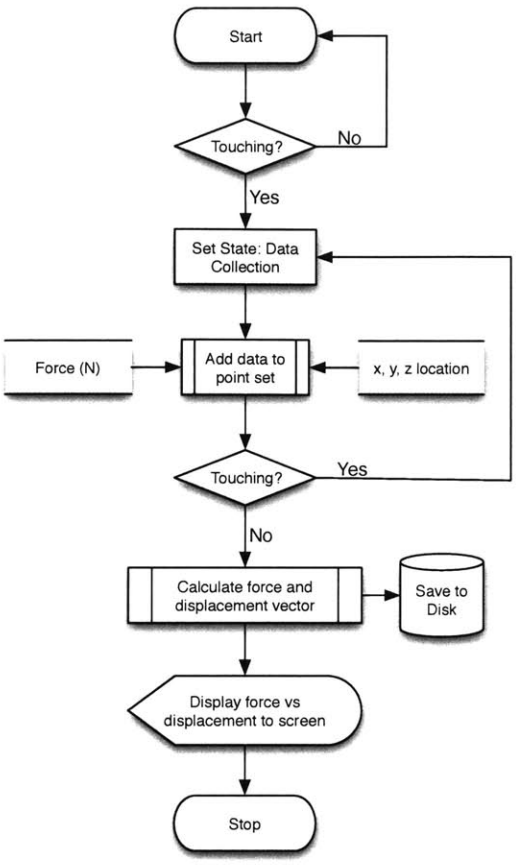

Figure 3-2: The FitPen software flow describes how the device collects biomechanical data.

The capacitive sensing tip of the FitPen was turned from a small round of 6061-T6 aluminum in with specific attention to accept a small copper disk and insulation layer for the sensor. In this way, the body of the tip is the ground electrode while the copper disk is subject to the charge rate sensing typical of charge-pump based capacitive sensors. It may be of interest to note that this very similar to how the projected capacitive touch screen on your smartphone works.

3.3 Software Description

The FitPen is software controlled using c on the embedded side and Java on the computer side. The Java displays a GUI that the user may use to control data collection while using the FitPen. Listing 3.1 details a function of particular interest in the calculation of force versus displacement in three-dimensional space. Because the FitPen is capable of moving in any direction in three-space, it is necessary to calculate the magnitude of the three-dimensional displacement vector at each measurement. This function is a helper function of the PointSet class, which relies on the Point class. The Point class is simply a data structure containing the four spatiotemporal variables – x, y, z, and time – and a fifth variable, force.

To begin, private arrays global to the class are initialized of the size of the ArrayList containing all the points. In the geometric fashion, the magnitude displacements between each successive point are calculated ($\delta d = \sqrt[2]{x^2 + y^2 + z^2}$) and added to the previous displacement. The displacements' corresponding forces are the average force between the two elements being used to calculate the magnitude displacement – since it would not make sense to use one or the other as there would then be a temporal mismatch between forces.

Listing 3.1: Calculation of Spring Constant

```
public double calculateForceDisplacementMagnitudes() {
```

```
    if (pointSet.size() < 2) return 0.0;

    distances = new double[pointSet.size()];
    forces = new double[pointSet.size()];

    for (int i = 0; i < pointSet.size(); i++) {
      forces[i] = pointSet.get(i).force;

      if (i == 0) {
        distances[i] = 0;
        forces[i] = 0;
      } else {
        double dx = (pointSet.get(i).x - pointSet.get(i - 1).x);
        double dy = (pointSet.get(i).y - pointSet.get(i - 1).y);
        double dz = (pointSet.get(i).z - pointSet.get(i - 1).z);

        distances[i] = distances[i - 1] + Math.sqrt(dx*dx + dy*dy + dz*dz);
        forces[i] = (pointSet.get(i).force + pointSet.get(i - 1).force) / 2;
      }
    }
  }
```

The resulting arrays may be used by other functions in the class since they are available to any function in the PointSet class. The resulting data are identical to those captured by the FitSocket and may be analyzed in much the same way. Because three to six distinct anatomical locations are able to inform the iFEA simulation created by David Sengeh and Kevin Moermon, the FitPen is a very useful device because it it much smaller than the FitSocket but able to collect (less precisely) the same type of data.

3.4 Future Work

The FitPen relies on a 3D digitizer arm currently in order to collect useful data. If the limb moves during this measurement, the data will not be accurate. The forces on the limb during a measurement applied by the FitPen are very low – on the order of 3N-5N – so they are unlikely to displace the bulk body part on which the measurement is taking place. Even so, an accurate optical distance measurement from the body of the FitPen device to the undeflected skin surface around the measurement site would be a better way to take measurements. The reason for this is twofold. First, the device would be agnostic to limb measurement during a test indentation. Second, the device could be much smaller because the digitizer arm is quite large compared to the rest of the FitPen device.

If the FitPen were coupled with a portable PC and an ultrasound probe to run biomechanical material optimizations during a test, the device would be capable of creating FEA type modeling information directly from measurements of the residual limb. This approach would require many more measurement

points, as the entire limb would need to be "scanned." The benefit of this approach is that a small, portable device that fits in a small case (including all equipment) could be capable of generating the necessary files to 3D print a quantitatively designed prosthetic socket. The addition of a three-axis force sensor on the tip of the FitPen would allow for shear measurements to be acquired in addition to linear force and displacement data.

Chapter 4

The Quasi-Passive, Variable Impedance Prosthetic Socket

Prosthetic sockets often cause pain for individuals with lower-extremity amputation. This pain is most often caused by poor socket fit due to either inaccurate initial fitting or limb volume change [Lacono et al., 1987, Molton et al., 2007, Davidson et al., 2010, Butler et al., 2014]. Current, commercially available prosthetic sockets are passive and therefore not adaptive to limb volume change or load transfer requirements of various activities — such as sitting, standing, walking, or running.

4.1 Introduction

Researchers have advanced active sockets that attempt to compensate for volume fluctuations in the residuum. State-of-the-art actuation strategies for sockets are accomplished through designs that feature pneumatic or hydraulic systems [Mak et al., 2001]. These systems address limb volume change through the inflation of flexible bladder elements either manually [Pirouzi et al., 2014, Montgomery et al., 2010b] or automatically, based on a sensor feedback configuration [Greeenwald et al., 2003]. These bladders may be actuated through negative or positive pressure. A recent patent application describes a combination of both negative and positive pressure inflation, dynamically during ambulation, using accelerometers to adjust the actuation of pneumatic valves in a vacuum socket system (VSS) type device [Galea et al., 2012].

Figure 4-1: The VIP socket shown being worn by a test subject on their left leg.

These active, pneumatic and hydraulic systems — while quite powerful — suffer the primary drawback of high added mass to the prosthesis. Increased noise is also a concern [Martin et al., 2012]. Further, while current work seeks to address pain primarily due to poor socket fit, it does little to address ischemia type deep tissue damage caused by the chronic pressure field applied to the residuum by temporally static prosthetic sockets [Stekelenburg et al., 2008]. Tissue degeneration typical to trans-tibial or trans-femoral residua [Portnoy et al., 2007a] include decubitus ulcers, deep tissue breakdown, and flap necrosis. These edema can, in the dark, moist environment of the prosthetic socket, quickly lead to serious infections and, if left untreated, to further amputation. Spatially varied impedance prosthetic sockets can be employed to reduce peak pressures on bony prominences [Sengeh and Herr, 2013a], but are unable to address temporally varied loading requirements of the wearer.

A seated or standing individual with lower extremity amputation need not transfer high forces to their prosthesis during activities such as sitting or quiet standing. These activities require a socket whose interface pressure on the residuum is lower in order to prevent ischemia type deep tissue damage — such as tissue acidification or glucose depletion [Stekelenburg et al., 2008]. Spatiotemporally static, elevated vacuum sockets fare relatively better at reduction of deep tissue damage than patellar tendon bearing or other hyperdiastollic pressure sockets [Gefen et al., 2013]; however, we hypothesize that spatiotemporally variable impedance socket positively affects a reduction in deep tissue damage through shear and pressure strain relief, and fluid flow redistribution.

In this study we advance a variable impedance socket that is low power and weight. A novel VIP socket design is demonstrated, providing reduced impedance during times of low versus high force transfer requirement for normal prosthesis use. This micro-controller, feedback controlled socket utilizes quasi-

passive actuation to accomplish temporal variation in impedance. The device uses an electrostatic clutch to modulate the impedance of the proximal- and distal-tibia regions of the socket–residuum interface. On a test participant with transtibial amputation, the socket is evaluated through sit-to-stand tests to determine the viability of computer-controlled electrolaminate engagement, and through a walking study to evaluate the ability of the electrolaminates to maintain their clutched state during ambulation at a self-selected walking speed.

Figure 4-2: The variable impedance socket shown without (left two images) and with (right image) its cosmetic and protective cover.

4.2 Method

The VIP socket employs elastomeric, dielectric clutches to accomplish stiffness control over the upper and lower tibial crest. These custom clutches are created from a specific layering of flexible conductive and insulative materials such that two thin electrolaminate sheets will — when provided with the correct voltage of 400V–800V DC[1] — electrostatically attract each other sans arcing. This electrostatic attraction causes an increase in the normal force to which the coefficient of static (0.3) or dynamic (0.2) sliding friction between the two electrolaminate strips is directly proportional. The increase in normal

[1]This voltage is highly dependent on the humidity of the environment in which the electrolaminates are performing.

force, and thereby, friction is substantial — resulting in effective electrostatic clutching of greater than 100N.

The use of elastomeric and/or nonelastomeric dielectric clutches add actuation or quasi-passive clutching to a VIP socket [Kornbluh et al., 1999]. This type of actuation or clutching is silent, low power, and low mass [Kornbluh et al., 2000]. SRI in Menlo Park, CA, has developed electrostatic clutches called electrolaminates, a microcontroller-actuated impedance variation technology (see Figure 4-3). Electrolaminates widely vary their impedance by more than two orders of magnitude while allowing for greater than 100% strain deformation. Further, electrolaminates operate quickly over a wide range of environmental conditions and consume very little power (<1mW) [Fitch, 1957].

The supply voltage to the electrolaminates is provided by two custom control printed circuit boards (PCBs) that feature a microcontroller, a 3-axis accelerometer, a radio, a battery management module, a high voltage production and sensing module (to drive two electrolaminates), two electrolaminate clutch position sensors, and two FSR type force sensors (located on the distal tibia and fibula head). The two PCBs and a 3.7V, 3.1Wh battery weigh a total of 45g. Each electrolaminate strip weighs 1.0g. All components including mechanical hinges, wiring, etc. weigh a total of 220g.

4.2.1 Electrolaminate and Mechanical Specification

Electrolaminates operate by changing the mutual attraction of layers in a laminated composite structure. This change in mutual attraction is accomplished by holding an electrostatic charge between the layers. As such, they can vary their stiffness from that of the softest material in the composite to that of the most rigid material in the composite. The softest materials are elastomers (or elastic fabrics) and the rigid materials are structural plastics. It is important to note that these rigid layers are typically thin and flexible. This flexibility is important in that it allows the clamping layers to form intimate contact and thus increase the clamping forces. The basic configuration employed on the VIP socket was a simple strap that slid along a curved, hinged, rigid arm. The tibial region of the socket interacts with this arm at the center through a stiff interface that transfers the forces exerted by the tibia to the electrolaminate system (see Figure 4-4).

4.2.1.1 Electrolaminate Specification

Electrostatic clamping can be a complex phenomenon and many factors are involved in determining the electrostatic clamping forces including the hardness, surface roughness and bulk, and surface conductivity of the interfacial layers. Typically, the interface is loaded in shear and so the frictional properties of the interface are critical. The electrolaminates developed for the VIP socket use clamping based on the Johnsen-Rahbek effect. The Johnsen-Rahbek effect allows for large clamping forces. This high force is due to the fact that the clamping is generated across the air gap between the two interfacial layers. If the dielectric coating (25µm–50µm thin) on the interfacial layers is slightly conductive then the charge travels to the surface of that layer and its thickness can be largely negated. The coating is based on a novel formulation of intercalated metal-oxide particles in a polymer matrix. Because of the dielectric properties of the coating, the electric field is applied only across the air gap. The thickness of this air gap is determined by the surface roughness of the materials at the interface. This surface roughness also minimizes the current flow across the interface and so there is a tradeoff between current flow and the magnitude of the electric field.

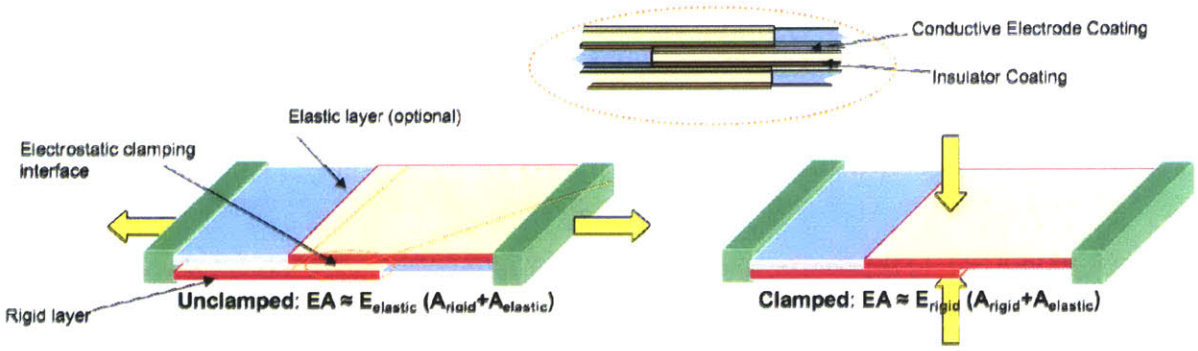

Figure 4-3: The electrolaminate clutch device works by electrostatic attraction between two thin conductive layers that are separated by an insulator. A series elastic element provides a restorative force when the clutch is stretched. This image is based on the original image by Roy Kornbluh, SRI

The dielectric surface clamped to a second surface that was a commercially available conductive polyimide film that was 50µm thin. In order to reduce the voltage drop associated with charge propagation over the length of this film, the backside (non-clamping surface) was spray-coated with a nickel particle-based conductive coating so that the resistance from one end of the strip to the other was less than $1M\Omega$. The electrolaminates function well from about 20% to about 80% relative humidity. Operation in drier or more humid environments would require environmental sealing such as offered by covers and/or fairings.

4.2.1.2 Mechanical Specification

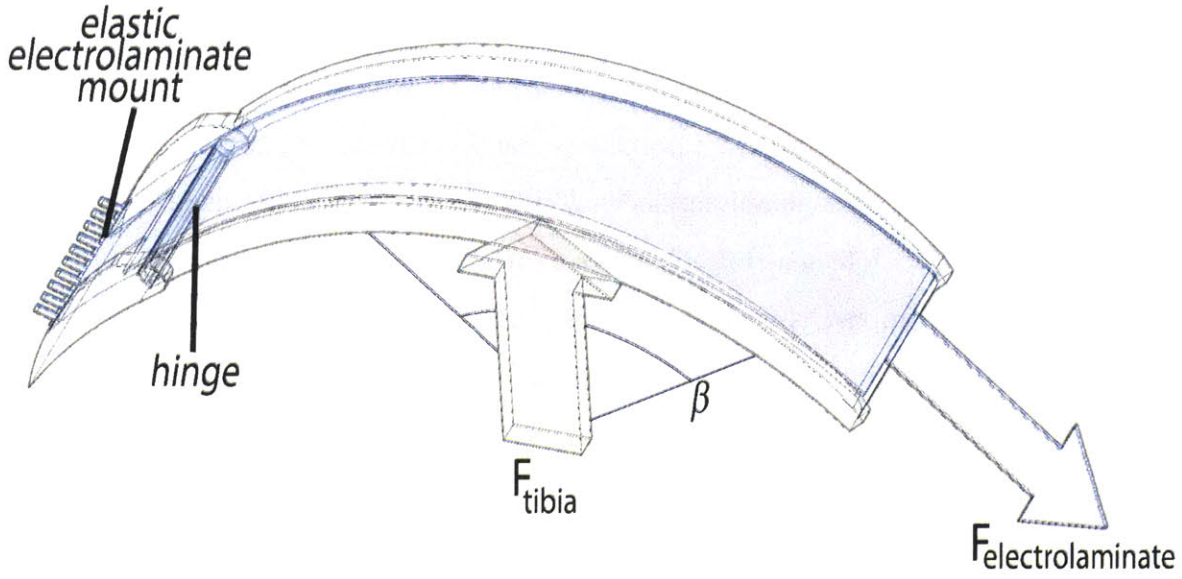

Figure 4-4: This diagram of one of the two hinge assemblies on the VIP socket helps to illustrate how the mechanism is able to use the capstan effect and levers to achieve a greater holding force than the electrolaminate can support on its own.

Based on force measurements both using a Tekscan F-Scan pressure measurement system (Model 9833, Teksan Inc., Boston, MA) and those using similar systems in literature [Appoldt et al., 1968, Pearson et al., 1974, Mak et al., 2001, Maurer et al., 2003, **?**, Pirouzi et al., 2014], the maximum mechanical load requirement at each quasi-passive electrolaminate clutch was 200kPa. The clamping strength parameter was derived through the physical parameters of the VIP socket mechanism — including the capstan effect — primarily,

Listing 4.1: Determination of Load Requirements

$$
\begin{aligned}
F_{electrolaminate} &= \frac{P_{tibia_{max}} A_{tibia}}{2e^{\mu\beta}} \\
F_{electrolaminate} &= \frac{F_{tibia}}{2e^{\mu\beta}} \\
F_{electrolaminate} &= \frac{200kPa \times 1.5 \times 10^{-3} m^2}{2 \times e^{0.3 \times 1.396 rad}} \\
F_{electrolaminate} &= 99N
\end{aligned}
$$

where $P_{tibia_{max}}$ is the maximum pressure provided by the tibial region by the residual limb on the corresponding area A_{tibia}, μ is the coefficient of static friction for the electrolaminate, and β is the angle of incidence between the two sliding portions of the clutch mechanism. The factor of two comes from the fact that the tibial region is applying a force on the capstan at half the length of the entire capstan

mechanism — creating a lever arm (see Figure 4-4).

The tension requirement derived in Listing 4.1 allows for the specification of the size of the electrolaminate straps (See Table 4.1) necessary to achieve clutching at a shear tension of 100N. The electrolaminates are able to maintain a clutched state with a shear force of 53.3kPa, resulting in the area requirement of $1.88^{-3}m^2$. The operating voltage must be kept below 1000V due to arcing and hardware availability[2]. The clamping time should be at most one-tenth of the time required to stand from sitting. Testing of a fast stand activity on biologically intact individuals (n=15) resulted in an average stand time of 0.55 seconds. Power dissipation should be kept below 100mW in order for the 3.1Wh battery powering the device to last for an entire day. If the device is using its radio, the power requirements are above 100mW but the radio is required for tuning and data collection purposes only. Based on an estimated 125 on-off cycles of the electrolaminates each day, the electrolaminates should last over two years; however, bench-top testing has shown that the electrolaminates may last up to twenty years. The humidity tolerance of the electrolaminates need to be as high as possible in order to cope with varied weather conditions. Unfortunately this requirement was not met, as the electrolaminates are extremely sensitive to changes in humidity. The stiffness of the material comprising the electrolaminates should be of relative stiffness to the prosthetic socket itself, or 1Gpa. The peak current at the electrolaminate must not exceed 1mA. This is primarily for electrical safety, as 1mA at 1000V, while reasonably shocking, is not dangerous[3]. Note that the achieved peak currents are substantially lower than 1mA.

The impedance map of the VIP socket shown in Figure 4-5 shows the many elements whose elastic properties should be taken into account during the design of the device. In particular we want to control the deflection of the tibial region of the residual limb (Callouts A and B) using computer control of the variable impedance prosthesis. The spatially varied impedance socket material (Callout C) has been thinned in the are of the tibia in order to reduce viscoelastic contributions and increase the elasticity. The electrolaminate attachment anchor (Callout D) is permanently attached to the carbon fiber shell of the VIP socket (see Figure 4-1) and is thus high stiffness. The electrolaminate return elasticity (Callout D) is relatively low; however, this elasticity is tuned to apply just enough restoring force for the clutch mechanism to return to its starting position even while worn by a user. This elasticity may be increased if the steady-state pressure on the wearer needs to be increased. The parallel elasticity (Callout F)

[2]It is quite difficult to acquire very small DC-DC buck converters that will allow for >1000V due to the inductive element requirements

[3]The author of this manuscript has tested this empirically and found that – if the device is fully assembled – it is nearly impossible to shock oneself. Capacitors hold charge for a long time.

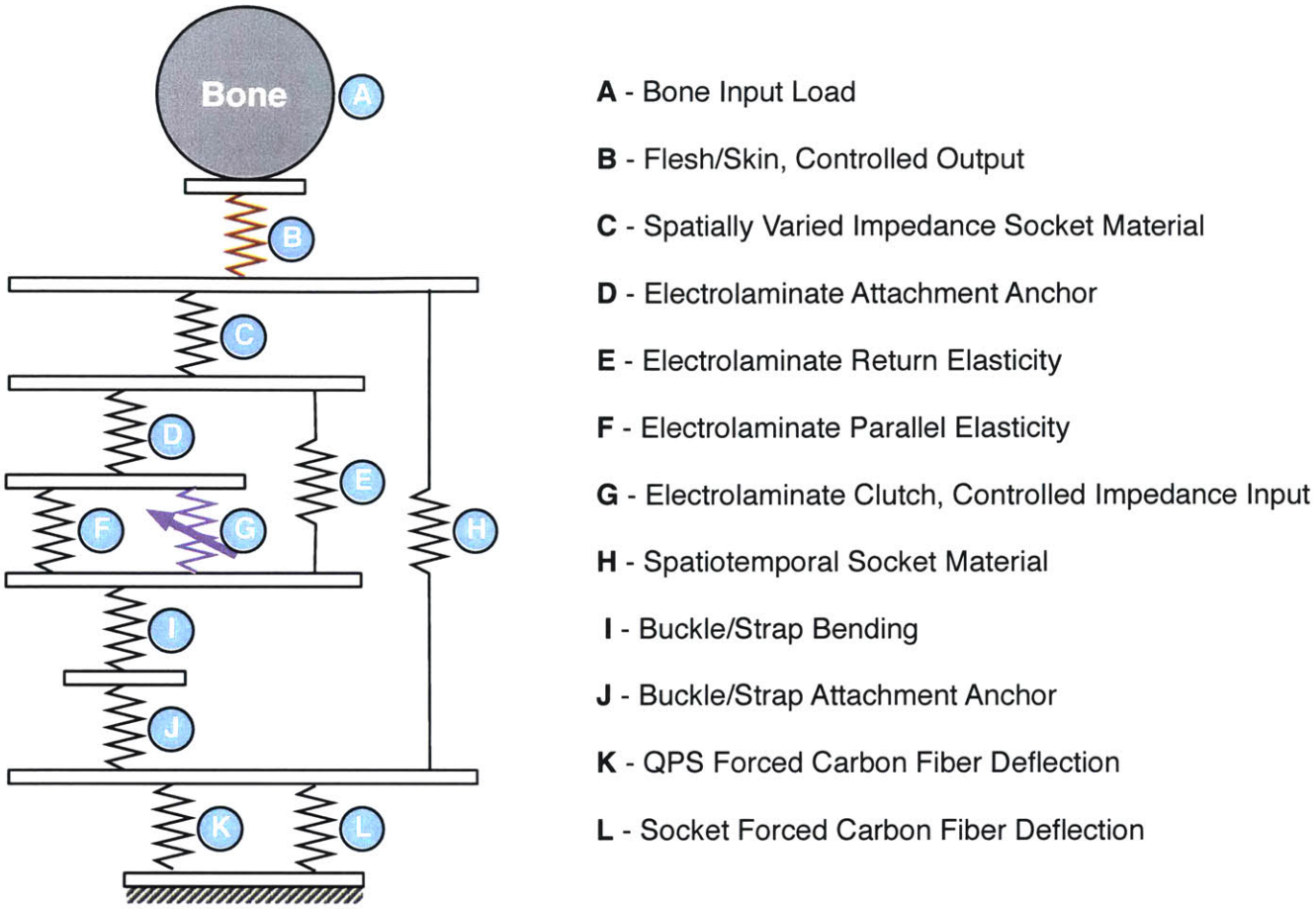

Figure 4-5: This spring diagram shows the mechanical impedance map for the entire VIP socket assembly. The red spring is the human wearer of the VIP socket while the violet spring is the electrolaminate control. All other impedances in the system were designed to amplify the effect of the electrolaminate clutch device.

is controlled to be very stiff by selecting electrical insulator material of high Young's modulus (see Table 4.1). The electrostatic clutch (Callout G) is able to electronically change from a state of zero elasticity, very low impedance (driven by friction), to a state of extremely high stiffness. There is a very stiff mechanical loading pathway from the tissue of the residual limb through the socket materials (Callouts H, K, L) to the rest of the prosthesis. These materials are made of carbon fiber, aluminum, and verowhite+ (Stratysis 3D printer material). The buckle (detail in Figure 4-4) is made of aluminum; while it does bend under load, the amount of deflection is quite low ($5 \times 10^{-3} mm$).

Table 4.1: Electromechanical Functional Requirements of the VIP Socket System

Parameter	Requirement	Achieved	Comment
Size	25mm x 75mm	25mm x 88mm	Size fits on VIP socket and achieves desired strength.
Operating Voltage	≤1000V	≤1000V	Voltage requirement depends on relative humidity.
Clamping Strength	100N	≥100N	Based on 200kPa max normal pressure for area of contact.
Claming Time	50ms	50ms	Benchtop test. Requirement to stiffen before full weight-bearing.
Clamping Power Dissipation	<100mW	10mW - 100mW	Power dissipation dependent on relative humidity.
Lifetime	>100,000 cycles	>1,000,000 cycles	Benchtop Test. Requirement based on estimated usage.
Humidity Tolerance	10% - 90%	20% - 80%	Tested at 20C. Performance is better at lower humidity.
Maximum Stiffness	1GPa	1GPa	Electrolaminate stiffness only. Defined by stiffness of polyamide.
Peak Current	<1mA	0.1mA - 0.2mA	Peak current dependent on relative humidity. Requirement for electrical safety.

4.2.2 Electrical and Software System Specification

The following is a brief description of the primary components that make up the controller circuit. The controller circuit is implemented in two separate PCBs. The mother-board contains all of the major circuitry and is able to function without the daughter-board. The daughter contains the XBEE radio, indicator LEDs, and the 9-pin 0.1" header connector for the external analog sensors. This header connector, along with a 3-pin connector on the mother-board, blind-mate with female headers in the back of the receptacle for the controller circuit.

The mother- and daughter- boards which implement the controller circuit are packaged into a 3D printed enclosure which slides into the base of the VIP socket. Guides allow for easy insertion and removal of the circuit while ensuring connectivity with the electrolaminates and sensors integrates into the the socket itself. Wiring under the surface of the 3D printed part run towards the buckle hinges where they interface with wires from the electrolaminates and extension sensors. Figure 4-6 details the overall module connections for the VIP socket control circuit.

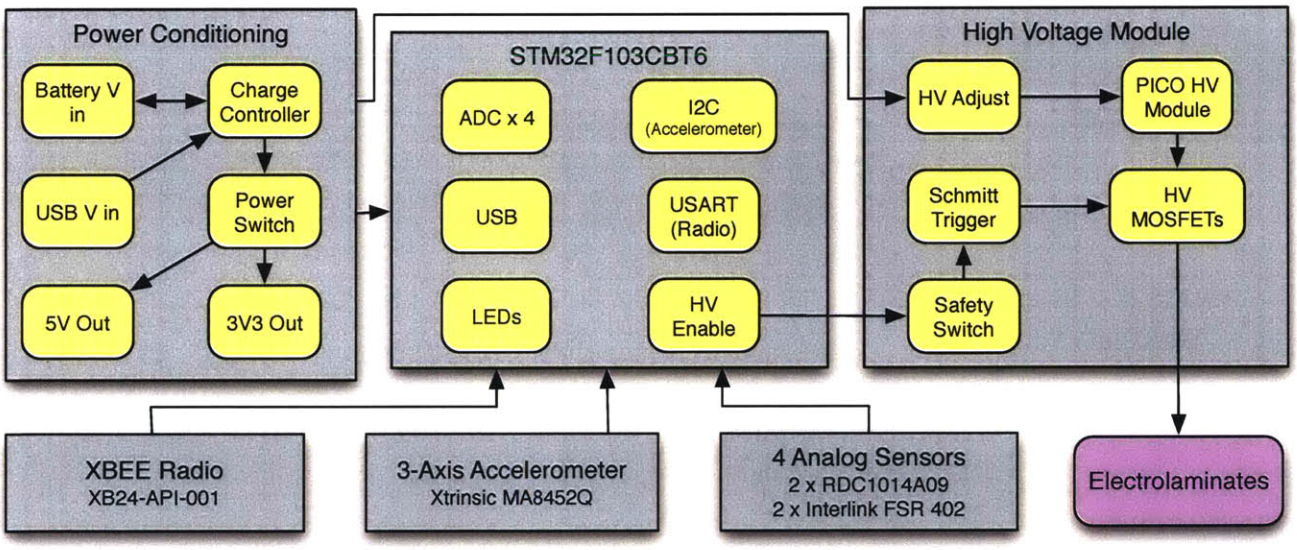

Figure 4-6: The basic module connections of the VIP socket controller circuit. Because of the many different voltage requirements, power handling is a large part of the PCB.

The overall system controller is a 72MHz ARM Cortex-M0 microcontroller that reads inputs from the accelerometer over I2C, utilizes 4 12-bit ADC channels to read additional sensors integrated into the VIP socket, and processes digital and analog sensor data and actuates electrolaminates via high-voltage N-MOSFETs accordingly (STM32F103CBT6, STMicroelectronics, Geneva, Switzerland). A momentary

Kornbluh SPDT safety switch allows for instant cut-off of power to the electrolaminates in case the user experiences discomfort due to the clamping action of the VIP socket (ED903, Switchcraft Inc., Chicago, IL). A 12-bit digital 3-axis accelerometer allows information about the movement of the VIP socket to be related to the control algorithm (Xtrinsic MA8452Q, Freescale Semiconductor Inc., Austin, TX). The high-voltage DC/DC step-up converter used to power the electrolaminates can operate between 400V - 1000V (5AV1000, PICO Electronics Inc., Pelham, NY). Communication through a XBEE 802.15.4 radio is used to transmit wireless telemetry (XB24-API-001, Digi International Inc., Minnetonka, MN). A linear battery charge management controller in a SOT-23-5 package suitable for USB charging keeps the charging circuit small and simple (MCP73831T-2ACI/OT, Microchip Technology Inc., Chandler, AZ). Linear potentiometers are used for position sensing of the electrolaminate buckle's displacement (RDC1014A09, Alps Electric Inc., Santa Clara, CA). Interlink 12.7mm (0.5") active area force sensitive resistors are used for pressure sensing within the socket (FSR 402, Interlink Electronics Inc., Westlake Village, CA). A 3.1Wh rechargeable lithium ion battery is able to power the VIP socket for over 36 hours (6SP063048, Wisdom Industrial Power Co. Ltd., KL, Hong Kong). 4.5kV photovoltaic optoisolators for high voltage controller isolation make sure that the high voltage circuit does not interfere with the TTL logic (VOM1271T, Vishay Intertechnology Inc., Malvern, PA). A dual inverter with Schmitt-trigger inputs to drive the high and low side high voltage MOSFETs automatically handles turn on and turn off timing for the 'FETs (74HC2G14GW-125, NXP Semiconductors, Eindhoven, Netherlands).

Sensor telemetry as well as electolaminate state (on/off) is available for viewing and recording via both wired and wireless (802.15.4) connections. The control system consists of a main board and daughterboard. The main board that has a microprocessor, battery charger, 3-axis accelerometer, USB port that is used for charging and wired telemetry, HV control electronics, 4 12-bit analog input channels (for sensors). The high-voltage electronics output up to 1000V. The high-voltage electronics use a commercially available DC-DC converter. A daughterboard has a Digi XBEE 802.15.4 radio that transmits telemetry packets every 20ms for system monitoring. The compact sensing and control circuit was packaged it into a box that slides into the base of the VIP socket. Guides allow for easy insertion and removal of the circuit while ensuring connectivity with the electrolaminates and sensors located on the socket. Wiring under the surface of the 3D printed part run towards the buckle hinges where they interface with wires from the electrolaminates and extension sensors.

The VIP socket has a resistance-based linear position sensor located on the upper surface of the buckles

and senses bending relative to the fixed hinge block on the shell. There are two force sensing-resistor (FSR) pressure sensors on the socket that also communicate with the sensing and control circuit. One is located on the upper surface of the soft material in the tibial region to measure pressure in that region. The sensing and control circuit accepts the analog inputs from the sensors. A rechargeable lithium ion battery pack (3.1Wh) internal to the sensing-control housing supplied power to the sensing-control board and electrolaminate driver board. The battery may be recharged using a USB cable attached to the front of the circuit (whether it is plugged into the socket or not). This same port is also be used for wired data transfer. The battery can provide operation for over 36 hours.

4.2.3 Clinical Experimental Design

The function of the VIP socket was validated with a single subject (bi-lateral, trans-tibial amputee; age 50) during treadmill walking, and in sit-to-stand-to-walking tests. The treadmill walking tests were conducted using long term on and off states in order to evaluate the deflection of the tibial crest region during walking in both states. The sit-to-stand tests evaluated the effectiveness of the simple control algorithms to provide the necessary stiffness required to control the prosthesis during the transition to standing, and eventually walking. Two different algorithms were tested. The first used the accelerometer readings of the two accelerometers in the saggital plane to determine if the upper leg was in a horizontal (sitting) or vertical (standing) position. The second used a combination of all three accelerometers to determine motion, which triggers the electrolaminates to turn on for a period of one second after any motion occurs. In other words, the electrolaminates will continue to stay on as long as motion of the VIP socket is present. The subject in the study (male; bi-lateral, transtibial amputation; age 50) was able to turn off the supplied voltage, thereby disengaging the electrolaminates at any time by releasing the momentary switch he was holding for safety. The participant in this study was consented through a research protocol approved by the Committee on the Use of Humans as Experimental Subjects (COUHES) through the Massachusetts Institute of Technology (MIT).

4.2.3.1 Sit to Stand - Angle Sensing

The sensing-control circuit was programmed to detect whether or not the wearer was seated or standing through accelerometers in the saggital plane for the purposes of sensing angle. If seated, the angle

indicates such and no voltage was applied to the electrolaminates and the impediance in the tibia region was low. If the subject stood up, the angle would change past a "stand threshold" and 720V was applied to the electrolaminates causing them to clamp and create a high impedance in the tibia region. The green light on the sensing and control circuit indicates that the sensors have detected that the individual is standing. While seated, the subject was asked to move his residuum in order to deflect the tibial region of the VIP socket. The subject was then asked to stand and repeat the same residuum movement. The differences in deflection were recorded in order to determine the effectiveness of the control algorithm. Data were analyzed using Logger Pro software to analyze the video taped experiments. A known distance was compared to the distance between the electrolaminate buckle and a reference point on the socket in order to report results in SI units. Sixteen trials were completed.

4.2.3.2 Sit to Stand - Motion Sensing

The sensing-control circuit was programmed to detect whether or not the wearer was seated or standing through accelerometers in all three orthogonal axes for the purposes of detecting bulk movement. If seated, no motion was detected and no voltage was applied to the electrolaminates and the impediance in the tibia region was low. If the subject stood up, the accelerometers would detect motion and 720V was applied to the electrolaminates causing them to clamp and create a high impedance in the tibia region. The green light on the sensing and control circuit indicates that the sensors have detected that the individual is standing. While seated, the subject was asked to move his residuum in order to deflect the tibial region of the VIP socket. The subject was then asked to stand and repeat the same residuum movement. The differences in deflection were recorded in order to determine the effectiveness of the control algorithm. Two trials were completed.

4.2.3.3 Walking

Walking trials (12 gait cycles in the on state, 6 gait cycles in the off state) were completed using manual control of the electrolaminates in order to evaluate the difference in deflection of the tibial region between the on and off states of the electrolaminates. The subject was asked to walk at self-selected speed (1.50 m/s) and the electrolaminates were turned on for 4 gait cycles and off for 2 gait cycles for a total of 18 gait cycles. The trial was video taped and the resulting deflections were displayed on a

portable computing device in real-time held next to the subject (as well as the on-off switch for the electrolaminates). Logger Pro software was used to analyze the video, separate gait cycles, and plot the corresponding electrolaminate displacements in each frame of the recorded video. Because some camera motion occurred during filming, reference points were used to create reliable relative measurements of these data rather than absolute points alone, which would be prone to error.

4.3 Results

4.3.1 Sit to Stand Results

Quantitatively, both sit-to-stand algorithms performed statistically the same. The walking study also shows statistically significant differences between the clutched and unclutched states. The average forced deflection during sitting was 6.55mm with a standard deviation of 1.69mm while standing deflection was on average 2.08mm with a standard deviation of 0.60mm. Subjectively, the wearer indicted that he could indeed perceive the difference between the clutched and unclutched states. He believed that the effects of clutched and unclutched in this manner were desirable.

4.3.2 Walking Study Results

The walking data show a significant difference in deflection between the clutched and unclutched states of the electrolaminate. Figure 4-7 shows that when the electrolaminate is unclutched, or off, the deflection data of the tibial region show an average, unclutched deflection of 16.35 times that of clutched deflection and a maximum unclutched deflection (3.71mm$\pm$0.90mm) of 16.56 times that of the maximum deflection while clutched. As is typical for gait data, the deflection drops around 64% as the subject enters swing phase with the VIP socket. Additionally, we can observe the double peak nature of the unclutched curve and determine that it agrees with typical walking tibial force curves seen in literature. While the electrolaminate is a clutch based device, the return spring stiffness provides sufficient restoring force to keep the electrolaminate tight on the tibial region when the device is clutched.

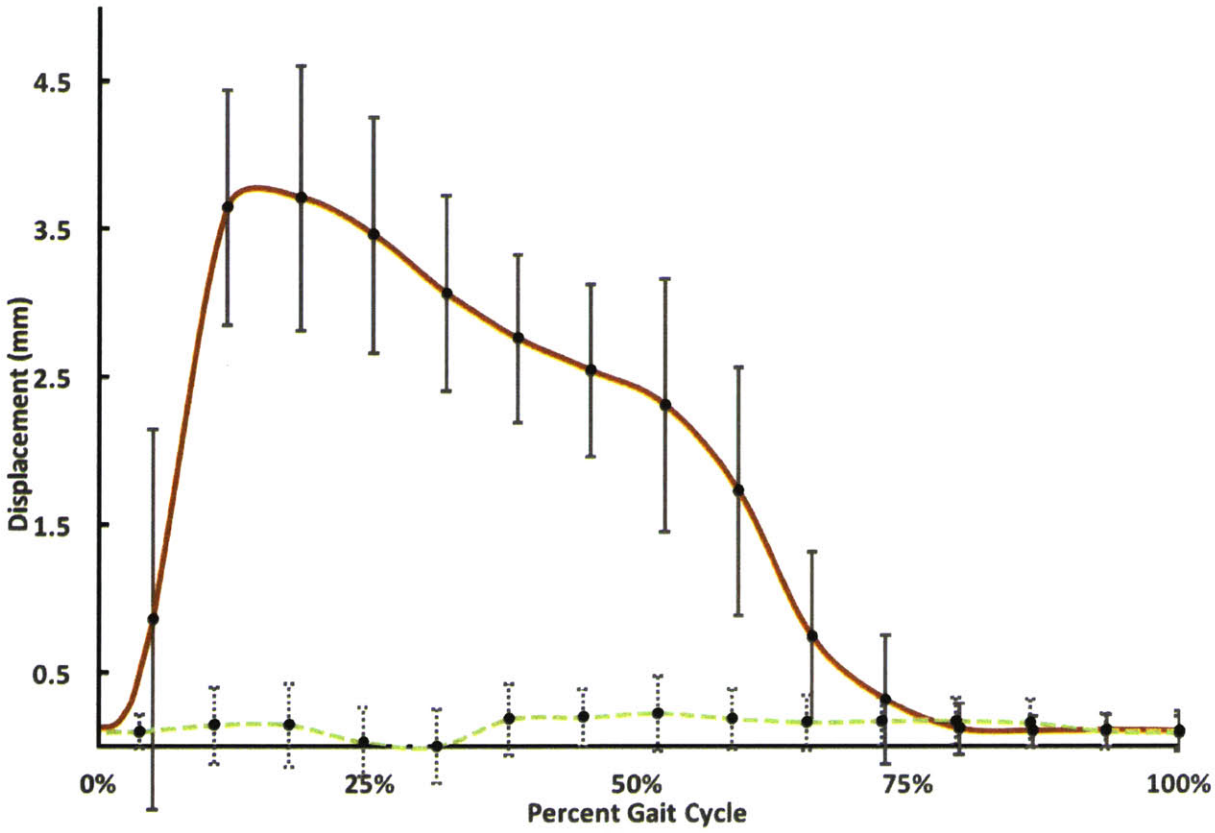

Figure 4-7: This graphs shows the deflection of an electrolaminate buckle as a function of gait cycle for the clutched (lower line) and unclutched (upper line) states. Twelve gait cycles were measured in the clutched state while six gait cycles were measured in the unclutched state.

4.4 Discussion

The basic functionality of the VIP socket (the ability to automatically control stiffness in the tibial region of the socket) was successfully demonstrated when worn by an individual with amputation. The VIP socket design was enabled by thin and flexible lightweight electrolaminate straps that were able to clamp and unclamp with sufficient strength to support normal activity without slippage. Each electrolaminate weighs a single gram. With all components that were added to the VIP socket in order for it to function, the total added weight was 220g. This included a radio, large battery, etc.

4.4.1 Refinement of the control algorithm to respond more fully to a variety of activities

Refinement of the control algorithm could provide affordances for a ratcheting type of effect. In this case, as the limb enters swing phase, the electrolaminate would unclutch and then clutch just before heel-strike. In this way the socket would take advantage of the negative force applied to the socket during swing phase to tighten the electrolaminate straps around the limb. This ratcheting effect would obviously only tighten to a certain amount – at which point the physical conditions would not allow for further tightening. Other algorithms may differentiate between sitting, standing, walking and running. The motion algorithm presented groups sitting and standing still together as "no motion" and walking and running together as "motion." This algorithm tended to work well; however, the addition of a full IMU on the control circuit would allow for real-time estimation of activity state and gait cycle location.

4.4.2 User acceptance testing on several individuals to further refine the design

The VIP socket was tested on a single subject, and as such, quantitative data are limited. A lighter weight, more robust version of the VIP socket could be more widely distributed and thus provide a clearer idea of the benefits of this spatiotemporally varied impedance technology. Instead of opening the shuttle lock of their prostheses, individuals with amputation would be able to simply sit down and their prostheses would relax for them. This technology may have application in those whose amputation is due to vascular disease.

4.4.3 Identification of additional socket areas that could benefit from stiffness control

In addition to the tibial region, the fibula head and distal end regions of the prosthetic socket may benefit from stiffness control. In general, areas that typically experience high pressures during prosthetic socket use are most likely to benefit from temporally varied mechanical impedance. Perhaps less obvious, regions that are along major blood flow pathways may also see a benefit from this type of approach.

4.4.4 Lifetime and robustness testing of the integrated socket

Humidity and the drastic effect it has on the performance of the electrolaminates is the primary lifetime and robustness concern with this device. Future designs will need to be environmentally sealed in order to prevent these effects, as it is otherwise impossible to negate the effects of moisture content in the air when utilizing an electrostatic device. Unexpected increases in humidity will cause the electrolaminates to arc across their layers – which permanently damages them. They can be repaired after such an event quite easily. In addition to environmental sealing, a robust current controller on the output of the device should be implemented. This task is surprisingly difficult as the output is generally 400V - 1000V, far too high for any of today's ICs.

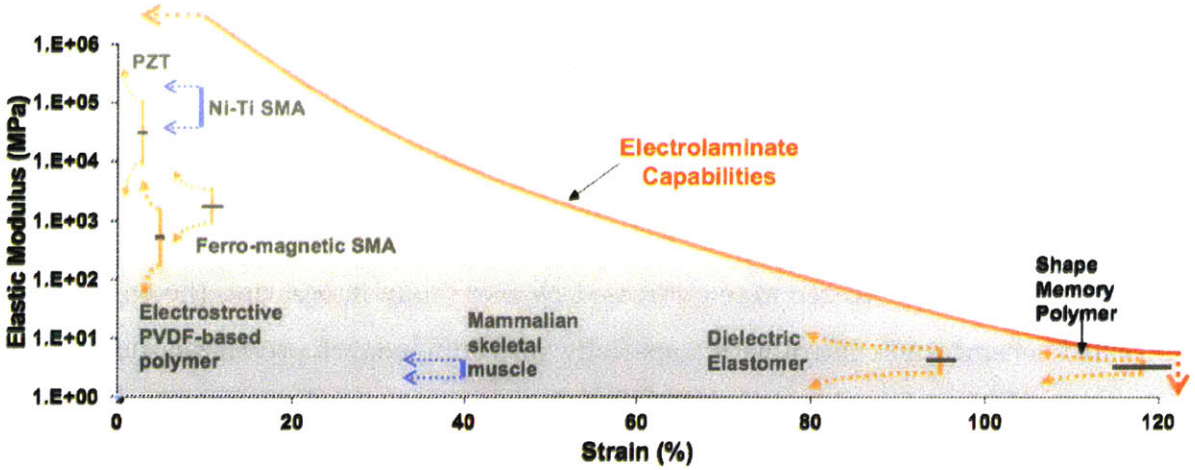

Figure 4-8: A comparison between electrolaminates and other methods of clutching in terms of elastic modulus versus strain.

4.4.5 Advantages over other methods of clamping

Aside from electrostatic clamping, one can imagine a few other viable methods for achieving a similar effects. These include motor and solenoid actuation (electromagnetic methods), piezo-electric clutches, pressure driven clutches[4], and chemical clutches. Of these, we generally consider electromagnetic-based clutching methods to be too heavy in general in addition to requiring much more power to drive. The electrolaminates in this work require less than 1mW to clutch. Chemical methods have yet to be explored as a viable alternative to electrolaminates, but one could imagine a bi-stable dielectric chemical

[4]Pressure driven clutches will also require a electromagnetic component, but are different enough to be considered separately

clutch. Piezo-electric devices are a good alternative to electrostatic clucthing. See Figure 4-8 for more information.

4.5 Conclusion

The quasi-passive socket seeks to increase comfort, reduce pain, and increase health for those who chronically use lower extremity, transtibial prosthetic sockets by regulating the pressure on certain areas of the residuum temporally through the use of electrostatic clutching mechanisms called electrolaminates. To put it simply, the socket aims to reduce the mechanical impedance in the tibial area when the socket wearer does not require high-fidelity load transfer between their residuum and their prosthesis.

The mechanical design allows for support of shear loads in the controllable stiffness region as well as decrease the friction and increase the stiffness. The performance and durability of the electrolaminates straps themselves is sufficient for use in a transtibial prosthetic socket.

The needs of the VIP socket wearer were addressed by more fully integrating the controllable stiffness functionality and sensing and control with a spatially varied impedance prosthetic socket. The goal was to add the stiffness control functionality without adding any significant mass, bulk, or logistical burden. It is believed that electrolaminate-based clamping system enabled the VIP socket to meet this goal. The resulting VIP socket successfully demonstrated the potential of adding temporal stiffness control to a socket.

Chapter 5

Conclusion

In this thesis, the field of digital, lower extremity, prosthetic socket design is defined and projects on the two opposite sides of the field work flow are presented. To review, the workflow is, in its simplest form, the basic experimental method. Following a defined hypothesis whose purpose is to address pain and health caused by the socket-human interface, data are collected, processed, and used to create a socket that may be tested with an individual with lower extremity amputation. The FitSocket and FitPen are data collection apparatūs. The Quasi-Passive Socket is an instantiation of data collection, processing, fabrication and quasi-passive algorithmic control implemented in a spatiotemporally varied impedance socket. With the exception of the FitPen, the projects presented were many year efforts that were completed simultaneously. In this way, increased understanding about how to measure an individual with amputation – or simply the hyperviscoelastic mechanical response of human soft tissue – allowed for increased specificity of hypotheses regarding all aspects of research.

5.1 Summary of the Thesis

The review of the field of digital socket design covers the current state of the art in lower extremity prosthetic socket design, improvements thereof, the measurable, quantitative benefits offered through data driven socket design, and the ways that these processes may be used for other applications other than prosthetic socket design – such as shoes, bras, backpacks, etc. The problems with the current state of the art are described in detail through a more thorough epitomization of traditional socket

manufacture, the specifics regarding the pain that those with lower extremity amputation experience day-to-day, the functional requirements of a socket that is hypothesized to reduce that pain and an exploration into the specifics of these functional requirements, and a brief summary of materials and material properties whose understanding is beneficial towards the rest of the document.

The primary independent variables of a prosthetic socket are elucidated as shape, spatially varied mechanical impedance, and spatiotemporally varied mechanical impedance. Each is given specific focus on their meaning, and the projects described in this thesis are introduced in these sections. Following the introduction of the knobs we can control, the field is reviewed in depth. Beginning with methods of residuum scanning and measurement, the topics covered include the shape and form of the digital biomechanical data gathered, how these data may be processed through forward and inverse finite element modeling, the form and function of the digital socket models output by these FEA or iFEA processes, the current and proposed rapid prototyping technologies that may aid in the production of digitally fabricated prosthetic sockets, the characteristics of the resulting socket or socket mold (to later be post-processed into a socket or socket liner), and finally the state of the art evaluation of the lower extremity, transtibial prosthetic socket.

The FitSocket is described in depth in Chapter 2. Following a brief introduction the device is fully characterized by specification of the design, electromechanical functional requirements, physical components that satisfy those requirements, methods of calibration and characterization, electrical system, software system, and clinical experimental design. The results are separated into device characterization and clinical experimental sections. These sections present detailed analysis of the performance of both the device itself and its ability to measure human subjects. In total 7 transtibial residua were measured and characterized. The discussion considers viscoelastic and boundary conditions for increased success of measurement, the difficulty of measurement over small bony prominences, different shapes of the indenter head and how hemispherical shaped indenter heads are ideal, various comments on the data acquisition time and methods, measured values of the residuum using the FitSocket as compared to those cited in literature, and future work with emphasis on full limb data capture using FitSocket related technology.

The FitPen discusses the benefits of a smaller, less accurate apparatus for the purposes of transportability. A workshop in Kenya is related where the FitPen is used in clinical practice and data are collected. The hardware and software are specified, and example code is shown to elucidate the finer points regard-

ing data processing. Finally the future of the FitPen is considered by describing technical affordances that would increase the efficacy of transportability and measurement accuracy.

The quasi-passive socket is introduced with a brief introduction to the general problem of pain during extended prosthetic socket use. The purpose of the device is given as a possible increase in comfort and long term residuum health through a temporally varied mechanical impedance socket design that only applies high impedance loading on the wearer when it is needed. The methods specify the electrolaminate and electromechanical, functional requirements, the software system and algorithms, and clinical experimental protocols for two sit to stand experiments and one walking study. The results succinctly present the data collected during these experiments. The discussion comprises future work and contains information about refinement of the control algorithms, methods for gauging user interest by engaging in larger studies involving multiple subjects, identification of additional spatial areas of the prosthetic socket that could benefit from temporally varied mechanical impedance, and lifetime and robustness with respect to electrolaminate integration into a prosthetic socket.

5.2 The Future of the Field

The current strategies employed for digital socket design are in bulk positively approaching a better understanding of clinically viable interventions; however, in specific cases research can be deemed superfluous. The problem of heat and moisture buildup within the prosthetic socket remains a chronic problem, and little research focus is allotted to this issue. The focus of the field's research on socket based strategies often ignore the silicone liner that is used to provide suspension for the socket[1]. The Poisson ratio of silicone is 0.48-0.50, effectively making it incompressible. A focus on a prosthetic liner that maintains suspension but has a lower, more compressible Poisson ratio may lead to low-cost, easy to manufacture custom liners with spatially varied impedance characteristics. This could alleviate the requirement of custom sockets all together. Sockets are much harder to fabricate due to the composite nature of their fabrication. This area has yet to be explored.

The tools used in the field of digital socket design are slowly beginning to reach a reasonable consensus on techniques and approaches that yield positive health benefits to the recipients of digital sockets.

[1]In this case suspension is a vacuum effect that keeps the socket attached to the residual limb during ambulation

Unfortunately these sockets are still primarily only research prototypes, as the path through FDA approval requires so much effort that no sufficiently undeveloped technologies or methodologies will approach this path before being extremely well validated. More work will need to be done, but more importantly, more data of an agreed upon specification must be shared among researchers (similar to how the biological engineering research fields share primers, gene sequences, etc.) in order to facilitate more rapid translation to clinical practice.

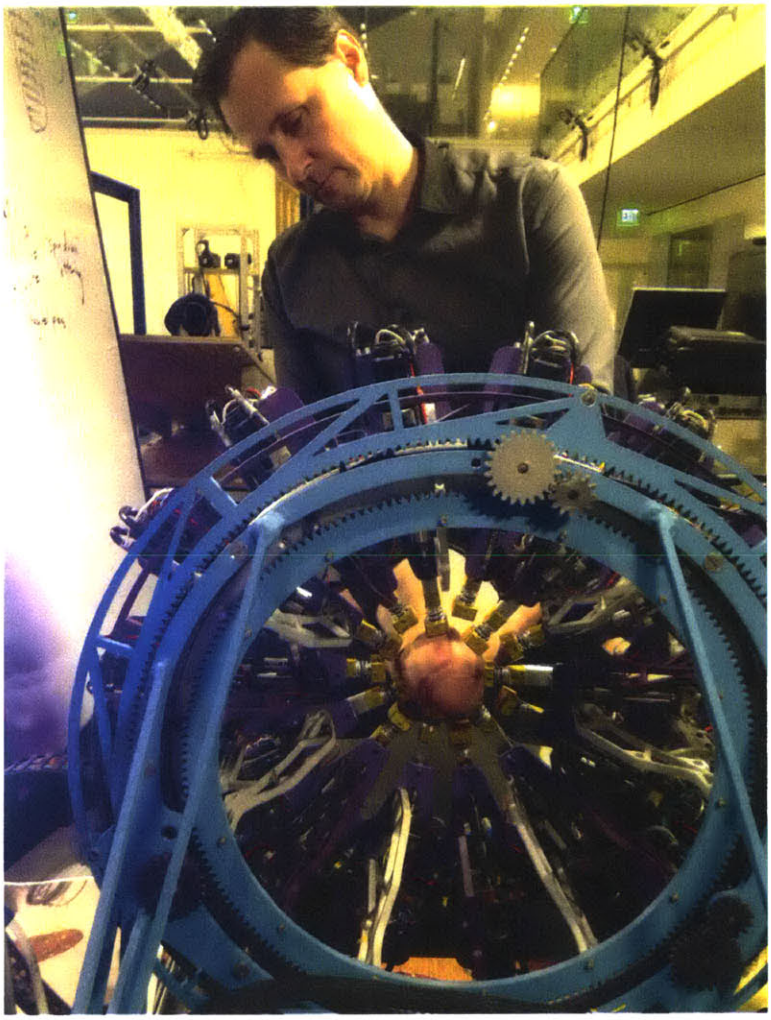

Appendix A

Summary of the Appendicies

A.0.1 Technical Proposal

This technical proposal was submitted to the the Department of Veterans Affairs in 2012 and granted in 2013. This proposal is the basis for the work described in the above thesis.

A.0.2 Project Management Plan

This management plan shows the updates and low-level tasks completed during the period of performance for the USVA grant.

A.0.3 FitSocket User Guide

The user guide gives a brief introduction into how to operate the FitSocket and run a test.

A.0.4 Spatially Varied Stiffness Socket Construction

This appendix describes the basics of spatially varied stiffness socket construction.

A.0.5 FitSocket Controller Board Assembly

Details of the PCB that holds the motor controller and communications board are presented in this appendix.

A.0.6 FitSocket Controller Board Buildbook

A buildbook is a summary of the electronics that gets sent to the board manufacturer in order for them to know what to make.

A.0.7 Software Constants

This appendix contains the software constants for the FitSocket controller program. They may be useful for someone developing similar software in the future.

A.0.8 Figures

This appendix contains bonus figures.

Appendix B

Technical Proposal

TECHNICAL PROPOSAL

1 Introduction

Research funding is sought to develop novel technologies to provide for a significantly more comfortable and healthy means to attach prostheses to an amputee's residual limb. Skin breakdown on the residual limb is a common occurrence, causing pain and discomfort in an amputee's daily life. Principal investigator **Hugh Herr** (MIT) along with co-investigators **Roy Kornbluh** (SRI International) and **Neri Oxman** (MIT) seek to advance a novel fabrication and design approach to socket interface technology.

Unfortunately today's socket technology does not leverage current state-of-the-art material, fabrication and robotic approaches that could facilitate socket designs that greatly improve both comfort and joint flexibility. In this proposal we put forth novel human measurement and fabrication tools to both increase socket functionality while simultaneously lowering the cost of prosthetic care. During the research program, an actuated test socket (ATS) will be designed, built and evaluated. The ATS is a computer-controlled, instrumented tool that will allow the prosthetist to independently control the shape and dynamics of a test socket in real time. This tool allows the prosthetist to adjust an actuated surface instead of a plastic test-socket to determine the ideal dynamic socket shape for a particular user with the aid of pressure field, blood flow, and dynamic anatomical data in real time.

Through the use of the actuated test socket, both passive variable-dynamic (PVD) sockets and quasi-passive, variable-dynamic (QPS) sockets will be constructed. PVD sockets make use of continuously variable-impedance 3D printing technologies to digitally fabricate not only ideal socket shapes, but also ideal dynamic properties of that shape (in other words, continuously variable resistance to flexing of the socket wall). For example, a socket could provide a soft interface in the area immediately supporting a boney protuberance of the residual limb, but gradually stiffen to accommodate higher loads on surrounding softer tissues. Current socket technology uses the practice of 'windowing' to provide an approximation of this technique. However, this windowing approach alone does not provide the needed spatial control of dynamics to ensure a comfortable interface. PVD sockets will be used to confirm design decisions about the ATS and QPS.

The QPS socket will extend the capabilities of the PVD socket by incorporating novel electrostatic, variable-stiffness materials into regions of the socket wall to provide for temporal variation of socket shape and stiffness. This microprocessor-controlled material will be employed to compensate for residual limb volume fluctuations as an amputee user goes about his day. Since the QPS socket technology is quasi-passive, where dynamics changes in the socket are infrequent, the final product will be low-

power, low-weight, highly robust and manufacturable -- design requirements for any successful socket technology.

Both socket technologies intend to address pain, costly return-visits to a prosthetist, lower than desired activity, skin pathologies, changes in residual limb volume and shape over time, and limits in tolerable duration wearing the socket. Through the use of dynamical skin (through subcutaneous) response measurements, ultrasound, an actuated test socket, and advanced 3D printing and electrostatic materials, we propose to advance repeatable – scientifically based – methodologies to create the most capable and comfortable sockets.

2 Impact

Users of a socket created with the actuated test socket will experience increased comfort, fewer skin pathologies, increased physical activity, and less pain than with traditionally fabricated sockets. Adjustments due to limb shape change can be completed quickly through the use of digitally stored pressure field and shape data. In addition, prosthetists should see a benefit in fewer repeat visits for adjustments, faster overall fitting times, and less labor cost per fitting. Because a patient-tested socket shape is created by the ATS, no plaster casts, positive molds, or test (diagnostic) sockets are required and this reduces overall costs to both the patient and prosthetist (Sewell 2000; Johannesson 2004).

Regarding scalability, the ATS allows the prosthetist – with a single purchase – to fit more patients more accurately at lower overall cost. Previously unavailable data provided exclusively by the ATS can be shared among experts to aid in further socket development, thereby increasing the rate of innovation in the field of socket technology.

3 Description

The project description contains information about the design and architecture of the main project deliverables and their new technology contribution with reference to current technology. A performance work statement follows these sections, detailing project requirements, deliverables with scheduling information, interdependencies between project sub-tasks, VA reporting format information, and any other special considerations.

3.1 Design and Architecture

This project will result in two main end products: the actuated test socket and the quasi-passive socket. The two differ in that the ATS is a desktop-sized device that is not usable as a traditional socket for mobility while the QPS is intended for use as a mobile, enhanced socket. The ATS is designed for use by prosthetists for the purpose of socket production, just as traditional test sockets are used for this purpose. The QPS intends to revolutionize socket technology by being the healthiest, most comfortable sockets in the world.

3.1.1 The Actuated Test Socket

In traditional socket manufacture, a male plaster mold is used to create a (usually clear) plastic test socket that a prosthetist uses to test the socket fit with a patient. The actuated test socket replaces all traditional tasks of socket fabrication up to and including the test socket fitting. Roughly the size of a CRT monitor, the ATS's patient interface is a surface that is variable in both size and shape while maintaining smooth, continuous contact with the amputee's limb and liner.

The data produced by the actuated test socket are the main purpose of the device. They will be used in all further development in the tasks that result in the creation of the quasi-passive socket. Using simple sensors – such as linear potentiometers and fluid pressure sensors – the ATS is capable of determining both the socket shape under load in real time and the pressure response at that shape due to physical interaction with the patient's tissue in his or her residual limb. These shape and pressure data also allow the stiffness of the residual limb's tissue to be calculated directly.

In order to gather this data in a way that is useful for further development, the ATS makes use of roughly 200 individually controlled bladders distributed around the surface of the patient interface that are actuated with the flow of incompressible fluid in and out of each bladder. This flow is controlled by electronic valves distal to the interface surface. The bladders are made of a rubber-like flexible material shaped to form bellows. Each bladder is designed to move normal to the surface of the residual limb while restricting tangential movement. The bladders are connected to each other at their inner surface with a rubber-like material and at their outer surface with a hard, structural plastic-like material. The structural connection also provides the main structure for the actuated part of the ATS and connects directly to the rest of the device's structure.

Electronics (both digital and analog), actuation valves, fluid transport lines, sensor wiring, power management, and computer interface ports are all housed within the ATS's casing. The device is self-contained and requires only a computer with a free USB port and power from a standard electrical outlet to function. The ATS does not consume any physical material (fluid or otherwise) during operation.

Typical prosthetist and patient interaction with the actuated test socket starts with a consultation. Following the consultation the amputee stands with their residual limb in the ATS while not placing load on the ATS. The ATS first makes contact only (no force) with the residual limb in order to determine the limb's unloaded shape. The patient is then asked to stand normally, loading the inner surface of the ATS. Through the onboard intelligence and the direction of the prosthetist, the ATS is adjusted to find the ideal shape for the patient. This fitting process will take roughly ten to fifteen minutes to complete.

After the patient has been measured by the ATS and both the patient and prosthetist agree on the socket fit, the data from the ATS are sent to a central fabrication facility where they are run through a novel processing algorithm that translates patient body stiffness and residual limb shape into socket wall stiffness and shape. These data are further processed to translate the socket stiffness and shape data into 3D computer aided drafting type files that are readable by a 3D printer. This processing is necessary to eliminate a tedious processing task, but more importantly to ensure the correct mapping between desired socket wall stiffness and the properties of the material used to create the physical quasi-passive socket.

Figure 3.1.1. A drawing of the imagined prosthetist patient interaction while using the ATS, which is pictured in the lower right of the figure.

3.1.2 The Quasi-Passive Socket

Traditional state-of-the-art sockets are the direct products of the knowledge gained from the clear plastic test sockets used in most socket fitting facilities. These sockets are generally created out of carbon-fiber composite because of its favorable

strength to weight ratio driven by the penalties associated with the high inertia caused by mass attached to the residual limb.

Carbon-fiber sockets are a proven technology. They are durable, lightweight, and extremely strong. The quasi-passive socket will leverage the advantages of traditional sockets by using carbon-fiber composite walls in areas of the socket that do not require variable stiffness. To explain, the strong composite will act as an excellent structural mounting surface for the electrolaminates that vary in stiffness. Also, socket fabrication using carbon-fiber composites is a known technology. This means that the resulting quasi-passive socket, which will leverage carbon-fiber for structure, can be designed as if it were a commercial product instead of a research prototype (Klasson 1995 and Wise 2010).

This design takes note of current best practices in socket manufacturing as well as manufacturing in general. The socket is fabricated by first 3D printing a male blank using very inexpensive 3D printing (the material is sacrificial). This male blank is used to create a carbon-fiber composite structure. The structure is finished using standard machining processes. Finally the electrolaminates and their support electronics are attached to the carbon-fiber structure, producing a finished socket.

The finished quasi-passive socket will change the experience of its user by varying the stiffness of the electrolaminate sections based on physical cues that tell the device about the activity in which the user is participating. If the amputee is sitting the electrolaminate areas will relax, providing increased comfort while maintaining a stable fit. During standing some or all of the electrolaminate sections will stiffen just enough to provide necessary holding force to the residual limb. During more active states such as walking, running, or leaping, the electrolaminate sections will stiffen further. This interaction between the amputee and the socket allows full, reliable physical control of the socket while providing high loads on the residual limb only when necessary (Portnoy 2010).

3.2 New Technology Identification

This project identifies four core technology innovations that make the quasi-passive socket possible. They are the electrolaminate material, the data processing techniques to translate limb shape and stiffness data to a functional socket, the actuated test socket's continuously variable patient interface surface, and the use of continuously variable durometer 3D printing to experimentally quantify socket fit.

3.2.1 Electrolaminates

Electrolaminates are a unique technology that allows for structures or structural elements to dramatically change their stiffness and/or damping. While many smart materials, such as piezoelectrics and piezoelectric composites, shape memory alloys and shape memory polymers, can change their properties based on electrical or thermal effects, electrolaminates are fundamentally different. Smart materials can generally change their properties by at most one order of magnitude. In contrast, electrolaminates

have been demonstrated to be able to change their stiffness by at least three orders of magnitude. Table 3.2.1a below shows this comparison.

Table 3.2.1a. Comparison between electrolminates and candidate "smart" materials. The maximum elastic energy density is a figure of merit combining the stiffness variation and elongation capbilities.

	Material Type (specific example)	Max Strain (%)	Typical Elastic Moduli (MPa)	Typical (Max.) Elastic Energy Density Change (J/cm³)	Relative Power Consumption	Relative Passive Damping	Relative Speed (full cycle)
NEW	**Electrolaminates**	**>100**	**<1 - >10⁴**	**>50,000**	**Low**	**Low**	**Fast**
INTRINSIC	Mammalian Skeletal Muscle	20 (40)	10 - 60	1 (2)	NA	Medium	Medium
	Shape Memory Alloy (TiNi)	2 (10)	20,000-80,000	12	High	Medium	Slow
	Shape Memory Polymer (polyurethane)	200 (rubbery) 5 (rigid, est.)	10,000-10	>1.3	High	Medium	Slow
	Magnetorheological Fluids	NA	NA	NA	Medium	Medium-High	Fast
	Electrorheological Fluids	NA	NA	NA	Low	Medium-High	Fast
	Mechano-chemical Polymer/Gels	> 100	wide range	<1	Medium	Medium	Slow
	Liquid Crystal Elastomer (Thermal)	>40	~0.05-0.5	0.04	Low	Medium	Slow
ACTIVE	Dielectric elastomer	>100	2	0.1 (3.4)	Low	Medium	Medium - Fast
	Electrostrictive Polymer	7.0	800	0.3 (>1.0)	Low	Medium	Fast
	Electrochemo-mechanical Conducting Polymer	2 (20)	1000	0.1 (1.0)	Medium	Medium	Medium-Slow
	Ionic Polymer Metal Composite	0.5 (3.3)	80	(0.006)	Medium	Medium	Medium - Slow
	Piezoelectric Polymer (PVDF)	0.1	450	0.0024	Low	Medium	Fast
	Piezoelectric Types						
	Ceramic (PZT)	0.2	50,000	0.10	Low	Low	Fast
	Single Crystal (PZN-PT)[1]	1.7	9000	1.0	Low	Low	Fast
	Magnetostrictive	0.2	40,000	0.025	Medium	Low	Fast
	Ferromagnetic Shape Memory Alloy	6(10)	2000	0.001 (1)	Medium	Low	Fast

Smart materials such as shape memory polymers must be operated within a relatively narrow range of temperatures to ensure proper functioning. As noted, unlike traditional smart material technologies, electrolaminates can be composed largely of a variety of commonly used structural materials including metal sheets and fiber composite laminates. Thus, the technology can be easily integrated into existing

structures, such as adaptive sockets, with little weight penalty or compromise in ruggedness or environmental tolerance.

Because they operate based on an electric field, electrolaminates are fast acting and energy efficient. Electrolaminates can also operate over a larger range of strains and forces than other field-operated materials such as piezoelectrics, since electrolaminates do not need to convert the energy of deformation into electricity (which is needed in active control concepts) in order to achieve their action. Rather, the material itself passively obtains the new performance characteristics. Table 3.2.1b below summarizes the key advantageous features of electrolaminates and their importance for the proposed work.

Table 3.2.1b Key features of electrolaminates and their importance for the proposed work.

Need addressed	Attribute	Engineering specification
Comfort and ease of motion	lightweight	Aerial mass density
Provide secure attachment even with variations in residual limb volume and shape	Stiffness modulation	Maximum and minimum stiffness, response speed
Cosmesis, quiet operation	Noise level, thin and conformal	Sound pressure level, thickness
Low power requirements	Power consumption	Average and peak power requirements

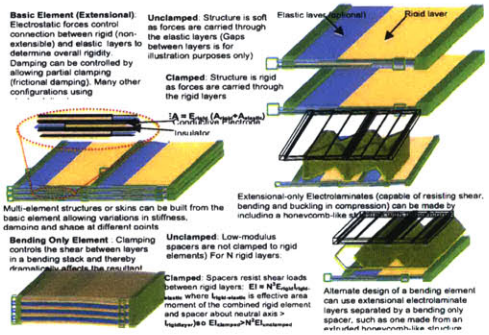

Figure 3.2.1c. Basic elements of electrolaminates.

The key to providing the benefits discussed above is that electrolaminates are essentially composites that can change the connectivity of materials or elements within their structure to achieve wide-ranging changes in overall material properties. While this principle can be incorporated in many ways, the simple elements shown in Figure 3.2.1c explain the principles and also allow for an understanding of how the principles can be incorporated into the adaptive socket system.

SRI has demonstrated the basic stiffness control capability of both the extensional and bending type of electrolaminate. Figure 3.2.1d and Figure 3.2.1e show bench-top tests of both types. These basic elements can be integrated into other structures or used in other forms. For example, the tensile strips could be woven into a fabric that in the unclamped state is stretchable and in clamped state is not stretchable. Figure SRI3 shows and example of such a configuration and how it might be incorporated into the overall socket design.

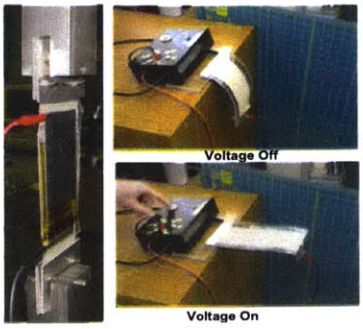

Figure SRI2. Two types of electrolaminates: extensional (left, being tested on a tensile test apparatus) and bending (right). Such devices have shown greater than 1000:1 stiffness variation.

Figure 3.2.1d. Candidate configuration of electrolaminates for socket windows.

Electrolaminates are comprised of rigid elements (e.g. carbon fiber sheets, metals, or any other structural material including high-stiffness elastomers) and compliant elements (e.g. softer elastomers, foams, or extensible truss-like structures). The connectivity between elements is controlled with electrostatic clamping.

Electrostatic clamping is fast, energy efficient and can be done with almost no added mass (generally only thin insulators and electrode coatings are needed). It is important to note that, while the clamping does require the application of electrical energy, the electrical energy does no external mechanical work and therefore the energy lost is minimal.

When the electrolaminate is in the clamped condition, its stiffness approaches that of the more rigid elements from which it is made (not unlike conventional composites). In the completely unclamped condition its stiffness is dominated by the more compliant material element. Thus the maximum and minimum stiffness states can be selected by selecting the individual component materials.

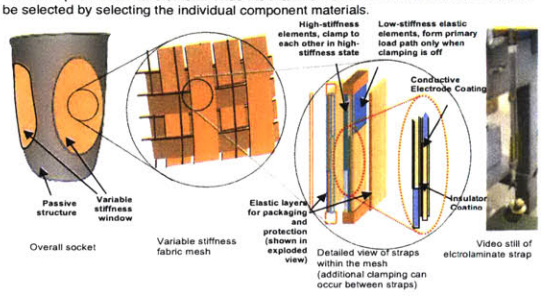

Figure 3.2.1e. Candidate configuration of electrolaminates for socket windows.

The basic elements can be stacked (connected in parallel) or attached end-to-end (connected in series). Gradations of stiffness between the completely clamped and unclamped states can be achieved by clamping only some elements within a multi-element structure. In general, you can achieve up to 2^N states where N is the number of unique stiffnesses of each single element in a series connection. Note that for the bending configuration, a series connection can be achieved in a single stack. If we choose a mesh configuration then we also have the option of controlling stiffness by clamping the orthogonal elements of the weave to each other in addition to controlling the extension of the individual elements. The best configuration will be selected during the execution of the proposed work.

3.2.2 Data Processing

The actuated test socket directly measures only the position of each bladder – giving a high-resolution shape of the loaded residual limb – and the pressure each bladder exerts on the limb – allowing control over areas that require more or less pressure. These data can in turn be used to directly calculate the non-linear, first-order stiffness of the tissue under each bladder, producing a high-resolution stiffness mapping of the residual limb (While skin is not first-order in its dynamical response to a displacement input, a first-order approximation will provide reliable data for the quasi-passive socket (Phillips 1981)).

Residual limb stiffness is an important set of data because it – in concert with various other data sets – is a key element in scientifically determining final socket shape and stiffness characteristics. Academic investigations into the role that residual limb (RL) stiffness plays in socket shape suggest that there is an inverse relationship between RL stiffness and socket pressure at a given location (Sanders 1993; Mak 1994; Silver-Thorn 1996). In reality, the correlation between the two is much more complicated than that.

The gradient of RS stiffness over limb topology along with the pressure and shape data from the ATS could be the key to determining an objective idea of socket comfort and health from measurable data. It is the intention of this project to determine not only what this mapping is, but also to test the suggested results iteratively in order to leverage experimental data.

The resulting novel software from this investigation will provide the first scientific method for determining socket comfort. As a tool, it will be tremendously valuable in supporting further research into new socket technology. In this project, it will provide the base data set for the creation of a new type of quasi-passive socket.

3.2.3 A Continuously Variable Smooth Inner Surface

The core component of the actuated test socket is its continuously variable smooth inner surface. This type of surface is important to provide comfort during the fitting process as well as to identify the socket shape accurately. The inner surface of the ATS adjusts to the amputee's residual limb shape accurately though hundreds of independently controlled, continuously variable surfaces. Each surface is mechanically designed to smoothly transition between itself and its surrounding surfaces.

The continuous variability of the socket wall is accomplished through precision control of the fluid valves using a closed-loop control system. Each bladder can be precisely controlled to move to any location in its range or accomplish any pressure against the residual limb.

The inner surface of the ATS that connects each bladder together, as seen in Figure 3.2.3b, is an elastic, rubber-like material that can increase in surface area though stretching. This allows the surface to change size and shape without uncomfortable wrinkling.

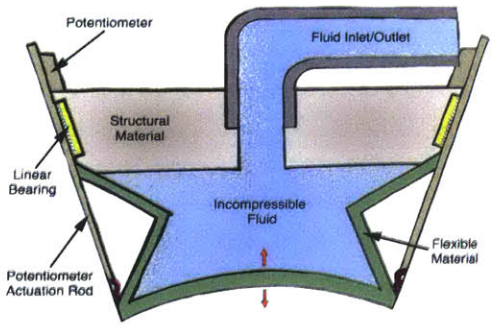

Figure 3.2.3a. shows a center cross-section of a single bladder. The potentiometers measure the shape of the bladder while pressure sensors at the valve location measure pressure.

3.2.4 Variable Durometer 3D Printing

The verification sockets will be 3D printed using the Connex500 technology developed by OBJET. The Connex500 is the first and only 3D printing system able to deposit multiple materials of varied mechanical and physical properties simultaneously within a single 'build' (i.e. a single 3D printing process). The technology is also known as the Poly-Jet Matrix Technology and is designed to 3D print two or more model materials based on an extensive range defined by matrix combinations.

Current socket designs and design technologies utilize processes of design assembly to cater for material variation. Such variations are traditionally achieved as discrete delineations in physical behavior by fabricating multiple parts comprised of different materials, and assembling them after the fabrication process has been completed (Laferrier 2010). This practice can only provide rough approximations to the mapping between tissue stiffness and socket interface response. However, the shape and size of the residual limb changes rapidly and often during each step due to muscle

contractions and forces associated with movement (Staker 2009; Sanders 2009). Ideally, a socket should be able to accommodate a broad range of movements without generating significant discomfort.

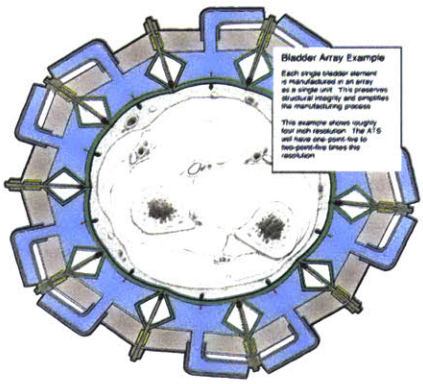

Figure 3.2.3b. shows a full bladder array cross-section.

Recent advances in Computational Topology Design (CTD) and Solid Free-Form Fabrication (SFF) are promoting the creation of components with controlled micro-, and macro-architectural features that can continuously vary impedance properties to provide an ideal interface complimentary to the properties mapped in the residual limb (Miyamoto 1999; Oxman 2010; Oxman 2011). In order to achieve highly articulated and ideally customized socket shapes and properties, we utilize a variable-property design approach and technology.

In order to iteratively test the progress of both the ATS's data collection quality as well as the calculated socket stiffness and shape based on the aforementioned data processing algorithm, wearable sockets will be created with varying durometer material as the socket wall. The socket location to durometer mapping will be derived using data provided by the ATS.

3.3 General Description

This project will result in the production of a quasi-passive socket that has undergone testing with amputees and is ready to transition to the clinical trial stage. In order to accomplish this result, four major tasks must be completed:

1. Develop and build the actuated test socket.
2. Create a passive variable stiffness socket through a defined process using continuously variable 3D printing techniques.
3. Develop and build electrolaminate materials.
4. Build and test both transfemoral and transtibial quasi-passive socket prototypes.

The actuated test socket is required to gather limb shape under load, pressure field, and stiffness field data. This data is processed and used to create both the passive variable stiffness socket – which is much like a traditional windowed socket – as well as the quasi-passive socket.

The passive variable stiffness socket will be used to validate the data processing algorithms used to define areas of high or low stiffness and overall socket shape. This data is taken unprocessed from the actuated test socket. Passive 3D printed sockets are used for validation because they can be made quickly, inexpensively, and at high precision.

Electrolaminate materials are thin sheets of material that are able to change stiffness characteristics through the application of an electric field. These materials will be used to create sections of the quasi-passive socket that will flex during some activity modes and remain stiff during others.

The quasi-passive socket prototypes will be 3D printed and modified to allow for the attachment of electrolaminate materials. Tests will be completed with both transfemoral and transtibial amputees. As the main deliverable of this project, all other tasks in this project are necessary in order to produce the quasi-passive socket prototypes.

The actuated test socket, 3D printing methods research, and electrolaminate development begin simultaneously at the start of the project. Each of these three main tasks are the responsibility of three different groups: Biomechatronics, Mediated Matter, and SRI respectively. On completion of the electrolaminate development early in year two of the project, the quasi-passive socket task will begin. The actuated test socket development is intended to reach completion at year 1.5 along with the 3D printing

technology research. At this point testing with amputees will commence, providing feedback and confirmation deliverables to the project.

3.4 Summary of Requirements

The milestones for this project are divided into four sections based on the four main tasks of the project. These evaluation criteria will be used to demonstrate the objective progress of the project.

1. Actuated Test Socket
   - A. Device: Demonstrate a working device through compliance with the device specification (see the methods section for more information).
   - B. Software: Demonstrate the usability and accuracy of the device control software through the IEEE 829 software test specification compliance and proof of usability through successful production of reliable data.
2. 3D Printed Variable Stiffness Passive Socket
   - A. Device: Demonstrate a 3D printed socket with passively variable stiffness walls through compliance with device specification.
   - B. Technology: Demonstrate capability in continuously variable stiffness material 3D printing through the production of controlled test blocks. These blocks will be mechanically tested to ensure the accuracy and precision of temporal stiffness data according to the ASTM D-1043 specification.
3. Electrolaminate Material
   - A. Device: Demonstrate a working device through compliance with the device specification.
   - B. Safety: Demonstrate that the design of the electrolaminate material is safe according to generally recognized electrical safety standards by showing, for example, that the maximum current output is kept to safe levels even in worse case failure scenarios.
4. Quasi-Passive Variable Dynamic Socket
   - A. Device: Demonstrate a working device through compliance with the device specification.
   - B. Human Testing: Demonstrate an increased comfort through human testing of the QPVD according to MIT and VA human testing protocols.

3.5 Period and Deliverables or End Products

3.5.1 Period of Performance

This project intends to perform for the duration of twenty-four months.

3.5.2 Deliverables

The main deliverables for this project are listed in the Summary of Requirements section. Below is a description of these main deliverables with more depth. Scheduling information in months is shown at the end of each heading in parentheses. The letter after the parentheses denotes the type of deliverable. 'R' suggests that the project will output a report for VA consumption. 'D' suggests that the project will output a demonstration for VA consumption. Demonstrations can either be in the form of an in-person visit or a video demonstration that is in-turn either live or recorded.

1. Actuated Test Socket (Biomechatronics)
   - A. Evaluate Relevant Technologies (0 – 2) R

     Determine the best mechanical solution for the actuated surface of the ATS through rapid benchmarking and simple prototypes.
   - B. Design and Fabricate ATS Rev 0 (3 – 8) D

     Using information learned in 1.A., design the first full ATS prototype. This includes not only the mechanical design and fabrication, but also the electronics and software to control it.
   - C. Test ATS Rev 0 with Mediated Matter (9 – 10) R

     Data gathered with ATS Rev 0 will be delivered to Mediated Matter in order to build passive prototype sockets that will be used to experimentally test the ATS and processing software performance.
   - D. Design and Fabricate ATS Rev 1 (11 – 13) D

     Using information from both 1.B. and 1.C., design a second ATS. This design will be used to create both trans-tibial and trans-femoral ATS builds.
   - E. Test ATS Rev 1 with Mediated Matter (14 - 23) D

     This testing round will have more depth than 1.C. Biomechatronics will test with Mediated Matter, trans-tibial and trans-femoral amputees, as well as beginning to incorporate the work of SRI on electrolaminates into the initial quasi-passive prototypes.
   - F. Support Technology Transfer Plan (24) R

     In order to support transfer of technology to the U.S. Department of Veterans Affairs, Biomechatronics will work with the VA to develop a technology transfer plan for the ATS.
2. 3D Printed Variable Stiffness Passive Socket (Mediated Matter)
   - A. Map ATS Data to Socket Structures and Materials (0 – 6) R

     Although this deliverable will be completed before real ATS data are available, the data structure and types are known. The mapping of mechanical properties to spatial orientation mappings will inform the structural and material deposition in satisfying the overall mechanical requirements. In this phase, the micro-composition of the material may be altered to achieve gradual variation of mechanical properties.
   - B. Map Material Data to STL files for 3D printing (7 – 9) R

     This deliverable will produce the mapping of material and structures to location and translate this mapping into an STL file that will contain all variable-property data in correspondence with Connex500 materials. The Connex500 printers require separate STL files for each durometer. In the case of continuously changing durometer, this step is best done by computer program than by hand.
   - C. Build Variable Stiffness Passive Sockets (10 – 13) D

     3D printed sockets will be created in order to test hypothesis with steps 2.A. and 2.B. in conjunction with steps 1.C. and 1.D. The results of these tests will help determine the system boundaries.
   - D. Refine Steps 2.A. and 2.B. Data Mappings (14 – 15) R

     Using the data from 2.C., the data mappings from ATS to STL files will be further refined. The software that presents the human interface to these algorithms will also be refined to meet user needs more directly.
   - E. Build Quasi-Passive Socket Prototypes (16 – 23) D

     In order to aid in the production of the quasi-passive socket, the Mediated Matter group will aid in the 3D printing of benchmark level prototypes of the quasi-passive socket. This production technique will allow the development process to investigate many factors at once, thus speeding production.
   - F. Support Technology Transfer Plan (24) R

In order to support transfer of technology to the U.S. Department of Veterans Affairs, Mediated Matter will work with the VA to develop a technology transfer plan for the material mapping technology.

3. Electrolaminate Material (SRI International)

   A. Develop Notional Design (0 – 2) R

   This deliverable will contribute to the overall system design by defining the range of performance and physical configurations of the electrolaminate technology and suggesting how it may best be used to achieve the goals of controlling spatial and temporal stiffness.

   B. Demonstrate Electrolaminate Performance (3 – 8) D

   Based on the preliminary notional design, the electrolaminate technology will be developed to demonstrate the level of performance, design configurations, and power requirements needed by the project requirements.

   C. Fabricate and Integrate Rev 0 Electrolaminates (9 – 11) D

   In order to incorporate electrolaminates into the rev 0 quasi-passive socket prototype, the electrolaminates will need to be structurally engineered and fabricated for this specific purpose. Electronics will be built to the prototype level for quick testing and reconfiguration.

   D. Refine Electrolaminate Design (12 – 14) R

   Based on the results of 3.C., the design of the electrolaminate technology will be refined to better suit the needs of the quasi-passive socket in terms of performance and mechanical integration with the socket structure with special considerations for user comfort, power requirements, and actuation methods.

   E. Fabricate and Integrate Rev 1 Electrolaminates (15 – 17) D

   Using the revisions to the electrolaminate technology completed in 3.D., the rev 1 electrolaminates will be integrated with rev 1 quasi-passive socket designs that are build by Biomechatronics and Mediated Matter.

   F. Design Testing and Final Refinement (18 – 23) D

   The final quasi-passive socket designs and electrolaminate designs will be integrated. Full, production level drive electronics will be integrated with the sensor and processing electronics developed by Biomechatronics. Human Subject testing will be experimentally controlled and documented to provide objective data.

   G. Support Technology Transfer Plan (24) R

   In order to support transfer of technology to the U.S. Department of Veterans Affairs, SRI will work with the VA to develop a technology transfer plan for the electrolaminate technology.

4. Quasi-Passive Variable Dynamic Socket (Biomechatronics)

   A. Design and Test QPS Rev 0 Prototype (9 – 14) D

   The first quasi-passive socket prototype will be designed and fabricated through 3D printing for the first integration tests with SRI's electrolaminate material.

   B. Design and Test QPS Rev 1 Prototype (15 – 18) D

   Using information from 1.C., 2.C., 3.C., 3.D., and 4.A. the QPS rev 1 prototype will be built and tested with both Mediated Matter and SRI for comfort, ease of use, battery life, and control.

   C. Design and Test QPS Rev 2 Prototypes (18 – 23) D

   Both trans-tibial and trans-femoral quasi-passive socket prototypes will be built using knowledge of best manufacturing processes in order to produce a final prototype that not only has the ability to be fabricated in a production setting, but has the ability to be fabricated efficiently and cost effectively.

   D. Support Technology Transfer Plan (24) R

   In order to support transfer of technology to the U.S. Department of Veterans Affairs, Biomechatronics will work with the VA to develop a technology transfer plan for the quasi-passive socket technology.

3.5.3 Delivery Schedule

Below is a table with the twenty-three aforementioned deliverables presented in chronological order. The delivery month is the end of the work time allocated for each deliverable. The delivery type is also listed in this table for convenience.

Deliverable	Delivery Month	Delivery Type
ATS Evaluate Relevant Technologies	2	Report
Electrolaminate Develop Notional Design	2	Report
Map ATS Data to Socket Structures and Materials	6	Report
Design and Fabricate ATS Rev 0	8	Demonstration
Demonstrate Electrolaminate Performance	8	Demonstration
Map Material Data to STL files for 3D printing	9	Report

Test ATS Rev 0 with Mediated Matter	10	Report
Fabricate and Integrate Rev 0 Electrolaminates	11	Demonstration
Build Variable Stiffness Passive Sockets	13	Demonstration
Design and Fabricate ATS Rev 1	13	Demonstration
Design and Test QPS Rev 0 Prototype	14	Demonstration
Refine Electrolaminate Design	14	Report
Refine Mediated Matter Material Data Mappings	15	Report
Fabricate and Integrate Rev 1 Electrolaminates	17	Demonstration
Design and Test QPS Rev 1 Prototype	18	Demonstration
Build Quasi-Passive Socket Prototypes	23	Demonstration
Design Testing and Final Refinement	23	Demonstration
Test ATS Rev 1 with Mediated Matter	23	Demonstration
Design and Test QPS Rev 2 Prototypes	23	Demonstration
ATS Technology Transfer Plan	24	Report
Mediated Matter Technology Transfer Plan	24	Report
Electrolaminate Technology Transfer Plan	24	Report
Quasi-Passive Socket Technology Transfer Plan	24	Report

3.5.4 Coordinating Performance/Delivery Schedules

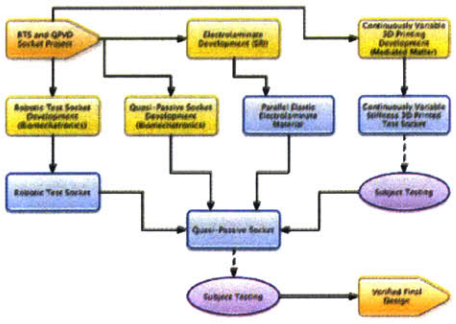

Figure 1: Methods diagram with dependencies. Yellow blocks are development tasks. Blue blocks are physical deliverables. Please see the Appendix for a full dependency diagram.

3.6 Progress and Compliance

Progress and Status Reports

Progress reports between project participants will be presented in the format described below. This format is based on the CEROS progress report format.

1. Title Page: A separate title page should contain the following information.
   A. Project Title
   B. Task Completion Title
   C. Principal Investigator(s)
   D. Reporter (if different than above)
   E. Affiliation, full mailing address, email address, telephone numbers)
   F. Beginning and ending dates of the reporting period
   G. Date Submitted

2. Project Overview: A summary in one or two short paragraphs of the background, objective, methods, and expected results of the project in plain English. This section can be identical in all task completion reports.

3. Task Report: A description of one task per section, if multiple tasks are included in a single progress report. Each task will begin with section with a verbatim restatement of the task as described in the contract. Progress made on task completion, difficulties encountered, preliminary data, and main findings and conclusions will be presented. Also any problems or unexpected findings will be presented, allowing for the opportunity to seek help resolving any issues. If the anticipated outcome of a task is different than envisioned, alternative ways to achieve the objectives should be suggested.

4. Schedule: A presentation of an updated timeline (e.g., a Gantt chart) showing the entire project, with indication of the planned versus actual schedule. Descriptions of project delays, if any, and their impact on the overall schedule should also be present.

5. Budget: Description of the planned versus actual expenditures; a simple graph or chart would be useful. Explanations and justifications for any significant

deviations from the contracted budget will be provided in the context of the contract.

6. Presentations: If any, presentations that have been made during the reporting period will be detailed with the location, audience, and results that were presented. Also, reports of any patents, trademarks, copyrights, and publications will be made in this section.

3.7 US-Government Furnished Equipment, Data, or Services

The final stages of this project will require human testing in order to gather objective data. We would like to request coordination with the VA with respect to this need. Because the VA currently has a leased space on MIT's campus, this coordination should be fairly straightforward.

3.8 Special Considerations

Done laid around, done stayed around This old town too long Summer's almost gone, winter's coming on Done laid around, done stayed around This old town too long And it seems like I've got to travel on And it seems like I've got to travel on.

4 Methods

This project intends to complete two main physical deliverables in the form of finished products. The actuated test socket provides intrinsically useful gains over traditional methods of socket production. The quasi-passive socket – through the use of the actuated test socket – objectively demonstrates the advantages of this technology to both the amputee and the prosthetist. These two main physical deliverables are supported by the electrolaminate variable stiffness material and the continuous 3D printing and data translation tools.

4.1 Electrolaminates

The basic extensional and bending configurations of electrolaminates have been demonstrated and may be employed in the proposed work. Typical performance specifications for the extensional type of electrolaminate are shown in Table 4.1a below. Since we can make the electrolaminates out of the same materials that we might expect to find in typical prosthetic sockets, the maximum stiffness can be similar. Alternatively, we can choose softer materials. Thus, the capability to address the needed range of stiffness would have low technical risk.

Table 4.1a. Typical demonstrated performance specifications for the extensional type of electrolaminate

Parameter	Value	Comments
Max Stiffness (EA)	8600N (875 lbs)	Per layer
Max elastic modulus	1 - 4 GPa (145 - 580 kpsi)	
Min stiffness/modulus	< Max/1000	Can be arbitrarily small
Max clamping shear stress	10 N/cm2 (14 psi)	Per layer
Clamping time	20 ms – 60 ms	
Unclamping time	20 ms – 800 ms	faster unclamping times can be achieved with AC voltage
Power to hold clamp	0.1 mW/cm2 (DC); 1.0 mW/cm2 (AC)	Per layer; some of AC power is recoverable
Capacitance	0.25 nF/cm2	Per layer
Peak current	0.025 mA/cm2 for 20 ms rise time	Per layer; partially recoverable. Longer rise times reduce peak current; Peak current can be produced by capacitors or from portions of the electrolaminate

A primary technical risk of the proposed work may be achieving the needed clamping strength. To date, we have shown that the clamping force on a per area basis should be sufficient to achieve the needed strengths for the proposed applications. Specifically, we can repeatedly achieve clamping forces of about 70 psi. This normal force translates to about 10 psi lateral force. In other words, we can produce about 10 lbf resistance to slippage for every square inch of clamping area. A simple extensional electrolaminate strip with 3 inches of overlap could then resist 30 lbf. Additional strength can be achieved by stacking individual layers. While the strength requirements have not yet been determined, we believe that they can be met with a practical number of stacked layers.

Note that if the maximum clamping strength is exceeded there is no catastrophic failure of the material. Rather, the material simply elongates with characteristic stiffness of the low-stiffness (unclamped) state. The electrolaminate can simply be cycled on and off to restore the desired stiffness and state of stretch.

Lifetime and wear is another technical risk. The insulating layer of an electrolaminate functions as both electrically as a dielectric and mechanically as a frictional braking surface. Wear of the insulating layer may be of concern. Such long-term wear studies have not been completed. Initial results do not show noticeable wear over many hundreds or thousands of cycles. An adaptive socket may have to operate for a million or more cycles. Several polymer materials have shown the ability to function well as the

insulating layer. In principle non-polymer materials, including rugged ceramic coatings, can function in this role. We will choose the best material during the execution of the proposed work.

Clamping and unclamping response times have been demonstrated to be on the order of 20 msec which should be fast enough for even dynamic modulation of the socket during normal activity.

Typical values for power consumption to hold a state are 1 mW/in^2. Although the total holding power required depends in turn on the maximum strength required (and thus the total clamping area required) we can estimate that the overall power requirements would be on the order of 1W or less. Such power levels are therefore feasible for the adaptive socket application. The proposed work may address the selection of the dielectric layer in the electrostatic clamping in an effort to further reduce this holding power. We have demonstrated electrolaminates that utilize other clamping mechanisms besides electrostatics. These approaches include electromagnetic, electrothermal and pneumatic approaches. These approaches can clamp with no holding power but, depending on the duty cycle, may require more overall power.

Figure 4.1b. Commercially available compact DC-DC converter (source: EMCO High Voltage).

Small commercially available DC-DC converters are available that allow for conversion of battery voltage to the needed operational voltages (typically about 2 kV). For example, EMCO High Voltage makes a 0.1 cu. Inch unit that is capable of putting out 1.5W at 2000V. Figure 4.1b shows this device.

It is simplest to think of electrostatic clamping as issuing a DC voltage. However, the optimum clamping considers both the dielectric material and the frequency of the applied voltage. Thus the ability to vary the frequency and duty cycle of the applied voltage is another design parameter that can determine the performance of the resulting electrolaminate.

4.1.1 Electrolaminate Risk Mitigation

The proposed work is based on electrolaminate performance levels that have already been demonstrated. As such, we hope that the risk is minimal. Nonetheless, as described above, there are challenges in areas such as achieving the needed maximum strength in the high-stiffness state, necessary speed of response, low holding power as well as achieving the needed lifetime.

Since electrolaminates have been demonstrated with a variety of component materials (high-stiffness component, low-stiffness component, electrodes and insulators), one

approach to risk mitigation is to select the materials that best allow us to meet the needed specifications. For example, electrode could be thin metal coatings, carbon or silver-impregnated polymers.

In addition to material selection, we can also choose from a large range of possible configurations of electrolaminates including extensional, bending, woven or combinations of these. This ability to design the electrolaminate structure to best meet the needed performance requirements can also help to minimize risk.

We have chosen electrostatic clamping as the most desirable approach to stiffness control due to its speed of response and energy efficiency. However, we can also explore alternate clamping means such as electrothermal approaches to reversible adhesion, electromagnetics or pneumatic approaches.

4.1.2 Electrolaminate Safety Issues

The electrostatic clamping typically operates at voltages of up to 2 kV. While this voltage is relatively high, we believe that it does not pose a significant health risk for two reasons: 1) there will be adequate insulation preventing contact with the skin and 2) the current will be ensured to be extremely low in all conceivable fault conditions. Indeed, since it is the maximum current that ultimately determines the safety of a device, it can be argued that the electrolaminate system is fundamentally safer than lower voltage systems that operate at higher currents (including electric motors, for example).

Even if we allowed a peak power of 10W, the resulting maximum operating current would be only 5 mA. This level of current may be associated with a slightly painful experience (akin to the shock one gets from touching a doorknob after shuffling ones feet across the carpet) but is not considered to be dangerous (Bernhardt 1988; Tans 1990).

We can ensure that the current would not exceed this threshold using redundant safety systems. First, the driving electronics will be designed to limit the current according to well-established current limiting schemes. Second, the electrodes can be designed to have a relatively high surface resistivity so that there is no possible way that a high current could discharge to the body even in the unlikely event of a direct short to the body caused by a puncture, tear or penetration of water or sweat. For example, an equivalent series resistance of 1 MΩ does not introduce significant electrical losses during normal operation but would limit the current to 2 mA with a maximum voltage of 2 kV.

Of course, the primary safety feature will be adequate insulation and arrangement of the electrodes to prevent contact with the body. The elastomers typically used in electrolaminates are good insulators. Further, we could ensure that the outermost electrodes will be at the same potential (equivalent to shielding for EMI). In order to produce a shock, the wearer would need to contact both electrodes, an unlikely event even with a catastrophic failure from puncture, tearing or water or sweat intrusion.

While operating at lower voltage is not a primary objective of the proposed work, we will take advantage of any advances in the technology that allow us to operate at lower voltages.

4.2 The Actuated Test Socket

The work required to create the actuated test socket (ATS) will be completed by Biomechatronics. The initial versions of the ATS's most critical module will be 3D printed using Objet's variable durometer printing technologies. The bladder array of the ATS is the most critical module of the device because it is the interface between the device and the amputee. It not only creates the shape and pressure field from which the amputee provides feedback to the prosthetist, but also sends data about the shape and pressure field in real-time to provide the prosthetist with computer processed data about the residual limb's current state.

Currently several different designs for the bladder system are being tested in order to determine the best mechanical solution. This determination is based on four main evaluation factors: the ability to collect accurate data, the ability to collect repeatable data, the maximum adjustability of the ATS inner wall, and user comfort.

There is no question that the accuracy of the shape and pressure field data collected by the ATS is extremely important. Unfortunately the required accuracy is defined by the accuracy of the electrolaminates that the quasi-passive socket uses for actuation. This is unfortunate because the algorithm that translates ATS data to QPS structure has not yet been developed, so exact requirements cannot be determined. Based on traditional socket data, we estimate that the ATS will need to accomplish at least 0.5mm (0.020 inches) resolution with shape, and at least 100Pa resolution with pressure. These requirements should be attainable using high-resolution potentiometers, as these sensors can be used to measure both pressure and shape.

The ATS's inner surface is by requirement an elastic, highly variable surface. At first this may suggest that repeatability in the data collected by the ATS would suffer drastically for small changes in subject leg placement, shifts in weight, or off-angle insertions. The solution to this problem has less to do with the design of the bladders themselves than with the control system that actuates them. The design of the bladders contributes a latency factor to the response time of the system. With the correct plant, the bladder control system is able to maintain the residual limb in exactly the right location even under external forces. The correct plant is a position control system that takes pressure data into account by cross-referencing position with non-linear stiffness data that are gathered during the fitting process. This method of control, while slightly more complicated, provides system stability and repeatability where there would be none with a plant that attempted to control pressure directly.

The maximum diameter change that the inner surface of the ATS can make is essentially double the maximum deflection of a single bladder. The larger the deflection of the bladder, the more non-linear the force response of the bladder becomes because

of the structure of the bellows that drive them. Additionally, trans-femoral sockets rise nearly to the insertion point of the gracilis, leaving very little space for large actuation distances. These space constraints make it impossible to create one device that can measure both trans-tibial and trans-femoral amputees. For this reason two versions of the device will be made: one for trans-femoral amputees, and one for trans-tibial amputees. The production of two ATS's will aid in the development process simply from making more devices.

User comfort during the fitting process is critical to a successful device. In order to be certain that the amputee will not be able to feel the discrete bladders that make up the ATS's inner surface, special consideration must be taken for the material properties and shape of the inner surface itself. The connection point between the flexible inner surface and the bellows that drive them must feel no different than the rest of the surface. This is a challenging problem mechanically because each bladder is able to exert an arbitrary force on the residual limb. First order calculations suggest that slight variations in the inner wall thickness will be able to alleviate this problem.

4.3 ATS Data Translation and QPS Test Socket 3D Printing

Mediated Matter's role will be to provide a 3D printed variable stiffness passive socket based on data generated from the ATS. The end product needs to have not only an ideal socket shape as determined by the ATS but also the appropriate dynamic shape properties. This will be accomplished by building on concepts and methodologies previously demonstrated by Neri Oxman and by utilizing commercially available 3D printing technology.

The general concept of mapping patient profiles to functionally graded, digitally fabricated materials and structures based on patients' anatomical and physiological requirements has been demonstrated previously in *Beast* and *Carpal Skin*. The first is a 3D printed chair designed to accommodate the unique load, curvature, and pressure profiles of each individual through variations in thickness, pattern density, stiffness, and flexibility. The second is a project that maps the pain-profile of a particular patient's hand and uses it to determine the correct distribution of hard and soft materials around the limb.

In the case of the 3D Printed Variable Stiffness Passive Socket, the mapping of patient residual limb stiffness profiles and necessary dynamic properties will be accomplished via the ATS. The ATS data will then be assigned to appropriate combinations of materials and structures that provide the required variations in mechanical properties (e.g. stiffness and flexibility) in a method similar to those used in *Beast* and *Carpal Skin*. The 3D printed socket prototypes will be printed using Objet Connex500 printers. Using up to 14 of Objet's Digital Materials for each socket, materials of different mechanical properties (e.g. durometer, toughness, or elasticity) can be placed in any structure at a resolution of 600 dpi in the x and y direction and 1600 dpi in the z direction using 16 micron layers.

Unique to the passive socket prototype will be the structure and types of materials used as well as an automated method of translating the ATS data mapping directly into STL files that can be directly read by most commercial 3D printers. Previous demonstrations of Functionally Graded Rapid Prototyping have involved manually creating files for each section of the end-product composed of a different materials using CAD software and then using additional software to combine multiple CAD files into a STL file for each different material. In order for it to be feasible to efficiently create passive socket prototypes for each patient, this process has to be automated.

There are limitations imposed by the number and variety of Digital Materials available through the Connex500. There are 51 different materials available that cover a large range of material properties such as high impact resistance (up to 1.22-1.5 ft lb/inch for ABS-like Digital Materials), flexural moduli (1026 MPa for Objet DurusWhite), and hardness variations (Shore A values from Shore 40 to Shore 95 for Objet Tango). Material properties exhibited by these Digital Materials are available only in discrete gradations. For example, within the rubber-like materials, Shore 27 A and 40 A values are attainable but Shore 30 A is not. It is feasible that material properties outside of or in between these ranges will be required. In these cases, it may be necessary to layer different materials or provide structural solutions in order to attain the desired overall mechanical properties. While further testing and calculations need to be done to determine the full range of mechanical properties that we will be able to achieve, we are confident that we can meet the requirements in a satisfactory manner using the materials available and layering and structural techniques.

The materials used by the Connex500 are not sufficiently sturdy for long-term use as production sockets. However, as the 3D printed passive socket prototype is only meant for use in a clinical setting to validate the data from the ATS, this should not be a major concern. Although some further testing should be done to characterize the life cycle of the sockets, material failures (e.g. small cracks or tears) – if they do occur – would occur under the supervision of a prosthetist and would not have sufficient opportunity to development into more catastrophic failures during the duration of the fitting.

5. Team Capabilities

This project boasts an extremely diverse team of scientists and engineers from all over the world. Below is a brief suggestion of the skills each of the three coordinating groups will bring to this project by describing their facilities and/or previous work.

5.1 SRI

As the inventors and primary developers of the **electrolaminate technology**, SRI is uniquely qualified to carry out the proposed work. SRI is a not-for-profit research institute with more than 60 years of experience in providing research and development

for a wide variety of government and commercial partners. SRI's headquarters in Menlo Park, California includes more than 1,000,000 square feet of general and special purpose laboratory space as well as model shop facilities for prototype fabrication.

The proposed work would be based in the Robotics Laboratory of the Engineering and Systems Group. This laboratory maintains the needed fabrication and test equipment required to carry out the proposed work. Additional facilities and expertise may be added as needed from other groups around the institute. These groups may include specific expertise in materials and coatings, for example.

The Robotics Laboratory has a long history of successful development efforts for DoD clients. These development efforts have included many projects based on a type of electroactive polymer invented by SRI. For TATRC, SRI is developing implantable artificial muscle based on their electroactive polymers in order to restore the ability to blink to those who have sustained neuromuscular damage. We have recently shown this capability in a human cadaver. SRI's electroactive polymer is an example of a successful technology transfer. In 2004, SRI created a spinoff, Artificial Muscle Inc. for the purpose of commercializing the technology. In 2010 this company was acquired by Bayer Material Science LLC. The first commercial consumer product, a haptic display actuator for an Apple iPod gaming add-on, will be available this summer.

For DARPA, SRI is exploring the use of electrolaminates for several applications including configuration control of low-cost underactuated robotic hands (DARPA ARM-H program), shape-locking of reconfigurable space structures, and skins and tunable structures for adaptive airfoils. Figure SRI5 below shows a close up of an electrolaminate joint-locking mechanism incorporated into an underactuated robotic finger. SRI is presently executing a project for DARPA that is aimed at improving our understanding of electrostatic clamping mechanisms so that we can make electrolaminates with greater clamping forces, faster response times and lower power consumption. The proposed effort can leverage these advances as they become available. We note, however, that the success of the proposed work does not depend on such improvements.

5.2 Mediated Matter

Previous work has been carried out setting up the theoretical, methodological, and technical foundations for Variable Property Design Fabrication. A variable-property 3-D printing prototype able to dynamically mix and vary the ratios of different materials in order to produce a continuous gradient in a 3-D printed part was developed. This project establishes a novel nozzle design coupled with a mixing chamber that can produce a continuous gradient, using colors as a substitute for material properties.

Potential design applications for **Functionally Graded Rapid Prototyping** occupy a vast range of possibilities in medical device design, product design, and architectural design. We present two examples facilitated by the FGF approach: ***Beast***, a prototype for a Chaise Lounge, is a 3-D printed chair. It combines structural,

environmental and corporeal performance by adapting its thickness, pattern density, stiffness, flexibility and translucency to load, curvature, and skin-pressured areas respectively. A single continuous surface acting both as structure and as skin is locally modulated to cater for structural support on the one hand, and corporeal performance on the other.

Carpal skin is a process by which to map the pain-profile of a particular patient – its intensity and duration - and distribute hard and soft materials to fit the patient's anatomical and physiological requirements limiting movement in a customized fashion. The formation process involves case-by-case pain registration and material property assignment. A 3-D scan of the patient's hand, including its pain registration, is mapped to a 2-D representation on which the distribution of elastic modulus is applied. This pain-map is then folded back to its 3-D form and 3-D printed using photopolymer composites.

5.3 Biomechatronics

We know from early Roman mosaics that physical rehabilitation and amplification technologies have been used during much of recorded history. Although the goal of constructing such technologies is not new, great scientific and technological hurdles still remain. Even today, permanent assistive devices are viewed by the physically challenged as separate, lifeless mechanisms and not intimate extensions of the human body—structurally, neurologically, and dynamically. The Biomechatronics group seeks to advance technologies that promise to accelerate the merging of body and machine, including device architectures that resemble the body's own musculoskeletal design, actuator technologies that behave like muscle, and control methodologies that exploit principles of biological movement.

The **Artificial Gastrocnemius** project investigates how human walking neuromechanical models show how each muscle works during normal, level-ground walking. They are mainly modeled with clutches and linear springs, and are able to capture dominant normal walking behavior. This suggests to us to use a series-elastic clutch at the knee joint for below-knee amputees. We have developed the powered ankle prosthesis, which generates enough force to enable a user to walk "normally." However, amputees still have problems at the knee joint due to the lack of gastrocnemius, which works as an ankle-knee flexor and a plantar flexor. We hypothesize that metabolic cost and EMG patterns of an amputee with our powered ankle and virtual gastrocnemius will dramatically improve.

The **Biomimetic Active Prosthesis for Above-Knee Amputees** proposes a novel biomimetic active prosthesis for above-knee amputees. The clinical impact of this technology focuses on improving an amputee's gait symmetry, walking speed, and

metabolic energy consumption on variant terrain conditions. The electromechanical design of this robotic device mimics the body's own musculoskeletal design, using actuator technologies that have muscle-like behaviors and can integrate control methodologies that exploit the principles of human locomotion. This work seeks to advance the field of Biomechatronics by contributing to the development of intelligent assistive technologies that adapt to the needs of the physically challenged.

The **Command of Powered Ankle Angle using Electromyography** shows that while the current powered ankle under development can readily adapt to constant surfaces while walking (including slopes and stairs), it is unable to predict slope transitions; particularly when the walking surface changes from a positive to a negative slope (or vice versa) within one step. This project explores to effect of using voluntary electromyography (EMG) signal from muscles in the residual limb to adjust ankle angle for better accommodation of slope transitions. Unilateral, trans-femoral amputees will walk across a course consisting of a series of changing slopes while using either a conventional prosthesis or the powered ankle with EMG commanded ankle position. It is thought that by giving the user a simple, effective, and rapid means of adjusting ankle angle, the safety and comfort of gait during rapid slope transitions can be improved.

6 Individual Resumes

Below are resumes in biographical sketch format for Hugh Herr, Neri Oxman, and Roy Kornbluh. Each contain information about education, employment status, publications/patents, honors/awards, and current research support.

6.1 Hugh Herr

NAME	POSITION TITLE
Hugh M. Herr, Ph.D.	**Associate Professor** Program in Media Arts and Sciences and Health Sciences and Technology, MIT **Lecturer** Department of Physical Medicine and Rehabilitation, Spaulding Rehabilitation Hospital, Harvard Medical School

6.1.1 Education/Training

INSTITUTION AND LOCATION	DEGREE	YEAR CONFERRED	FIELD OF STUDY

Millersville University Millersville, PA	B.A.	1990	Physics
Massachusetts Institute of Technology Cambridge, MA	S.M.	1993	Mechanical Eng.
Harvard University Cambridge, MA	Ph.D.	1998	Biophysics
Massachusetts Institute of Technology Cambridge, MA	Postdoc	1998-99	Bioengineering

6.1.2 Positions, Employment and Honors

6.1.2.1 Positions and Employment

Postdoctoral Fellow
1998 to 1999, Electrical Engineering and Computer Science, MIT

Instructor
1999 to 2003, *Department of Physical Medicine and Rehabilitation, Spaulding Rehabilitation Hospital, Harvard Medical School*

Instructor
1999 to 2003, *MIT-Harvard Division of Health Sciences and Technology*

Assistant Professor
2003 to 2004, *Department of Physical Medicine and Rehabilitation, Spaulding Rehabilitation Hospital, Harvard Medical School*

Lecturer
2004 to present, *Department of Physical Medicine and Rehabilitation, Spaulding Rehabilitation Hospital, Harvard Medical School*

Assistant Professor
2004 to 2006, *Program in Media Arts and Sciences and Health Sciences and Technology, MIT*

Associate Professor
2006 to present, *Program in Media Arts and Sciences and Health Sciences and Technology, MIT*

Associate Professor with Tenure
2009 to present, *Program in Media Arts and Sciences and Health Sciences and Technology, MIT*

6.1.2.2 Honors/Awards

YEAR	NAME OF HONOR
1989	Pennsylvania Sports Hall of Fame
1990	United States College Academic Team
1990	Young American Award, National Boy Scouts Council of America
1992 to 1995	Office of Naval Research Fellow
2001	Howard R. Thranhardt Lecture Honorarium, American Academy of Orthotists & Prosthetists
2003	Science Magazine Next Wave: Best of 2003
2004	Best Invention of the Year, Time Magazine
2005	Popular Mechanics Breakthrough Leadership Award
2005	NEC Career Development Professorship
2006	Howard R. Thranhardt Lecture Honorarium, American Academy of Orthotists & Prosthetists
2007	Heinz Award in Technology, the Economy and Employment
2007	Best Invention of the Year, Time Magazine
2008	Action Maverick Award
2008	Spirit of Da Vinci Award

6.1.3 Selected Peer-Reviewed Recent Publications

1. **Herr** H, Wilkenfeld A. User-Adaptive Control of a Magnetorheological Prosthetic Knee. Industrial Robot Journal: Special Issue on Biomedical Devices 2002 (In press).
2. Seyfarth A, Geyer H, **Herr** H. Leg Retraction: A Simple Control Strategy for Stable Running. The Journal of Experimental Biology 2003; 206: 2547-2555.
3. Blaya J., **Herr** H. Adaptive Control of a Variable-Impedance Ankle-Foot Orthosis to Assist Drop Foot Gait. IEEE Transactions on Neural Systems & Rehabilitation Engineering 2004; 12(1): 24-31.

4. Johansson J., Sherrill D., Riley P., Paolo B., **Herr** H. A Clinical Comparison of Variable-Damping and Mechanically-Passive Prosthetic Knee Devices. American Journal of Physical Medicine & Rehabilitation. 2005; 84(8): 563-575.

5. Farahat W., **Herr** H. An Apparatus for Generalized Characterization and Control of Muscle. IEEE Transactions on Neural Systems & Rehabilitation Engineering. 2005; 13(4): 473-481.

6. Popovic M., Goswami A., **Herr** H. Ground Reference Points in Legged Locomotion: Definitions, Biological Trajectories and Control Implications. International Journal of Robotics Research. 2005; 24(10): 1013-1032.

7. Paluska D., **Herr** H. The Effect of Series Elasticity on Actuator Power and Work Output: Implications for Robotic and Prosthetic Joint Design. Robotics and Autonomous Systems. 2006; 54: 667-673.

8. Conor W., Endo K., **Herr** H. A Quasi-passive Leg Exoskeleton for Load-carrying Augmentation. International Journal of Humanoid Robotics. 2007; 4 (3): 487-506.

9. Dollar A., **Herr** H. Lower Extremity Exoskeletons and Active Orthoses: Challenges and State-of-the-Art. IEEE Transactions on Robotics, Special issue on Biorobotics. 2008; 24(1): 144-158.

10. **Herr** H., Popovic M. Angular Momentum in Human Walking. Journal of Experimental Biology. 2008; 211, 467-481.

11. Au S., Berniker M., **Herr** H. Powered Ankle-Foot Prosthesis for Level-Ground and Stair Descent Ambulation. International Journal of Neural Networks. Special Issue in Robotics and Neuroscience. 2008; 21: 654-666.

12. Au S., **Herr** H. On the Design of a Powered Ankle-Foot Prosthesis: The Importance of Series and Parallel Motor Elasticity. Special Issue of the IEEE Robotics & Automation Society IEEE Magazine on Adaptable Compliance for Robotic Applications. September 2008; 52-59.

13. Au S., Weber J., **Herr** H. Powered Ankle-foot Prosthesis Improves Walking Metabolic Economy. IEEE Transactions on Robotics. 2009; 25 (1): 51-66.

14. Eilenberg M.F., Geyer H., and **Herr**, H. Control of a powered ankle-foot prosthesis based on a neuromuscular model. IEEE Transactions on Neural Systems and Rehabilitation Engineering, 18(2): 164-73, 2010.

15. Farahat, W. and **Herr**, H. Optimal Workloop Energetics of Muscle-Actuated Systems: An Impedance Matching View. PLoS Computational Biology, 6(6):e1000795. doi:10.1371/journal.pcbi.1000795, 2010.

16. Markowitz J., Krishnaswamy P., Eilenberg M.F., Endo K., Barnhart C., and **Herr** H. Speed Adaptation in a powered transtibial prosthesis controlled with a neuromuscular model. Phil. Trans. R. Soc. B, 366:1621-1631, 2011.

17. Krishnaswamy P., Emory, B., **Herr**, H. Human Leg Model Predicts Ankle Muscle-Tendon Morphology, State, Roles and Energetics in Walking. PLoS Computational Biology, March 2011.

6.1.4 Current Research Support

Government Award 10/01/09 – 9/30/14
Department of Veteran Affairs
Rebuilding, Regenerating, and Restoring Function After Traumatic Limb Loss

MIT shall develop a fully robotic transfemoral prosthesis comprising a motorized ankle and knee components. A muscle reflex model-based control will be advanced for the transfemoral system and compared to the performance of an intact limb for level ground ambulation.

Government Award 09/01/09 – 08/31/14
Army
Prosthetic Knee-ankle-foot System with Biomechatronic Sensing, Control, and Power Generation

MIT shall develop a knee prosthesis capable of emulating intact-limb knee mechanics in level-ground walking without requiring net power from an onboard battery.

Government Award 09/01/09 – 08/31/14
Army
Development of a Neural Interface for Powered Lower Limb Prostheses

MIT shall develop neural control strategies for a powered ankle-foot prosthesis using surface electrodes.

Government Award 09/01/09 – 08/31/12
Department of Veteran Affairs
Implantable Myoelectric Sensors for Control of a Powered Foot Prosthesis

MIT shall develop neural control strategies for a powered ankle-foot prosthesis using an implantable myoelectric sensor.

6.2 Neri Oxman

NAME	POSITION TITLE
Neri Oxman, Ph.D.	**Assistant Professor** Program in Media Arts and Sciences and Health Sciences and Technology, MIT **Presidential Fellow** Massachusetts Institute of Technology

6.2.1 Education/Training

INSTITUTION AND LOCATION	DEGREE	YEAR CONFERRED	FIELD OF STUDY
Hebrew University Medical School Jerusalem, ISRAEL		1996-1999	Medicine
Technion Institute of Technology Haifa, ISRAEL		1999-2002	Architecture & Urban Planning
Architectural Association London, UK	Dipl Eng (RIBA Hons)	2002-2004	Architecture & Urban Planning
Massachusetts Institute of Technology Cambridge, MA	Ph.D.	2005-2010	Design Computation

6.2.2 Positions, Employment and Honors

6.2.2.1 Positions and Employment

First Lieutenant
1994 to 1996, *Air Force Base Headquarters*

Architect
2002 to 2004, *Ram Carmi Associates, Israel*

Architect
2004 to 2006, *KPF Associates, London, UK*

Visiting Associate
2004 to 2005, *Smart Geometry Group, London, UK*

Instructor
2004 to 2005, *Emergent Technologies & Design, Architectural Association, London*

Presidential Fellow
2005 to 2010, *Design Computation, Department of Architecture, MIT*

Assistant Professor
2010 to present, *Program in Media Arts and Sciences, MIT*

6.2.2.2 Honors/Awards

YEAR	NAME OF HONOR
2002	Eileen Grey Award
2002	Ian Davidson Future Practice Award
2003	Bentley Award
2004	Presidential Fellowship
2005	America Israel Cultural Foundation Award
2006	Harold Horowitz Award
2004	Archiprix International Award
2006	FEIDAD Design Top 30 Award
2007	Young CAADRIA Award
2007	Schintzer Prize, MIT
2008	Revolutionary Mind Award, SEED Magazine
2008	Carter Manny Award, Graham Foundation for the Arts
2008	HOLCIM Next Generation Award for Sustainable Construction
2009	Earth Award for Future Crucial Design
2009	METROPOLOSI Next Generation Award
2010	SONY Career Development Professor

6.2.3 Selected Peer-Reviewed Recent Publications

Papers in Refereed Journals

Oxman, N. (2011). "Variable property rapid prototyping." Virtual and Physical Prototyping **6**(1): 3-31.

Oxman, N. (2011). "Variable property design fabrication." Building Research & Information. In publication

Oxman, N., Keating, S., Tsai, E. (2011). "Variable property design fabrication." "Innovative developments in virtual and physical prototyping ", 2011, P.J. Bártolo et al., published by Taylor & Francis. Under review

Oxman, N., Keating, S., Tsai, E. (2011). "Finite Element Synthesis." "Innovative developments in virtual and physical prototyping ", 2011, P.J. Bártolo et al., published by Taylor & Francis. Under review

Oxman, N. Get Real: Towards Performance Driven Computational Geometry. International Journal of Architectural Computing (IJAC). 2007; 4(5): 663 -684.

Oxman, N. and J. L. Rosenberg. Material-based Design Computation: An Inquiry into Digital Simulation of Physical Material Properties as Design Generators. International Journal of Architectural Computing (IJAC). 2007; 5(1): 26-44.

Oxman, N. Material-based Design Computation: Tiling Behavior. In publication for ACADIA Proceedings, 2009.

Oxman, N. Rapid Gestalt(en). Proceedings of Euro U-Rapid: International User's Conference on Rapid Prototyping, Rapid Tooling and Rapid Manufacturing; 2008; Berlin, Germany, 61-69.

Oxman, N. Oublier Domino: On the Evolution of Architectural Theory from Spatial to Performance-based Programming. Proceedings of Critical Digital Conference: What Matters? Harvard Graduate School of Design, Harvard University, 2008; Cambridge, MA, 393-403.

Oxman, N. Rapid Craft: Machine Immanence and Naïve Materialization. Proceedings of IASS 2007, Shell and Spatial Structures: Structural Architecture: Towards the Future Looking to the Past, 2007; Venice, Italy; 269 – 276.

Oxman, N., Rosenberg, J., L. Material Based Design Computation. Proceedings of CAADRIA: the 12th International Conference on Computer Aided Architectural Design Research in Asia. April 2007; Nanjing, China; 5-12

Oxman, N. FAB Finding. Proceedings of The 25th eCAADe Conference: Predicting the Future. September 2007; Frankfurt am Main, Germany; 785-792.

Oxman, N. Rapid Craft: Material Experiments Towards an Integrated Sensing Skin System. Proceedings of the 27th Annual Conference of the Association for Computer Aided Design in Architecture: Expanding Bodies: Art • Cities• Environment. October 2007;

Halifax, Nova Scotia; 182-191.

Oxman, N. Rapid Craft: Machine Immanence and Naïve Materialization. Proceedings of UbiComp: International Conference on Ubiquitous Computing. September 2007; Innsbruck, Austria; 534-538

6.2.4 Current Research Support

Government Award 01/01/10 – 1/01/12
Institute for Soldier Nanotechnologies

Morphometric Origins of Biological and Bio-inspired Flexible Exoskeleton Design via Mechanics of Macroscale Prototypes

Co PI's: Christine Ortiz (ICB), Mary C. Boyce (ISN)

6.3 Roy Kornbluh

NAME	POSITION TITLE
Roy Kornbluh, S.M.	**Principal Research Engineer** SRI International
	Associate Editor Journal of NeuroEngineering and Rehabilitation

6.3.1 Education/Training

INSTITUTION AND LOCATION	DEGREE	YEAR CONFERRED	FIELD OF STUDY
Cornell University Ithaca, New York	B.S.	1982	Mechanical Engineering
Massachusetts Institute of Technology Cambridge, MA	S.M.	1984	Mechanical Engineering

6.3.2 Positions, Employment and Honors

6.3.2.1 Positions and Employment

Principal Research Engineer

1984 to 1991, 1994 to Present, SRI International, Menlo Park, CA

U.S. Peace Corps Volunteer

1991 to 1993, Manabi, Ecuador

6.3.2.2 Honors/Patents

YEAR	NAME OF HONOR/PATENT
2002 to 2008	International Program Committee of the Electroactive Polymers and Devices Conference of SPIE, a Biannual Conference
2004	Biologically Powered Electroactive Polymer Generators, US 6,768,246
2005	Variable stiffness electroactive polymer systems, US 6,882,086
2005	Master/slave electroactive polymer systems, US 6,876,135
2008	Electroactive Polymer Generators US 7,368,862
2009	Mechanical meta-materials, US 7,598,652

6.3.3 Selected Peer-Reviewed Recent Publications

Roy Kornbluh, Annjoe Wong-Foy, Ron Pelrine, Harsha Prahlad, Brian McCoy, 2010 "Long-lifetime All-polymer Artificial Muscle Transducers." To be published in the *Proc. of the 2010 MRS Spring Meeting Symposium JJ*

F. Carpi, D. De Rossi, R. Kornbluh, R. Pelrine, and P. Sommer-Larsen, Eds., 2008 *Dielectric Elastomers as Electromechanical Transducers. Fundamentals, Materials, Devices, Models and Applications of an Emerging Electroactive Polymer Technology.* Amsterdam, The Netherlands: Elsevier

Chiba S., Waki M., Kornbluh .R and Pelrine R. 2008 "Innovative power generators for energy harvesting using electroactive polymer artificial muscles", *Proc. SPIE* 6927 692715

Kornbluh, R.D., Prahlad, H., Pelrine, R., Stanford, S., Rosenthal, M.A., von Guggenberg, P.A.,"Rubber to rigid, clamped to undamped: toward composite materials with wide-range controllable stiffness and damping", Proceedings of SPIE -- Volume 5388, Smart Structures and Materials 2004: Industrial and Commercial Applications of Smart Structures Technologies, Eric H. Anderson, Editor, 2004, pp. 372-386

Herr, H. and Kornbluh, R.D., 2004. "New horizons for orthotic and prosthetic technology: artificial muscle for ambulation," Smart Structures and Materials 2004: Electroactive Polymer Actuators and Devices, ed. Y. Bar-Cohen, Proc. SPIE, Vol. 5385, pp. 1-9.

R. Kornbluh, R. Pelrine, Q. Pei, M. Rosenthal, S. Stanford, N. Bonwit, R. Heydt, H. Prahlad, S. Shastri, "Application of Dielectric Elastomer EAP Actuators", Chapter 16 in *Electroactive polymer (EAP) actuators as artificial muscles: reality, potential and challenges*, Y. Bar-Cohen, ed. 2nd edition., SPIE Press, Bellingham, Washington, 2004, pp. 529-589.

Kornbluh, R.D., D.S. Flamm, H. Prahlad, K.M. Nashold, S. Chhokar, R. Pelrine, D.L. Huestis, J.Simons, T. Cooper, and D.G. Watters. 2003. "Shape control of large lightweight mirrors with dielectric elastomer actuation," *Smart Structures and Materials 2003: Electroactive Polymer Actuators and Devices (EAPAD), Proc. of the SPIE*, Volume 5051, pp. 143-158 (2003)

Kornbluh, R.D., R.E. Pelrine, Q. Pei, R. Heydt, S.E. Stanford, S. Oh, and J. Eckerle. 2002. "Electroelastomers: Applications of Dielectric Elastomer Transducers for Actuation, Generation and Smart Structures," *Smart Structures and Materials 2002: Industrial and Commercial Applications of Smart Structures Technologies, Proc. SPIE*, Vol. 4698, pp. 254-270.

R. Pelrine, R. Kornbluh, J. Eckerle, P. Jeuck, S. Oh, Q. Pei, and S. Stanford, "Dielectric Elastomers: Generator Mode Fundamentals and Applications," in *Smart Structures and Materials 2001: Electroactive Polymer Actuators and Devices*, ed. Y. Bar-Cohen, *Proc. of SPIE*, Vol. 4329, pp. 148–156, 2001

Pelrine, R., R. Kornbluh, Q. Pei, and J. Joseph. 2000 "High-Speed Electrically Actuated Elastomers with Over 100% Strain," *Science*, Vol. 287, No. 5454, pp. 836–839

Pelrine R., Kornbluh R. and Joseph J. 1998 "Electrostriction of polymer dielectrics with compliant electrodes as a means of actuation" *Sensors Actuators A*", 64 77–85

6.3.4 Current Research Support

Government Award
Autonomously Deployed Energy Harvesting System in Coastal and Riverine Environment, Air Navy SBIR Phase I **5/9/11 – 11/7/11**

Mr. Kornbluh is leading SRI's effort ias a subcontractor on a Phase I contract whose goal is to develop energy harvesting systems using electroactive polymer (EAP) elements that can be be easily deployed and capture energy form a varoiety of hydrokinetic energy sources. SRI is responsible for the development of the EAP elements and overall design of energy harvesting device.

Government Award
Electrostatic interface characterization and enhancement for tunable materials, DARPA **6/1/11 - 2/28/12**

Mr. Kornbluh is the project leader in support of a DARPA-sponsored effort to better understand the factors that are involved in electrostatic clamping and leverage this knowledge to demonstrate improved electrolaminate materials. As such, this project can benefit the proposed VAI2 effort. The proposed work, this effort looks at the physics of the electrolaminates at a fundamental level rather than application level.

7 References

Bernhardt, J.H. (1988) iThe establishment of frequency dependent limits for electric and magnetic fields and evaluation of indirect effects.ĩ Radiation and Environmental Biophysics 27(1): p1-27

Johannesson, A., G.U. Larsson, and T. Oberg. (2004) "From major amputation to prosthetic oucome: a prospective study of 190 patients in a defined population." Prosthetics and Orthotics International 28: p9-21.

Klasson, B.L. (1995) "Carbon fibre and fibre lamination in prosthetics and orthotics: some basic theory and practical advice for the practitioner." Prosthetics and Orthotics International 19: 74-91.

Laferrier, J.Z. and R. Gailey. (2010) "Advances in lower-limb prosthetic technology." Physical Medicine and Rehabilitation Clinics of North America 21(1): p87-110.

Mak, A.F.T, G.H.W Liu, and S.Y. Lee. (1994) "Biomechanical assessment of below-knee residual limb tissue." Journal of Rehabilitation Research and Development 31(3): p188-198.

Miyamoto, Y., W. Kaysser, et al. (1999) "Functionally graded materials: design, processing, and applications." Chapman & Hall.

Oxman, N. (2011) "Variable property rapid prototyping." Virtual and Physical Prototyping 6(1): p3-31.

Oxman, N. (2010) "Structuring materiality: design fabrication of heterogenous materials." Architectural Design 80(4): p78-85.

Phillips, J.R. and K.O. Johnson. (1981) "Tactile spatial resolution. III. A continum mechanics model of skin predicting mechanoreceptor responses to bars, edges, and gratings. Journal of Neurophysiology 46(6): p1204-1225.

Portnoy, S., J. van Haare, R.P.J. Geers, A. Kristal, I. Siev-Ner, H.A.M. Seelen, C.W.J. Oomens, and A. Gefen. (2010) "Real-time subject-specific analyses of dynamic internal tissue loads in the residual limb of transtibial amputees. Medical Engineering and Physics 32(4): p312-323.

Sanders, J.E. and C.H. Daly. (1993) "Normal and shear stresses on a residual limb in a prosthetic socket during ambulation: Comparison of finite element results with experimental measurements." Journal of Rehabilitation Research 30(2): p191-204.

Sanders, J.E., D.S. Harrison, K.J. Allyn, and T.R. Myers. (2009) "Clinical utility of in-socket residual limb volume change measurements: case study results." Prosthetics and Orthotics International 33(4): p178-190.

Sewell, P., S. Noroozi, J. Vinney, and S. Andrews. (2000) "Developments in the trans-tibial prosthetic socket fitting process: A review of past and present research." Prosthetics and Orthotics International 24(2): p97-107.

Silver-Thorn, M.B., J.W. Steege, D.S. Childress. (1996) "A review of prosthetic interface stress investigations." Journal of Rehabilitation Research and Development 33(3): p253-266.

Staker, M., K. Ryan, and K.LaBat. (2009) "Medicine and design investigate residual limb volume fluctuations: three case studies." Australasian Medical Journal 12(1): p156-161.

Tans, K.S. and D.L. Johnson. (1990) iThreshold of sensation for 60-Hz leakage current: results of a survey.ĩ Biomedical Instruments Technology 24(3): p207-2011

Wise, D.L., D.J. Trantolo, D.E. Altobelli, M.J. Yaszemski, and J.D. Gresser. (2006/2010) "Human Biomaterials Applications." Humana Press.

Appendix C

USVA Grant Project Management Plan

VA118-12-C-0040 Project Management Plan

MIT Prosthetic Socket Project

Period of Performance: September 28, 2012 – September 27, 2014
Collaborating Organizations: VA, MIT, SRI

Points of Contact:

MIT: Hugh Herr, hherr@media.mit.edu
SRI: Roy Kornbluh, roy.kornbluh@sri.com
VA: Allison Amrhein, allison.amrhein@va.gov and Derek Maselli, derek.maselli@va.gov

Project Description

The MIT Prosthetic Socket project seeks to create more comfortable sockets through better measurement techniques and improved socket fabrication practices. At first, we will create the robotic test socket that will consist of several actuated plates that will measure shape and dynamical information about a subject's residual limb. We will design a computation method by which this information can be used to inform the design of prosthetic sockets. From here, we will create sockets that reflect our models in order to demonstrate their performance. These sockets will incorporate both spatially variable, temporally constant stiffness and spatially variable, temporally variable stiffness paradigms.

Participants and Positions

MIT	VA	SRI
Hugh Herr *Lead PI for VA118-C-0040* *Biomechatronics*	**Jonah Czerwinski** *VACI Director* *Dept. Veterans Affairs*	**Roy Kornbluh** *PI for Electrolaminates* *SRI*
Neri Oxman *Co-PI at MIT* *Mediated Matter*	**Patricia Dorn** *Science Program Manager* *Dept. Veterans Affairs*	**Richard Mahoney** *Director of Robotics* *SRI*
Arthur Petron *Ph.D. candidate* *Biomechatronics*	**Allison Amrhein** *Innovation Coordinator* *Dept. Veterans Affairs*	**Allegra Shum** *Research Engineer* *SRI*
David Sengeh *Ph.D. candidate* *Biomecatronics*	**Summer Spalliero** *Contracts Specialist* *Dept. Veterans Affairs*	**Brian McCoy** *Research Engineer* *SRI*
Bryan Ranger *Ph.D. Candidate* *Biomechatronics*		**Tom Egan** *Product Design Engineer* *SRI*

Deliverables

Deliverables can be separated into five main areas:

1. Actuate Test Socket (ATS)

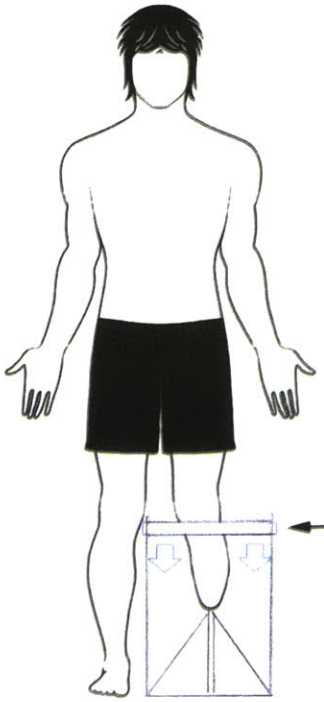

ATS is a ring that surrounds the residual limb

The ring is moved up and down on the residual limb to collect data about the entire residuum

After data is collected, it is processed by computer in order to determine the socket shape and impedance

2. 3D Printed Variable Stiffness Socket (VTS)

Able to print multiple material 3D parts using Objet's Connex500 3D printer

Material strength information programmed into CAD software for FEA analysis

We have tested this method of socket fabrication and know it can be used to testing purposes

3. Data Mapping from ATS to VTS/QPS
    1. We will explore the inverse stiffness mapping approach
        A. Where amputee is hard, we make the socket wall soft
        B. Where amputee is soft, we make the socket wall hard
    2. Use ATS data to inform the inverse mapping approach
    3. Establish algorithms that are able to translate data from ATS to VTS 3D print files

4. Electrolaminate Material Development
    - Almost passive – ultra-low power
    - Fast response

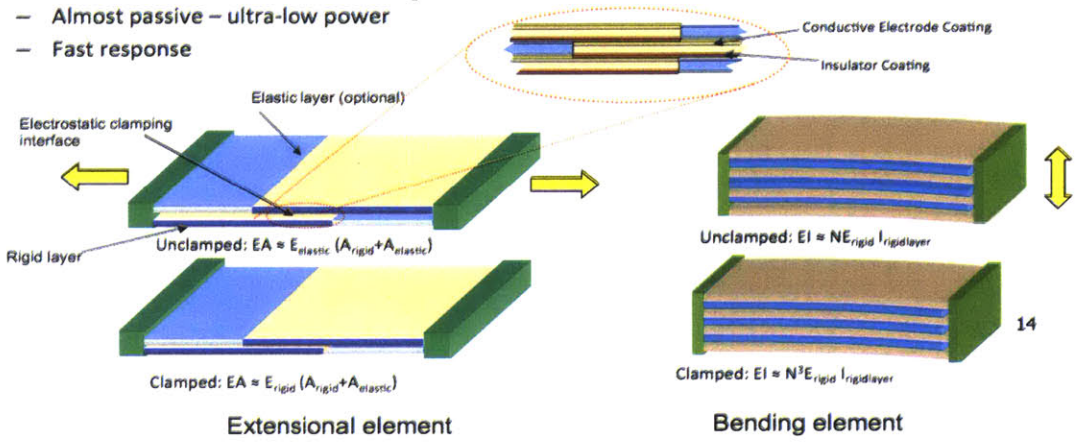

5. Quasi-Passive Socket (QPS)

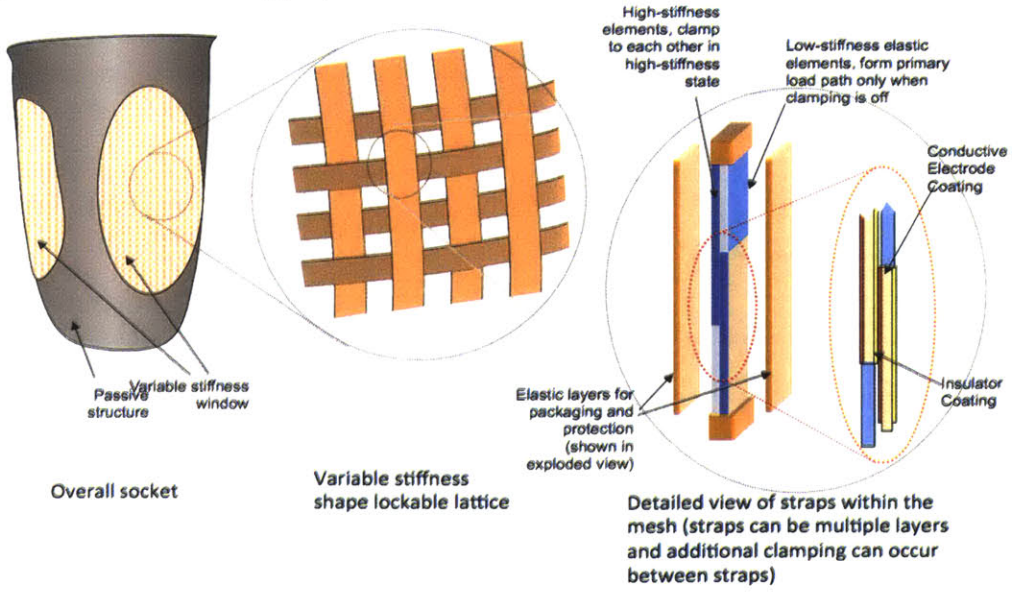

Deliverables Flowchart

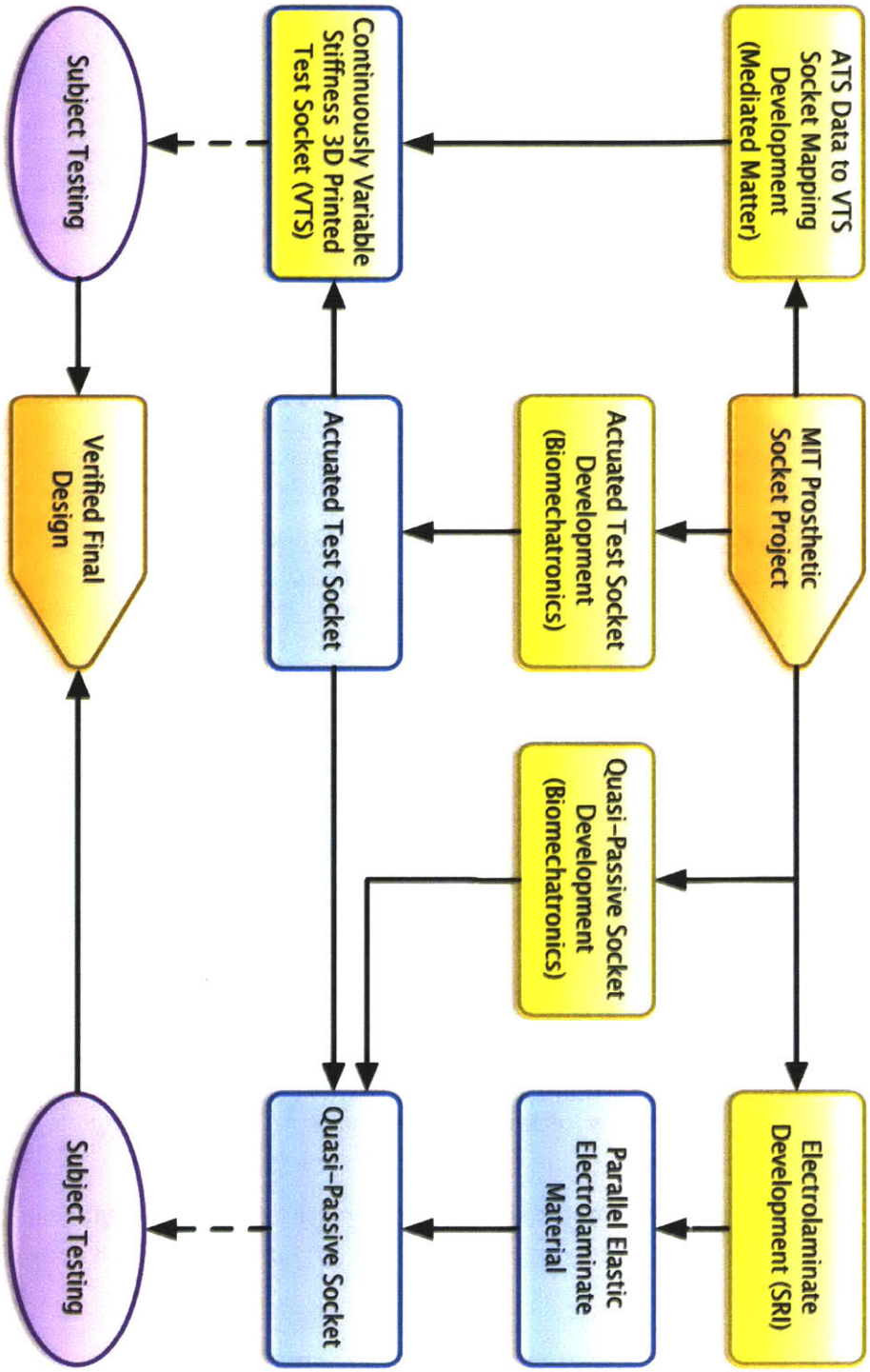

Deliverables Reference Sheet

Project Management Plan Updated Last – *September 5, 2014*

Pending Monthly Progress Reports - Complete

Bi-Annual Progress Presentations – April 18, 2014
September 12, 2014

Annual Progress Presentation Minutes – *Due 5 BD after presentation - Complete*

Actuated Test Socket (ATS) Development

- **ATS Relevant Technologies Report** – *Due November 27, 2012 – Complete*
- **ATS Prototype Demonstration** – *Due March 27, 2013 - Complete*
- **ATS V1.0 Demonstration** – *Due September 20, 2013 - Complete*
- **ATS V1.0 Prototype Performance Report** - *Due October 11, 2013 - Complete*
- **ATS V2.0 Demonstration** – *Due September 12, 2014 - Complete*
- **ATS V2.0 Prototype Performance Report** –*September 27, 2014 - Complete*
- **ATS Operational Guide** - *Due September 27, 2014 - Complete*
- **ATS User Guide** - *Due September 27, 2014 - Complete*

Variable Impedance Socket (VTS)

- **VTS Demonstration** - *Due September 20, 2013 - Complete*
- **VTS Prototype Performance Report** – *Due September 27, 2014 - Complete*
- **VTS STL Files** - *Due November 8, 2013 - Complete*

Actuated Test Socket Data Mapping

- **ATS Data Mapping Demonstration** - *Due March 27, 2013 - Complete*

Electrolaminate (EL) Technology Development

- **EL Relevant Technologies Report** - *Due November 27, 2012 – Complete*
- **EL Demonstrate Technology** – *Due March 27, 2013 - Complete*
- **EL V1.0 Demonstration** - *Due September 20, 2013 - Complete*
- **EL V2.0 Integration** – *Due April 18, 2014 – Complete*
- **EL V2.0 Demonstration** - *Due September 12, 2014 - Complete*
- **EL Design Report** - *Due September 20, 2013 - Complete*

Quasi-Passive Socket (QPS) Development

- **QPS V1.0 Demonstration** - *Due September 20, 2013 - Complete*
- **QPS V2.0 Demonstration** - *Due September 12, 2014 - Complete*
- **QPS Prosthesis Report** - *Due September 27, 2014 – Complete*

Prostheses

- **Transtibial Prosthesis** - *Due September 27, 2014 – Complete*

***Deliverable* Gantt Chart**

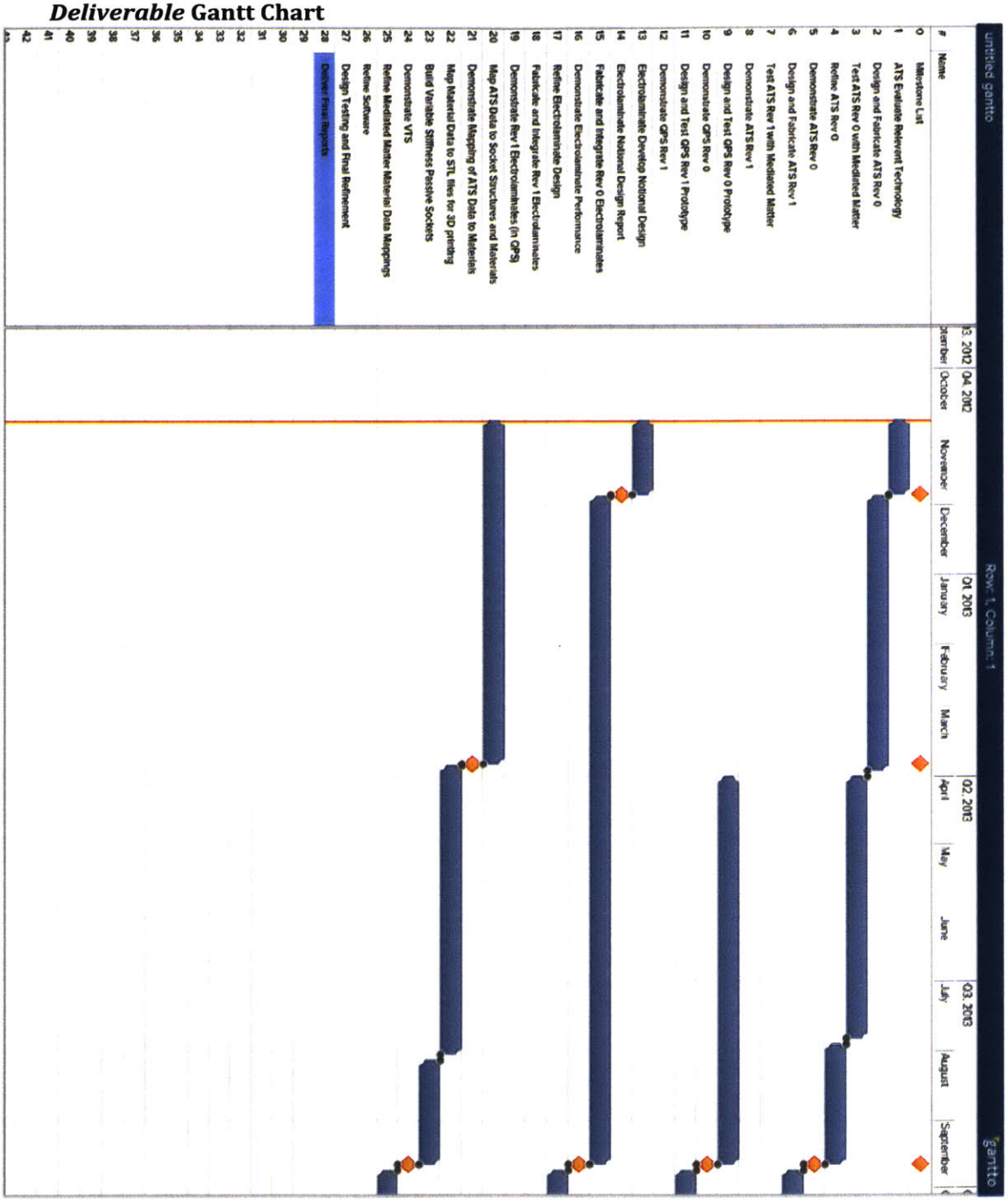

untitled gantto
Row: 1, Column: 2
gantto
Q4, 2013
Q1 2014
Q2, 2014
Q3, 2014
Q4, 2014
October
November
December
January
February
March
April
May
June
July
August
September
October
Name
0 Milestone List
1 ATS Evaluate Relevent Technology
2 Design and Fabricate ATS Rev 0
3 Test ATS Rev 0 with Mediated Matter
4 Refine ATS Rev 0
5 Demonstrate ATS Rev 0
6 Design and Fabricate ATS Rev 1
7 Test ATS Rev 1 with Mediated Matter
8 Demonstrate ATS Rev 1
9 Design and Test QPS Rev 0 Prototype
10 Demonstrate QPS Rev 0
11 Design and Test QPS Rev 1 Prototype
12 Demonstrate QPS Rev 1
13 Electrolaminate Develop Notional Design
14 Electrolaminate Notional Design Report
15 Fabricate and Integrate Rev 0 Electrolaminates
16 Demonstrate Electrolaminate Performance
17 Refine Electrolaminate Design
18 Fabricate and Integrate Rev 1 Electrolaminates
19 Demonstrate Rev 1 Electrolaminates (in QPS)
20 Map ATS Data to Socket Structures and Materials
21 Demonstrate Mapping of ATS Data to Materials
22 Map Material Data to STL files for 3D printing
23 Build Variable Stiffness Passive Sockets
24 Demonstrate VTS
25 Refine Mediated Matter Material Data Mappings
26 Refine Software
27 Design Testing and Final Refinement
28 Deliver Final Reports
29
30
31
32
33
34
35
36
37
38
39
40
41
42
Current Progress Line

Detailed Deliverables

1. ATS
    a. Evaluate relevant technology
        i. Analyze functional requirements
        ii. Determine specifications necessary to satisfy requirements
        iii. Select mechanical design that meets specifications
        iv. Select components for intended design
    b. Design and fabricate ATS Rev 0
        i. Order components
            1. Motors
            2. Ballscrews
            3. Raw Materials (screws, metal)
            4. Bearings (linear and rotary)
            5. Motor Controllers
            6. Electronics (capacitors, ICs resistors)
            7. PCBs
            8. Computer
            9. Force Sensors
            10. Position Sensors
        ii. Manufacture Components
            1. End Effector
            2. Bearing Blocks
            3. Motor Mounts
        iii. Develop control schemes
            1. Test motor controller
            2. Develop motor control software
                a. Design EtherCAT master
                    i. Work with experts to implement EtherCAT Master
                    ii. Program lab computer with expert input to run motion tests
                    iii. Program computer to log data from ATS
                b. Design GUI interface
                c. Design Data translation algorithms
            3. Develop ATS calibration schema
                a. Calibrate Position Error
                    i. LVDT not necessary
                    ii. Assemble testing hardware
                b. Calibrate Force Error
                c. Determine bandwidth of mechanical system
                d. Calibrate Force Value to Force Reading
            4. Debug as necessary
                a. Debug malfunctioning force sensors
                b. Increase sampling frequency
        iv. Assemble unit prototypes (Projected February 14)

1. Manufacture ring base plate
2. Assemble motor, ball screw, etc.
3. Integrate electronics with sensors and motors
4. Calibrate unit
5. Run system test

v. Assemble full prototypes (Projected March 18)

1. Manufacture vertical positioning system
2. Merge units into ring
3. Test/Develop controls for ring
4. Calibrate ring
5. Run system test
6. Run experiment

c. Refine ATS Rev 0

i. Test unit with experimental controls

ii. Finalize hardware and software

1. Determine software structure
2. Lay out software objects
   a. Machine object
   b. Test object
   c. Experiment object
   d. Analysis object
   e. Results object
   f. Visualizer object
   g. GUI object

iii. Iterate design

1. Decide between EtherCAT control or MCBMini control
   a. Flop back and forth between the two
   b. Choose EtherCAT because there's no time
2. Assemble experimental system for test
   a. Add additional sensors (capacitive)
   b. Integrate all electronics with Java
   c. Debug everything

d. Demonstrate ATS Rev 0

e. Design and Fabricate ATS Rev 1

i. Use knowledge from previous ATS rev to provide new design

ii. Order new parts where necessary

iii. Assemble ATS Rev 1

iv. Finalize hardware control and software interface

f. Test ATS Rev 1 with Mediated Matter

i. Collect data from an amputee

ii. Use data to inform socket design through MM's software

iii. 3D print test socket (VTS)

iv. Test socket fit on amputee

g. Demonstrate ATS

2. VTS

a. Generate residual limb data format

b. Create residual limb data to socket data translation algorithms
c. Collect data from ATS and modeling software
d. 3D print test socket
    i. Create Objet socket files
    ii. Send Objet 3D files
    iii. Receive 3D printed socket
e. Explore alternative methods of variable stiffness socket manufacture
    i. Look into composite variable stiffness technology
    ii. Test various composites and determine properties/specs
    iii. Create test sockets for evaluation purposes
f. Test VTS on amputees
    i. Schedule amputees for visit
    ii. COUHES
    iii. Develop evaluation criteria
    iv. Test sockets
    v. Demonstrate VTS

3. QPS
    a. Determine electrolaminate design parameters
    b. Schedule initial test with subject for mid-summer 2013
    c. Receive electrolaminate prototype from SRI
    d. Fabricate socket for amputee with electrolaminate mounting
    e. Develop electrolaminate control electronics
    f. Integrate electrolaminate, control hardware, and socket
    g. Test QPS on amputee
4. Electrolaminate
    a. Develop notional design
    b. Develop electrolaminate proof of concept
        i. Order materials for R and D on weaving tech
        ii. Test weaving techniques on EL
    c. Fabricate Rev 0 electrolaminates
    d. Assist MIT with electrolaminate Rev 0 integration
    e. Demonstrate Electrolaminate performance
    f. Refine electrolaminate design based on performance demonstration
    g. Fabricate electrolaminate Rev 1 design
    h. Assist MIT with electrolaminate Rev 1 integration
    i. Demonstrate Rev 1 electrolaminates in QPS
5. Modeling
    a. Establish data structure and types
    b. Populate data structure with test data
    c. Design model to convert data to socket properties
    d. Create 3D models from model and test in CAD
    e. 3D print VTS 1
    f. Refine model based on VTS 1 demonstration
    g. 3D print VTS 2
    h. Refine model based on VTS 2
    i. 3D print VTS 3

6. Subject Testing
    a. Year 1
        i. Get initial subject list
        ii. Schedule subjects for testing with ATS
        iii. Test subjects with ATS
        iv. Schedule subjects for socket testing
        v. Test subjects with sockets and Tekscan system
    b. Year 2
        i. Schedule subjects for testing with ATS
        ii. Test subjects with ATS
        iii. Schedule subjects for socket testing
        iv. Test subjects with sockets and Tekscan system
        v. Finalize results
    c. General Testing
        i. Schedule subjects as needed to test various parts for the FitSocket
        ii. Test subjects, create sockets and test as time allows

Management Organizational Structure

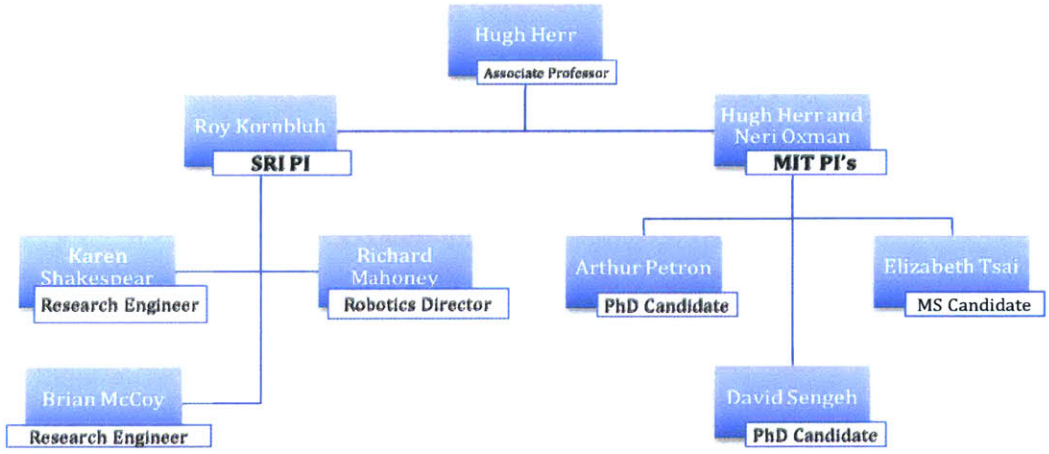

Reporting

The Contractor shall provide the Contracting Officer's Technical Representative (COTR) with Monthly Progress Reports in electronic form in Microsoft Word and Project formats. The report shall include detailed instructions/explanations for each required data element, to ensure that data is accurate and consistent. These reports shall reflect data as of the last day of the preceding Month.

The Monthly Progress Reports shall cover all work completed during the reporting period and work planned for the subsequent reporting period. The report shall also identify any problems that arose and a description of how the problems were resolved. If problems have not been completely resolved, the Contractor shall provide an explanation including their plan and timeframe for resolving the issue. The Contractor shall monitor performance against the PMP and report any deviations. It is expected that the Contractor will keep in communication with VA accordingly so that issues that arise are transparent to both parties to prevent escalation of outstanding issues.

An annual progress meeting including the primary and sub-contractors will be held to review the progress of the contract. MIT Contractor and SRI Sub-contractor presence shall be required at the VA DC facility. Other sub-contractor participation shall be remote.

Reports will be electronically submitted to Allison Amrhein and/or Derek Maselli.

- Monthly Progress Reports (5th day of each month except those which are demo months)
- Meeting Minutes (after each meeting)
- Performance Reports (twice yearly)
- User Guides/Manuals (end of POP)

Monthly reports will be submitted in *.doc and/or PDF format. Each monthly report will adhere to the same formatting template for ease of consumption.

Change Management Plan

Change management is used to implement the following changes to management plans:

- Communication Strategy
- Training Methods
- Separation Strategies
- Risk Management Strategy
- Team Structure Changes
- Special Tactics
- Scheduling Changes
- Budget Changes
- Scope Changes

Using the established management structure will make any change management related to this project more effective. The size and complexity of the change may require special tactics. It is prudent to anticipate and document points of resistance, as well as strategies necessary to address these points before the change

management plan is initiated. Risk must be assessed during the change management planning period in order to move forward with both low organizational resistance as well as minimal disruptiveness. While some change management strategies may require disruptive actions, these shall be well justified.

Feedback will be acquired from all individuals involved with the project in order to convey:

- Awareness of the need for change
- Desire to support the change
- Knowledge on how to change
- Ability to execute the change
- Reinforcement for accepting the change

1. Approach

The change management approach for the MIT Prosthetic Socket Project will ensure that all proposed changes are defined, reviewed and agreed upon so they can be properly implemented and communicated to all involved parties. This approach will also ensure that only changes within the scope of this project are approved and implemented.

In general, we seek to ensure that changes are beneficial to the project, determine how the changes will be put into place, and manage the change as it is performed.

2. Roles and Responsibilities

The following section describes the roles and responsibilities of each member of the project team with respect to change management activities. The following roles and responsibilities are related to the MIT Prosthetic Socket Project.

Project Sponsor:

- Approve changes to budget/funding allocation
- Approve changes to schedule
- Approve changes in project scope

Project Manager:

- Initiate change process
- Conduct risk, cost, schedule, scope etc. analysis of any proposed changes
- Document all changes
- Address any change concerns

Project Team:

- Submit change requests to project manager
- Provide reasoning and data to support change

3. Change Management Process

This section describes the change management process from beginning to end. Typically all change processes shall be well documented in the event that they require repetition. The project manager is responsible for executing the change management process for each change.

1. Identify a need for a change
2. Log change (What, Why, How, When)
3. Evaluate change
4. Submit change request to VA
5. Obtain decision from VA
6. Execute change

Risk Management and Mitigation Strategy

1. Risk Identification

A risk is any event that could prevent the project from progressing as planned. Tasks can be identified from a number of different sources Some may be quite obvious and will be identified prior to project kick-off. Others will be identified during the project life cycle, and a risk can be identified by anyone associated with the project. Some risk will be inherent to the project itself, while other risk will be the result of external influences that are completely out side the control of the project team.

Any identified risks need to be logged by the project manager, as should thus be reported to the project manager with the following information:

- Description of risk factor or event
- Probability that event will occur
- Predicted impact on project schedule
- Scope of risk
- Impact on quality of work or project deliverable
- Impact on cost of project/budgeting

2. Risk Assessment

Risk assessment is the act of determining the probability that a risk will occur and the impact that event would have, should it occur. This is basically

a "cause and effect" analysis. The cause" is the event that might occur, while the "effect" is the potential impact to a project, should the event occur.

Good risk assessment involves two main factors. These factors are the probability of the risk event occurring. For this factor we use a percentage to express how likely a risk event is of occurring. For example: A 100% chance of occurrence means that the risk event will absolutely occur with no doubt, while a 20% chance means that the risk event would occur 1 time out of every 5 times that risk event were encountered.

The second risk assessment factor is the impact of the risk event occurring. Impact factors can help us understand the full nature of risk impact. These factors are:

- Cost – an estimated dollar amount lost/gained
- Scope – changes to the end deliverables of the project
- Schedule – changes in the deliverable schedule
- Quality – changes in the quality of deliverables

3. Risk Mitigation

Risk mitigation involves both identification of steps to reduce the probability and/or impact of adverse risk as well as identification of a contingency plan to deal with risk should it occur. Taking early steps to reduce the probability of adverse risk is generally more effective than repairing a situation where a risk has occurred.

4. Risk Contingency Planning

Contingency planning is the act of preparing a plan, or a series of activities, should an adverse risk occur. Having a contingency plan in place forces the project team to think in advance as to a course of action if a risk event takes place. Contingency plans should follow the following steps:

1. Identify the contingency tasks or activates necessary to address a specific risk in order to mitigate that risk
2. Identify the necessary resources (money, equipment, labor) for mitigation
3. Develop a schedule for the contingency plan
4. Define emergency/escalation procedures if necessary
5. Publish plan to project team
6. Review and update plan as necessary

5. Risk Tracking and Reporting

As project activities are conducted and completed, risk factors and events will be monitored to determine if in fact trigger events have occurred that would indicate that any risk has become a reality. Based on these trigger events that have been documented during the risk analysis and mitigation processes, the project manager will initiate any necessary contingency plans. Large scale risk mitigation may be initiated by the VA.

Risk management is an ongoing activity that will continue throughout the life of the project. This process includes risk identification, assessment, mitigation, contingency planning, and tracking and reporting. Project status reporting shall include this risk assessment information.

Project Management Plan Updates

Date	Update Description and Page Number	Reason for Update
11/5/2012	Added CMP (9-10), Deliverable list (5), update sec. (11)	VA Request
12/3/2012	Updated Deliverables Reference Sheet (5)	Standard Update
12/12/2012	Added Detailed Deliverables List (8)	VA Request
1/4/2013	Updated Detailed Deliverables List (8)	Standard Update
2/4/2013	Updated Detailed Deliverables List (8)	Standard Update
3/5/2013	Updated Deliverables Reference Sheet (5)	Standard Update
3/5/2013	Updated Detailed Deliverables List (8)	Standard Update
7/5/2014	Updated Detailed Deliverables List (8-9)	Standard Update

Appendix D

FitSocket User Guide

ATS User Guide

Table of Contents

1. Installation of Device

The ATS is intended for installation in a clinical practice having standard wall power. Since the control computer is collocated with the device, no internet connection is necessary to run a test with a patient. However, if remote data processing or remote control is desired, an internet connection must be provided to the ATS.

i. Component List

Component Name	Quantity
Actuated Test Socket	1
Multi-Outlet Power Strip (120V)	1
Position Calibration Tool	1
Force Calibration Tool	1
Desktop Style PC	1
Beckhoff NIC	1
Required Software (see below)	4

ii. Space Requirements

The ATS will require at minimum a 92 inch by 128 inch space for clinician, patient, and the device itself. The ATS measures 30 inches by 72 inches and it is 52 inches tall. While it is intended to fit through standard doorways, it is important to check that the ATS can be maneuvered into the intended space before attempting with the device.

For best measurement comfort, it is suggested that at least 2 – 3 feet of clearance around the ATS be provided in the measurement space in order to allow (1) the patient to comfortably engage with the ATS and (2) the clinician to interact with the patient effectively.

iii. Power and Computer Requirements

The ATS requires standard US wall power. At maximum draw, the ATS will draw 720 watts from the wall outlet. For reference, wall outlets are specified for 10 amperes at minimum. The ATS will operate at maximum 6 amperes. While this is below the minimum specification for a wall outlet, it is important to make sure that the circuit that the ATS is plugged into does no have any other high power devices on it.

The provided computer for the ATS is a standard desktop PC with custom network card for interfacing with the ATS system. If necessary, it is possible to use any desktop PC for control of the ATS provided the correct network card it used. It is currently not possible to operate the ATS with a laptop unless the laptop has a Beckhoff approved NIC. For a list of approved network cards, see Beckhoff Automations list of EtherCAT approved NICs: Appendix A.

In order to run LimbViewer software, the PC must have at least 4GB of RAM, and a recent graphics card meant for gaming. The exact type of graphics card is not important.

2. Installation of Software

The FitSocket requires a significant software setup in order to run the device. Future versions should have a more integrated software suite.

i. System Requirements

The FitSocket controller computer must be a multi-core PC capable of running Windows XP or 7. It can be a 64-bit machine (recommended) or 32-bit. The specific requirements are as follows:

1. Multi-core 2.4 GHz processor (4 cores recommended)
2. 4 Gb RAM (8 Gb Recommended)
3. 500 Gb HDD (1 Tb recommended)
4. Windows XP or Windows 7 OS
5. Beckhoff, Intel-based dedicated Ethernet Controller Card Installed
6. Secondary Ethernet Controller for external communication

ii. TwinCAT

The ATS's computer is running TwinCAT software under a license from Beckhoff Automation. This license will need to be renewed yearly. Obtain the TwinCAT install CD either online or from Beckhoff directly. Follow the manufacturer's installation instructions. Once TwinCAT is installed, open the FitSocketController.twe file to instantiate the device mapping. (http://www.beckhoff.com/english.asp?twincat/tcatdow.htm)

iii. Controller Program

The FitSocket controller program is a Java executable file. You must have JRE runtime 7.0 or greater to execute this file. Running the controller program will present the user with a GUI interface that will allow them to interact with the FitSocket, run tests, and collect data.

iv. LimbViewer

LimbViewer allows device operators to visualize the data that the FitSocket has collected. To install LimbViewer, run the installer file and follow the on screen instructions. The operator can then visualize data by opening the appropriate dataset of his or her choice with the File → Open command in the programs GUI interface. LimbViewer requires at least 4GB SDDR5 memory, 144Gb/s memory bandwidth and a 384-bit interface for graphics. To install LimbViewer, please use the LimbViewer CD provided. With the TT package.

v. EasyMotion Studio

EasyMotion Studio is used to update the low-level control parameters of the FitSocket's motor controllers. In order to obtain EasyMotion Studio, contact Technosoft Motion and ask to purchase their latest release (http://www.technosoftmotion.com/en/contact-us). After you have installed the program by following the on screen instructions, you will be able to program the FitSocket's motor controllers by connecting a USB ←→ RS-485 cable between the FitSocket controller PC and the motor controller that you would like to interact with. EasyMotion Studio should recognize the controller and allow you to interact with it.

2. Setting up the Device for Your First Test

Getting the ATS up and running for your first test is intended to be a straightforward process. Follow these steps:

i. Power On Sequence

1) Make sure the ATS is plugged in (as well as the control PC if using different circuits)

2) Turn on the PC with the button on the back-bottom-left of the ATS

3) Turn on the black toggle switch on the back-bottom-middle of the ATS

4) Turn on the white toggle switch on the front-bottom-middle of the device

ii. Software Sequence

1) Open TwinCAT

2) In the TwinCAT toolbar, select "Restart in RUN Mode"

3) Check the "Device" tab on the left side of the window and make sure all devices are in "OP" mode

4) Open Eclipse IDE

5) Select the type of test (see 'Selecting a Test')

6) Press the green "Run" button to start the test. Follow the on screen instructions.

3. Running a Test

i. Calibration

a. Position Calibration

The ATS will not allow movement of an uncalibrated pin. Instead of restricting movement, the ATS will automatically calibrate any uncalibrated pin that the program attempts to move.

The user can also ask the ATS to calibration the position of any pin at any time by running the calibratePosition function on that pin's object.

b. Force Calibration

Force calibration requires the use of the provided calibration pen.

1) Make sure nothing is touching the pins of the ATS

2) Run the force calibration program using Eclipse

3) Wait until the program asks you to place the calibration tool between two pins (specifically which pins will be noted by the program)

4) Press enter in the console window to indicate that you are ready to proceed.

5) The specified pins will calibrate.

6) Catch the calibration tool as the pins relax

7) Repeat steps 3 – 6 six more times, calibrating all 14 pins.

ii. Selecting a test

In the Eclipse IDE, you can select a test from the TestApp by simply deleting the '//' from the front of the test you'd like to run. Any tests that you would not like to run should have '//' in front of them.

iii. How to Position a Patient

Place the subject chair on the ATS platform. Wait until the selected test has been run before placing the subject into the ATS. Position the subject in the ATS. Press 'OK' on the dialogue window in order to proceed with the test.

The ATS will run the selected test and prompt for further steps on the control computer.

It is important that the patient's limb be in line with the central axis of the ATS. Position the patient's chair so that this can be accomplished.

iv. Test Results

Test results are generated in .csv format. The ATS controller understands how to read and write these files in terms of the ATS physical configuration. If any adjustments need to be made to the data, they can be easily done by adjusting the native Java objects that contain the ATS data.

In order to view the output from the ATS, it is possible to open the standard output files in programs like Excel, Matlab, Numbers, or LimbViewer.

4. Troubleshooting

i. Actuators not all in 'OP' mode

If you notice that – under the 'Device' tab in TwinCAT – all the actuators are not in 'OP' mode, the process for resolving is simple.

1) Right-click on the actuators not in 'OP' mode.

2) Select 'Request OP mode' from the pop up menu.

ii. ATS does not initialize

If the ATS does not initialize, which is indicated by the ATS's status lights not turning solid blue, turn the ATS off and back on again using the white toggle switch in the front-bottom-middle of the ATS. Repeat until the ATS initializes. Wait 10 seconds between each change in switch position.

Apendix A – Beckhoff Supported Network Interface Cards

Supported Network Controller by Beckhoff Ethernet Driver

Intel Fast Ethernet Controllers (Vendor ID: 0x8086)

Device ID	Description
0x1029	82559
0x1030	82559
0x1031	82801CAM
0x1032	82801CAM
0x1033	82801CAM
0x1034	82801CAM
0x1038	82801CAM
0x1039	82801CAM
0x103A	82801DB
0x103B	82801DB
0x103 C	82801DB
0x103D	82801DB
0x103E	82801DB
0x1050	82801EB/ER
0x1051	82801EB/ER
0x1052	82801EB/ER
0x1053	82801EB/ER
0x1054	82801EB/ER
0x1055	82801EB/ER
0x1056	82801EB/ER
0x1057	82801EB/ER
0x10 59	82551QM
0x1064	82801EB/ER
0x1067	Intel PRO/100
0x1068	82562
0x1069	Intel PRO/100
0x106A	Intel PRO/100
0x106B	Intel PRO/100
0x1094	Intel PRO/100
0x1209	8255xER/IT

0x12 29	82557/8/9/0/1
0x12 49	82559ER
0x12 59	82801E
0x245D	82801E
0x27DC	Intel PRO/100

Intel Gigabit Ethernet Controllers (Vendor ID: 0x8086)

Device ID	Description
0x1000	82542
0x1001	82543GC
0x1004	82543GC
0x1008	82544EI
0x1009	82544EI
0x100C	82544EI
0x100D	82544GC
0x100 E	82540EM
0x100F	82545EM
0x1010	82546EB
0x1011	82545EM
0x1012	82546EB
0x1013	82541EI
0x1014	82541ER
0x1015	82540EM
0x1016	82540EP
0x1017	82540EP
0x1018	82541EI
0x1019	82547EI
0x101A	82547EI
0x101D	82546EB
0x101E	82540EP
0x1026	82545GM
0x1027	82545GM
0x1028	82545GM
0x1049	82566MM
0x104A	82566DM
0x104B	82566DC
0x104C	82562V

0x104D	82566MC
0x104E	82571EB
0x104F	82571EB
0x1060	82571EB
0x1075	82547EI
0x1076	82541GI
0x1077	82547EI
0x1078	82541ER
0x1079	82546EB
0x107A	82546EB
0x107B	82546EB
0x107C	82541GI
0x107D	82572EI
0x107E	82572EI
0x107F	82572EI
0x10 8A	82546GB
0x10 8B	82573E
0x108C	82573E
0x1096	80003ES2LAN
0x1098	80003ES2LAN
0x109 9	82546GB
0x109A	82573L
0x10A4	82571EB
0x10A7	82575
0x10A9	82575
0x10B5	82546GB
0x10B9	82572EI
0x10BA	80003ES2LAN
0x10BB	80003ES2LAN
0x10BC	82571EB
0x10BD	82566DM
0x10C4	82562GT
0x10C5	82562G
0x10C9	82576
0x10CB	82567V - ICH9
0x10D3	82574L
0x10E5	82567LM-4 - ICH9

0x10E6	82576 (Fiber)
0x10E7	82576 (Serdes)
0x10E8	82576 (Quad Copper)
0x10EA	82577LM
0x10EB	82577LC
0x10EF	82578DM
0x10F0	82578DC
0x10F2	82579LM
0x10F3	82567LM
0x10F5	82579V

Appendix E

Spatially Varied Stiffness Socket Construction

VTS Material to 3D Printable Files

Introduction

This report details the technical processing required to translate the biomechanical requirements of the VTS into 3D printable files that a 3D printer is able to print. Additionally, we will review the entire process generally.

Prosthetic socket comfort and quality affects the ability of a patient to use his or her prosthesis and plays a role in preventing the development of future pathological conditions. Unlike standardized prosthetic components such as knees or ankle-foot prostheses, prosthetic sockets are typically custom fabricated for each patient by individual prosthetists. This process is labor intensive and iterative and can take several weeks to complete. Given the skills and experiences of different prosthetists and the highly custom nature of the socket fabrication process, socket geometry – and hence comfort and socket-residual limb interface pressure distributions – are highly variable across different sockets.

Although computer-aided design and computer-aided manufacturing (CAD/CAM) tools are available, the design and fabrication of a functional socket still remains largely an art. Even prosthetic clinics that do use CAD/CAM techniques generally rely on 3D scan surface data alone to generate their models. Quantitative anthropomorphic data collected via internal and surface image capturing technologies such as MRI, CT and ultrasound can provide some insight into tissue distribution within the residual limb. The Actuated Test Socket as proposed allows a prosthetist to control the shape of a test socket and efficiently measure residual-limb tissue impedance during both unloaded and dynamic socket loading conditions. This quantitative data, in combination with continuously variable-impedance 3D printing technologies allows for the repeatable fabrication of sockets designed with ideal shapes and dynamic properties.
Here, residual limb stiffness plays a key role in scientifically determining final socket shape and material stiffness. Prior research suggests that there is an inverse relationship between residual limb stiffness and socket pressure along the socket-residual limb interface. For example, areas of the limb with boney protuberances require softer interfaces while softer tissues may be able to interface with stiffer materials.

Variable-Impedance Test Socket

In conventional carbon fiber sockets, pressure distribution within the socket is controlled through areas of compression, contact and voids. More recent technologies achieve varying degrees of compliance over certain anatomical features through changing socket wall thickness or adding mechanical features.

"Windowing" techniques where patches of softer materials are added to a socket provides some variation of socket compliance over the residual limb but lack the necessary spatial control of dynamics to ensure a comfortable interface. Fabricated using an Objet Connex500 3D printer, the Variable-Impedance Test Socket (VTS) is designed using data collected from the ATS. The inner shape of the VTS socket is computationally determined from this data set and the wall stiffness of the VTS is inversely proportional to the tissue stiffness estimated. The VTS is passive and relatively lightweight allowing for dynamic testing under typical use conditions in a prosthetics facility.

The commercially sold Objet Connex500 3D printer and its affiliated software is capable of working with fourteen Digital Materials with a range of elastic modulus and durometer. The high resolution of the printer (600 dpi in X, 300 dpi in Y and 845 dpi in Z) allows for a high spatial resolution of material to tissue stiffness gradient matching. Smooth transitions between hard and soft materials can be designed, avoiding the edges and hard transitions seen in windowing techniques. The socket is printed layer-by-layer in the Z direction and all materials are incorporated in one process. For a full list of materials, please see Appendix A.

If quantitative feedback is required, especially with regard to peak pressures over anatomical features of interest, off-the-shelf solutions may be employed, for example the Tekscan F-Socket Pressure Analysis System. Ongoing work in this direction is exploring the feasibility of incorporating 3D printed optical sensors into the current fabrication process of the VTS. Such sensors may be able to provide real-

time feedback on socket wall deformation, shear stresses and pressure.

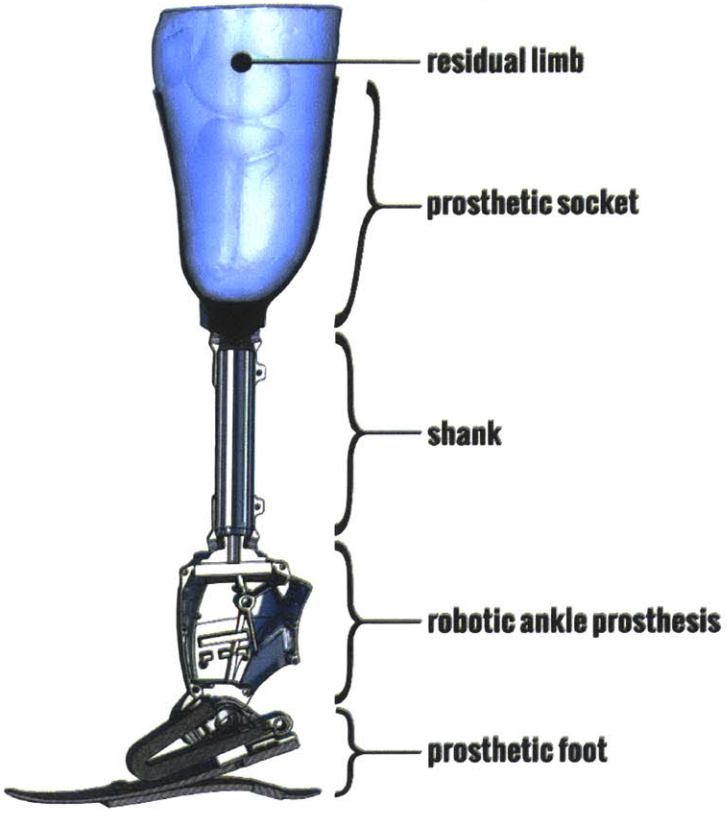

VTS Design

The VTS design and fabrication process begins with data collected by the ATS, including local tissue stiffness. This data is then used in addition to magnetic resonance images to computationally generate socket shape and socket material distribution. These shapes are also compared with those from surface laser scans of the residual limb at no load. Images of molds of the residual limb at known pressure loads are also incorporated into the design mechanism. The socket shape and material distribution are incorporated into bitmaps or STL files that are then sent to a 3D printer for fabrication. After fabrication, carbon fiber is added to the socket for structural integrity by a clinical prosthetist using the standard vacuum bag technique.

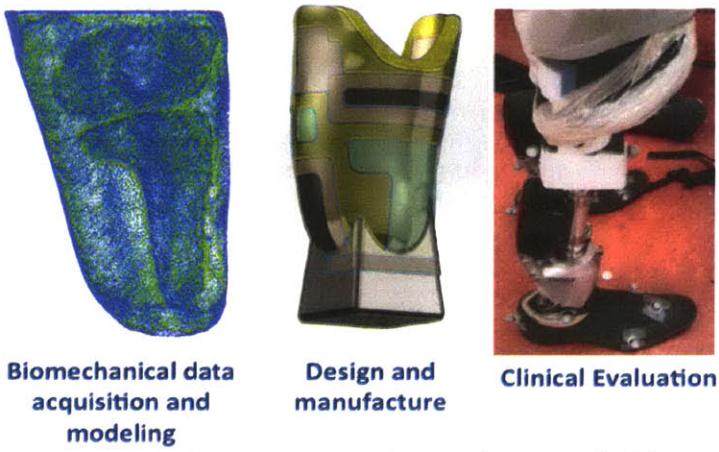

Figure 1: Design process for production of VTS

Data Collection

ATS data

In the final system, data will be collected physically using the ATS. The socket shape under load in real time, the pressure response at different tissue displacements and the local impedance of residual limb tissue may be measured. From these measurements, the local nonlinear first order stiffness at each location on the residual limb will be passed on to the VTS generation process. Since the ATS and VTS development tracks run in parallel, a set of realistic test data was constructed to allow data to socket structure and material mapping to commence. Test data was derived from three sets of data taken from the same residual limb: an MRI scan of the limb encased within a silicone liner, Tekscan F- Socket pressure distribution along the socket-limb interface under unloaded.

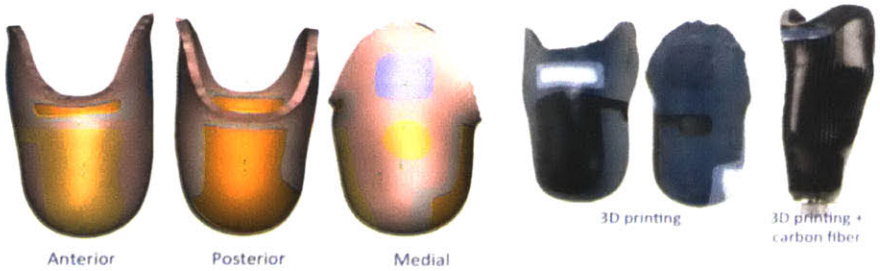

Figure 2: STL showing different materials, 3D printed part and 3D printed parts with carbon fiber

Data Evaluation

1) **Interface Pressure**: Contact pressure is measured over various anatomical landmarks at the residual limb—prosthetic socket interface for both a conventional and a variable-impedance socket during:

    a. Quiet standing (double leg support), and
    b. Level ground walking

Special attention is placed over the tibia, tibia region, patella tendon, femoral head, medial and lateral femoral condyles and the posterior wall. These anatomical points are highlighted particularly because of high soft tissue strain in the residual limb under mechanical load, which lead to deep tissue injury in these locations.

Using the *F-Socket Pressure System* provided by Tekscan, Inc. (307 West First Street. South Boston, MA 02127- 1309, USA T: 800.248.3669), interface contact pressure is recorded at 100 Hz within the socket for quiet standing and level ground walking. The thin pressure sensors of thickness 0.2 mm are attached using adhesives to the outside surface of a prosthetic liner worn by a patient to avoid displacement during tests.

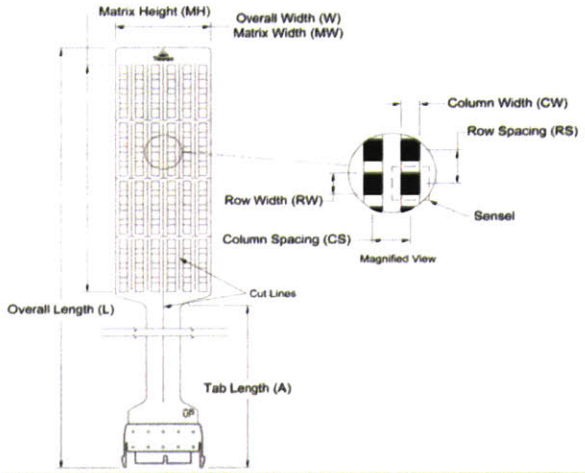

Overall Length L	Overall Width W	Tab Length A	Matrix Width MW	Matrix Height MH	Columns			Rows			Total No. of Sensels	Resolution
					CW	Pitch CS	Qty.	RW	Pitch RS	Qty.		Sensel Density
(in.)	(in.)	(in.)	(in.)	(in.)	(in.)	(in.)		(in.)	(in.)			(sensel per in.^{2})
21.45	3.00	12.43	3.00	8.00	0.250	0.500	6	0.310	0.500	16	96	4.0
(mm)	(mm)	(mm)	(mm)	(mm)	(mm)	(mm)		(mm)	(mm)			(sensel per cm^2)
544.8	76.2	315.7	76.2	203.2	6.3	12.7	6	7.9	12.7	16	96	0.6

Figure 3: TekScan sensor detail

For level ground walking over an instrumented treadmill walkway, the patient chooses a comfortable self-selected speed over many gait cycles.

The pressure readings are synchronized with the motion capture data thus allowing for accurate determination of the different phases of the gait cycle.

From the images below, it is evident that over a chosen self-selected walking speed, the contact pressure over various anatomical landmarks are much lower in the VTS than the conventional socket.

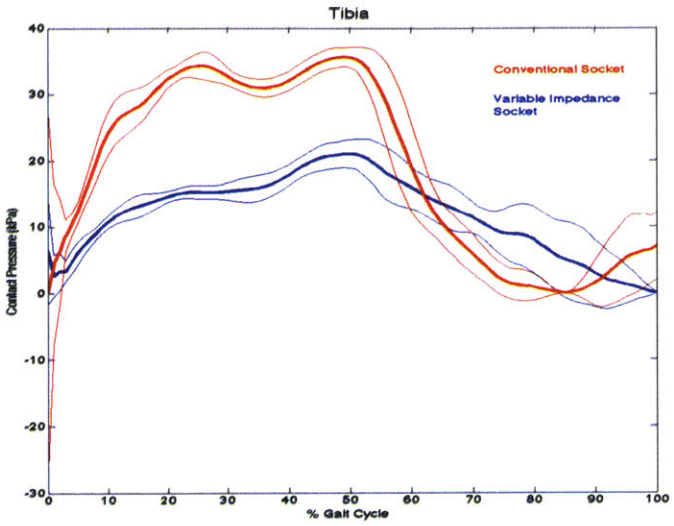

Figure 4: Subject 1 data

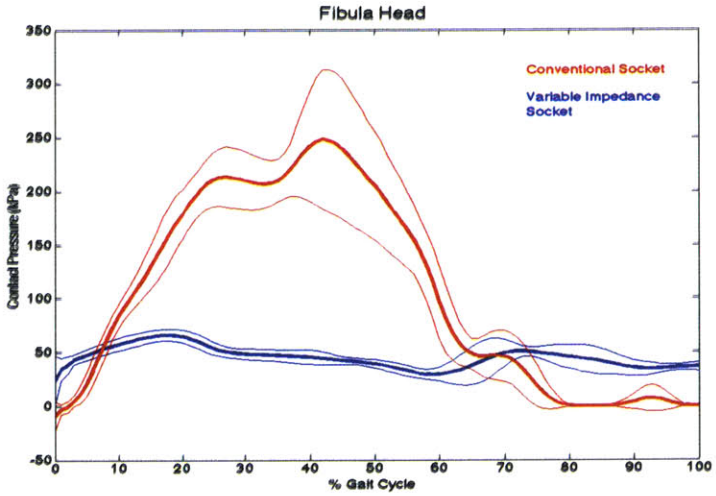

Figure 5: Subject 2 data

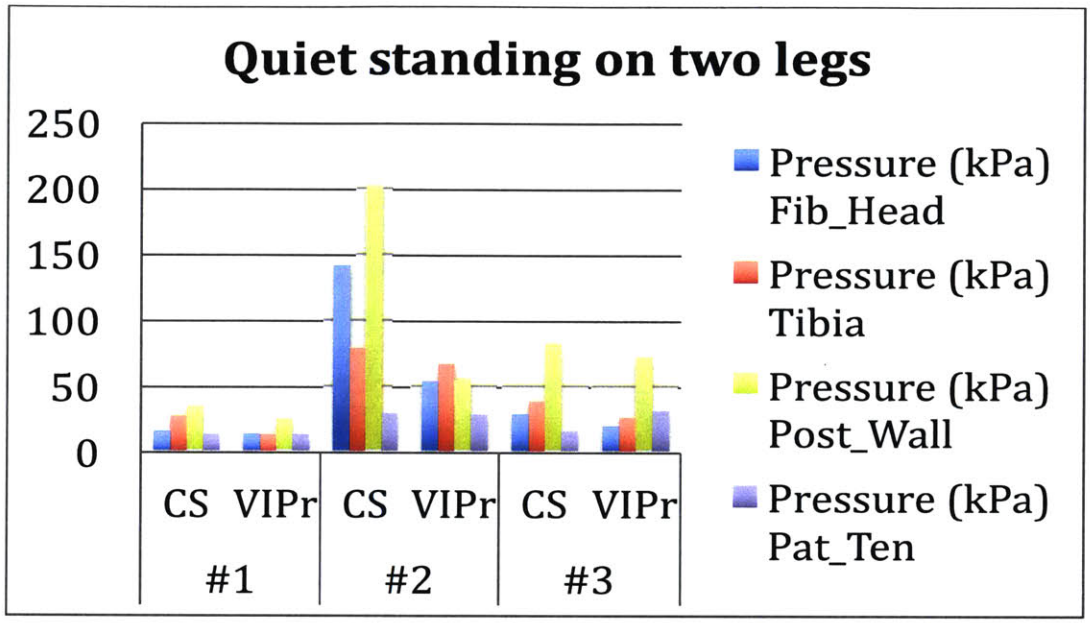

Figure 6: Three subjects TekScan pressure data

2) Inverse models of locomotion can be used to measure gait kinetics and kinematics from motion capture data. Kinetic and kinematic data is use to capture joint states and moments during gait.

Kinetic Data An instrumented force plate treadmill (Bertec Corporation, Columbus, OH) is used to measure ground reaction forces of patients during level ground walking. The force plates measure foot contact centers of pressure. The treadmill, composed of two side-by-side belts, ensures that each foot is measured separately. The sampling rate used for data collection is 1000 Hz.

Kinematic Data An infrared camera system (12 cameras, T-Series Vicon Motion Capture Systems, Denver, USA) is used to track the motion of patients during gait in the capture volume. Reflective markers are placed at 43 (bilateral) locations on the patient's body. These are used to measure their three dimensional trajectories at frequencies of 500 Hz. The marker locations were chosen specifically to track joint motion, as prescribed by the Helen Hayes marker model.

Appendix A – Connex500 Materials

Digital Materials
http://www.stratasys.com/~/media/Main/Secure/Material%20Specs%20MS/PolyJet-Material-Specs/Digital_Materials_Datasheet.pdf

Poly-Jet Materials
http://www.stratasys.com/~/media/Main/Secure/Material%20Specs%20MS/PolyJet-Material-Specs/PolyJet_Materials_Data_Sheet.pdf

Appendix F

FitSocket Controller Board Assembly

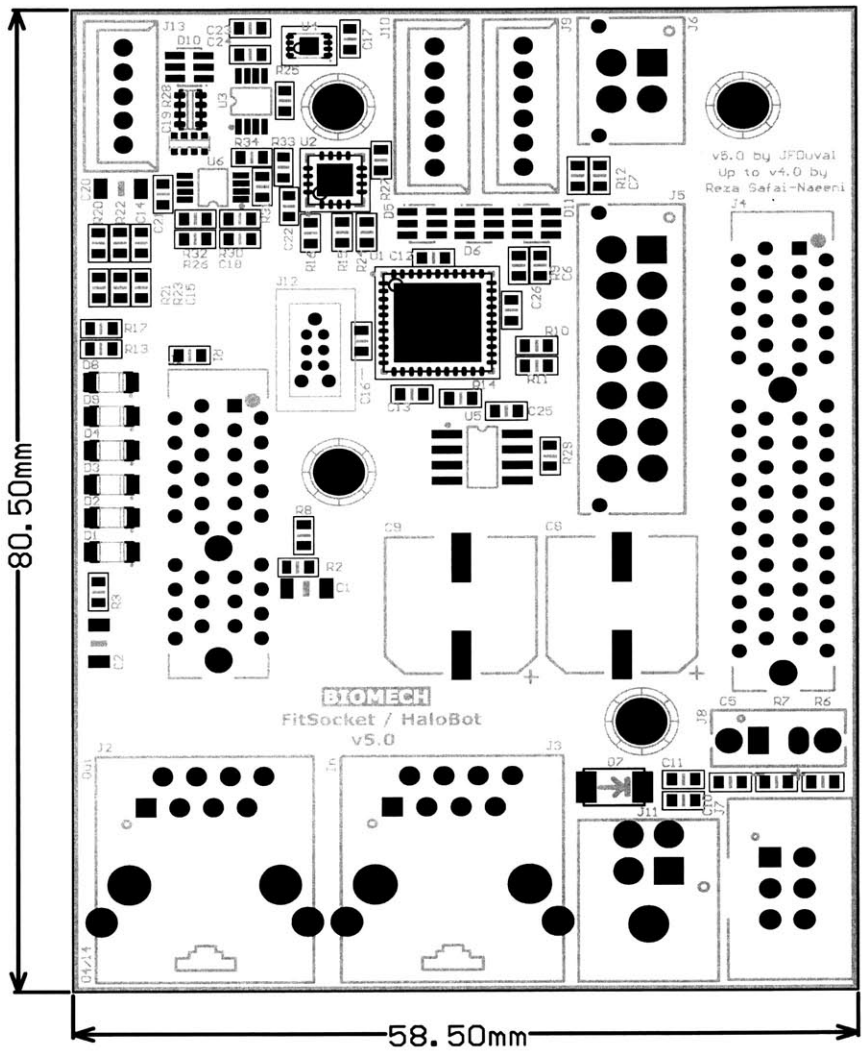
80.50mm
58.50mm
BIOMECH
FitSocket / HaloBot
v5.0
v5.0 by JFDuval
Up to v4.0 by
Reza Safai-Naeeni

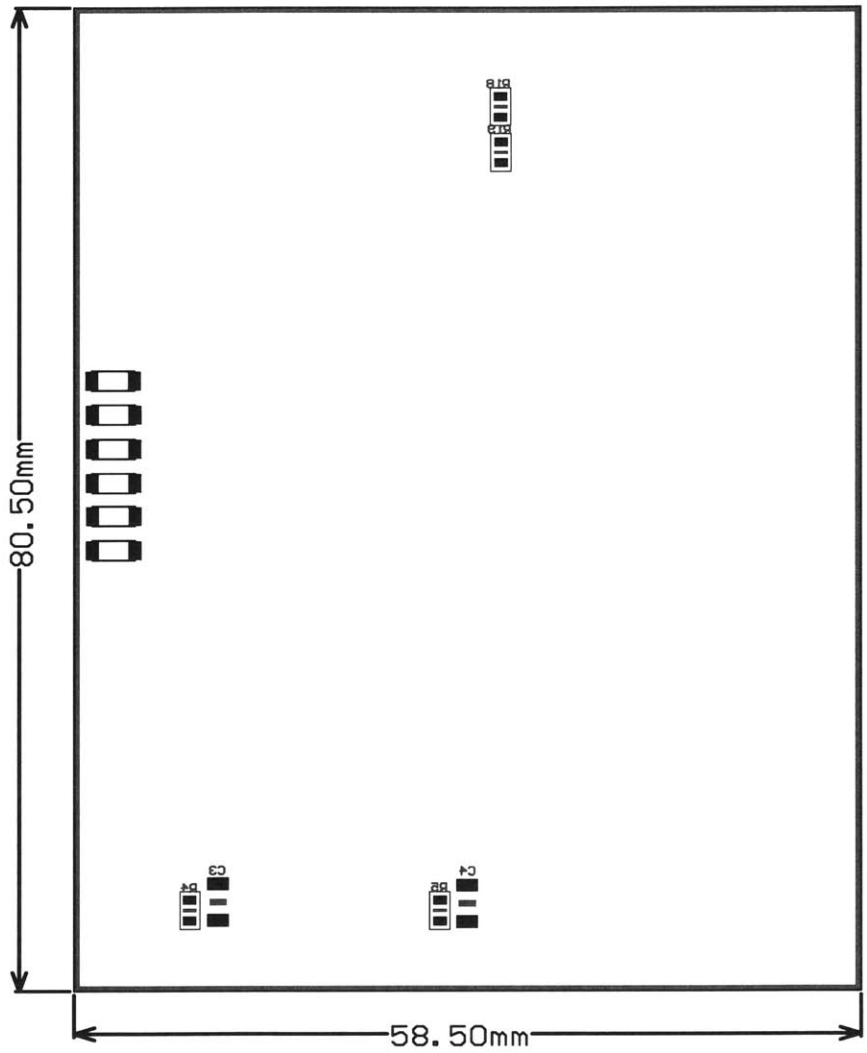
80.50mm
58.50mm

Appendix G

FitSocket Controller Board Buildbook

Buildbook – FitSocket / HaloBot v5.0

MIT Media Lab – Biomechatronics – 04/09/2014

Contact :

Jean-François Duval

jfduval@mit.edu

408-215-8748

Extension	Layer
.GTO	Top Overlay/Silkscreen
.GTP	Top Paste
.GTS	Top Soldermask
.GTL	Top Layer
.G1	Internal plane #1 (GND)
.G2	Internal plane #2 (+5V)
.GBL	Bottom Layer
.GBS	Bottom Soldermask
.GBP	Bottom Paste
.GBO	Bottom Overlay/Silkscreen
.GM15	Mechanical, board outline

Stackup (from top to bottom):

Top Layer (GTL)

Plane 1 (G1)

Plane 2 (G2)

Bottom Layer (GBL)

PCB specs:

Layers: 4

Traces/spacing: 6/6 mils

Smallest hole: 8 mils

Minimum annular ring: 7 mils

Number of holes: 397

Soldermask color: Black

Silkscreen color: White

Size - X: 58.5mm

Size - Y: 80.5mm

Copper rating: 2 Oz on external layers, 1 Oz internal

Stackup: L1/5.5mil prep/L2/47mil core/L3/5.5mil prep/L4

Build time: 2 days

Number of PCBs: 20

Finish: ENIG

Via tenting: All the vias need to be tented.

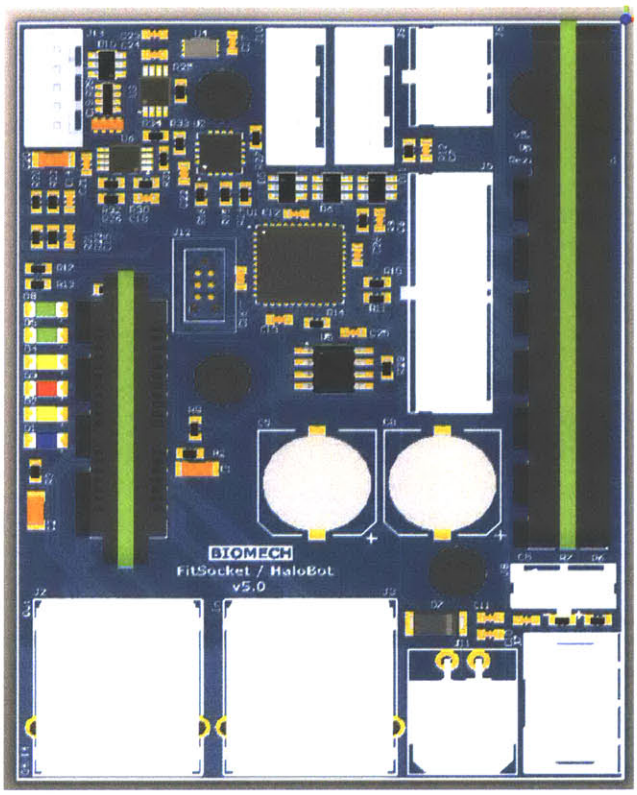

Notes:

- The black and green boards on the picture will be assembled by us after delivery. Their connectors are PCI-E.
- 6 SMT components are on the bottom layer. Please solder them manually to avoid an additional stencil and setup fee.
- Parts indicated as DNS (Do Not Solder) should not be assembled.

Appendix H

Software Constants

Listing H.1: Constants Used in the Software Control of the FitSocket

```
public static final boolean DEBUG = false;
public static final boolean USING_DUE = false;
public static final boolean RS485_ENABLED = false;

// File IO Stuff
public static final String FORCE_CALIBRATION_DATA_FILENAME = "ForceCalibrationData.dat";
public static final String FILE_SAVE_LOCATION="C:\\Users\\FitSocket\\Documents\\";

// Constants for Tests
public static final int NUMBER_OF_SLICES = 10;
public static final int NUMBER_OF_TEST_POINTS = 10;
public static final int NUMBER_OF_SAMPLES_PER_TEST = 1500;
public static final double MAX_TESTING_FORCE_NEWTONS = 12; // How much force is too much?
    About 10N.
public static final double MAX_TESTING_FORCE_SINGLE_PIN = 8;
public static final long MAX_CLAMPING_TIME_MILLISECONDS = 5000;
public static final double TOTAL_TESTING_TIME = 16000;

// Constants for SinglePinExperiment.java
public static final boolean HOLD_BETWEEN_INDENTATION = true; // Between inward indentation
    and outward.
public static final int HOLD_NUMBER_OF_EXTRA_SAMPLES = 1000; // If "hold between
    indentation" == true, then this.
public static final int TIME_TO_HOLD_BETWEEN_INDENTATION = 10000; // If "hold between
    indentation" == true...

// PID Force controller constants
public static final double KP = 0.025;
public static final double KI = 0.008;
public static final double KD = 0.006;

// Physical Characteristics of the robot
public static final double TICKS_PER_REVOLUTION = 1440;
public static final double TICKS_PER_MM = 720;
public static final double PIN_LINEAR_TRAVEL_RANGE = 44;
public static final double MAX_LINEAR_TRAVEL_MM = PinCalibrationZeros.getMinValue();
public static final double MIN_LINEAR_TRAVEL_MM = MAX_LINEAR_TRAVEL_MM -
    PIN_LINEAR_TRAVEL_RANGE;
public static final double MAX_LINEAR_TRAVEL_TICKS = MAX_LINEAR_TRAVEL_MM * TICKS_PER_MM *
    2; // Zero adjusted ticks only
public static final double MIN_LINEAR_TRAVEL_TICKS = MIN_LINEAR_TRAVEL_MM * TICKS_PER_MM;
    // Zero adjusted ticks only
```

```
public static final double MIN_RADIUS_ALL_PINS = 50; // The smallest radius that all the
    pins are able to fit.
public static final int MAX_ROTARY_TRAVEL_TICKS = (int) (MAX_LINEAR_TRAVEL_MM *
    TICKS_PER_MM);
public static final int MIN_ROTARY_TRAVEL_TICKS = (int) (MIN_LINEAR_TRAVEL_MM *
    TICKS_PER_MM);
public static final int MM_PER_SECOND_TO_TICKS_PER_MINUTE = 720 * 60;
public static final int DEFAULT_ACTUATOR_VELOCITY_TICKS_PER_MINUTE = (int)
    (MM_PER_SECOND_TO_TICKS_PER_MINUTE * 0.5);
public static final int DEFAULT_ACTUATOR_VELOCITY_MM_PER_SECOND = 8;
public static final double MAX_VELOCITY_MM_PER_SECOND = 50;
public static final double MIN_VELOCITY_MM_PER_SECOND = 0;
public static final double MAX_VELOCITY_TICKS_PER_MINUTE = MAX_VELOCITY_MM_PER_SECOND *
    MM_PER_SECOND_TO_TICKS_PER_MINUTE;
public static final double MIN_VELOCITY_TICKS_PER_MINUTE = MIN_VELOCITY_MM_PER_SECOND *
    MM_PER_SECOND_TO_TICKS_PER_MINUTE;

public static final double PIN_RADIUS_OFFSET_TICKS = MAX_LINEAR_TRAVEL_MM * TICKS_PER_MM;
    // Ticks
public static final double PIN_RADIUS_OFFSET_MM = MAX_LINEAR_TRAVEL_MM; // MM
//public static final boolean MM = true;
//public static final boolean TICKS = false;

// Constants for calibration
public static final int MAX_POSITION_CALIBRATION_CURRENT = 30500;
public static final double MAX_DISTANCE_BETWEEN_PLATES = 129.097699; // MM
public static final double MAX_SPRING_LENGTH_MM = 120.1928; // MM
public static final double SPRING_LENGTH_MM = MAX_SPRING_LENGTH_MM * 0.90; // MM
public static final double MIN_SPRING_LENGTH_MM = 93.43; // MM
public static final double MAX_SPRING_DEFLECTION = (MAX_SPRING_LENGTH_MM -
    MIN_SPRING_LENGTH_MM) * .90;
public static final double POSITION_CALIBRATION_VELOCITY_MM_PER_SECOND = 0.5;
public static final int FORCE_CALIBRATION_VELOCITY_MM_PER_SECOND = 3;
public static final double SPRING_CONSTANT_NEWTONS_PER_MM = 0.349; // Newtons/mm
public static final int NUMBER_OF_ZERO_FORCE_TESTS = 2;
public static final int NUMBER_OF_MAX_FORCE_ADJUSTMENTS = 3;
public static final double MIN_SPRING_HOLDING_FORCE_NEWTONS = 3; // Newtons
public static final int NUMBER_OF_LINEAR_REGRESSION_POINTS = 500;

// Pin Calibration Constants
public static final int START_WITH_LIMIT_SWITCH_NOT_TRIGGERED = 0;
public static final int START_WITH_LIMIT_SWITCH_TRIGGERED = 1;
public static final int MOVING_AWAY_FROM_LIMIT_SWITCH = 2;
public static final int MOVING_TOWARD_LIMIT_SWITCH = 3;
public static final int TRIGGERED_LIMIT_SWITCH_ON_PURPOSE = 4;
public static final int MOVING_AWAY_FROM_LIMIT_SWITCH_FOR_FINAL_POSITION = 5;
public static final int CALIBRATED = 6;

// EtherCAT Communication Constants
public static final int ETHERCAT_COMM_PORT = 301;
public static final int ETHERCAT_UPDATE_DELAY = 15;

// EtherCAT Drive Control Word Commands
public static final int RESET_FAULT = 0x80;
public static final int DISABLE_VOLTAGE = 0x04;
public static final int SHUTDOWN = 0x06;
public static final int SWITCH_ON = 0x07;
public static final int ENABLE_OPERATION = 0x0F;
public static final int QUICK_STOP = 0x02;
public static final int BEGIN_HOMING = 0x1F;
public static final int END_HOMING = 0x0F;

// EtherCAT Drive Status Word Values
public static final int NOT_READY = 0;
public static final int SWITCH_ON_DISABLED = 1;
public static final int READY_TO_SWITCH_ON = 2;
public static final int SWITCHED_ON = 3;
public static final int OPERATION_ENABLED = 4;
public static final int FAULT = 5;
public static final int QUICK_STOP_ENABLED = 6;
```

```
// EtherCAT Modes of Operation
public static final int PROFILE_POSITION_MODE = 0x01;
public static final int PROFILE_VELOCITY_MODE = 0x02;
public static final int PROFILE_TORQUE_MODE = 0x04;
public static final int HOMING_MODE = 0x06;
public static final int CYCLIC_SYNCHRONOUS_POSITION_MODE = 0x08;
public static final int CYCLIC_SYNCHRONOUS_VELOCITY_MODE = 0x09;
public static final int CYCLIC_SYNCHRONOUS_TORQUE_MODE = 0x0A;
public static final int CONFIG_0_MODE = 0x9E;
public static final int CONFIC_1_MODE = 0xDE;
public static final int NONE_MODE = 0xFF;

// Serial Communication
public static final String PORT_NAMES[] = {
  "/dev/tty.usbserial-A9007UX1",  // Mac OS X
  "/dev/ttyUSB0",          // Linux
  "COM3",              // Windows
};
public static final String DEFAULT_PORT_NAME = "COM3";
public static final int DEFAULT_SERIAL_RATE_INDEX = 2;
public static final int SERIAL_RATES[] = {
  4800, 9600, 19200, 38400, 57600
};

public static final String SERIAL_RATES_STR[] = {
  "4800", "9600", "19200", "38400", "57600"
};

// Serial Protocol
public static final int SERIAL_BUFFER_SIZE = 5;
public static final byte SERIAL_DATA_INIT = 0x23;
public static final byte SERIAL_DEBUG_END = 0x21;
public static final byte SERIAL_DATA_END = 0x0A;
public static final byte SERIAL_INIT_ID = 0x61;

public static final int SERIAL_DATA_INIT_INDEX1 = 0;
public static final int SERIAL_DATA_INIT_INDEX2 = 1;
public static final int SERIAL_DATA_ID_INDEX = 2;
public static final int SERIAL_DATA_INDEX = 3;
public static final int SERIAL_DATA_END_INDEX = 4;

// Capacitive Sensor
public static final int NUM_CAPACTIVE_ELECTRODES_USED = 14;
public static final int NUM_CAPACTIVE_ELECTRODES_PER_BOARD = 12;
public static final byte CAPACITIVE_ID_BEGIN_INDDEX = 0x30;
public static final byte[] CAP_IDS = {0,1,2,3,4,36,37,38,39,24,25,26,27,28};


// Data codes for HALOBOT boards
public static final int DATA_CONFIG_PARAM = 40;  // What the hell is this?
public static final int DATA_CAPACITIVE_SENSE = 41;  // Also this

// Strain Gauge suggested values
public static final int MEAN_FORCE_VALUE_TICKS = 20000; // I'm aiming a little low on 2^16/2
public static final int MAX_FORCE_VALUE_TICKS = 50000;  // And that's why.  We need some
    wiggle room here.

// Motor Control
public static final byte MOTOR_CONTROL_BEGIN_ID = 0x55;
public static final byte DEFAULT_MOTOR_SPEED = (byte)255;
public static final byte MAX_MOTOR_SPEED = (byte)255;
public static final byte MIN_MOTOR_SPEED = 0;
public static final int MIN_MOTOR_POSITION = 0;
public static final int MAX_MOTOR_POSITION = 255;
public static final int DEFAULT_MOTOR_POSITION = 50;

// Stepper Motor Control
public static final byte STEPPER_MOTOR_CONTROL_BEGIN_ID = 0x5D;
public static final int STEPPER_MOTOR_FAULT_PIN = 30;
public static final byte DEFAULT_STEPPER_SPEED = 15;    //RPM
public static final byte DEFAULT_STEPPER_RESOLUTION = 0;  //Full step
public static final boolean DEFAULT_STEPPER_DIRECTION = false;
```

```
public static final byte MIN_STEPPER_SPEED = 15;
public static final byte MAX_STEPPER_SPEED = 127;
public static final int NUM_STEPS_PER_REVOLUTION = 200;
public static final byte DEFAULT_STEPPER_MOVE_ANGLE = 1;
public static final int MIN_STEPPER_ANGLE = 1;
public static final int MAX_STEPPER_ANGLE = 15;

// GUI Stuff
public static final int DEFAULT_WINDOW_WIDTH = 1024;
public static final int DEFAULT_WINDOW_HEIGHT = 345;

// Units
public static final int TICKS_PER_MINUTE = 1; // Multiply by this to get ticks per minute
public static final int TICKS_PER_SECOND = 60; // Multiply by this to get ticks per minute
public static final int MM_PER_SECOND = 43200; // Multiply by this to get ticks per minute
public static final double METERS_PER_SECOND = 43200000; // Multiply by this to get ticks
    per minute
public static final double MILES_PER_HOUR = 96635808; // Multiply by this to get ticks per
    minute
public static final int FORCE_NEWTONS = 2; // This is just a constant as the actual force
    is dependent on the calibration value
public static final int FORCE_TICKS = 1; // This is just a constant as the actual force is
    dependent on the calibration value
public static final int MM = 720; // Multiply this to get ticks
public static final int MILES = 1609344 * MM; // Multiply this to get ticks
public static final double TICKS_DISTANCE = 1/720; // in mm
public static final int CM = 7200; // Multiply this to get ticks
public static final int METERS = 72000; // Multiply this to get ticks
public static final int SMOOTS = 1225000; // Multiply this to get ticks
public static final double POTRZEBIES = 1629.6109; // Multiply this to get ticks
public static final double BEARD_SECONDS = 0.0036; // Multiply by this to get ticks
public static final double ATTOPARSECS = 22216.9; // Multiply by this to get ticks
public static final int TICKS = 1;
public static final int RAW_TICKS = -3;

// RS485 constants
// Board IDS
public static final byte HALO_MASTER = 14;
public static final byte[] HALOBOT_SLAVES =
  {0,1,2,3,4,5,6,7,8,9,10,11,12,13};

// Modify these values to match rs485 protocol established by Jake Isenhart
public static final int CAP_BIT_BYTE_OFFSET = 2;
public static final int CAP_BIT_BYTE_LENGTH = 0;
public static final int CAP_BIT_BIT_OFFSET = 7;
public static final int LIMIT_BIT_BYTE_OFFSET = 3;
public static final int LIMIT_BIT_BYTE_LENGTH = 0;
public static final int LIMIT_BIT_BIT_OFFSET = 6;
public static final int AMPLIFIER_GAIN_BYTE_OFFSET = 0; // Assumed that the length is 1 byte
public static final int AMPLIFIER_OFFSET_BYTE_OFFSET = 1; // Assumed that the length is 1
    byte
public static final int COMMAND_BYTE_OFFSET = 3;

public static final int RS485_UPDATE_DELAY = 7; // milliseconds
public static final int RS485_SCHEDULED_UPDATE_PERIOD = RS485_UPDATE_DELAY * 13;
public static final int RS485_BAUDRATE = 19200; // non-standard, but standard ones have
    more errors
public static final int RS485_SERIAL_IN_BUFFER_CAPACITY = 100;

/*  Possible Received Commands:
*               Dump Data ('d'),
*               Dump Data and Call Next Slave ('n'),
*               Set Gain ('g'),
*               Set Offset ('o'),
*               Auto-Calibrate Capacitive Sense ('c'),
*               Auto-Calibrate Offset ('a')
*/

// A list of possible commands that can be sent to the FitSocket HALOBOT boards
public static final char DUMP_DATA = 'd';
public static final char DUMP_DATA_AND_CALL_NEXT = 'n';
```

```
public static final char SET_AMPLIFIER_OFFSET = 'o';
public static final char AUTO_ADJUST_OFFSET = 'a';
public static final char SET_AMPLIFIER_GAIN = 'g';
public static final char AUTO_ADJUST_CAP_SENSE = 'c';

// Data codes for HALOBOT boards
public static final int DATA_CAP_LIMIT_STRAIN_GAIN_OFFSET= 40; //
    capsense,limit,strain,gain,offset
public static final int DATA_BOARD_ID = 41;

//Common defines:
public static final int BOARD_ID = HALO_MASTER;         //Slave address - pick from Board
    list
public static final int ID_MATCH = 1;
public static final int ID_NO_MATCH = 0;
public static final int STR_LEN = 12;               //Maximum number of bytes in CP string

// Packet Specific Constants:
public static final int PACKET_LEN = 12;
public static final int MAX_PACKET_LEN = 16;
public static final byte HEADER = 'a';
public static final byte ESCAPE = 'e';
public static final byte FOOTER = 'z';

//Communication protocol fields:
public static final int CP_XID = 0;                 //Emitter ID
public static final int CP_RID = 1;                 //Receiver ID
public static final int CP_CMDS = 2;                //Number of Commands sent
public static final int CP_CMD1 = 3;                //First command
public static final int CP_DATA1 = 4;               //First data

//Parser:
public static final int PARSE_DEFAULT = 0;
public static final int PARSE_ID_NO_MATCH = 1;
public static final int PARSE_SUCCESSFUL = 2;
public static final int PARSE_UNKNOWN_CMD = 3;
public static final int PARSE_ACK_RECEIVED = 4;
public static final int PARSE_BAD_XID = 5; //TODO: why do I sometimes get bad XIDs?

// Constants for PinMovementTest
// THIS IS A SEPARATE CLASS THAN CONSTANTS.JAVA!
public static class PinMovementTestConstants {

  public static final int INIT = 0;
  public static final int FINDING_TESTING_POSITION = 1;
  public static final int NEW_POSITION_COMMAND_SET = 2;
  public static final int TRYING_OPPOSITE_DIRECTION = 3;
  public static final int MOVING_TO_ORIGINAL_POSITION = 4;
  public static final int TRIGGERING_LIMIT_SWITCH = 5;
  public static final int TEST_COMPLETE = 6;

  public static final int ERROR_TOLERANCE_TICKS = 10;

  public static final boolean MOVE_TO_ORIGINAL_POSITION = false;
}

public static class PinGeometricConstants {
  public static final int INWARD = -1;
  public static final int OUTWARD = 1;
  public static final boolean TO = true;
  public static final boolean FROM = false;
}

public static class PinSizeConstants {
  public static final double PIN_AND_HEAD_LENGTH_MM = 106.68;
}

public static class PinCalibrationZeros {
  public static final double PIN_0_ZERO_LOCATION = 67.99584;
  public static final double PIN_1_ZERO_LOCATION = 66.9142;
  public static final double PIN_2_ZERO_LOCATION = 66.23812;
  public static final double PIN_3_ZERO_LOCATION = 68.08522;
```

```
    public static final double PIN_4_ZERO_LOCATION = 67.52285;
    public static final double PIN_5_ZERO_LOCATION = 67.20706;
    public static final double PIN_6_ZERO_LOCATION = 68.39495;
    public static final double PIN_7_ZERO_LOCATION = 67.95004;
    public static final double PIN_8_ZERO_LOCATION = 67.02;
    public static final double PIN_9_ZERO_LOCATION = 67.17792;
    public static final double PIN_10_ZERO_LOCATION = 65.17842;
    public static final double PIN_11_ZERO_LOCATION = 66.10655;
    public static final double PIN_12_ZERO_LOCATION = 69.13506;
    public static final double PIN_13_ZERO_LOCATION = 67.41885;

    static final double[] PIN_ZEROS = new double[] {
      PIN_0_ZERO_LOCATION,
      PIN_1_ZERO_LOCATION,
      PIN_2_ZERO_LOCATION,
      PIN_3_ZERO_LOCATION,
      PIN_4_ZERO_LOCATION,
      PIN_5_ZERO_LOCATION,
      PIN_6_ZERO_LOCATION,
      PIN_7_ZERO_LOCATION,
      PIN_8_ZERO_LOCATION,
      PIN_9_ZERO_LOCATION,
      PIN_10_ZERO_LOCATION,
      PIN_11_ZERO_LOCATION,
      PIN_12_ZERO_LOCATION,
      PIN_13_ZERO_LOCATION};

    public static double getZeroLocationById(int id) {
      return PIN_ZEROS[id];
    }

    public static double getMinValue() {
      int index = 0;
      for (int i = 0; i < PIN_ZEROS.length; i++) {
        if (PIN_ZEROS[i] < PIN_ZEROS[index]) index = i;
      }
      return PIN_ZEROS[index] - 2;
    }
  }
```

Appendix I

Figures

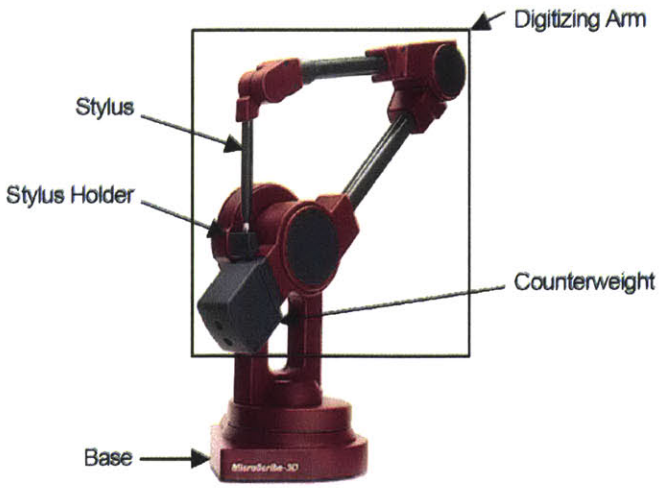

Figure I-1: Anatomy of the Microscribe

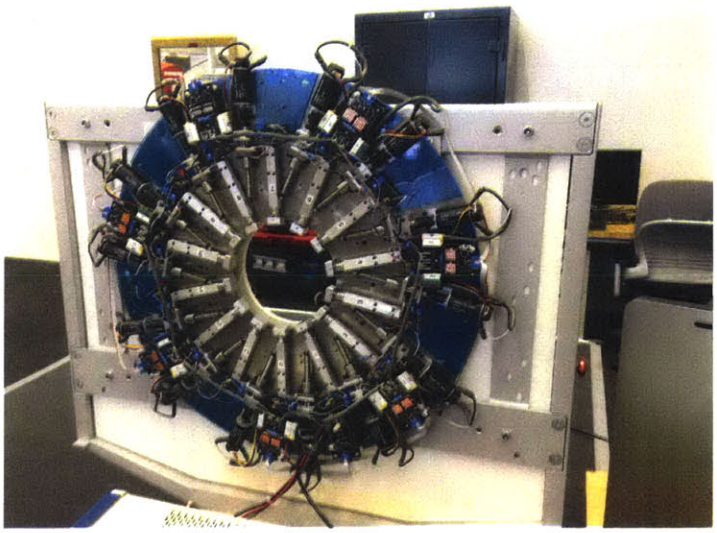

Figure I-2: The original FitSocket

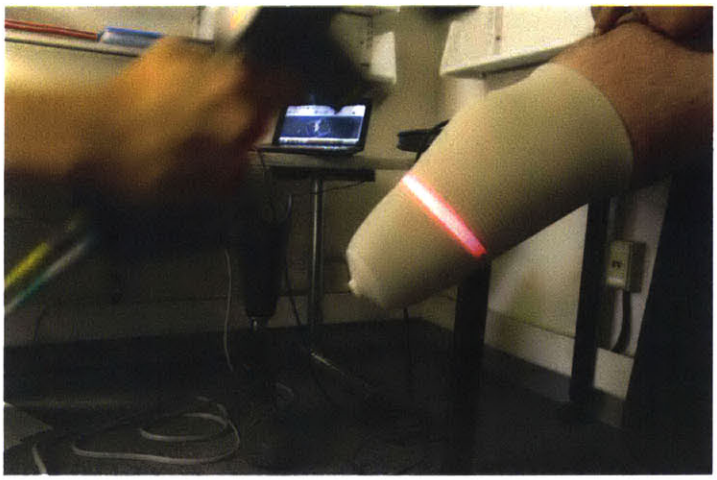

Figure I-3: 3D Scanning of a Subject

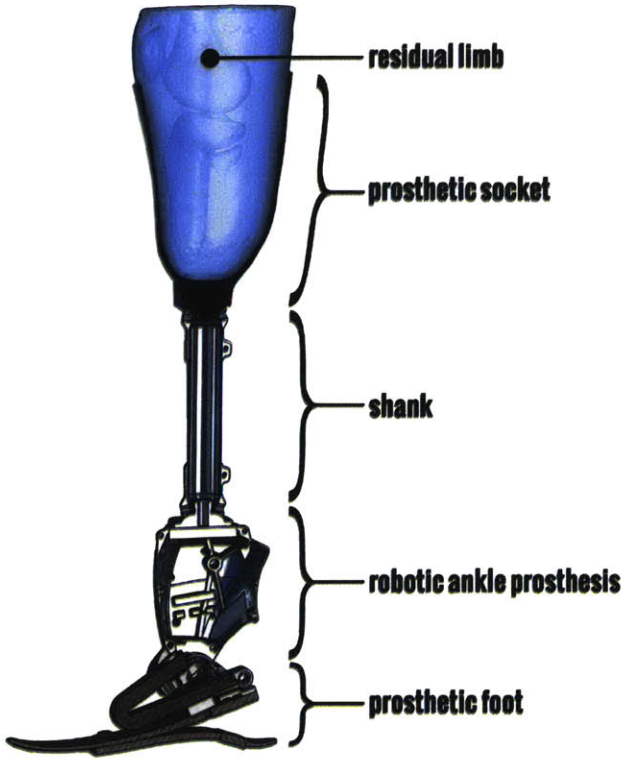

Figure I-4: Anatomy of a Prosthesis

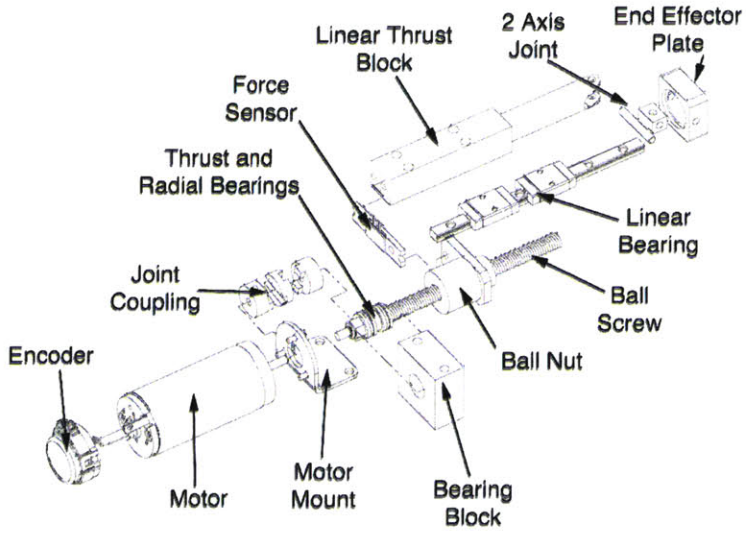

Figure I-5: Anatomy of the First Actuator Layout for the FitSocket

Bibliography

[Agache et al., 1980] Agache, P. G., Monneur, C., Leveque, J. L., Rigal, J., Agache, P. G., Monneur, C., Monneur, C., Leveque, J. L., Leveque, J. L., Rigal, J., and Rigal, J. (1980). Mechanical properties and Young's modulus of human skin in vivo. *Arch. Dermatol. Res.*, 269(3):221–232.

[Aherwar et al., 2014] Aherwar, A., Singh, A., and Patnaik, A. (2014). A review paper on rapid prototyping and rapid tooling techniques for fabrication of prosthetic socket. *High Value Manuf. Adv. Res. Virtual Rapid Prototyp. - Proc. 6th Int. Conf. Adv. Res. Rapid Prototyping, VR@P 2013*, pages 345–353.

[Ahn and Kim, 2010] Ahn, B. and Kim, J. (2010). Measurement and characterization of soft tissue behavior with surface deformation and force response under large deformations. *Med. Image Anal.*, 14(2):138–148.

[Antich et al., 1991] Antich, P. P., Anderson, J. a., Ashman, R. B., Dowdey, J. E., Gonzales, J., Murry, R. C., Zerwekh, J. E., and Pak, C. Y. (1991). Measurement of mechanical properties of bone material in vitro by ultrasound reflection: methodology and comparison with ultrasound transmission. *J. Bone Miner. Res.*, 6(4):417–26.

[Appoldt et al., 1968] Appoldt, F. A., Bennett, L., and Contini, R. (1968). Stump-socket pressure in lower extremity prostheses. *J. Biomech.*, 1(4):247–257.

[Arwert et al., 2007] Arwert, H. J., van Doorn-Loogman, M. H., Koning, J., Terburg, M., Rol, M., and Roebroeck, M. E. (2007). Residual-limb quality and functional mobility 1 year after transtibial amputation caused by vascular insufficiency. *J. Rehabil. Res. Dev.*, 44:717–722.

[Avril et al., 2010] Avril, S., Bouten, L., Dubuis, L., Drapier, S., and Pouget, J.-F. (2010). Mixed experimental and numerical approach for characterizing the biomechanical response of the human leg under elastic compression. *J. Biomech. Eng.*, 132(3):031006.

[Awtar, 2004] Awtar, S. (2004). Synthesis and analysis of parallel Kinematic XY flexure mechanisms.

[Bakody, 2009] Bakody, E. (2009). Orthopaedic plaster casting: nurse and patient education. *Nurs. Stand.*, 23(51):49–56.

[Behr et al., 2009] Behr, J., Friedly, J., Molton, I., Morgenroth, D., Jensen, M. P., and Smith, D. G. (2009). Pain and pain-related interference in adults with lower-limb amputation: comparison of knee-disarticulation, transtibial, and transfemoral surgical sites. *J. Rehabil. Res. Dev.*, 46(7):963–972.

[Berke et al., 2010] Berke, G. M., Fergason, J., Milani, J. R., Hattingh, J., McDowell, M., Nguyen, V., and Reiber, G. E. (2010). Comparison of satisfaction with current prosthetic care in veterans and servicemembers from Vietnam and OIF/OEF conflicts with major traumatic limb loss. *JOURNAL OF REHABILITATION RESEARCH AND DEVELOPMENT*, 47(4):361–371.

[Berryman, 1989] Berryman, J. G. (1989). Fermat's Principle and Nonlinear Traveltime Tomography. *Phys. Rev. Lett.*, 62(25):2953–2957.

[Bossy et al., 2005] Bossy, E., Padilla, F., Peyrin, F., and Laugier, P. (2005). Three-dimensional simulation of ultrasound propagation through trabecular bone structures measured by synchrotron microtomography. *Phys. Med. Biol.*, 50(23):5545–56.

[Boutwell et al., 2012] Boutwell, E., Stine, R., Hansen, A., Tucker, K., and Gard, S. (2012). Effect of prosthetic gel liner thickness on gait biomechanics and pressure distribution within the transtibial socket. *J. Rehabil. Res. Dev.*, 49(2):227.

[Boyer et al., 2007] Boyer, G., Zahouani, H., Le Bot, A., and Laquièze, L. (2007). In vivo characterization of viscoelastic properties of human skin using dynamic micro-indentation. In *Conf. IEEE EMBS*, number 2, pages 4584–4587.

[Bronzino, 2006] Bronzino, J. D. (2006). *Biomedical Engineering Fundamentals (The Biomedical Engineering Handbook, Third Edition).*

[Buis et al., 2006] Buis, A. W. P., Condon, B., Brennan, D., McHugh, B., and Hadley, D. (2006). Magnetic resonance imaging technology in transtibial socket research: a pilot study. *J. Rehabil. Res. Dev.*, 43(7):883–890.

[Butler et al., 2014] Butler, K., Bowen, C., Hughes, A.-M., Torah, R., Ayala, I., Tudor, J., and Metcalf, C. D. (2014). A systematic review of the key factors affecting tissue viability and rehabilitation outcomes of the residual limb in lower extremity traumatic amputees. *J. Tissue Viability*, 23(3):81–93.

[Candes et al., 2011] Candes, E. J., Strohmer, T., and Voroninski, V. (2011). PhaseLift: Exact and Stable Signal Recovery from Magnitude Measurements via Convex Programming.

[Capone et al., 2013] Capone, S. H., Dufresne, M., Rechel, M., Fleury, M.-J., Salsac, A.-V., Paullier, P., Daujat-Chavanieu, M., and Legallais, C. (2013). Impact of Alginate Composition: From Bead Mechanical Properties to Encapsulated HepG2/C3A Cell Activities for In Vivo Implantation. *PLoS ONE*, 8(4):e62032.

[Catheline et al., 1999] Catheline, S., Wu, F., and Fink, M. (1999). A solution to diffraction biases in sonoelasticity: the acoustic impulse technique. *J. Acoust. Soc. Am.*, 105(5):2941–2950.

[Chen, 2010] Chen, Y. (2010). *Nonlinear Stochastic System Identification.* PhD thesis, Massachusetts Institute of Technology.

[Christopher et al., 1996] Christopher, D. A., Burns, P. N., Armstrong, J., and Foster, F. S. (1996). A High-Frequency Continuous-Wave Doppler Ultrasound System for the Detection of Blood Flow in the Microcirculation. *Ultrasound Med. Biol.*, 22(9):1191–1203.

[Coleman, 1998] Coleman, M. J. (1998). A stability study of a three-dimensional passive-dynamic model of human gait. *Ann. Phys. (N. Y).*, 54:286.

[Colombo et al., 2011] Colombo, G., Facoetti, G., Morotti, R., and Rizzi, C. (2011). Physically based modelling and simulation to innovate socket design. *Comput. Aided. Des. Appl.*, 8(4):617–631.

[Convery and Murray, 2000] Convery, P. and Murray, K. D. (2000). Ultrasound study of the motion of the residual femur within a trans-femoral socket during gait. *Prosthet. Orthot. Int.*, 24:226–232.

[Cosgrove and Lassau, 2010] Cosgrove, D. and Lassau, N. (2010). Imaging of perfusion using ultrasound. *Eur. J. Nucl. Med. Mol. Imaging*, 37(S1):65–85.

[Cua et al., 1990] Cua, A. B., Wilhelm, K.-P., and Maibach, H. I. (1990). Elastic properties of human skin: relation to age, sex, and anatomical region. *Arch. Dermatol. Res.*, 282(5):283–288.

[Davidowitz and Kotick, 2011] Davidowitz, G. and Kotick, P. G. (2011). The Use of CAD/CAM in Dentistry. *Dent. Clin. North Am.*, 55(3):559–570.

[Davidson et al., 2010] Davidson, J. H., Khor, K. E., and Jones, L. E. (2010). A cross-sectional study of post-amputation pain in upper and lower limb amputees, experience of a tertiary referral amputee clinic. *Disabil. Rehabil.*, 32(22):1855–1862.

[Deimel et al., 2013] Deimel, G. W., Jelsing, E. J., and Hall, M. M. (2013). Musculoskeletal Ultrasound in Physical Medicine and Rehabilitation. *Curr. Phys. Med. Rehabil. Reports*, 1(1):38–47.

[Delalleau et al., 2008] Delalleau, A., Josse, G., Lagarde, J. M., Zahouani, H., and Bergheau, J. M. (2008). Characterization of the mechanical properties of skin by inverse analysis combined with an extensometry test. *Wear*, 264(5-6):405–410.

[Diridollou et al., 1998] Diridollou, S., Berson, M., Vabre, V., Black, D., Karlsson, B., Auriol, F., Gregoire, J. M., Yvon, C., Vaillant, L., Gall, Y., and Patat, F. (1998). An in vivo method for measuring the mechanical properties of the skin using ultrasound. *Ultrasound Med. Biol.*, 24(2):215–224.

[Dou et al., 2006] Dou, P., Jia, X., Suo, S., Wang, R., and Zhang, M. (2006). Pressure distribution at the stump/socket interface in transtibial amputees during walking on stairs, slope and non-flat road. *CLINICAL BIOMECHANICS*, 21(10):1067–1073.

[Doubrovski et al., 2014] Doubrovski, E., Tsai, E., Dikovsky, D., Geraedts, J., Herr, H., and Oxman, N. (2014). Voxel-based fabrication through material property mapping: A design method for bitmap printing. *Comput. Des.*, 60:3–13.

[Engsberg et al., 2008] Engsberg, J. R., Sprouse, S. W., Uhrich, M. L., Ziegler, B. R., and Luitjohan, F. D. (2008). Comparison of Rectified and Unrectified Sockets for Transtibial Amputees. *J Prosthet Orthot.*, 18(1):1–7.

[Faustini et al., 2005] Faustini, M. C., Crawford, R. H., Neptune, R. R., Rogers, W. E., and Bosker, G. (2005). Design and Analysis of Orthogonally Compliant Features for Local Contact Pressure Relief in Transtibial Prostheses. *J. Biomech. Eng.*, 127(6):946.

[Faustini et al., 2006] Faustini, M. C., Neptune, R. R., and Crawford, R. H. (2006). The quasi-static response of compliant prosthetic sockets for transtibial amputees using finite element methods. *Med. Eng. Phys.*, 28(2):114–121.

[Fernie et al., 1985] Fernie, G. R., Griggs, G., Bartlett, S., and Lunau, K. (1985). Shape sensing for computer aided below-knee prosthetic socket design. *Prosthet. Orthot. Int.*, 9(1):12–16.

[Ferris et al., 1999] Ferris, D. P., Liang, K., and Farley, C. T. (1999). Runners adjust leg stiffness for their first step on a new running surface. *J. Biomech.*, 32(8):787–794.

[Finocchietti et al., 2013] Finocchietti, S., Takahashi, K., Okada, K., Watanabe, Y., Graven-Nielsen, T., and Mizumura, K. (2013). Deformation and pressure propagation in deep tissue during mechanical painful pressure stimulation. *Med. Biol. Eng. Comput.*, 51(1-2):113–122.

[Fitch, 1957] Fitch, C. (1957). Development of the electrostatic clutch. *IBM J. Res. Dev.*, 1(1):49–56.

[Foisneau-Lottin et al., 2003] Foisneau-Lottin, A., Martinet, N., Henrot, P., Paysant, J., Blum, A., and Andre, J. (2003). Bursitis, adventitious bursa, localized soft-tissue inflammation, and bone marrow edema in tibial stumps: The contribution of magnetic resonance Imaging to the diagnosis and management of mechanical stress complications. *ARCHIVES OF PHYSICAL MEDICINE AND REHABILITATION*, 84(5):770–777.

[Freeman and Wontorcik, 1998] Freeman, D. and Wontorcik, L. (1998). Stereolithography and Prosthetic Test Socket Manufacture: A Cost/Benefit Analysis. *J. Prosthetics Orthot.*, 10(1):17–20.

[Frillici et al., 2008] Frillici, F. S., Rissone, P., Rizzi, C., and Rotini, F. (2008). The role of simulation tools to innovate the prosthesis socket design process. *Pham, DT, Eldukhri, EE, Soroka, AJ Innov. Prod. Mach. Syst. MEC Cardiff Univ. Cardiff.*

[Fuchs et al., 1999] Fuchs, M. B., Paley, M., and Miroshny, E. (1999). The Aboudi micromechanical model for topology design of structures. *Comput. Struct.*, 73:355–362.

[Galea et al., 2012] Galea, A. M., LeRoy, K., and Truong, T. Q. (2012). ACTIVE PROSTHETIC SOCKET.

[Gard and Konz, 2003] Gard, S. a. and Konz, R. J. (2003). The effect of a shock-absorbing pylon on the gait of persons with unilateral transtibial amputation. *J. Rehabil. Res. Dev.*, 40(2):109–24.

[Gefen et al., 2013] Gefen, A., Farid, K. J., and Shaywitz, I. (2013). A review of deep tissue injury development, detection, and prevention: shear savvy. *Ostomy. Wound. Manage.*, 59(2):26–35.

[Geil, 2007] Geil, M. D. (2007). Consistency, precision, and accuracy of optical and electromagnetic shape-capturing systems for digital measurement of residual-limb anthropometrics of persons with transtibial amputation. *J. Rehabil. Res. Dev.*, 44(4):515–524.

[Geisheimer et al., 2002] Geisheimer, J. L., Geisheimer, J. L., Greneker, E. F., Greneker, E. F., Marshall, W. S., and Marshall, W. S. (2002). A High-Resolution Doppler Model of Human Gait. *Proc. SPIE*, 4744(2002):8–18.

[Gilbertson and Anthony, 2012] Gilbertson, M. and Anthony, B. (2012). Ergonomic control strategies for a handheld force-controlled ultrasound probe. *Intell. Robot. Syst. (IROS), 2012 IEEE/RSJ Int. Conf.*, pages 1284–1291.

[Greeenwald et al., 2003] Greeenwald, R. M., Dean, R. C., and Board, W. J. (2003). Volume management: smart variable geometry socket (SVGS) technology for lower-limb prostheses. *J. Prosthetics Orthot.*, 15(3):107–112.

[Han et al., 2002] Han, L., Burcher, M., and Noble, J. (2002). Non-invasive Measurement of Biomechanical Properties of in vivo Soft Tissues. In *Med. Image Comput. Comput. Interv. — MICCAI 2002*, volume 2488, pages 208–215.

[Han et al., 2003] Han, L., Noble, J. A., and Burcher, M. (2003). A novel ultrasound indentation system for measuring biomechanical properties of in vivo soft tissue. *Ultrasound Med. Biol.*, 29(6):813–823.

[Hanley et al., 2007] Hanley, M. A., Jensen, M. P., Smith, D. G., Ehde, D. M., Edwards, W. T., and Robinson, L. R. (2007). Preamputation Pain and Acute Pain Predict Chronic Pain After Lower Extremity Amputation. *J. Pain*, 8(2):102–109.

[Hansen et al., 2008] Hansen, C., Hiittebrauker, N., Schasse, A., Wilkening, W., Ermert, H., Hollenhorst, M., Heuser, L., and Schulte-Altedomeburg, G. (2008). Ultrasound breast imaging using full angle spatial compounding: in-vivo results. *Proc. - IEEE Ultrason. Symp.*, pages 54–57.

[Hanspal et al., 2003] Hanspal, R. S., Fisher, K., and Nieveen, R. (2003). Prosthetic socket fit comfort score. *Disabil. Rehabil.*, 25(22):1278–1280.

[He et al., 1996] He, P., Xue, K., Chen, Q., Murka, P., and Schall, S. (1996). A PC-based ultrasonic data acquisition system for computer-aided prosthetic socket design. *IEEE Trans. Rehabil. Eng.*, 4(2):114–9.

[He et al., 1999] He, P., Xue, K., Fan, Y., and Wang, Y. (1999). Test of a vertical scan mode in 3-D imaging of residual limbs using ultrasound. *J. Rehabil. Res. Dev.*, 36(2):86–93.

[He et al., 1997] He, P., Xue, K., and Murka, P. (1997). 3-D imaging of residual limbs using ultrasound. *J. Rehabil. Res. Dev.*, 34(3):269–78.

[Hendriks, 2005] Hendriks, F. (2005). *Mechanical behaviour of human epidermal and dermal layers in vivo.*

[Herr and Maes, 2013] Herr, H. and Maes, P. (2013). Pattern Classification of Terrain During Amputee ARQ Accepted by Pattern Classification of Terrain During Amputee Walking. (2009).

[Hoskins and Svensson, 2012] Hoskins, P. R. and Svensson, W. (2012). Current state of ultrasound elastography. *Ultrasound*, 20(1):3–4.

[Hospital and Womwn´S, 2011] Hospital, B. and Womwn´S (2011). Standard of Care : Lower Extremity Amputation. pages 1–46.

[Hsu et al., 2008] Hsu, L., Huang, G., Lu, C., Lai, C., Chen, Y., Yu, I., and Shih, H. (2008). The Application of Rapid Prototyping for the Design and Manufacturing of Transtibial Prosthetic Socket.

[Huang et al., 2005] Huang, Q. H., Zheng, Y. P., Lu, M. H., and Chi, Z. R. (2005). Development of a portable 3D ultrasound imaging system for musculoskeletal tissues. *Ultrasonics*, 43(3):153–163.

[INMAN et al., 1961] INMAN, V., LOON, H., LEVY, S., RALSTON, H., and BARNES, G. (1961). MEDICAL PROBLEMS OF AMPUTEES. *CALIFORNIA MEDICINE*, 94(3):132–&.

[Jia et al., 2005] Jia, X., Zhang, M., Li, X., and Lee, W. C. C. (2005). A quasi-dynamic nonlinear finite element model to investigate prosthetic interface stresses during walking for trans-tibial amputees. *Clin. Biomech.*, 20(6):630–635.

[Jr, 2006] Jr, J. P. (2006). Adjustable prosthetic socket. *US Pat. 6,991,657*, 1(12).

[Kane et al., 2004] Kane, D., Grassi, W., Sturrock, R., and Balint, P. V. (2004). A brief history of musculoskeletal ultrasound: 'From bats and ships to babies and hips'. *Rheumatology*, 43(7):931–933.

[Kang and Wang, 2011] Kang, Z. and Wang, Y. (2011). Structural topology optimization based on non-local Shepard interpolation of density field. *Comput. Methods Appl. Mech. Eng.*, 200(49-52):3515–3525.

[Keesman, 2011] Keesman, K. J. (2011). *System Identification*.

[Khatyr et al., 2004] Khatyr, F., Imberdis, C., Vescovo, P., Varchon, D., and Lagarde, J. M. (2004). Model of the viscoelastic behaviour of skin in vivo and study of anisotropy. *Ski. Res. Technol.*, 10:96–103.

[Kisiel et al., 2007] Kisiel, R., Bukat, K., Drozd, Z., Szwech, M., Syryczyk, P., and Girulska, A. (2007). *Recent Advances in Mechatronics*.

[Korenberg, 1990] Korenberg, M. J. (1990). The Identification of Nonlinear Biological Systems - Wiener .pdf. 18:629–654.

[Kornbluh et al., 1999] Kornbluh, R. D., Pelrine, R., Joseph, J., Heydt, R., Pei, Q., and Chiba, S. (1999). High-field electrostriction of elastomeric polymer dielectrics for actuation. *Proc. SPIE*, 3669(1):149–161.

[Kornbluh et al., 2000] Kornbluh, R. D., Pelrine, R., Pei, Q., Oh, S., and Joseph, J. (2000). Ultra-high strain response of field-actuated elastomeric polymers. *SPIE 3987, Smart Struct. Mater. 2000 Electroact. Polym. Actuators Devices*, 3987:51–64.

[Krouskop et al., 1987a] Krouskop, T. A., Dougherty, D. R., and Vinson, F. S. (1987a). A pulsed Doppler ultrasonic system for making noninvasive measurements of the mechanical properties of soft tissue. *J. Rehabil. Res. Dev.*, 24(10):1–8.

[Krouskop et al., 1987b] Krouskop, T. a., Muilenberg, a. L., Doughtery, D. R., and Winningham, D. J. (1987b). Computer-aided design of a prosthetic socket for an above-knee amputee. *J. Rehabil. Res. Dev.*, 24(2):31–38.

[Krouskop et al., 1987c] Krouskop, T. a., Muilenberg, a. L., Doughtery, D. R., and Winningham, D. J. (1987c). Computer-aided design of a prosthetic socket for an above-knee amputee. *J. Rehabil. Res. Dev.*, 24(2):31–38.

[Kuo, 2001] Kuo, A. D. (2001). Energetics of Actively Powered Locomotion Using the Simplest Walking Model. *J. Biomech. Eng.*, 124(1):113.

[Lacono et al., 1987] Lacono, R. P., Linford, J., and Sandyk, R. (1987). Pain management after lower extremity amputation. *Neurosurgery*, 20(3):496–500.

[Lalitha et al., 2011] Lalitha, P., Balaji Reddy, M., and Jagannath Reddy, K. (2011). Musculoskeletal applications of elastography: A pictorial essay of our initial experience. *Korean J. Radiol.*, 12(3):365–375.

[Lang, 2004] Lang, P. (2004). Optical Tactile Sensors for Medical Palpation Pencilla Lang. *Sensors (Peterborough, NH)*, (March 2004):1–7.

[Larrabee, 1986] Larrabee, W. F. (1986). A finite element model of skin deformation. I. Biomechanics of skin and soft tissue: a review. *Laryngoscope*, 96(4):399–405.

[Laugier et al., 1997] Laugier, P., Droin, P., Laval-Jeantet, a. M., and Berger, G. (1997). In vitro assessment of the relationship between acoustic properties and bone mass density of the calcaneus by comparison of ultrasound parametric imaging and quantitative computed tomography. *Bone*, 20(2):157–65.

[Lee et al., 2011] Lee, T., Leok, M., and McClamroch, N. H. (2011). Geometric numerical integration for complex dynamics of tethered spacecraft. *Proc. 2011 Am. Control Conf.*, (March):1885–1891.

[Lee et al., 2005] Lee, W., Zhang, M., and Mak, A. (2005). Regional differences in pain threshold and tolerance of the transtibial residual limb: Including the effects of age and interface material. *ARCHIVES OF PHYSICAL MEDICINE AND REHABILITATION*, 86(4):641–649.

[Lee et al., 2004] Lee, W. C. C., Zhang, M., Jia, X., and Cheung, J. T. M. (2004). Finite element modeling of the contact interface between trans-tibial residual limb and prosthetic socket. *Med. Eng. Phys.*, 26(8):655–662.

[Lempitsky and Boykov, 2007] Lempitsky, V. and Boykov, Y. (2007). Global optimization for shape fitting. *Proc. IEEE Comput. Soc. Conf. Comput. Vis. Pattern Recognit.*, (June):1–14.

[Lempitsky et al., 2009] Lempitsky, V., Kohli, P., Rother, C., and Sharp, T. (2009). Image segmentation with a bounding box prior. *Proc. IEEE Int. Conf. Comput. Vis.*, pages 277–284.

[Lenka, 2011] Lenka, P. K. (2011). Analysis of trans tibial prosthetic socket materials using finite element method. *J. Biomed. Sci. Eng.*, 04(12):762–768.

[Lester et al., 2005] Lester, J., Choudhury, T., and Borriello, G. (2005). Sensing and modeling activities to support physical fitness. *to Support Fitness),*, pages 5–8.

[Lilja et al., 1993] Lilja, M., Johansson, T., and Oberg, T. (1993). Movement of the tibial end in a PTB prosthesis socket: a sagittal X-ray study of the PTB prosthesis. *Prosthet. Orthot. Int.*, 17(1):21–26.

[Lin et al., 2004] Lin, C. C., Chang, C. H., Wu, C. L., Chung, K. C., and Liao, I. C. (2004). Effects of liner stiffness for trans-tibial prosthesis: A finite element contact model. *Med. Eng. Phys.*, 26(1):1–9.

[Lin and Chao, 2000] Lin, C.-Y. and Chao, L.-S. (2000). Automated image interpretation for integrated topology and shape optimization. *Struct. Multidiscip. Optim.*, 20(2):125–137.

[Lu et al., 2009] Lu, C. T., Hsu, L. H., Huang, G. F., Lai, C. W., Peng, H. K., and Hong, T. Y. (2009). The Development and Strength Reinforcement of Rapid Prototyping Prosthetic Socket Coated with a Resin Layer for Transtibial Amputee. *IFMBE Proc.*, 23:1128–1131.

[Lustig et al., 2013] Lustig, S., Scholes, C. J., Leo, S. P. M., Coolican, M., and Parker, D. A. (2013). Influence of soft tissues on the proximal bony tibial slope measured with two-dimensional MRI. *Knee Surgery, Sport. Traumatol. Arthrosc.*, 21(2):372–379.

[Mahmud et al., 2012] Mahmud, J., Evans, S. L., and Holt, C. a. (2012). An Innovative Tool to Measure Human Skin Strain Distribution in Vivo using Motion Capture and Delaunay Mesh. *J. Mech.*, 28(02):309–317.

[Mak et al., 2001] Mak, a. F., Zhang, M., and Boone, D. a. (2001). State-of-the-art research in lower-limb prosthetic biomechanics-socket interface: a review. *J. Rehabil. Res. Dev.*, 38(2):161–174.

[Mak et al., 2010] Mak, A. F. T., Zhang, M., and Tam, E. W. C. (2010). Biomechanics of Pressure Ulcer in Body Tissues Interacting with External Forces during Locomotion. In Yarmush, ML and Duncan, JS and Gray, ML, editor, *ANNUAL REVIEW OF BIOMEDICAL ENGINEERING, VOL 12*, volume 12 of *Annual Review of Biomedical Engineering*, pages 29–53. ANNUAL REVIEWS, 4139 EL CAMINO WAY, PO BOX 10139, PALO ALTO, CA 94303-0897 USA.

[Martin et al., 2012] Martin, J. J., Butel, T., Markmiller, M., Kozlowski, M., and Boone, D. (2012). PUMP SYSTEM FOR PROSTHESIS.

[Mattmann et al., 2007] Mattmann, C., Amft, O., Harms, H., Tröster, G., and Clemens, F. (2007). Recognizing upper body postures using textile strain sensors. *Proc. - Int. Symp. Wearable Comput. ISWC*, pages 29–36.

[Maurer et al., 2003] Maurer, J., Ronsky, J., Loitz-ramage, B., Andersen, M., and Harder, J. (2003). Prosthetic socket interface pressures: customized calibration technique for the Tekscan F-Socket system. *2003 Summer Bioeng. Conf.*, (1):1073–74.

[Mcelligott et al., 2002] Mcelligott, L., Dillon, M., Leydon, K., Richardson, B., Fernström, M., and Paradiso, J. a. (2002). ' ForSe FIElds ' – Force Sensors for Interactive Environments. *Proc. Int. Conf. Ubiquitous Comput. (UbiComp '02)*, pages 168–175.

[McGeer, 1993] McGeer, T. (1993). Dynamics and control of bipedal locomotion.

[Milano et al.,] Milano, P., Meccanica, D. I., and Masa, L. 3D Digital Models Reconstruction : Residual Limb. *Body Model. Crime Scene Investig.*, pages 96–103.

[Moerman et al., 2013] Moerman, K. M., Sprengers, A. M. J., Nederveen, A. J., and Simms, C. K. (2013). A novel MRI compatible soft tissue indentor and fibre Bragg grating force sensor. *Med. Eng. Phys.*, 35:486–499.

[Moerman et al., 2012] Moerman, K. M., Sprengers, A. M. J., Simms, C. K., Lamerichs, R. M., Stoker, J., and Nederveen, A. J. (2012). Validation of continuously tagged MRI for the measurement of dynamic 3D skeletal muscle tissue deformation. *Med. Phys.*, 39(4):1793.

[Mojra et al., 2011] Mojra, A., Najarian, S., Mohsen, S., Kashani, T., Panahi, F., and Yaghmaei, M. (2011). A novel haptic robotic viscogram for characterizing the viscoelastic behaviour of breast tissue in clinical examinations. *Int J Med Robot. Comput Assist Surg*, (7):282–292.

[Molton et al., 2007] Molton, I. R., Jensen, M. P., Ehde, D. M., and Smith, D. G. (2007). Phantom limb pain and pain interference in adults with lower extremity amputation: The moderating effects of age. *Rehabil. Psychol.*, 52(3):272–279.

[Monetti and Minafra, 2007] Monetti, G. and Minafra, P. (2007). The musculoskeletal elastography. *MEDIX suppl*, pages 43–45.

[Montgomery et al., 2010a] Montgomery, J. T., Vaughan, M. R., and Crawford, R. H. (2010a). Design of an actively actuated prosthetic socket. *RAPID PROTOTYPING JOURNAL*, 16(3):194–201. International Solid Freeform Fabrication Symposium, Austin, TX, AUG 03-05, 2009.

[Montgomery et al., 2010b] Montgomery, J. T., Vaughan, M. R., and Crawford, R. H. (2010b). Design of an actively actuated prosthetic socket. *Rapid Prototyp. J.*, 16(3):194–201.

[Moo et al., 2009] Moo, E. K., Abu Osman, N. a., Pingguan-Murphy, B., Wan Abas, W. a. B., Spence, W. D., and Solomonidis, S. E. (2009). Interface pressure profile analysis for patellar tendon-bearing socket and hydrostatic socket. *Acta Bioeng. Biomech.*, 11(4):37–43.

[Morimoto et al., 1995] Morimoto, A. K., Bow, W. J., Strong, D. S., Dickey, F. M., Krumm, J. C., Vick, D. D., Kozlowski, D. M., Partridge, S., Warsh, N., Faulkner, V., and Rogers, B. (1995). 3D Ultrasound Imaging for Prosthesis Fabrication and Diagnostic Imaging. pages 1–70.

[Natterer and Wubbeling, 1995] Natterer, F. and Wubbeling, F. (1995). A propagation-backpropagation method for ultrasound tomography. *Inverse Probl.*, 11(Copyright 1996, IEE):1225–1232.

[Neptune et al., 2008] Neptune, R. R., Sasaki, K., and Kautz, S. A. (2008). The effect of walking speed on muscle function and mechanical energetics. *Gait Posture*, 28(1):135–43.

[Nolan et al., 2003] Nolan, L., Wit, A., Dudziñski, K., Lees, A., Lake, M., and Wychowañski, M. (2003). Adjustments in gait symmetry with walking speed in trans-femoral and trans-tibial amputees. *Gait Posture*, 17(2):142–151.

[Normann et al., 2011] Normann, E., Olsson, A., and Brodtkorb, T.-H. (2011). Modular socket system versus traditionally laminated socket: a cost analysis. *Prosthet. Orthot. Int.*, 35:76–80.

[Novacheck, 1998] Novacheck, T. F. (1998). The biomechanics of running. *Gait Posture*, 7(1):77–95.

[Nowozin and Lampert, 2009] Nowozin, S. and Lampert, C. H. (2009). Global connectivity potentials for random field models. *2009 IEEE Comput. Soc. Conf. Comput. Vis. Pattern Recognit. Work. CVPR Work. 2009*, pages 818–825.

[Oflaz and Baran, 2014] Oflaz, H. and Baran, O. (2014). A new medical device to measure a stiffness of soft materials. *Acta Bioeng. Biomech.*, 16(1).

[OK-Denis et al., 1995] OK-Denis, F., Basset, O., and Gimenez, G. (1995). Ultrasonic Transmission Tomography in Refracting Media: Reduction of Refraction Artifacts by Curved-Ray Techniques. *IEEE Trans. Med. Imaging*, 14(1):173–188.

[Omasta et al., 2011] Omasta, M., Paloušek, D., Návrat, T., and Rosický, J. (2011). Finite element analysis for the evaluation of the structural behaviour, of a prosthesis for trans-tibial amputees. *Med. Eng. Phys.*, 34(1):355–356.

[Ophir, 1991] Ophir, J. (1991). Elastography: A quantitative method for imaging the elasticity of biological tissues. *Ultrason. Imaging*, 13(2):111–134.

[Oxman et al., 2010] Oxman, N., Mitchell, W. J., Arts, M., Supervisor, T., and Beinart, J. (2010). Material-based Design Computation.

[Ozcakar et al., 2013] Ozcakar, L., Carli, A. B., Tok, F., Tekin, L., Akkaya, N., and Kara, M. (2013). The utility of musculoskeletal ultrasound in rehabilitation settings. *Am J Phys Med Rehabil*, 92(9):805–817.

[Pailler-Mattei et al., 2008] Pailler-Mattei, C., Bec, S., and Zahouani, H. (2008). In vivo measurements of the elastic mechanical properties of human skin by indentation tests. *Med. Eng. Phys.*, 30(5):599–606.

[Palousek et al., 2009] Palousek, D., Krejci, P., and Rosicky, J. (2009). Long-Term Monitoring of Transtibial Prosthesis Deformation. *Recent Adv. Mechatronics 2008-2009*, pages 419–424.

[Pandy and Anderson, 1992] Pandy, M. and Anderson, F. (1992). A parameter optimization approach for the optimal control of large-scale musculoskeletal systems.

[Papaioannou et al., 2010] Papaioannou, G., Mitrogiannis, C., Nianios, G., and Fiedler, G. (2010). Assessment of amputee socket-stump-residual bone kinematics during strenuous activities using Dynamic Roentgen Stereogrammetric Analysis. *J. Biomech.*, 43(5):871–878.

[Pearson et al., 1974] Pearson, J. R., Grevsten, S., Almby, B., and Marsh, L. (1974). Pressure variation in the below-knee, patellar tendon bearing suction socket prosthesis. *J. Biomech.*, 7(6):487–496.

[Peery et al., 2005] Peery, J. T., Ledoux, W. R., and Klute, G. K. (2005). Residual-limb skin temperature in transtibial sockets. *J. Rehabil. Res. Dev.*, 42(2):147–154.

[Philen, 2009] Philen, M. (2009). ON THE APPLICABILITY OF F(2)MC VARIABLE IMPEDANCE MATERIALS FOR PROSTHETIC DEVICES. In *SMASIS 2008: PROCEEDINGS OF THE ASME CONFERENCE ON SMART MATERIALS, ADAPTIVE STRUCTURES AND INTELLIGENT SYSTEMS - 2008, VOL 2*, pages 637–646, THREE PARK AVENUE, NEW YORK, NY 10016-5990 USA. ASME, Nanotechnol Inst, AMER SOC MECHANICAL ENGINEERS. Conference on Smart Materials, Adaptive Structures and Intelligent Systems, Ellicot, MD, OCT 28-30, 2008.

[Pinzur et al., 1996] Pinzur, M. S., Reddy, N., Charuk, G., Osterman, H., and Vrbos, L. (1996). Control of the residual tibia in transtibial amputation. *Foot ankle Int. / Am. Orthop. Foot Ankle Soc. [and] Swiss Foot Ankle Soc.*, 17(9):538–540.

[Pirouzi et al., 2014] Pirouzi, G., Osman, N., Oshkour, A., Ali, S., Gholizadeh, H., and Abas, W. (2014). Development of an Air Pneumatic Suspension System for Transtibial Prostheses. *Sensors*, 14(9):16754–16765.

[Polliack et al., 2000a] Polliack, A., Sieh, R., Craig, D., Landsberger, S., McNeil, D., and Ayyappa, E. (2000a). Scientific validation of two commercial pressure sensor systems for prosthetic socket fit. *PROSTHETICS AND ORTHOTICS INTERNATIONAL*, 24(1):63–73.

[Polliack et al., 2000b] Polliack, a. a., Sieh, R. C., Craig, D. D., Landsberger, S., McNeil, D. R., and Ayyappa, E. (2000b). Scientific validation of two commercial pressure sensor systems for prosthetic socket fit. *Prosthet. Orthot. Int.*, 24(1):63–73.

[Portnoy et al., 2009] Portnoy, S., Siev-Ner, I., Shabshin, N., Kristal, A., Yizhar, Z., and Gefen, A. (2009). Patient-specific analyses of deep tissue loads post transtibial amputation in residual limbs of multiple prosthetic users. *JOURNAL OF BIOMECHANICS*, 42(16):2686–2693.

[Portnoy et al., 2006] Portnoy, S., Yarnitzky, G., Yizhar, Z., Kristal, A., Oppenheim, U., Siev-Ner, I., and Gefen, A. (2006). Real-time patient-specific finite element analysis of residual limb stresses in transtibial amputees during treadmill walking. *J. Biomech.*, 39(2005):S539.

[Portnoy et al., 2007a] Portnoy, S., Yarnitzky, G., Yizhar, Z., Kristal, a., Oppenheim, U., Siev-Ner, I., and Gefen, a. (2007a). Real-time patient-specific finite element analysis of internal stresses in the soft tissues of a residual limb: A new tool for prosthetic fitting. *Ann. Biomed. Eng.*, 35(1):120–135.

[Portnoy et al., 2007b] Portnoy, S., Yarnitzky, G., Yizhar, Z., Kristal, A., Oppenheim, U., Siev-Ner, I., and Gefen, A. (2007b). Real-time patient-specific finite element analysis of internal stresses in the soft tissues of a residual limb: A new tool for prosthetic fitting. *ANNALS OF BIOMEDICAL ENGINEERING*, 35(1):120–135.

[Potts et al., 1983] Potts, R. O., Chrisman, D. A., and Buras, E. M. (1983). The dynamic mechanical properties of human skin in vivo.

[Radegran, 1997] Radegran, G. (1997). Doppler Ultrasound Estimates of Femoral Artery Blood Flow During Dynamic Knee Extensor Exercises in Humans. *J. Am. Physi*, (1):1383–1388.

[Rheinstein, 2001] Rheinstein, J. (2001). Checklist for evaluating a transtibial prosthesis. *Foot Ankle Clin.*, 6(2):265–269, vi.

[Safari et al., 2013] Safari, M. R., Rowe, P., and Buis, A. (2013). Examination of anticipated chemical shift and shape distortion effect on materials commonly used in prosthetic socket fabrication when measured using MRI: a validation study. *J. Rehabil. Res. Dev.*, 50(1):31–42.

[Sanders and Daly, 1993a] Sanders, J. and Daly, C. (1993a). Measurement of stresses in three orthogonal directions at the residual limb-prosthetic socket interface. *IEEE Trans. Rehabil. Eng.*, 1(2):79–85.

[Sanders and Daly, 1993b] Sanders, J. E. and Daly, C. H. (1993b). Normal and shear stresses on a residual limb in a prosthetic socket during ambulation: comparison of finite element results with experimental measurements. *J. Rehabil. Res. Dev.*, 30:191–204.

[Sanders et al., 1992] Sanders, J. E., Daly, C. H., and Burgess, E. M. (1992). Interface shear stresses during ambulation with a below-knee prosthetic limb. *J. Rehabil. Res. Dev.*, 29(4):1–8.

[Sanders et al., 2009] Sanders, J. E., Harrison, D. S., Allyn, K. J., and Myers, T. R. (2009). Clinical utility of in-socket residual limb volume change measurement: case study results. *Prosthet. Orthot. Int.*, 33(4):378–390.

[Sanders et al., 2006] Sanders, J. E., Jacobsen, a. K., and Fergason, J. R. (2006). Effects of fluid insert volume changes on socket pressures and shear stresses: case studies from two trans-tibial amputee subjects. *Prosthet. Orthot. Int.*, 30(3):257–69.

[Sanders and Lee, 2008] Sanders, J. E. and Lee, G. S. (2008). A means to accommodate residual limb movement during optical scanning: a technical note. *IEEE Trans. Neural Syst. Rehabil. Eng.*, 16(5):505–509.

[Sanders et al., 2007] Sanders, J. E., Rogers, E. L., Sorenson, E. a., Lee, G. S., and Abrahamson, D. C. (2007). CAD/CAM transtibial prosthetic sockets from central fabrication facilities: how accurate are they? *J. Rehabil. Res. Dev.*, 44(3):395–405.

[Sanders and Severance, 2011] Sanders, J. E. and Severance, M. R. (2011). Assessment technique for computer-aided manufactured sockets. *J. Rehabil. Res. Dev.*, 48(7):763.

[Sanders et al., 2012a] Sanders, J. E., Severance, M. R., and Allyn, K. J. (2012a). Computer-socket manufacturing error: How much before it is clinically apparent? *J. Rehabil. Res. Dev.*, 49(4):567.

[Sanders et al., 2012b] Sanders, J. E., Severance, M. R., and Allyn, K. J. (2012b). Computer-socket manufacturing error: How much before it is clinically apparent? *J. Rehabil. Res. Dev.*, 49(4):567.

[Sanders et al., 2013] Sanders, J. E., Severance, M. R., Swartzendruber, D. L., Allyn, K. J., and Ciol, M. a. (2013). Influence of prior activity on residual limb volume and shape measured using plaster casting: Results from individuals with transtibial limb loss. *J. Rehabil. Res. Dev.*, 50(7):1007–16.

[Sengeh and Herr, 2013a] Sengeh, D. M. and Herr, H. (2013a). A Variable-Impedance Prosthetic Socket for a Transtibial Amputee Designed from Magnetic Resonance Imaging Data. *JPO J. Prosthetics Orthot.*, 25(3):129–137.

[Sengeh and Herr, 2013b] Sengeh, D. M. and Herr, H. (2013b). A Variable-Impedance Prosthetic Socket for a Transtibial Amputee Designed from Magnetic Resonance Imaging Data. *J. Prosthetics Orthosis*, 25(3):129–137.

[Sewell et al., 2012] Sewell, P., Noroozi, S., Vinney, J., Amali, R., and Andrews, S. (2012). Static and dynamic pressure prediction for prosthetic socket fitting assessment utilising an inverse problem approach. *Artif. Intell. Med.*, 54(1):29–41.

[Shimazu et al., 1989] Shimazu, H., Ito, H., and Yamakoshi, K. (1989). SYSTEM FOR MEASURING THE VOLUME OF A PART OF A HUMAN BODY.

[Shirley and Mermelstien,] Shirley, L. G. and Mermelstien, M. S. Apparatus and Methods for Surface Countour Measurement.

[Shuxian et al., 2005] Shuxian, Z., Wanhua, Z., and Bingheng, L. (2005). 3D reconstruction of the structure of a residual limb for customising the design of a prosthetic socket. *Med. Eng. Phys.*, 27(1):67–74.

[Silver et al., 2002] Silver, F. H., Seehra, G. P., Freeman, J. W., and DeVore, D. (2002). Viscoelastic properties of young and old human dermis: A proposed molecular mechanism for elastic energy storage in collagen and elastin. *J. Appl. Polym. Sci.*, 86(8):1978–1985.

[Silver-Thorn and Childress, 1996] Silver-Thorn, M. B. and Childress, D. S. (1996). Parametric analysis using the finite element method to investigate prosthetic interface stresses for persons with trans-tibial amputation. *J. Rehabil. Res. Dev.*, 33(3):227–238.

[Stekelenburg et al., 2008] Stekelenburg, A., Gawlitta, D., Bader, D. L., and Oomens, C. W. (2008). Deep tissue injury: how deep is our understanding? *Arch. Phys. Med. Rehabil.*, 89(7):1410–3.

[Terzopoulos, 2011] Terzopoulos, D. (2011). Computational Vision and Medical Image Processing. 19:125–143.

[Tran et al., 2007] Tran, H. V., Charleux, F., Rachik, M., Ehrlacher, A., and Ho Ba Tho, M. C. (2007). In vivo characterization of the mechanical properties of human skin derived from MRI and indentation techniques. *Comput. Methods Biomech. Biomed. Engin.*, 10(6):401–407.

[Vannah and Childress, 1996] Vannah, W. M. and Childress, D. S. (1996). Indentor tests and finite element modeling of bulk muscular tissue in vivo. *J. Rehabil. Res. Dev.*, 33(3):239–252.

[Vannah et al., 1999] Vannah, W. M., Drvaric, D. M., Hastings, J. a., Stand, J. a., and Harning, D. M. (1999). A method of residual limb stiffness distribution measurement. *J. Rehabil. Res. Dev.*, 36(1):1–7.

[Vukobratović and Borovac, 2004] Vukobratović, M. and Borovac, B. (2004). Zero-Moment Point — Thirty Five Years of Its Life. *Int. J. Humanoid Robot.*, 01(01):157–173.

[Wachinger et al., 2007] Wachinger, C., Wein, W., and Navab, N. (2007). Three-dimensional ultrasound mosaicing. *Med. Image Comput. Comput. Assist. Interv.*, 10:327–335.

[Wang et al., 2007] Wang, Q., Zheng, Y. P., Niu, H. J., and Mak, a. F. T. (2007). Extraction of mechanical properties of articular cartilage from osmotic swelling behavior monitored using high frequency ultrasound. *J. Biomech. Eng.*, 129(3):413–422.

[Webber and Davis, 2015] Webber, C. M. and Davis, B. L. (2015). Design of a novel prosthetic socket: assessment of the thermal performance. *J. Biomech.*, 48(7):1294–9.

[Werner et al., 2000] Werner, a., Lechniak, Z., Skalski, K., and Kedzior, K. (2000). Design and manufacture of anatomical hip joint endoprostheses using CAD/CAM systems. *J. Mater. Process. Technol.*, 107:181–186.

[Wiskin et al., 2007] Wiskin, J., Olsen, S., and Hanover, B. (2007). NON-INVASIVE BREAST TISSUE CHARACTERIZATION USING ULTRASOUND SPEED AND ATTENUATION In Vivo Validation. pages 147–154.

[Wolf et al., 2009] Wolf, S. I., Alimusaj, M., Fradet, L., Siegel, J., and Braatz, F. (2009). Pressure characteristics at the stump/socket interface in transtibial amputees using an adaptive prosthetic foot. *Clinical Biomechanics*, 24(10):860 – 865.

[Wu et al., 2012] Wu, C. H., Chen, W. S., Park, G. Y., Wang, T. G., and Lew, H. L. (2012). Musculoskeletal Sonoelastography: A Focused Review of its Diagnostic Applications for Evaluating Tendons and Fascia. *J. Med. Ultrasound*, 20(2):79–86.

[Wu et al., 2003] Wu, Y., Casanova, H., Smith, W. K., Edwards, M., and Childress, D. S. (2003). CIR sand casting system for trans-tibial socket. *Prosthet. Orthot. Int.*, 27:146–152.

[Xiong et al., 2010] Xiong, S., Goonetilleke, R. S., Witana, C. P., and Rodrigo, W. D. A. S. (2010). An indentation apparatus for evaluating discomfort and pain thresholds in conjunction with mechanical properties of foot tissue in vivo. *J. Rehabil. Res. Dev.*, 47(7):629–641.

[Yang and Chuang, 1994] Yang, R. and Chuang, C. (1994). Optimal topology design using linear programming. *Comput. Struct.*, 52(2):265–275.

[Yeung et al., 2012] Yeung, L. F., Leung, A. K. L., Zhang, M., and Lee, W. C. C. (2012). Effects of long-distance walking on socket-limb interface pressure, tactile sensitivity and subjective perceptions of trans-tibial amputees. *Disabil. Rehabil.*, 35(July 2012):1–6.

[Yigiter et al., 2002] Yigiter, K., Sener, G., and Bayar, K. (2002). Comparison of the effects of patellar tendon bearing and total surface bearing sockets on prosthetic fitting and rehabilitation. *PROSTHETICS AND ORTHOTICS INTERNATIONAL*, 26(3):206–212.

[Zach and Pollefeys, 2010] Zach, C. and Pollefeys, M. (2010). Practical methods for convex multi-view reconstruction. *Comput. Vision–ECCV 2010.*

[Zachariah and Sanders, 2001] Zachariah, S. G. and Sanders, J. E. (2001). Standing interface stresses as a predictor of walking interface stresses in the trans-tibial prosthesis. *Prosthet. Orthot. Int.*, 25(1):34–40.

[Zagzebski et al., 1991] Zagzebski, J. a., Rossman, P. J., Mesina, C., Mazess, R. B., and Madsen, E. L. (1991). Ultrasound transmission measurements through the os calcis. *Calcif. Tissue Int.*, 49(2):107–11.

[Zajac et al., 2002] Zajac, F. E., Neptune, R. R., and Kautz, S. a. (2002). Biomechanics and muscle coordination of human walking: Part I: Introduction to concepts, power transfer, dynamics and simulations. *Gait Posture*, 16(3):215–232.

[Zakrzewski and Anthony, 2013] Zakrzewski, A. M. and Anthony, B. W. (2013). Quantitative elastography and its application to blood pressure estimation: Theoretical and experimental results. *Proc. Annu. Int. Conf. IEEE Eng. Med. Biol. Soc. EMBS*, pages 1136–1139.

[Zakrzewski et al., 2013] Zakrzewski, A. M., Anthony, B. W., and Reconstruction, A. E. (2013). Quantitative Elastography and its Application to Blood Pressure Estimation : Theoretical and Experimental Results. (2011):1136–1139.

[Zhang et al., 1998] Zhang, M., Mak, a. F. T., and Roberts, V. C. (1998). Finite element modelling of a residual lower-limb in a prosthetic socket: A survey of the development in the first decade. *Med. Eng. Phys.*, 20(5):360–373.

[Zheng et al., 1999] Zheng, Y., Mak, a. F., and Lue, B. (1999). Objective assessment of limb tissue elasticity: development of a manual indentation procedure. *J. Rehabil. Res. Dev.*, 36(2):71–85.

[Zheng and Mak, 1999] Zheng, Y. P. and Mak, a. F. (1999). Extraction of quasi-linear viscoelastic parameters for lower limb soft tissues from manual indentation experiment. *J. Biomech. Eng.*, 121(June 1999):330–339.

[Zheng et al., 2001] Zheng, Y. P., Mak, a. F., and Leung, a. K. (2001). State-of-the-art methods for geometric and biomechanical assessments of residual limbs: a review. *J. Rehabil. Res. Dev.*, 38(5):487–504.

[Zhi et al., 2007] Zhi, H., Ou, B., Luo, B.-M., Feng, X., Wen, Y.-L., and Yang, H.-Y. (2007). Comparison of ultrasound elastography, mammography, and sonography in the diagnosis of solid breast lesions. *J. Ultrasound Med.*, 26(6):807–815.

[Zhou and Zheng, 2012] Zhou, G. and Zheng, Y. P. (2012). Human motion analysis with ultrasound and sonomyography. *Proc. Annu. Int. Conf. IEEE Eng. Med. Biol. Soc. EMBS*, pages 6479–6482.

[Ziegert and Lewis, 1978] Ziegert, J. C. and Lewis, J. L. (1978). In-Vivo Mechanical Properties of Soft Tissue Covering Bony Prominences.